

UNCLASSIFIED

AD NUMBER
AD853957
NEW LIMITATION CHANGE
TO Approved for public release, distribution unlimited
FROM Distribution authorized to U.S. Gov't. agencies and their contractors; Critical Technology; MAY 1969. Other requests shall be referred to Air Force Material Lab., Wright-Patterson AFB, OH 45433.
AUTHORITY
AFML ltr, 12 Jan 1972

THIS PAGE IS UNCLASSIFIED

SECTION for	
STI	WHITE SECTION <input type="checkbox"/>
IC	BUFF SECTION <input checked="" type="checkbox"/>
ANNOUNCED	<input type="checkbox"/>
STIFICATION	
DISTRIBUTION/AVAILABILITY CODES	
DIST.	AVAIL. INFO or SPECIAL
2	

NOTICE

When Government drawings, specifications, or other data are used for any purpose other than in connection with a definitely related Government procurement operation, the United States Government thereby incurs no responsibility nor any obligation whatsoever; and the fact that the Government may have formulated, furnished, or in any way supplied the said drawings, specifications, or other data, is not to be regarded by implication or otherwise as in any manner licensing the holder or any other person or corporation, or conveying any rights or permission to manufacture, use, or sell any patented invention that may in any way be related thereto.

Copies of this report should not be returned unless return is required by security considerations, contractual obligations, or notice on a specific document.

COMPATIBILITY OF TANKAGE MATERIALS WITH LIQUID PROPELLANTS

AD853957

P.M. Lorenz

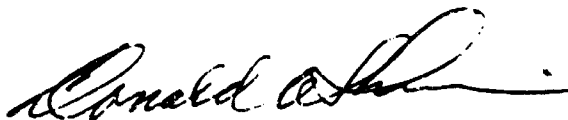
This document is subject to special export controls and each transmittal to foreign governments or foreign nationals may be made only with prior approval of the Air Force Materials Laboratory (MAAA), Wright-Patterson Air Force Base, Ohio (45433).

FOREWORD

This report describes an investigation by the Space Division of The Boeing Company on "Compatibility of Tankage Materials with Liquid Propellants" under Air Force Contract F33(615)-67-C-1698. This contract was initiated under Project 7381 ("Materials Application" Task 738107 "Prevention and Control of Corrosion.") The work was performed under the direction of Air Force Materials Laboratory, Air Force Systems Command, Wright Patterson Air Force Base Ohio. The contract period was from May 1967 through October 1968. The work was administered by Capt. N. Tupper USAF from May through July 1967, by Mr. George Young from August 1967 through February 1968 and by Mr. Fred Meyer from February 1968 through October 1968; as project engineers. Manuscript was released by the authors in March 1969 for publication as a technical report.

Boeing personnel who participated in the investigation include: C. F. Tiffany, Project Supervisor; P. M. Lorenz, Technical Leader; and Dr. L. R. Hall, Research Specialist. Structural testing of specimens was conducted by A. A. Ottlyk and Glenn Vermillion. Design and functional checkout of aggressive propellant test systems were done by A. J. Kacoroski and H. M. Oiden. Metallurgical support was provided by Don Lovell and J. Trzil. Don Good prepared the technical illustrations and artwork. The information contained in this report is also available in Boeing Document D2-121040-1

This Technical Report has been reviewed and is approved.



Donald A. Shinn
Chief, Aeronautical Systems
Support Branch
Materials Support Division
Air Force Materials Laboratory

ABSTRACT

Fracture toughness and flaw growth characteristics of several materials were evaluated in the environment of aggressive propellants. The combinations evaluated were 2219-T851 aluminum/ N_2O_4 , 2219-T851 aluminum/ F_2 , 2219-T851 aluminum/ ClF_5 , 6A1-4V(ELI) titanium/ F_2 , 6A1-4V(ELI) titanium/ ClF_5 , 410(MOD) stainless steel/ N_2O_4 , and 2021-T81 aluminum/ N_2O_4 . Results indicate that described experimental technique is useful in screening engineering materials and establishment of service life requirements for pressurized components. 6A1-4V(ELI) titanium was found to be incompatible with the ClF_5 . Furthermore, it was established that 2021-T81 aluminum is most likely to create functional problems if used to make pressurized N_2O_4 storage vessels.

TABLE OF CONTENTS

	<u>PAGE</u>
1.0 INTRODUCTION	1
2.0 BACKGROUND	3
2.1 Stress Intensity Solutions	3
2.1.1 Surface-Flawed Specimens	3
2.1.2 Uniform Double-Cantilever-Beam Specimen	10
2.1.3 Surface-Flawed Bend Specimen	16
2.2 Sustained-Stress Flaw Growth	18
2.3 Subcritical Cyclic Flaw Growth	22
3.0 EXPERIMENTAL PROCEDURE	27
3.1 Phase I—Qualitative Screening Test	27
3.1.1 Surface-Flawed-Bend (SFB) Specimens	28
3.1.2 Double-Cantilever Beam (DCB) Specimen	42
3.2 Phase II—Quantitative Crack Growth Test	48
3.2.1 Static K_{Ic} Test	59
3.2.2 Sustained Flaw Growth Test	59
3.2.3 Cyclic Flaw Growth Test	60
3.3 Fractographic Technique	60
4.0 MATERIALS	69
5.0 EXPERIMENTAL TEST RESULTS	73
5.1 Phase I—Screening Test	73
5.1.1 2219-T851 Aluminum	74
5.1.1.1 N_2O_4 and 2219-T851 Aluminum	75
5.1.1.2 F_2 and 2219-T851 Aluminum	75
5.1.1.3 ClF_5 and 2219-T851 Aluminum	75
5.1.2 2021-T81 Aluminum and N_2O_4	83
5.1.3 6Al-4V(ELI) Titanium	83
5.1.3.1 F_2 and 6Al-4V(ELI) Titanium	87
5.1.3.2 ClF_5 and 6Al-4V(ELI) Titanium (First Run Test)	87
5.1.3.3 ClF_5 and 6Al-4V(ELI) Titanium (Second Run Test)	93
5.1.3.4 ClF_5 and 6Al-4V(ELI) Titanium (Third Run Test)	99

	<u>PAGE</u>
5.2 Phase II—Fracture Toughness Tests	109
5.2.1 2219-T851 Aluminum As-Welded Weldments	111
5.2.1.1 N ₂ O ₄ and 2219-T851 Aluminum	114
5.2.1.2 F ₂ and 2219-T851 Aluminum	123
5.2.1.3 ClF ₅ and 2219-T851 Aluminum	133
5.2.2 2021-T81 Aluminum	141
5.2.2.1 N ₂ O ₄ and 2021-T81 Aluminum (Base Metal)	141
5.2.2.2 N ₂ O ₄ and 2021-T81 Aluminum Weldment	151
5.2.3 6Al-4V(ELI) Titanium	155
5.2.3.1 F ₂ and 6Al-4V(ELI) Titanium	165
5.2.3.2 ClF ₅ and 6Al-4V(ELI) Titanium	179
5.2.4 410(MOD) Stainless Steel	187
5.2.4.1 N ₂ O ₄ and 410(MOD) Stainless Steel	193
6.0 DISCUSSION	199
6.1 Application to Pressure Vessel Design	199
6.2 Limitations Inherent in Specific Cases	203
6.2.1 Baseline Fracture Toughness, K _{Ic}	204
6.2.2 Threshold Stress Intensity, K _{TH}	205
6.2.3 Proof Test Factor	205
6.2.4 Data Scatter and Proof Test Logic	206
7.0 CONCLUSIONS	209
REFERENCES	211
DISTRIBUTION LIST	215

LIST OF ILLUSTRATIONS

	<u>Page</u>
1 Shape Parameter Curves for Surface and Internal Flaws	5
2 Resultant Stress Magnification Due to Deep Flaw and Plastic Yielding for Plane Strain	7
3 Stress Intensity Factor for a Semi-Circular Surface Flaw	8
4 Schematic Representation of Possible Fracture Initiation at a Semi-Circular Surface Flaw	9
5 Stress Intensity Factor for a Semi-Elliptical Surface Flaw	11
6 Elastic Stress Intensity Magnification Factors for Deep Surface Flaws	12
7 Uniform Double Cantilever Beam Specimen	13
8 Compliance Relationship for DCB Specimens	15
9 Approximate Stress Intensity Factors for Semi-Elliptical Surface Flaws in Bending at $\alpha = 0$	17
10 K_{TH} for 4340 Steel Tested in Three Different Specimen Configurations	19
11 Crack Growth in Inert Atmosphere	21
12 Screening Test Retort	29
13 Schematic Diagram of the N_2O_4 Pressurization System	30
14 Schematic Diagram of the F_2 Pressurization System	31
15 Schematic Diagram of the ClF_5 Pressurization System	32
16 Typical Bend Specimen Assembly for Phase I Testing	33
17 2219-T81 Base Metal Bend Specimen	34
18 2219-T81 As-Welded Bend Specimen	35
19 2021-T81 Aluminum Base Metal Bend Specimen	36
20 2021-T81 Aluminum Weld Metal Bend Specimen	37
21 6Al-4V Base Metal Titanium Bend Specimen	38
22 6Al-4V Weld Metal Titanium Bend Specimen	39
23 SPB Specimen Assembly Preloading (Three-Point Bend)	40
24 SPB Specimen Assembly Preloading (Four-Point Bend)	41
25 Preload Curve for 2021-T81 Aluminum (Base Metal)	43
26 Preload Curve for 2021-T81 Aluminum (Weldment)	44
27 Plain Double Cantilever Beam Specimen	45
28 Grooved Double Cantilever Beam Specimen	46
29 Prestressed DCB Specimen	47
30 Load Compliance Curve for 6Al-4V(ELI) Titanium DCB Specimen	49

LIST OF ILLUSTRATIONS

	<u>Page</u>
31 Typical Surface Flaw	50
32 2219-T851 Aluminum Surface Flawed Specimen (Weldment)	51
33 6A1-4V(ELI) Titanium Surface-Flawed Specimen (Weldment)	52
34 2021 Aluminum Surface-Flawed Specimen (Base Metal)	53
35 2021 Aluminum Surface Flawed Specimen (Weld Metal)	54
36 410(MOD) Stainless Steel Surface Flawed Specimen (Base Metal)	55
37 2219-T851 Aluminum Weld Test Panel	56
38 6A1-4V(ELI) Titanium Weld Test Panel	57
39 2021-T81 Aluminum Weld Test Panel (Virgin and Repair Welds)	58
40 Schematic Illustration of Fractographic Setup	62
41 Cross-sections of Photographically Discrete Zones in Cyclically Tested 2219-T87 Aluminum Specimen	63
42 2219 Aluminum Fatigue Specimen	64
43 Fractographs of 2219-T87 Aluminum Specimen Tested at Room Temperature (Specimen No. CA-43)	66
44 Fractographs of 2219-T87 Aluminum Specimen Tested at Room Temperature (Specimens CA-34 and DA-33)	67
45 Fractographs of 2219-T87 Aluminum Tank Tested at Room Temperature (Tank No. 0001)	68
46 General View of the Test Apparatus After Explosion	94
47 Close-up View of High Pressure Test Chamber	95
48 Close-up View of the Only Two Remaining Specimen Assemblies	96
49 Sustained Flaw Growth in 6A1-4V(ELI) Titanium in Liquid ClF_5	104
50 Absence of Sustained Flaw Growth in 6A1-4V(ELI) Titanium in Vapor ClF_5	105
51 Initiation of the Sustained Flaw Growth in 6A1-4V(ELI) Titanium in ClF_5	110
52 Mechanical Properties of 2219-T851 Aluminum As-Welded Weldments	113
53 Static Fracture Toughness Data for 2219-T851 Aluminum As-Welded Weldments	115
54 Static Fracture Toughness for 2219-T851 Aluminum As-Welded Weldments	116
55 Fractographs of 2219-T851 Aluminum As-Welded Weldment Specimens (Sustained Test in N_2O_4)	117
56 Sustained Flaw Growth Data for 2219-T851 Aluminum As-Welded Weldments (N_2O_4 at 155°F and 100 psig)	118

LIST OF ILLUSTRATIONS

	<u>Page</u>
57 Fractographs of 2219-T851 Aluminum As-Welded Weldment Specimens (Cyclic Test in N_2O_4)	124
58 Cyclic Flaw Growth Data for 2219-T851 Aluminum As-Welded Weldments (N_2O_4 at 155°F and 100 psig)	125
59 Fractographs of 2219-T851 Aluminum As-Welded Weldment Specimens (Sustained Test in F_2 at -320°F and 450 psig)	126
60 Sustained Flaw Growth Data for 2219-T851 Aluminum As-Welded Weldments (F_2 at -320°F and 450 psig)	127
61 Fractographs of 2219-T851 Aluminum As-Welded Weldment Specimens (Sustained Test in ClF_5 at 155°F and 450 psig)	134
62 Sustained Flaw Growth Data for 2219-T851 Aluminum As-Welded Weldments (ClF_5 at 145°F and 450 psig)	135
63 Cyclic Flaw Growth Data for 2219-T87 Aluminum As-Welded Weldments (ClF_5 at 145°F and 450 psig)	136
64 Fractographs of 2021-T81 Aluminum Base Metal (Static Test, White Light Illumination)	142
65 Fractographs of 2021-T81 Aluminum Base Metal (Static Test, Polarized Light Illumination)	143
66 Static Fracture Toughness Data for 2021-T81 Aluminum Base Metal	144
67 Fractographs of 2021-T81 Aluminum Base Metal (Sustained Test, White Light Illumination)	145
68 Fractographs of 2021-T81 Aluminum Base Metal (Sustained Test, Polarized Light Illumination)	146
69 Sustained Flaw Growth Data for 2021-T81 Aluminum Base Metal (N_2O_4 at 145°F and 100 psig)	147
70 Static Fracture Toughness for 2021-T81 Aluminum Weldment	152
71 Crack Path and Fracture Appearance in 2021-T81 Aluminum Weldment (Specimens A1-2 and A1-3)	156
72 Crack Path and Fracture Appearance in 2021-T81 Aluminum Weldment (Specimen A1-4)	157
73 Crack Path and Fracture Appearance in 2021-T81 Aluminum Weldment (Specimens A2-1 and A2-2)	158
74 Crack Path and Fracture Appearance in 2021-T81 Aluminum Weldment (Specimens A2-3 and A2-4)	159
75 Crack Path and Fracture Appearance in 2021-T81 Aluminum Weldment (Specimens B1-1 and B1-2)	160
76 Crack Path and Fracture Appearance in 2021-T81 Aluminum Weldment (Specimens B1-3 and B1-4)	161

LIST OF ILLUSTRATIONS

	<u>Page</u>
77 Crack Path and Fracture Appearance in 2021-T8 ¹ Aluminum Weldment (Specimens AW1-1 and AW1-3)	162
78 Sustained Flaw Growth Data for 2021-T8 ¹ Aluminum Weldments (N ₂ O ₄ at 145°F and 100 psig)	163
79 Mechanical Properties for 6A1-4V(ELI) Titanium As-Welded Weldments	164
80 Fractographs of 6A1-4V(ELI) Titanium As-Welded Weldments Static Test at Room Temperature and -320°F)	167
81 Fractographs of 6A1-4V(ELI) Titanium As-Welded Weldment (Static Test at 140°F and -230°F)	168
32 Static Fracture Toughness Data for 6A1-4V(ELI) Titanium As-Welded Weldments	169
83 Effect of Flaw Depth Upon Calculated Fracture Toughness (6A1-4V(ELI) Titanium As-Welded Weldment)	170
84 Fractographs of 6A1-4V(ELI) Titanium As-Welded Weldment (Sustained Test in F ₂ at -320°F and 450 psig)	174
85 Sustained Flaw Growth Data for 6A1-4V(ELI) Titanium As-Welded Weldment (F ₂ at -320°F and 450 psig)	175
86 Fractographs of 6A1-4V(ELI) Titanium As-Welded Weldment (Sustained and Cyclic Test in ClF ₅ at 140°F and 450 psig)	180
87 Sustained Flaw Growth Data for 6A1-4V(ELI) Titanium As-Welded Weldment (ClF ₅ at 140°F and 450 psig)	186
88 Fractographs of 410(MOD) Stainless Steel Base Metal Specimens (Static Test in Air At Room Temperature)	189
89 Static Fracture Toughness Data for 410(MOD) Stainless Steel Base Metal	190
90 Fractographs of 410(MOD) Stainless Steel Base Metal Specimens (Sustained Test in N ₂ O ₄)	194
91 Sustained Flaw Growth Data for 410(MOD) Stainless Steel Base Metal (N ₂ O ₄ at 120°F and 450 psig)	195

NOTE: There are also four text-incorporated stress vs. flow graphs in Section 6.

LIST OF TABLES

	<u>Page</u>
1 2219-T851 Aluminum in N_2O_4 (SFB Specimen Data)	77
2 2219-T851 Aluminum in F_2 (SFB Specimen Data)	79
3 2219-T851 Aluminum in ClF_5 (SFB Specimen Data)	81
4 2021-T811 Aluminum in N_2O_4 (SFB Specimen Data)	85
5 6A1-4V(ELI) Titanium in F_2 (SFB Specimen Data)	89
6 6A1-4V(ELI) Titanium in ClF_5 (SFB Specimen Data, First Run)	91
7 6A1-4V(ELI) Titanium in ClF_5 (SFB Specimen Data, Second Run)	97
8 6A1-4V(ELI) Titanium in ClF_5 (SFB Specimen Data, Third Run)	101
9 6A1-4V(ELI) Titanium in ClF_5 (DCB Specimen Data, Third Run)	107
10 Mechanical Properties of 2219-T851 Aluminum As-Welded Weldments	112
11 Static Fracture Toughness Data 2219-T851 Aluminum As-Welded Weldments	119
12 Sustained Flaw Growth Data 2219-T851 Aluminum Weldment in the Environment of N_2O_4 at 155°F and 100 psig Pressure	121
13 Cyclic Flaw Growth Data 2219-T851 Aluminum Weldment in the Environment of N_2O_4 at 155°F and 100 psig Pressure	129
14 Sustained Flaw Growth Data 2219-T851 Aluminum Weldment in the Environment of F_2 at -320°F and 450 psig Pressure	131
15 Sustained Flaw Growth Data 2219-T851 Aluminum Weldment in the Environment of ClF_5 , at 145°F and 450 psig Pressure	137
16 Cyclic Flaw Growth Data 2219-T851 Aluminum Weldment in the Environment of ClF_5 at 145°F and 450 psig Pressure	139
17 Sustained Flaw Growth Data 2021-T811 Aluminum Base Metal in the Environment of N_2O_4 at 155°F and 100 psig Pressure	149
18 Sustained Flaw Growth Data 2021-T811 Aluminum Weldment in the Environment of N_2O_4 at 155°F and 100 psig Pressure	153
19 Mechanical Properties of 6A1-4V(ELI) Titanium As-Welded Weldment	166
20 Static Fracture Toughness Data for 6A1-4V(ELI) Titanium As-Welded Weldments	171
21 Sustained Flaw Growth Data for 6A1-4V(ELI) Titanium As-Welded Weldment (F_2 at -320°F and 450 psig Pressure)	177
22 Sustained Flaw Growth Data for 6A1-4V(ELI) Titanium As-Welded Weldment (ClF_5 at 140°F and 450 psig Pressure)	181
23 Cyclic Flaw Growth Data for 6A1-4V(ELI) Titanium As-Welded Weldment (ClF_5 at 140°F and 450 psig Pressure)	183
24 Mechanical Properties of 410(MOD) Stainless Steel Base Metal	188
25 Static Fracture Toughness Data of 410(MOD) Stainless Steel Base Metal	191
26 Sustained Flaw Growth Data 410(MOD) Stainless Steel Base Metal in the Environment of N_2O_4 at 120°F and 450 psig Pressure	197

NOMENCLATURE

K_{TH}	Threshold stress intensity for a given material-environment
K_I	Plane strain stress intensity factor
K_{Ii}	Plane strain stress intensity factor at initial conditions
K_{Ic}	Plane strain fracture toughness of material
a	Crack depth of the semielliptical surface flaw; half crack length for through-the-thickness center-cracked specimen; crack depth of a double-centiliver-beam (DCB) specimen
N	Number of cycles
K	Plane stress stress intensity factor
ΔK	Value of $(K_{max} - K_{min})$ during a typical loading cycle
K_c	Plane stress fracture toughness of the material
$R = \frac{K_{min}}{K_{max}}$	Load ratio
$2c$	Crack length of a semielliptical surface flaw
ϕ	Defined as $x = a \cos \phi$ and $y = a \sin \phi$
α	Polar angle measured from minor axis
Φ	Complete elliptical integral of second kind having modulus k defined as
$k = \left(\frac{c^2 - a^2}{c^2} \right)^{\frac{1}{2}}$	
σ	Uniform stress applied at infinity and perpendicular to the plane of crack
σ_{ys}	Uniaxial tensile yield strength
Q	$\Phi^2 - 0.212 (\sigma / \sigma_{ys})^2$
ν	Poisson's ratio of the material
E	Young's modulus
t	Thickness of plate
M_{kf}	Elastic stress magnification due to deep flaw
M_{kp}	Stress magnification due to plastic yielding
M_K	$M_{kf} \times M_{kp}$
M_I	Peripheral stress intensity correction factor for semicircular surface flaw
M_I^s	Peripheral stress intensity correction factor for semielliptical surface flaw - Smith's analysis

NOMENCLATURE

M_K^I	Deep flaw stress intensity magnification - Smith's analysis
P	Force in pounds
b	Thickness of DCB specimen
b_n	Net thickness of DCB specimen as measured at the root of the side groove
h	One half of the DCB specimen depth

1.0 INTRODUCTION

This program is designed to establish an experimental procedure for evaluation of engineering materials exposed to the environment of aggressive propellants. The experimental approach is based on the principles of linear elastic fracture mechanics and consists of two phases. Phase I is devoted to screening tests to identify the most severe combinations of test variables, which include pressure-temperature combinations, location of the surface flaws, (weld, base metal, or heat affected zone), and liquid or vapor state of the propellant. Phase II effort is to utilize this information in scheduling fracture toughness testing under static, cyclic, and sustained loading conditions. Results of the investigation and description of the experimental procedure, together with the underlying philosophies in selecting certain approaches, are presented in the form useful in design of propellant-containing pressure vessels.

Material-propellant combinations selected for the present program include: 2219-T851 aluminum in combination with N_2O_4 , F_2 , and ClF_5 ; 6Al-4V(ELI) titanium in combination with F_2 and ClF_5 ; 410(MOD) stainless steel in combination with N_2O_4 , and 2021-T81 aluminum also in combination with N_2O_4 . An overall description of the analytical background and the general experimental approach are given in sections preceding presentation of test results.

2.0 BACKGROUND

Quantitative characterization of stress corrosion cracking can be developed by testing preflawed specimens of the type suitable for application of basic principles of applied fracture mechanics. Considerable experimental data has been generated by many investigators supporting usefulness of such approach. It is the purpose of this section to review some of the pertinent background information utilized in the present program and to provide a short summary of basic relationships between specimen dimensions, type of loading, crack shapes and sizes, as well as applied stress levels. Together with the summary of stress intensity solutions the section also contains a short description of sustained and cyclic crack growth at subcritical stress intensity levels and how such growth can be characterized using existing analytical solutions of linear elastic fracture mechanics.

2.1 Stress Intensity Solutions

Most of the experimental data presented in this report has been generated using surface-flawed-bend (SFB) specimens for the Phase I screening tests and surface-flawed-tensile (SFT) specimens for the Phase II flaw growth tests. Toward the end of the Phase I testing it became apparent that the surface-flawed-bend specimens were inadequate for generation of high initial stress intensities and could not serve as an effective screening tool for qualification of various material-propellant combinations. Double-cantilever-beam (DCB) specimens were added to the program to supplement whenever possible the screening test data obtained using surface-flawed-bend specimens. Applicable formulas for the three types of specimens used are summarized in the following paragraphs.

2.1.1 Surface-Flawed Specimens

Irwin (Ref 1) first obtained a solution for a semielliptical surface flaw in a plate and estimated that the solution may be valid for flaws with depth up to about half the material thickness. As part of the Boeing Independent Research and Development program (IR&D), Kobayashi (Ref 2)

arrived at an approximate stress intensity solution for deep flaws having small depth-to-length ratios, that is $a/2c$ values. Smith (Ref 3) derived a solution for the semicircular flaw in a semi-infinite body. This solution provided further refinement of the free surface correction Irwin used in his equation. As part of Boeing IR&D, Smith (Ref 4) estimated free surface corrections for semielliptical surface flaws in a semi-infinite body. He also obtained an approximation of the stress intensity for the semicircular surface flaws, which become very deep with respect to thickness (Ref 4). Using the single-edge-notch solution, (that is, $a/2c = 0$) of Gross, et al. (Ref 5), and his own solution for deep semicircular flaw, Smith roughly estimated stress intensity factors for deep surface flaws of intermediate shape, that is, $a/2c$ ratios between 0 and 0.5 (Ref 4).

Irwin Analysis---The Irwin relationship for the semielliptical surface flaw in a finite thickness plate is as follows:

$$K_I = 1.1 \sqrt{\pi} \sigma (a/Q)^{1/2} \left[\frac{1}{c^2} (a^2 \cos^2 \phi + c^2 \sin^2 \phi) \right]^{1/4} \quad (1)$$

The maximum value of K_I , which occurs at the end of the semiminor axis of the ellipse, is:

$$K_I = 1.1 \sqrt{\pi} \sigma (a/Q)^{1/2} \quad (2)$$

A plot of Q versus $a/2c$ is shown in Figure 1.

The 1.1 coefficient was an estimate to account for free surface effect. The equations were believed to be valid for flaw depths up to about half the plate thickness.

Kobayashi Analysis---For surface flaws that have a small depth-to-length ratio, that is, $a/2c$, but are deep with respect to the plate thickness, Kobayashi assumed the following form for the stress intensity:

$$K_I = 1.1 K_K \frac{\sigma \sqrt{\pi a}}{\sqrt{Q}} \quad (3)$$

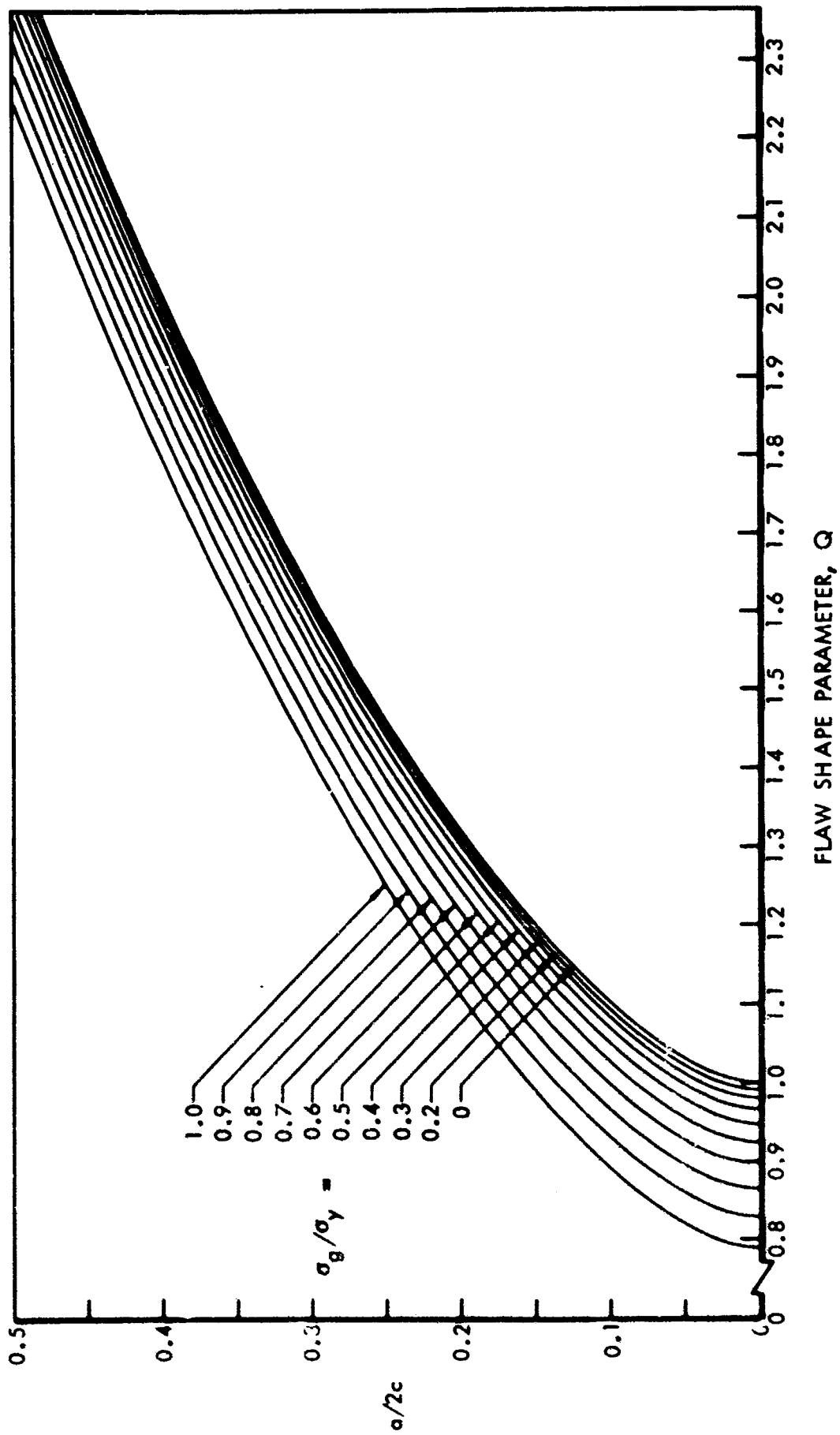


Figure 1: SHAPE PARAMETER CURVES FOR SURFACE AND INTERNAL FLAWS

where:

$$M_K = M_{kf} \times M_{kp}$$

Following Irwin, the multiplying constant 1.1 is taken to account for the effect of free surface on the stress intensity factor.

M_{kf} is elastic stress magnification due to deep flaw in an infinite strip under the conditions of plane-strain. M_{kp} is the stress magnification due to plastic yielding in an infinite plate under the conditions of plane-strain.

A plot of M_K (that is, $M_{kf} \times M_{kp}$) versus a/t is given in Figure 2 for $(\sigma/\sigma_{ys}) = 0.4$, and 0.8 for $\nu = 1/3$. Kobayashi solution is considered valid for small $a/2c$ values and flaw depths up to about 70% of the plate thickness. Experimental evidence accumulated to date suggests that for some engineering materials the applicability of the solution can be extended to $a/t \approx 0.95$.

Smith Analysis---Smith's linear elastic analysis of a semicircular surface flaw in a semi-infinite body resulted in the following stress-intensity relationship:

$$K_I = M_I \frac{2\sigma\sqrt{a}}{\sqrt{\pi}} \quad (4)$$

This result corresponds to that shown in Equations 1 and 2, except that the 1.1 free surface correction assumed by Irwin is replaced by the M_I coefficient, which is dependent upon location on the flaw periphery (Figure 3), and plasticity correction is not incorporated. From the illustration it can be seen that M_I varies from about 1.03 at the point of maximum flaw depth to 1.21 at the free surface. Unlike the Irwin equation, the point of maximum stress intensity is predicted at the surface rather than at maximum flaw depth. However, for most materials the resistance to fracture is higher at the surface (i.e., higher than the plane-strain fracture toughness value) so it is probable that fracture will initiate at a point below the surface where the applied stress intensity becomes tangent to the fracture toughness value. This is illustrated schematically in Figure 4.

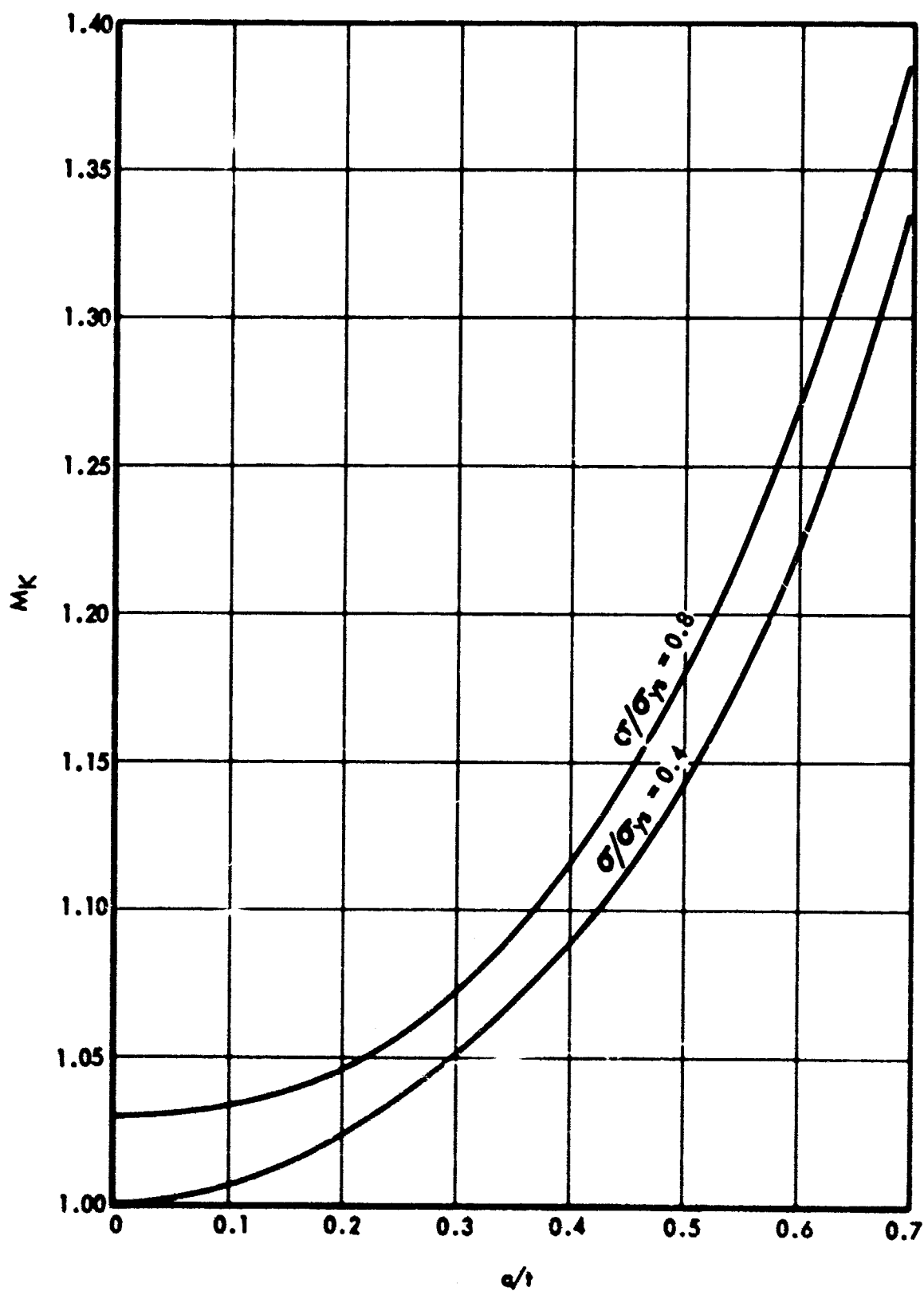


Figure 2 : RESULTANT STRESS MAGNIFICATION DUE TO DEEP FLAW AND PLASTIC YIELDING FOR PLANE STRAIN.
 $\nu = 1/3$, $a/2c < 0.3$

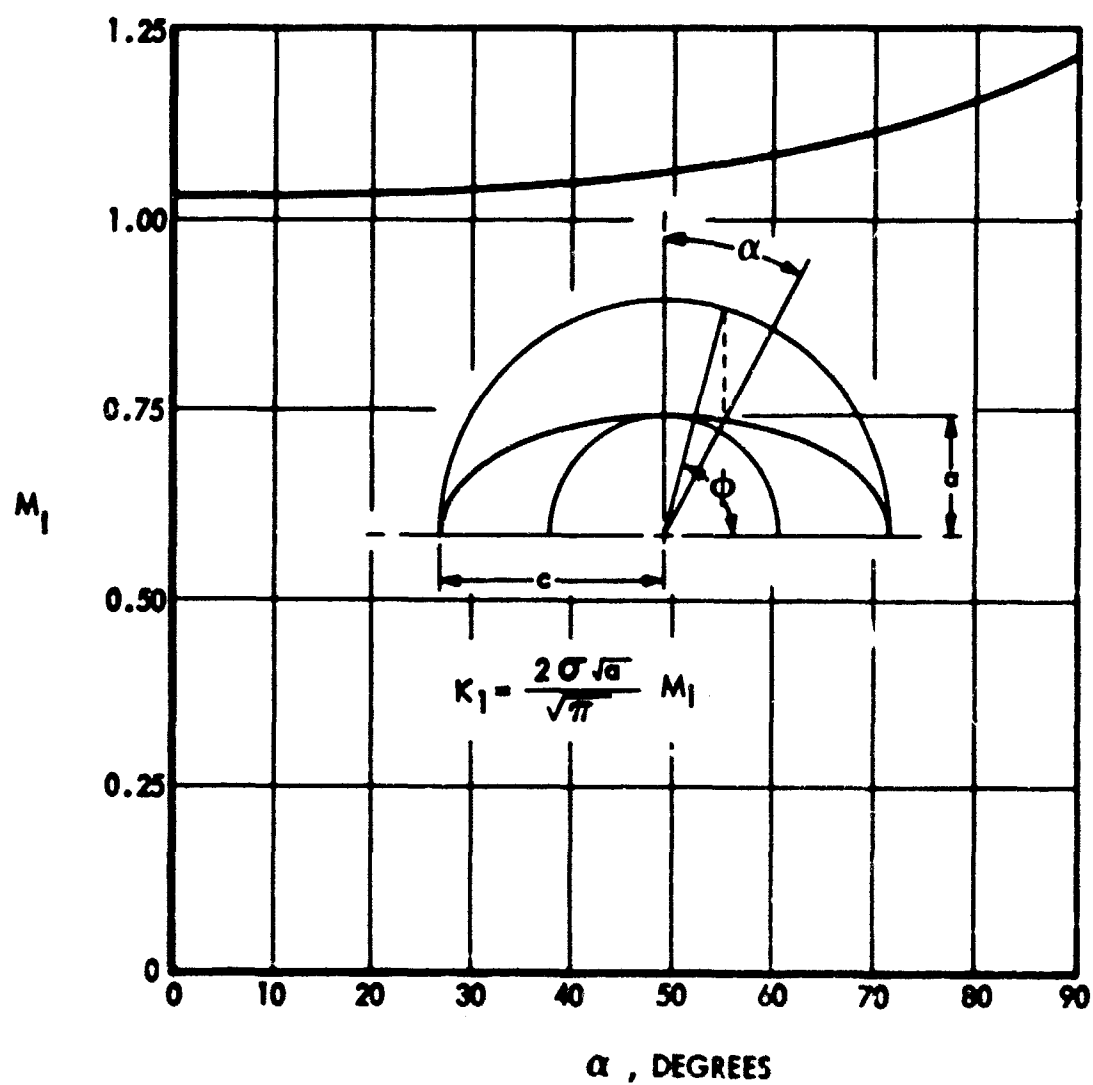


Figure 3: STRESS INTENSITY FACTOR FOR A SEMI-CIRCULAR SURFACE FLAW

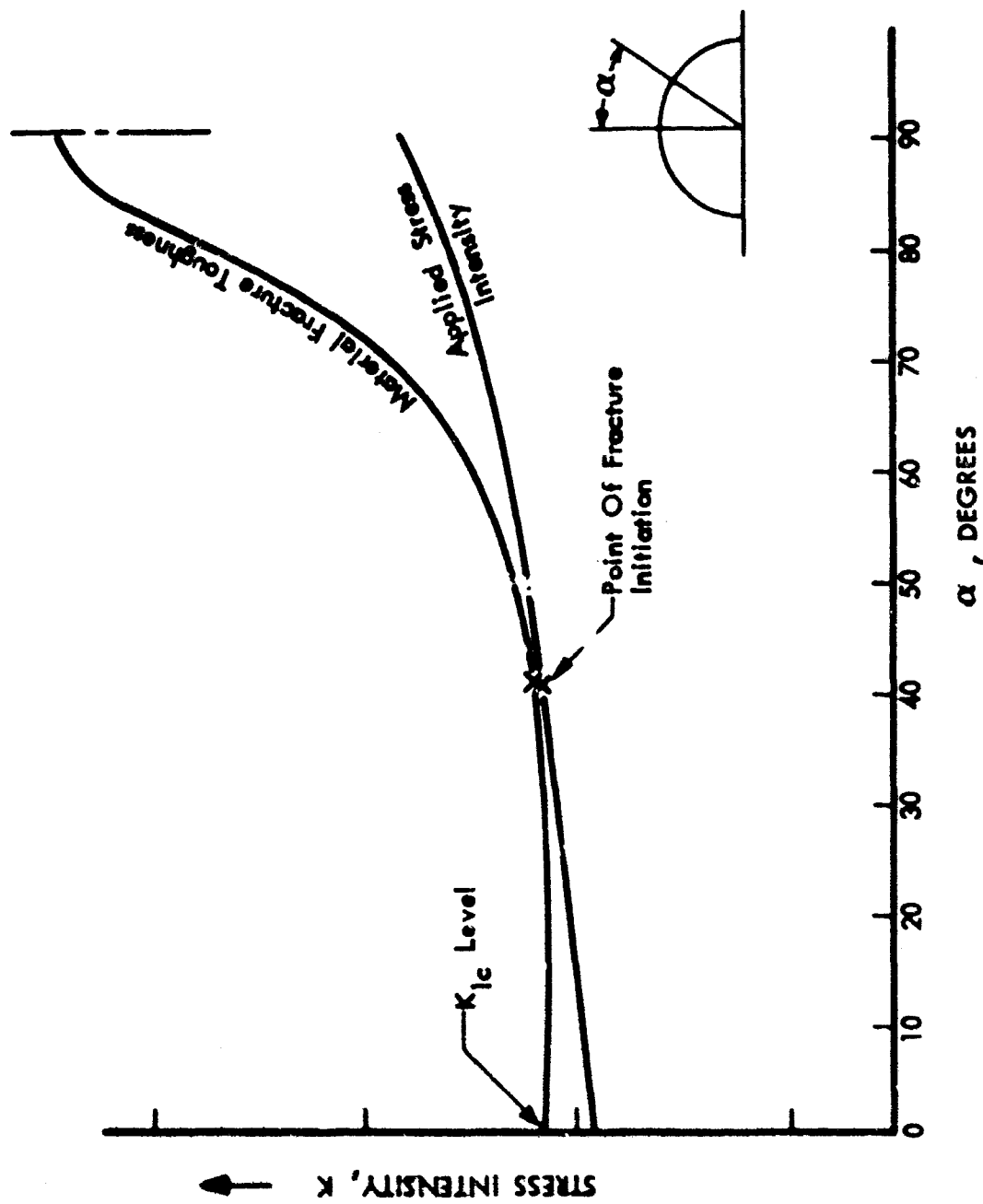


Figure 4 : SCHEMATIC REPRESENTATION OF POSSIBLE FRACTURE INITIATION AT A SEMI-CIRCULAR SURFACE FLAW

For semielliptical flaws in semi-infinite bodies, Smith estimated the free surface coefficient, M_I^1 . This result is shown in Figure 5. The stress intensity relation thus becomes:

$$K_I = M_I^1 \sqrt{\pi} \sigma (a/Q)^{1/2} \quad (5)$$

where:

$$M_I^1 = M_I \left[(a/c)^2 \cos^2 \phi + \sin^2 \phi \right]^{1/4} \left[\frac{1.1}{M_I} - \left(\frac{1.1}{M_I} - 1 \right) a/c \right]$$

As seen in Figure 5, the point of maximum stress intensity occurs at the point of maximum flaw depth for all flaws with $a/2c$ ratios less than about 0.35 to 0.40. This is consistent with Irwin's analysis; however, the magnitude of the free surface corrections is slightly less than the 1.1 he estimated. Smith obtained the stress intensity factors for semicircular flaws in a finite-thickness plate and estimated the stress intensity factors for semielliptical surface flaws in a plate as a function of $a/2c$ and a/t ratios. The resulting relationship is:

$$K_I = M_I^1 M_K^1 \sqrt{\pi} \sigma (a/Q)^{1/2} \quad (6)$$

M_K^1 is the finite thickness (or deep flaw stress intensity magnification) correction. The M_K^1 versus a/t curve for the semicircular flaw and the estimated curves for semielliptical flaws with $a/2c$ ratios of 0.20, 0.25, and 0.30 are shown in Figure 6. Smith's solution is considered accurate for semicircular flaws but becomes less and less reliable as $a/2c$ decreases.

2.1.2 Uniform Double-Cantilever-Beam Specimen

An approximate expression for the uniform height DCB specimen is given in Ref 6 as

$$K_I = \frac{2P}{b} \left[\frac{3(a + 0.6h)^2 + h^2}{(1 - \mu^2) h^3} \right]^{1/2} \quad (7)$$

where specimen configuration and symbols are defined in Figure 7.

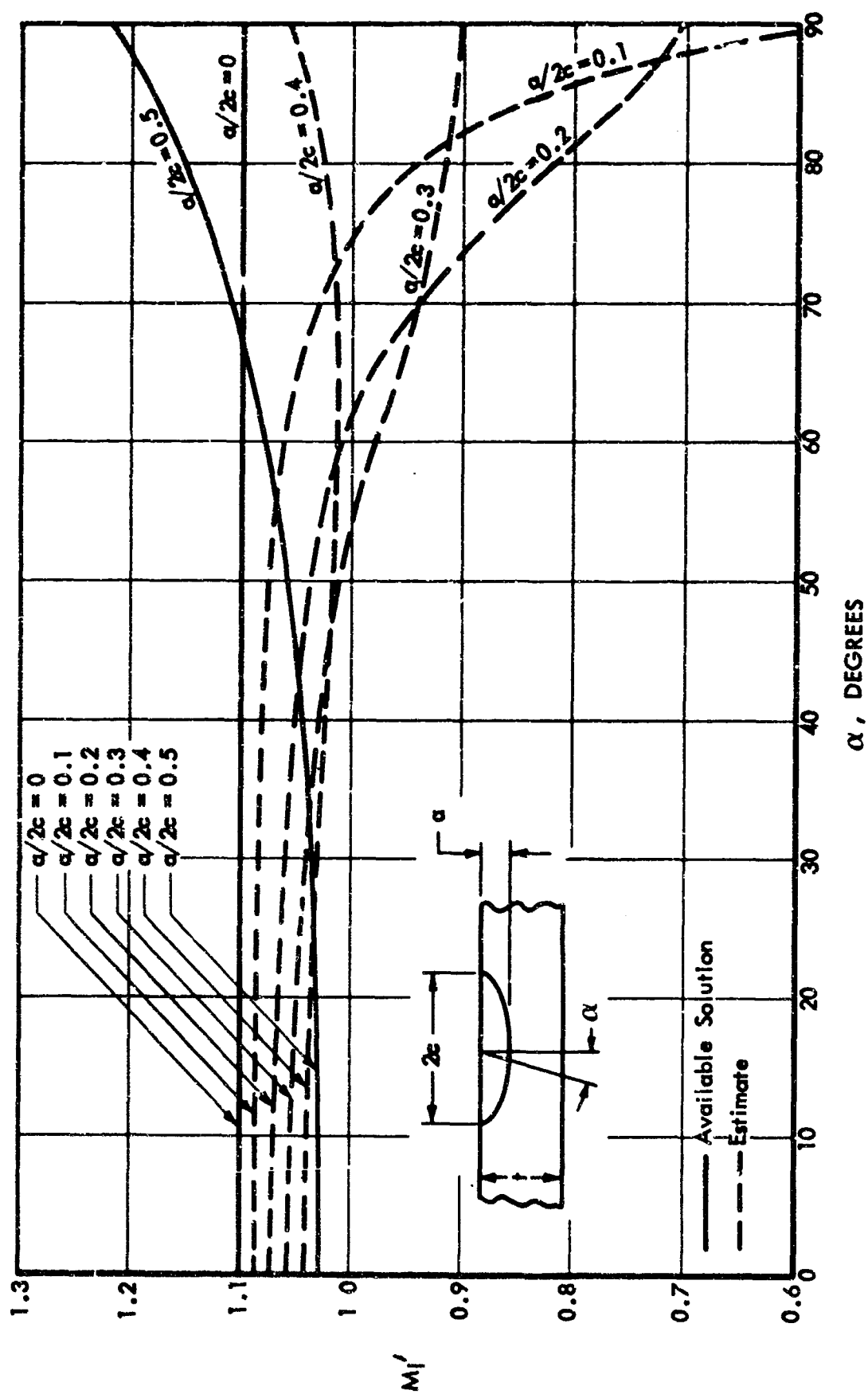


Figure 5: STRESS INTENSITY FACTOR FOR A SEMI-ELLIPTICAL SURFACE FLAW

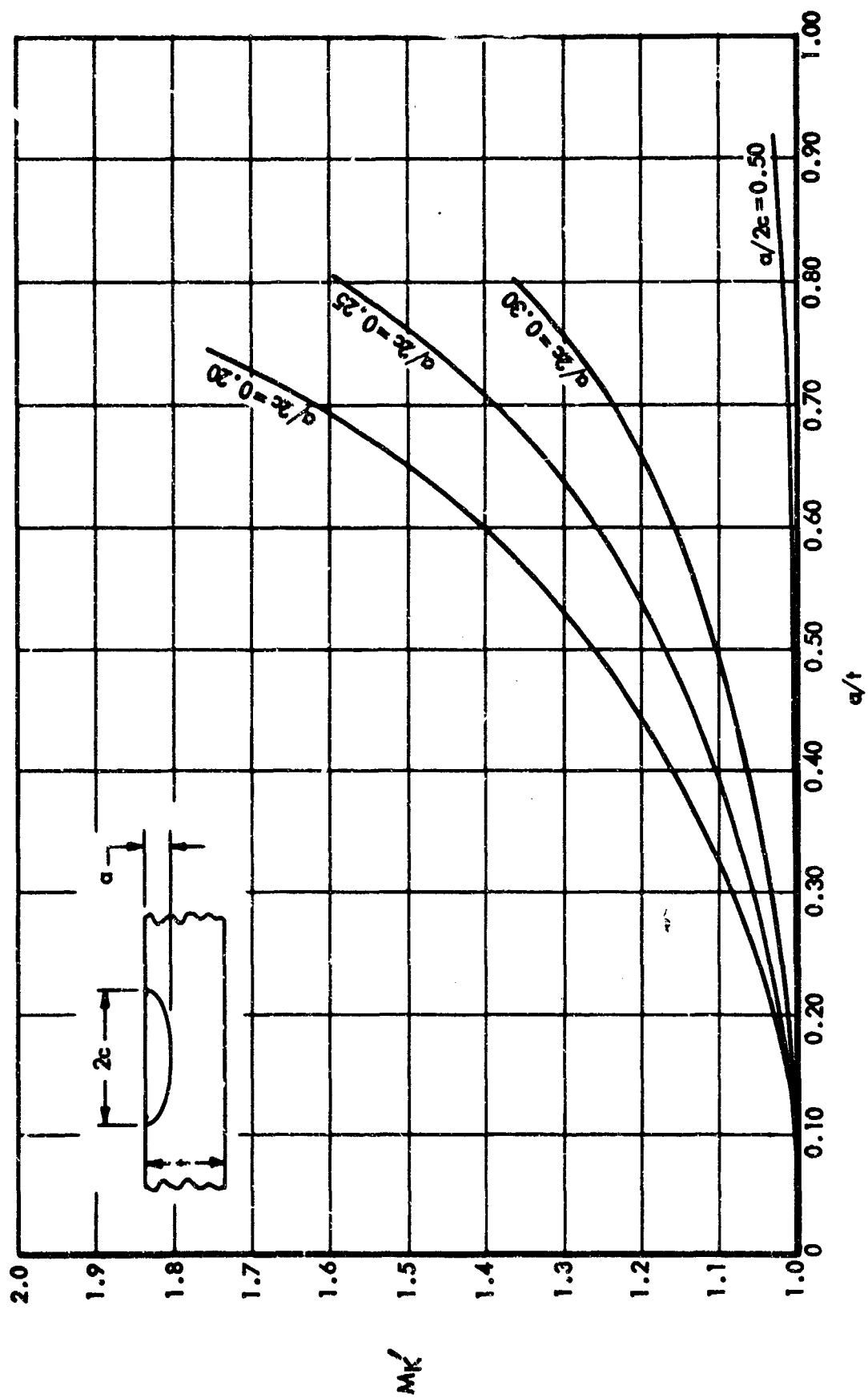


Figure 6: ELASTIC STRESS INTENSITY MAGNIFICATION FACTORS FOR DEEP SURFACE FLAWS

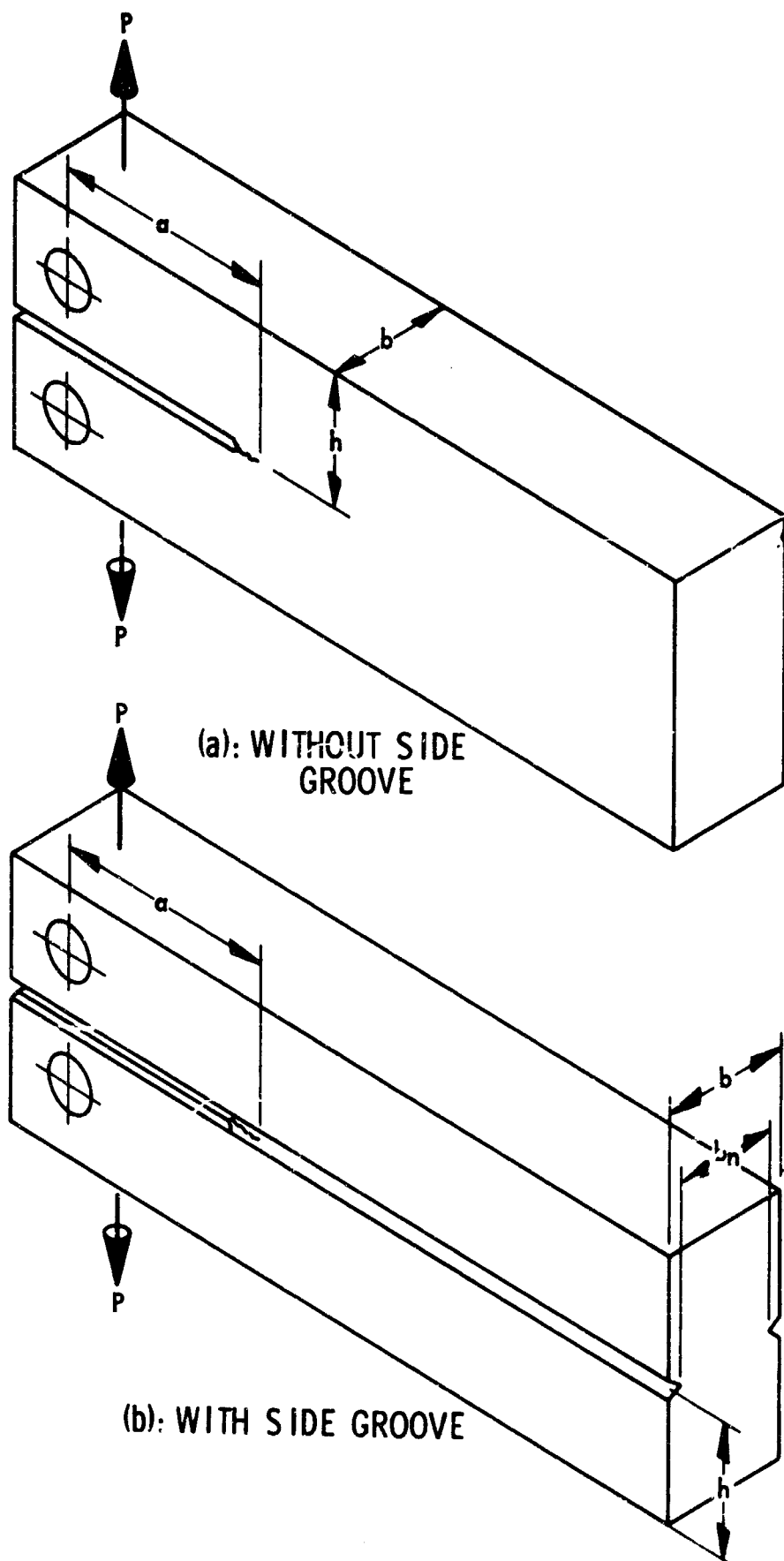


Figure 7: UNIFORM DOUBLE CANTILEVER BEAM SPECIMEN

Equation 7 has been substantiated at the University of Washington by a numerical solution based on the direct stiffness method. Stress intensities calculated from Equation 7 are compared in Figure 8 with those resulting from the numerical analysis. The two methods give essentially the same result except for crack length of less than 1.0 inch (for a 6.0-inch specimen). Compliance measurements (Ref 6) have shown that the remaining unbroken ligament in a DCB specimen must be large enough or the linear compliance of the specimen is disturbed by a plastic flow "hinging action" in the ligament. In a 5.5-inch specimen, Mostovoy measured linear compliance with crack lengths from 1 to 3 inches.

If the crack surfaces of a DCB specimen are given a fixed relative normal displacement in the plane of the pinholes, the applied stress intensity decreases as the crack length increases; therefore, a crack can be arrested without complete fracture of the specimen, and crack arrest values of K_{TH} can be determined.

In the DCB specimen, cracks do not always grow in the original crack plane but may turn from that plane and break off one arm of the test specimen. This problem can be alleviated by side grooving the specimen as shown in Figure 7. When side grooved, the expression for stress intensity for the DCB specimen becomes

$$K_I = \frac{2P}{b} \left(\frac{b}{b_n} \right)^m \left[\frac{3(a + 0.6h)^2 + h^2}{(1 - \mu^2) h^3} \right]^{1/2} \quad (8)$$

Values of m must be between 0.5 and 1.0.

For 7075-T651 aluminum, Mostovoy (Ref 6) found that a value of $m = 1/2$ correlated critical K_I values measured from face-grooved DCB specimens with comparable K_{Ic} values reported in the literature (Ref 7). Freed and Krafft (Ref 8) found that when fracture toughness in the flank direction relative to the forward cracking direction is high, m approaches $1/2$; when it is low, m increases toward unity. The value of m can be determined experimentally; however, with shallow side grooves, the error in using an incorrect value of m will be small; for example, with 10% groove, K_{Ic} would be 93% of the

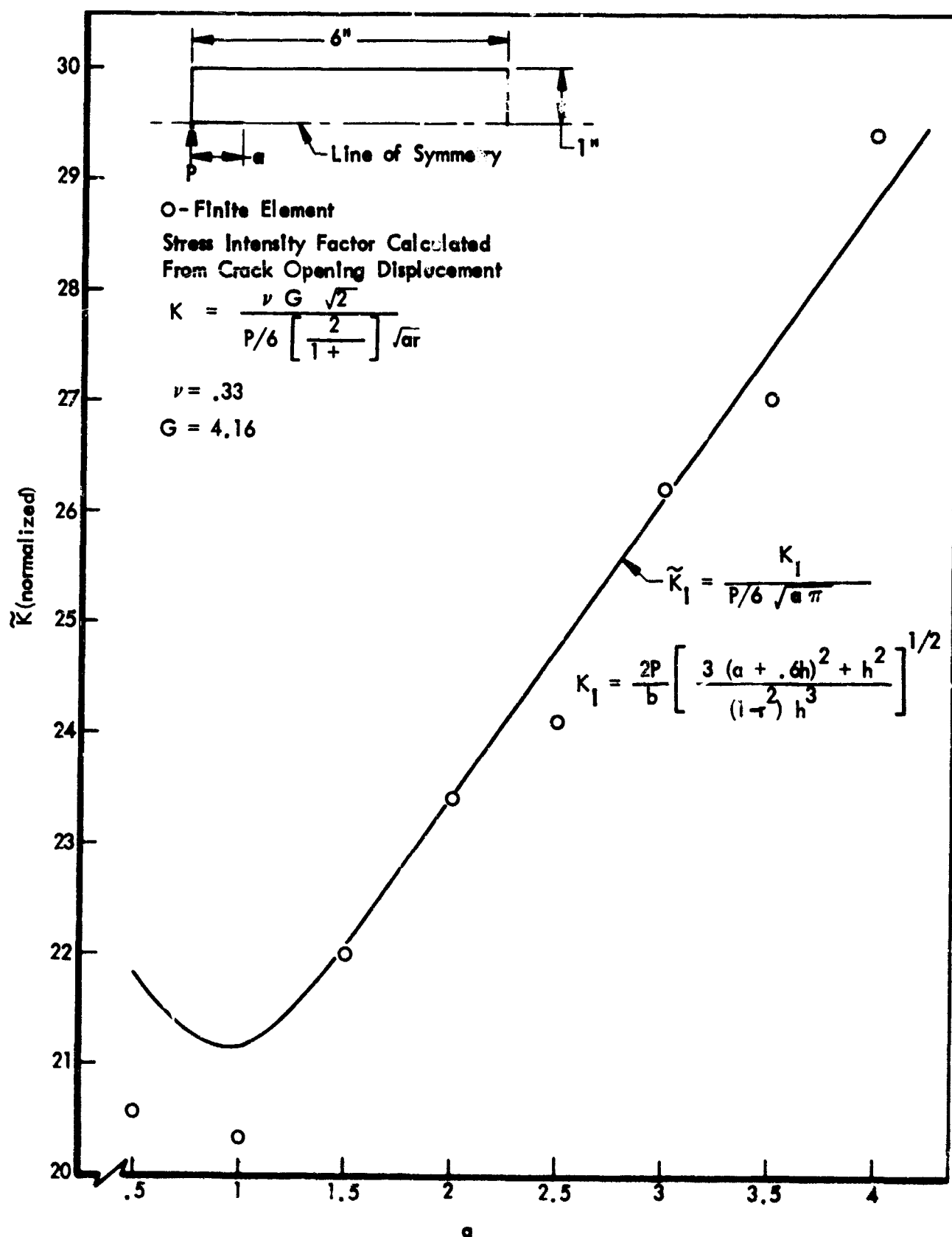


Figure 8: COMPLIANCE RELATIONSHIP FOR DCB SPECIMENS

"correct" value if $m = 1/2$ were used in Equation 8, when the correct value of m was actually 0.8.

Side grooving not only constraints crack propagation to a single plane, but it also suppresses side boundary plastic zone formation, thereby more closely simulating plane-strain deformation conditions at the crack front.

The effect of side grooving has not been systematically studied. Test results reported by Mostovoy, et al. (Ref 6) using 7075-T651 aluminum show that over a wide range of thicknesses (0.25 inch to 1.0 inch) and groove depths ($0.30 < b_n/b < 0.90$), the critical stress intensities calculated using side grooved-DCB specimens, and Equation 8 with $m = 1/2$ are plane-strain fracture toughness values. Freed and Krafft (Ref 8) state that the acuity of the side groove up to $R = 0.020$ inch appears to have little effect on the value of m or K_{Ic} . They also state that the thickness of specimen required for valid K_{Ic} measurement appears to be $5r_y$ (where $r_y = 1/2 (K_{Ic}/\sigma_{ys})^2$) independent of the depth of the side groove, and that the value of K_{Ic} calculated from maximum load with specimens not meeting this requirement appears to underestimate the true K_{Ic} .

2.1.3 Surface-Flawed Bend Specimen

The solution for a semicircular surface flaw in a thick plate in bending was presented by Smith (Ref 3). Smith showed that the back surface correction for bending will be smaller for bending than for tension. If a/t values for bend specimens are restricted to be less than 0.5, it may be concluded that in this range of a/t values no correction for the back surface effect is necessary for bending.

Gross (Ref 9) presented the solution for an edge notch ($a/2c = 0$) in bending. This solution with that of Smith (Ref 3) for $a/2c = 0.5$ gives two limiting cases of surface flaws in bending. Stress intensities for other shape ratios were estimated (Ref 4) by assuming logarithmic variation between $a/2c = 0$ and $a/2c = 0.5$. The resulting relationships are plotted in Figure 9. These curves present stress intensities only at $\alpha = 0$.

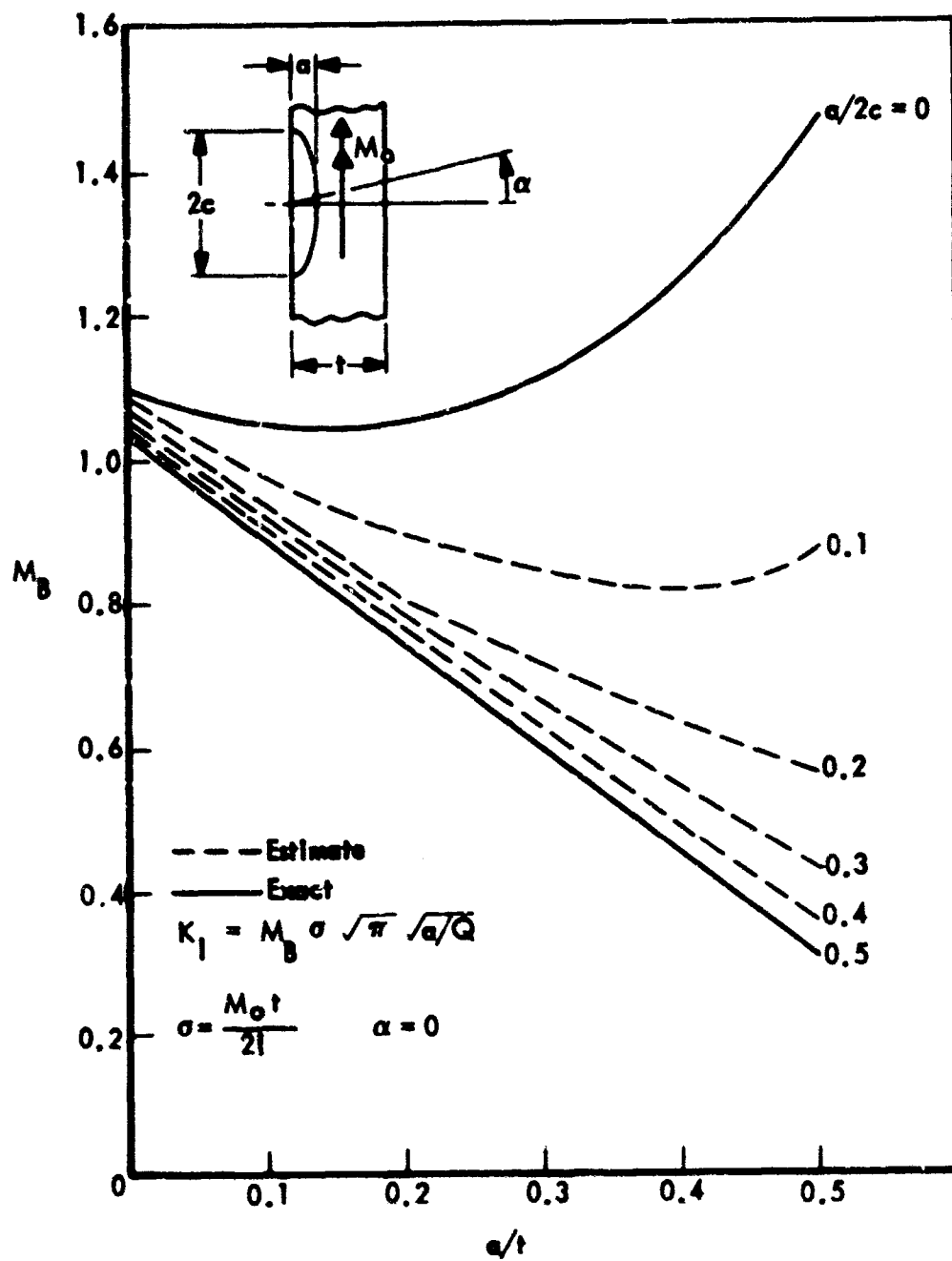


Figure 9: APPROXIMATE STRESS INTENSITY FACTORS FOR SEMI-ELLIPTICAL SURFACE FLAWS IN BENDING AT $\alpha = 0$

The resultant equation for calculating stress intensity K for a given flaw size and applied bending moment becomes

$$K_I = M_B \sigma_B \sqrt{\pi} (a/Q)^{1/2} \quad (9)$$

where M_B is the bend specimen correction and σ_B is the outer fiber applied bending stress level.

2.2 Sustained-Stress Flaw Growth

The most significant phenomenon noted in sustained-stress testing of precracked specimens is the observation that there is an apparent threshold stress intensity level above which the flaws would grow in a given environment-material combination, but remain stationary under identical conditions if the stress intensity is below that level. Moreover, the same phenomenon is noted both in aggressive as well as in relatively inert environments. The value of threshold is designated by K_{TH} where K is the stress intensity value calculated for a given stress-flaw size combination and subscript TH signifies "threshold". Actual calculations are made in the usual manner using any one of the applicable formulas discussed in the previous section.

A striking example of threshold phenomena is provided by Beachem and Brown (Ref 10), who explored the consistency in sustained-stress crack growth test results using three different specimen types: the center-cracked plate, the surface-flawed plate, and the precracked cantilever beam. For 4340 steel in dilute salt solution, the same K_{TH} value was obtained from all three specimens as illustrated in Figure 10. The three specimen types did yield differences in failure time at a given K_{II} level. This result is due to the different functional dependencies of stress intensity upon crack length for the three specimens. The shortest failure times were observed for the precracked cantilever beam, which has the most rapid increase of stress intensity with increasing crack length; the longest failure times were observed for center-cracked specimens, for which the rate of increase of stress intensity with crack length is the least.

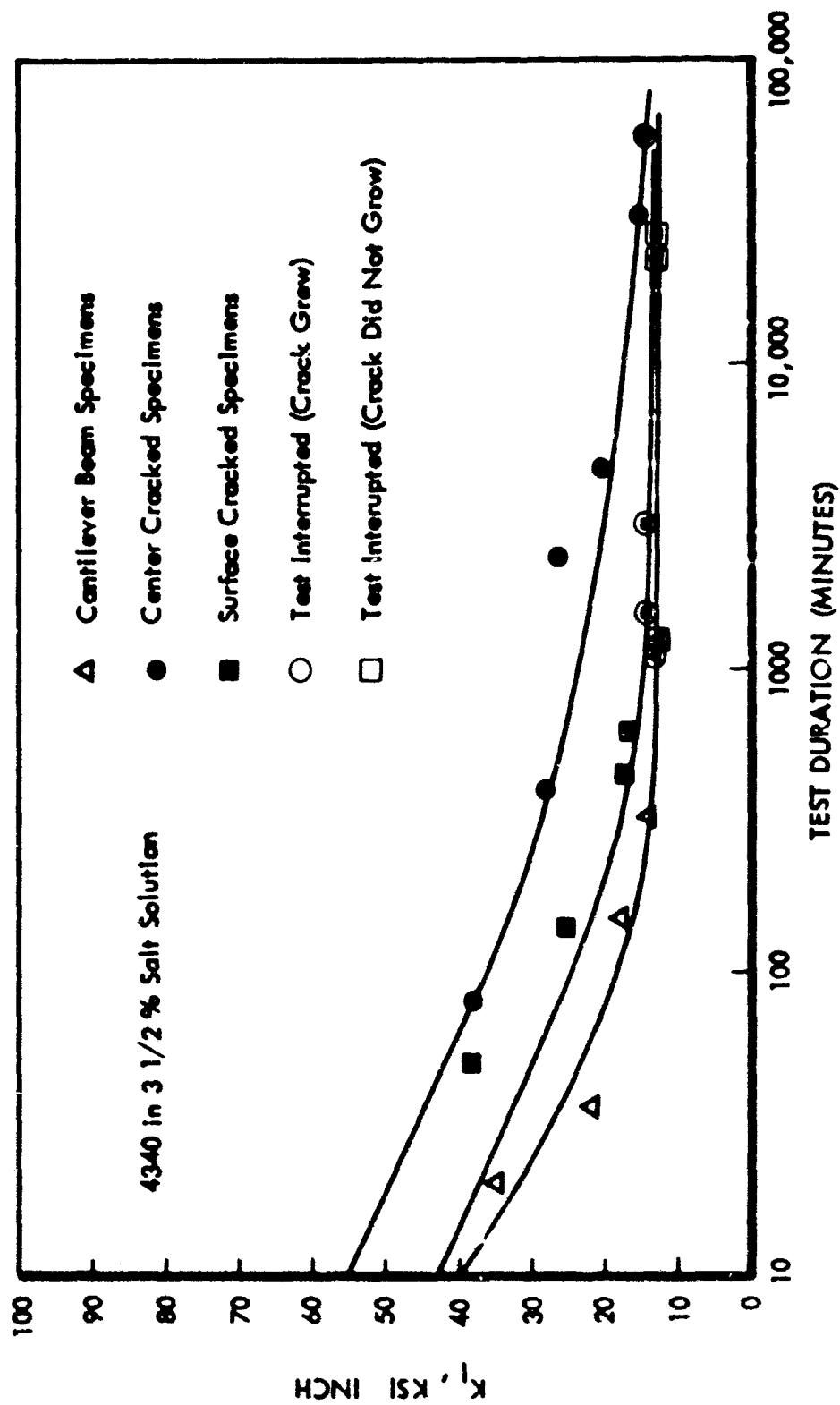


Figure 10: K_{TH} FOR 4340 STEEL TESTED IN THREE DIFFERENT SPECIMEN CONFIGURATIONS

The work of Smith, Piper, and Downey (Ref 11) has shown that specimens for which stress decreases with crack length are useful in the determination of K_{TH} . The authors used center-cracked specimens to determine the threshold stress intensity for crack initiation, and the wedge opening load (WOL) specimens for crack arrest. For Ti-8Al-1Mo-1V alloy in 3.5% salt solution, the threshold stress intensity for crack initiation was 20 to 25 ksi $\sqrt{\text{in.}}$, and for crack arrest, 20 to 22 ksi $\sqrt{\text{in.}}$, in excellent agreement. For end-loaded specimens under constant load, stress-intensity factor and net section stress both increase with increasing crack length; for wedge-force loading, the net section stresses increase, whereas the stress intensity decreases with increasing crack length. The excellent agreement between initiation and arrest K_{TH} values clearly shows that it is the stress-intensity parameter that is the controlling factor in the sustained stress crack growth, not the net section stress.

The state of deformation at the crack tip influences environmental cracking. There is considerable experimental evidence that indicates that environmental cracking is most severe under conditions of plane-strain, and less severe under conditions of plane-stress. Brown (Ref 12) has shown that environmentally induced cracks will not propagate under stress conditions that result in substantial shear lip formulation, that is, plane-stress conditions. Piper et al., (Ref 13) have demonstrated that K_{TH} for two titanium alloys decreases as specimen thickness is increased.

Sustained stress crack growth has been also observed in chemically inert environments. Johnson (Ref 14) has reported subcritical flaw growth over a substantial range of stress intensity for AM350 in a purified argon environment. Test results show that crack growth behavior in inert environments differs from that in aggressive environments. In aggressive environments, crack growth rates increase uniformly with increasing stress intensity (Refs 11, 15 through 18). In inert environments, the crack growth rate initially decreases with increasing stress intensity (Figure 11). If the initial stress intensity is sufficiently low, the crack growth may stop altogether. At higher stress intensities, the crack growth rate passes through a minimum and then increases steadily until fracture.

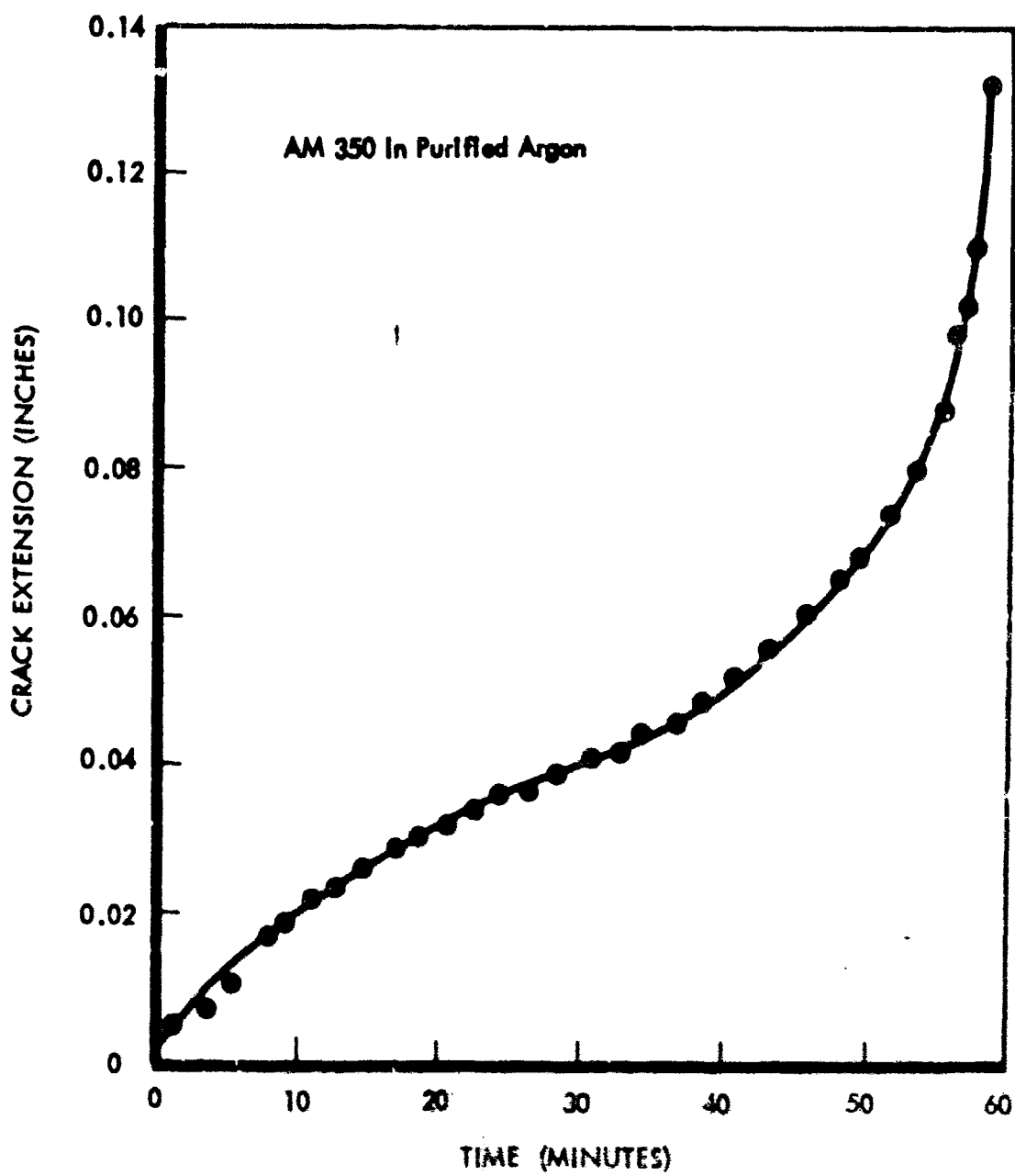


Figure 11: CRACK GROWTH IN INERT ATMOSPHERE

This behavior was also noted by Tiffany (Ref 19), who defined two threshold stress intensities for 5Al-2.5Sn(ELI) titanium and 2219-T67 aluminum in an environment of ambient air, liquid nitrogen, and liquid hydrogen. The one threshold stress intensity was defined as that value above which growth could be expected to occur without resulting in failure. A higher threshold stress intensity was defined as the value above which growth to failure could be expected. Presumably, sustained stress flaw growth in inert environments involves time-dependent deformation processes at the crack tip which manifest themselves in slow crack extension. Greater plastic relaxation, associated with plane-stress deformation, seems to accentuate inert environment growth. If there is uncertainty concerning the state of deformation at the crack tip, one must be careful to differentiate inert environment type of growth with environmental cracking.

2.3 Subcritical Cyclic Flaw Growth

Observations of crack growth caused by fluctuating loads indicate that crack growth in metals can be looked at as a continuous process proceeding at a characteristic rate. Many investigators have formulated crack growth rate laws for through-the-thickness cracks growing under conditions of plane-stress in thin metallic sheets. Many of these laws and the results from which they were derived are based on fracture mechanics analyses, which provide considerable information on which to base the analysis of plane-strain flaw growth rates.

Since fatigue crack growth is caused by fracture of material in the plastic zone at the crack tip, it follows that two different cracked sheets with identical sheet thickness and material properties should undergo reasonably identical fatigue crack extensions if each is subjected to the same history of variation of elastic stress intensity. Thus, where da/dN is the extension of a crack tip per cycle of loading, elastic-plastic analyses suggest that

$$da/dN = f(K_{max}, \Delta K) \quad (10)$$

A crack growth rate correlation similar to Equation 10 was first proposed by Paris, et al. (Ref 20). Subsequent investigations (Refs 21 through 26) have adequately substantiated the validity of the stress-intensity approach. Other crack growth rate laws have been proposed that are based on dimensional analysis (Refs 27, 28, and 29) and the direct use of elastic-plastic analyses (Refs 30 through 34). Although successful correlations were established between limited amounts of data and laws based on dimensional analysis, it has been shown (Ref 21) that such laws are inadequate when compared to the broad trend of cyclic crack growth data. The direct use of elastic-plastic models to develop crack growth rate laws is not yet firmly established. Hence, the stress-intensity approach provides the most powerful tool presently available for the evaluation and correlation of cyclic crack growth rates.

After looking at a broad trend of data, Paris (Ref 20) concluded that plane-stress crack growth rates could be adequately represented for sinusoidally loaded metal specimens by the expression

$$da/dN = C \Delta K^n$$

where

C is a coefficient that incorporates the effects of material properties, mean load, frequency, environment, etc.;

K is the value of $(K_{max} - K_{min})$ during a typical loading cycle.

A value of $n = 4$ was found to be in agreement with test results obtained from a number of materials (steel, aluminum, titanium, and molybdenum).

A value of C has been estimated by Krafft (Ref 35), who has proposed the crack growth rate formula

$$\frac{da}{dN} = \frac{16 \times 10^6}{7 E^3 K_{Ic}^2} \frac{f(\gamma)}{n} K_{max}^4 \quad (11)$$

where E is the Young's modulus of the material, n is the tensile strain that can be applied before plastic instability ensues, K_{max} is the maximum value

of K during the loading sequence, $\gamma = (K_{\max} - K_{\min})/K_{\max}$ where K_{\min} is the minimum value of K during the loading sequence, and

$$f(\gamma) = \left[1 - (1 - \gamma)^2 \right] \left[1 + \gamma \right]^4$$

Forman, et al. (Ref 36) compared the Paris law with an even larger range of data and found that the law did not predict the observed behavior of crack growth rates tending to increase rapidly toward an instability as the maximum applied stress intensity approaches the fracture toughness of the material. Forman then modified the Paris law to take into account the instability and to explicitly express the effect of load ratio, $R = \frac{K_{\min}}{K_{\max}}$. Forman's expression is

$$\frac{da}{dN} = \frac{C (\Delta K)^n}{(1 - R) K_c - \Delta K} \quad (12)$$

where:

C is a coefficient that incorporates the effects of material properties, frequency environment, etc.;

K_c is the plane stress fracture toughness of the material;

R and ΔK are as previously defined.

The experimental determination of flaw growth rate data for surface or embedded flaws is more complex than for through-the-thickness cracks. A surface flaw grows along its entire periphery and continually changes, not only in size but also in shape. Furthermore, the inaccessibility of the flaw prevents direct visual measurements of the flaw shape and size during the test.

A method of determining plane-strain flaw growth rates from the testing of surface-flawed specimens has been developed by Tiffany, et al. (Ref 37). Tiffany noted that the cyclic life of any specimen in which the flaw was growing under conditions of plane-strain at a constant maximum cyclic stress was primarily a function of the maximum initial stress intensity applied to the specimen at the beginning of the test. Accordingly, cyclic flaw growth

data for a given material, environment, and load ratio was represented by a single curve on a plot of K_{I1} versus cycles to failure (K_{I1} versus N).

Flaw growth rates were computed on the basis of the slopes of the K_{I1} versus N curve. Although Tiffany presents flaw growth rates graphically, the rates could be expressed by an equation of the form

$$\frac{d(\text{flaw size})}{dn} = \frac{C \left(\frac{\sigma}{\sigma_o}\right)^2 (K_{\max})^n}{\left[1 - \frac{K_{\max}}{K_{Ic}}\right]^m} \quad (13)$$

where:

- σ_o is an arbitrarily chosen stress level used to evaluate C ;
- C is a constant depending on material properties, load ratio environment, and σ_o .

In the absence of data showing the inverse square root stress effect of Equation 13 over a wide range of maximum stress levels, the equation should be considered valid only for the stress range levels used to generate a particular K_{I1} versus N curve.

In a recent experimental work Hall (Ref 38) derived an expression to represent cyclic life and flaw-growth-rate data obtained for 2014-T62 aluminum and 6Al-4V(ELI) titanium. An equation of the form

$$d(a/Q)/dN = C \left(\sigma_o/\sigma\right)^2 (1 + \lambda)^m (\Delta K)^n \left(1 - K_{\max}/K_{Ic}\right)^{-p} \quad (14)$$

was chosen where:

- C = a constant for a particular material-environment combination;
- σ = peak cyclic stress level;
- σ_o = an arbitrarily chosen peak cyclic stress level for which the value of C is derived;
- K_{\max} = peak stress intensity at the tip of the flaw during the loading cycle;

K_{\min} = minimum stress intensity corresponding to K_{\max} ;

$$\Delta K = (K_{\max} - K_{\min});$$

$$\lambda = K_{\min} / \Delta K;$$

m, n, p = exponents to be experimentally evaluated.

In Equation 14, C represents the effect of material properties, environmental conditions, and minor variables (such as frequency) on flaw-growth rate. Lambda (λ) is a modified value of the Roberts and Erdogan β (Ref 39), that accounts for the effect of mean-applied K during the loading cycle;

$\lambda = 0$ for a zero-to-tension loading cycle and 1.0 for a half-tension-to-tension loading cycle. The $(\Delta K)^n$ term expresses the dominating effect of stress intensity range in the manner originally suggested by Paris (Ref 21). Flaw-growth rates rapidly increase as K_{\max} approaches K_{Ic} , and the $(1 - K_{\max}/K_{Ic})^{-p}$ term was included to account for this observed behavior. Finally, the stress ratio $(\sigma_o/\sigma)^2$ was used to express the experimental result that the cyclic life data for specimens cycled to failure at different elastic peak cyclic stress levels can be represented by a unique K_{I1}/K_{Ic} - or K_{I1} -versus-cycles-to-failure curve. This result implies that flaw-growth rates are inversely proportional to the square of the peak cyclic stress (Ref 37). Although no systematic investigation of the stress level dependence of plane-strain flaw-growth rates has been undertaken over large ranges of peak cyclic stress, the data herein and in References 19, 37, and 40 show that it is experimentally justified to consider flaw-growth rates to be stress-level dependent for the ranges of peak cyclic stress normally encountered in spacecraft pressure vessels. Further experimental work in this area seems likely to provide added measure of confidence in experimental test data generated utilizing preflawed specimens in conjunction with basic principles of applied fracture mechanics.

3.0 EXPERIMENTAL PROCEDURE

Experimental work intended to establish compatibility of several candidate materials in given environments may be divided into two distinct phases: Phase I - qualitative screening tests intended to reveal inherent weaknesses or critical areas for a given material-environment combination; and Phase II -- quantitative fracture toughness tests aiming to provide test data usable in actual design for establishing conditions for initial and in-service inspection criteria, functional testing, and assurance of structural integrity under service conditions.

Qualitative screening tests used in this program are suitable for evaluation of numerous variables, such as liquid or vapor state of the environmental fluids; pressure, temperature, and stress levels; base metal and weldment areas; and even different regions of the weldments such as weld center, fusion zone, or heat-affected zones. Test data generated during screening test indicates relative severity of the many variables affecting the behavior of engineering materials. The primary purpose of the screening test is to cover as many variables as possible and to ensure that none of the critical parameters escape detection.

Once the qualitative screening tests are completed, the Phase II testing is then started to determine more specific information such as basic fracture toughness, sustained or cyclic flaw growth characteristics, and applicable threshold stress intensity levels. The number of specimens which should be tested depends largely on the intended service requirements of the structural components. The level of experimentation in the present program may be considered to be typical for initial indication of service capability for a highly stressed flight component with relatively short mission time. The key features of the experimental approach applicable to Phase I as well as Phase II testing are summarized in the following sections.

3.1 Phase I -- Qualitative Screening Test

The main feature is the experimental approach used for the screening test is the simultaneous testing of several sets of precracked specimens in the completely enclosed, pressurized, and heated (or cooled) test retort (pressure

cooker) schematically illustrated in Figure 12. Several such retorts, if used simultaneously, would permit variation in temperature and pressure for liquid as well as vapor phases of the environmental fluid or introduction of several fluids for a given temperature-pressure combination. The test specimens of either surface-flawed-bend (SFB) or double-cantilever-beam (DCB) type are preloaded and placed in liquid and vapor regions of the retort and then exposed to the environment for a predetermined period of time. Environmental test systems for the N_2O_4 , F_2 , and ClF_3 propellants are schematically illustrated in Figures 13, 14, and 15, respectively.

3.1.1 Surface-Flawed-Bend (SFB) Specimens

A typical prestressed bend specimen assembly is shown in Figure 16. Each weld bend specimen contains three surface flaws (depicted as A, B, and C in Figure 16). Flaw A is located on the weld fusion line, parallel to the weld bead. The centerline of the weld bead is shifted by an angle θ away from the specimen transverse axis so that each region of the weldment is exposed to the maximum bend stress. (Use of a four-point bending specimen load would eliminate the necessity for doing this.) Flaw B is on the weld centerline and parallel to the axis. Flaw C traverses the fusion line and is oriented parallel to the specimen axis. Each bend specimen assembly is composed of two specimens, one of which is narrower than the other, so that when the specimens are prestressed by tightening bolts to a predetermined displacement, high and low stress levels are generated. The applied stress intensity levels are calculated by using Equation 9 of the Smith's analysis for SFB specimens. Configuration of the selected SFB specimen types and their dimensions are listed in Figures 17 through 22.

Preloading of the SFB specimens is illustrated in Figure 23 for the three-point bend and in Figure 24 for the four-point bend. Each specimen assembly is preloaded to produce outer fiber stresses in the narrowest (high-stress) specimen equal to the yield strength of the material. The load level is established by loading dummy SFB specimens (no surface cracks) past the yield strength of the material at the outer layers. Typical load versus

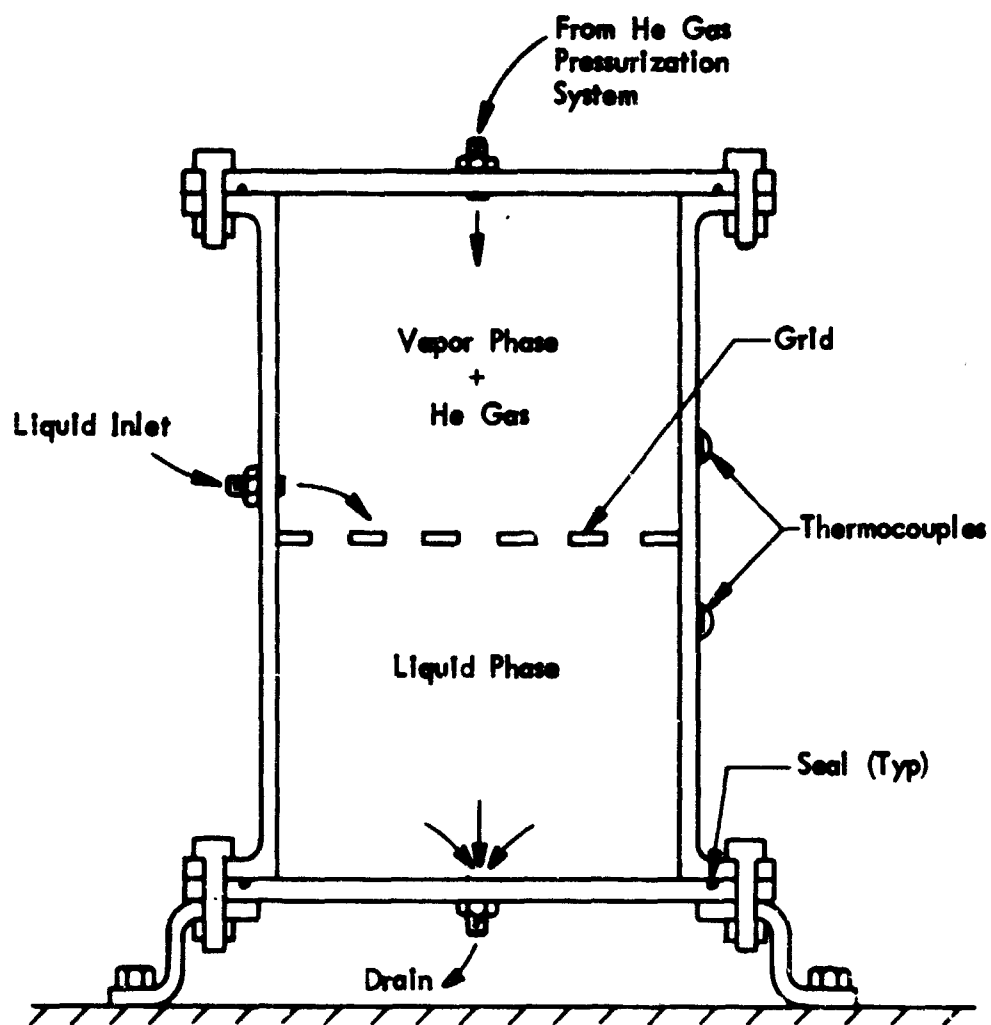


Figure 12: SCREENING TEST RETORT

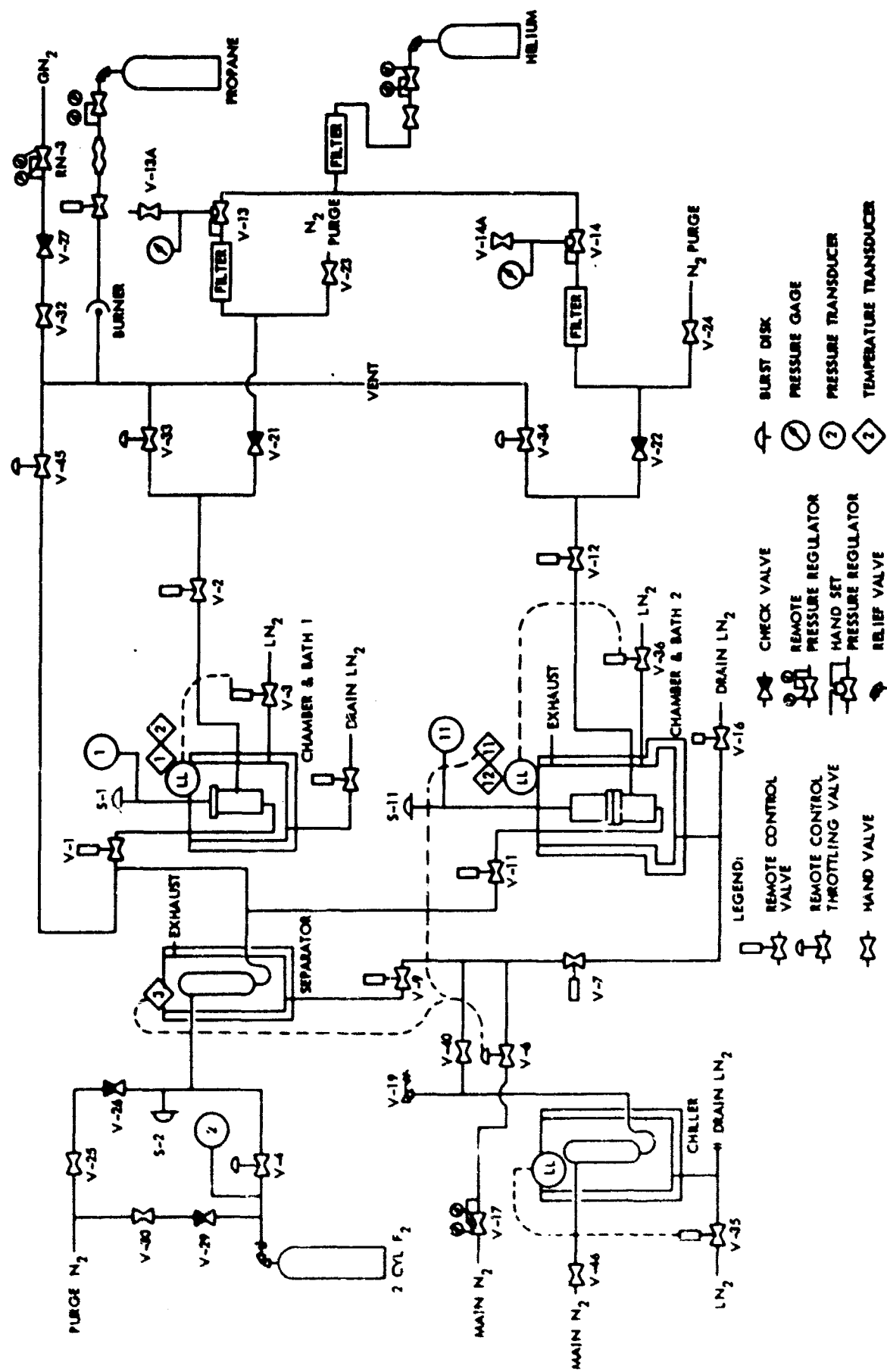


Figure 14: SCHEMATIC DIAGRAM OF THE F2 PRESSURIZATION SYSTEM

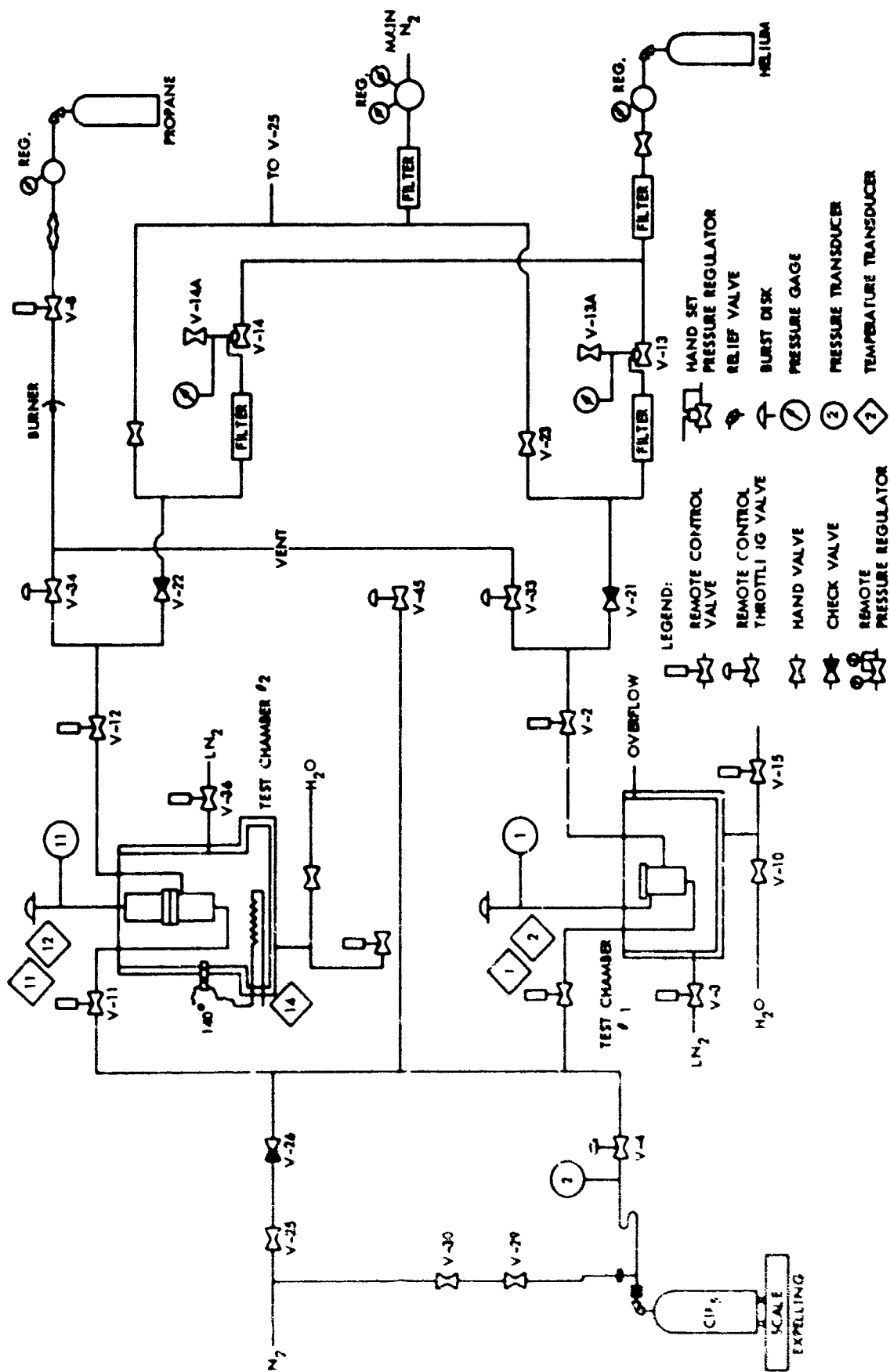


Figure 15: SCHEMATIC DIAGRAM OF THE CIF5 PRESSURIZATION SYSTEM

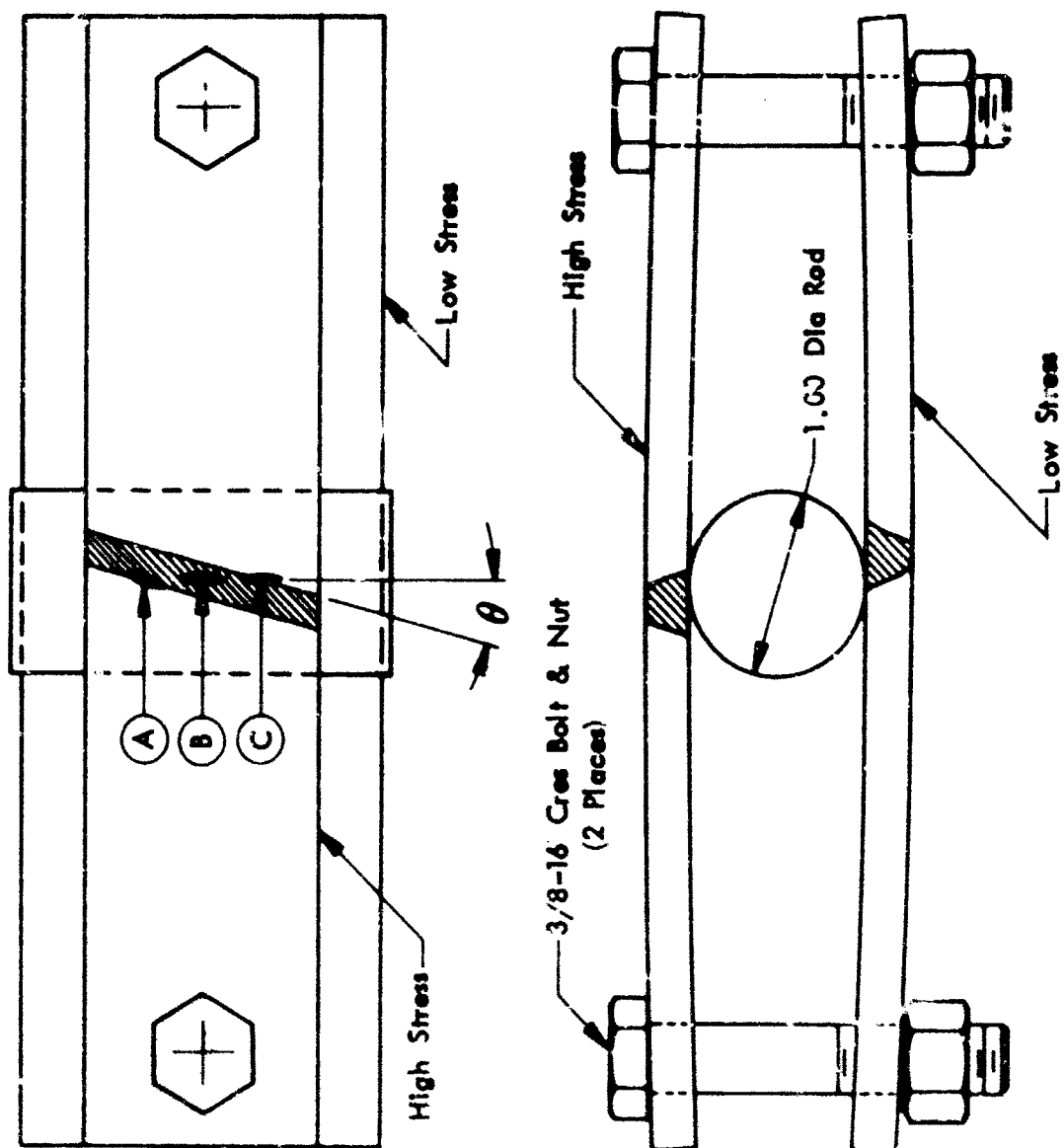
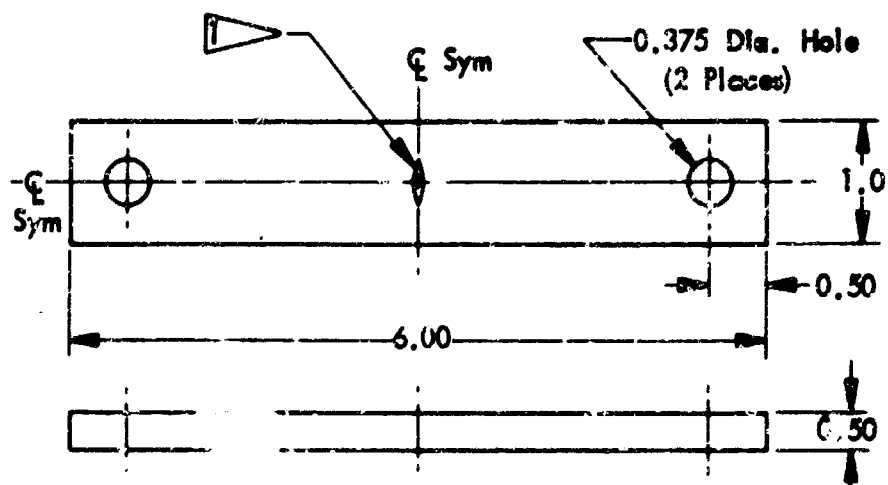


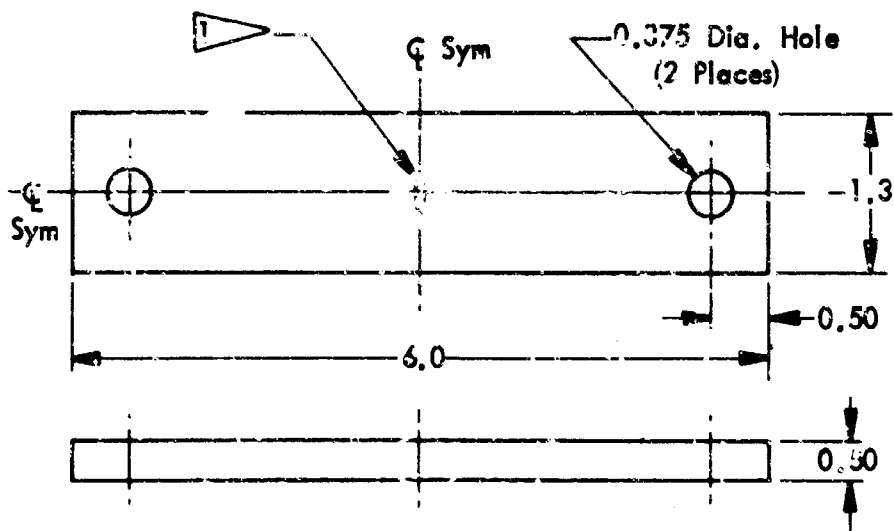
Figure 16: TYPICAL BEND SPECIMEN ASSEMBLY FOR PHASE I TESTING



All Dimensions are in Inches

1 Surface Flaw Made by Using Sharp (.001 radius) EDM Cutter

(HIGH STRESS)

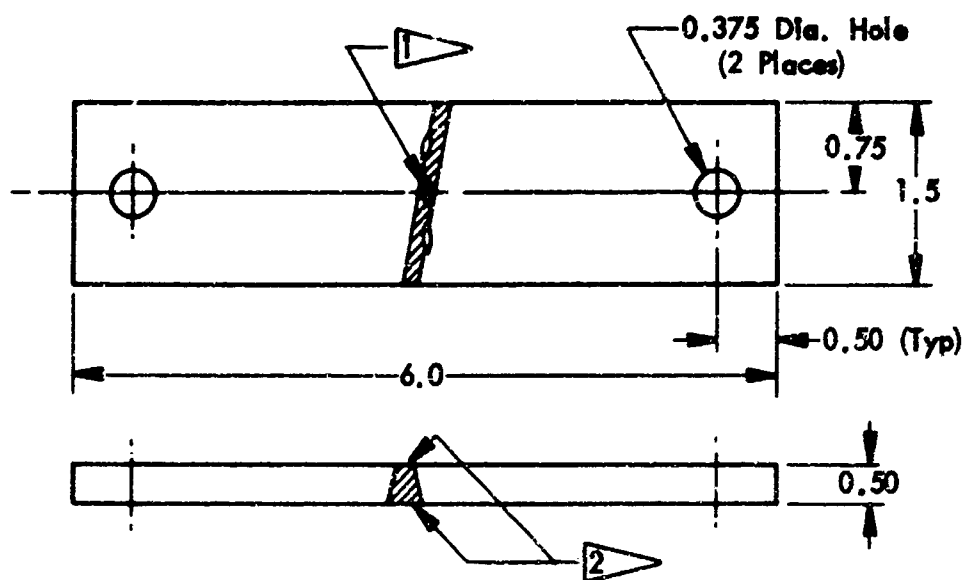


All Dimensions are in Inches

1 Surface Flaw Made by Using Sharp (.001 radius) EDM Cutter

(LOW STRESS)

Figure 17: 2219-T81 BASE METAL BEND SPECIMEN

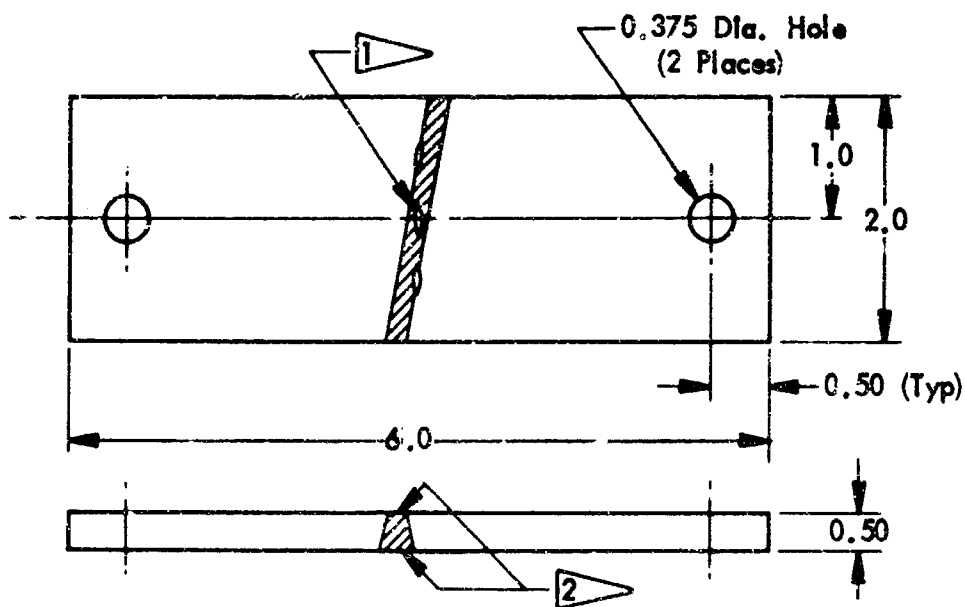


All Dimensions are in Inches

1 Surface Flaw Made by Using Sharp (.001 radius) EDM Cutter
(3 places as shown)

2 Weld Bead to be Removed Flush with the Base Metal

(HIGH STRESS)



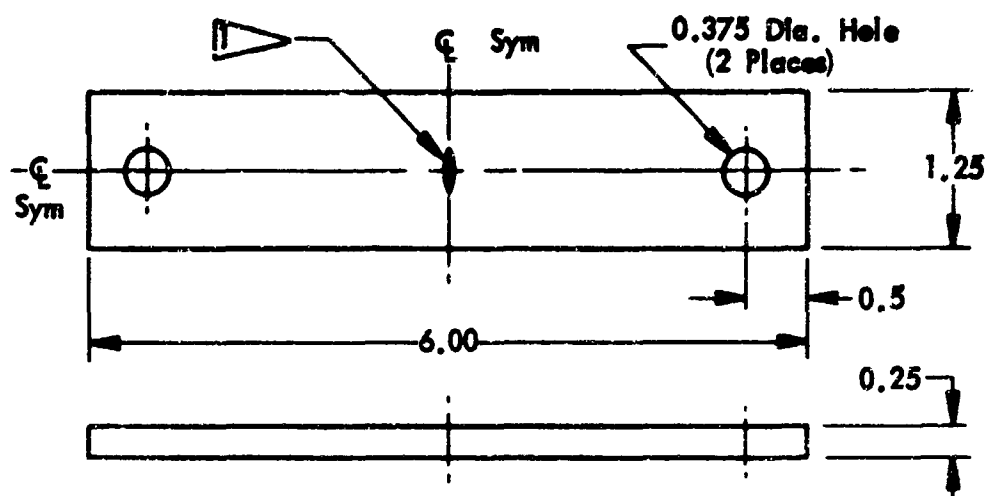
All Dimensions are in Inches

1 Surface Flaw Made by Using Sharp (.001 radius) EDM Cutter
(3 places as shown)

2 Weld Bead to be Removed Flush with the Base Metal

(LOW STRESS)

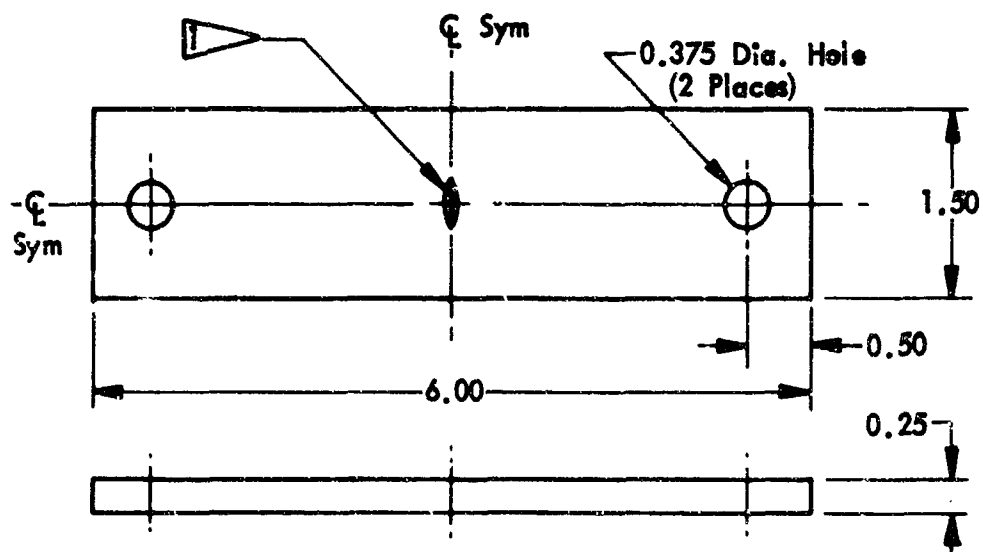
Figure 18: 2219-T81 AS-WELDED BEND SPECIMEN



All Dimensions are in Inches

1 Surface flaw made by sharp (.001 Radius) EDM cutter.

(High Stress)

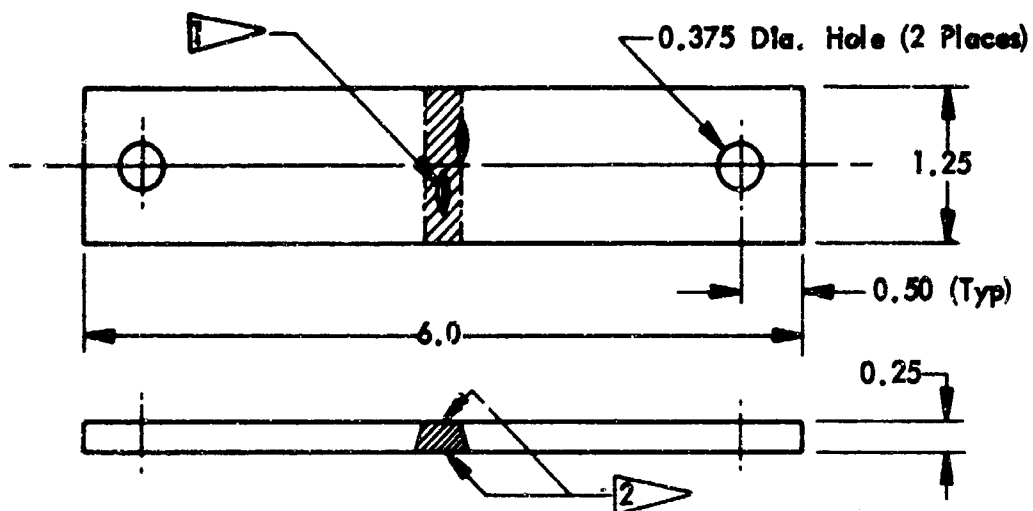


All dimensions are in Inches

1 Surface flaw made by sharp (.001 Radius) EDM cutter.

(Low Stress)

Figure 19: 2021-T81 ALUMINUM BASE METAL BEND SPECIMEN

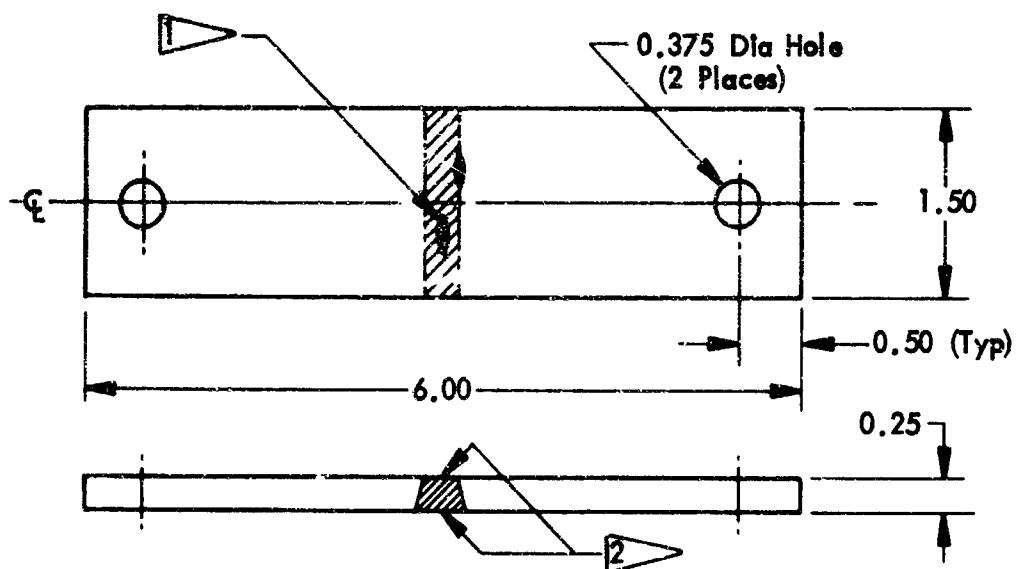


All dimensions are in inches

1 Surface Flaw made by using sharp (.001 Radius) EDM cutter.
(2 Places as Shown)

2 Weld Bead to be Removed Flush with Base Metal

(High Stress)



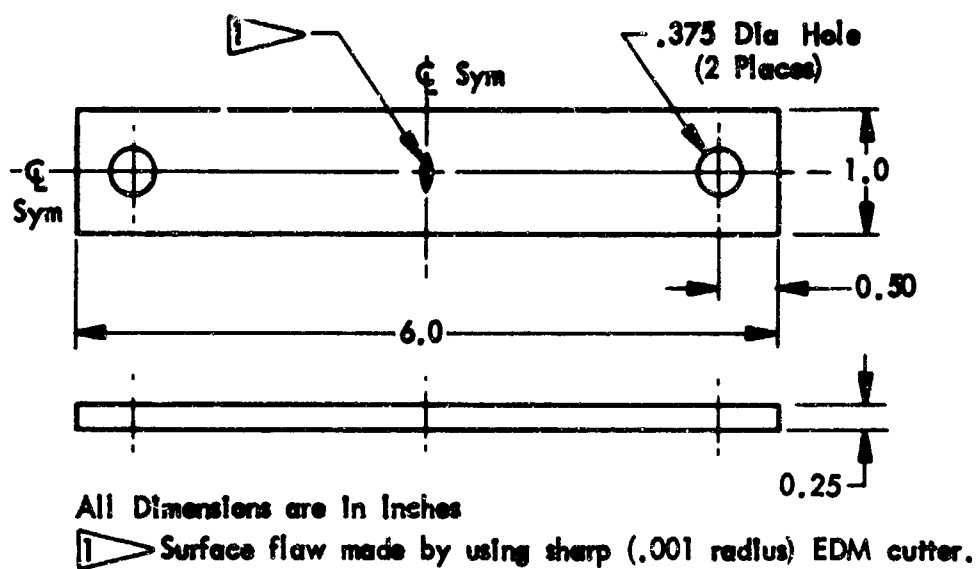
All Dimensions are in inches

1 Surface flaw made by using sharp (.001 Radius) EDM cutter
(2 places as shown)

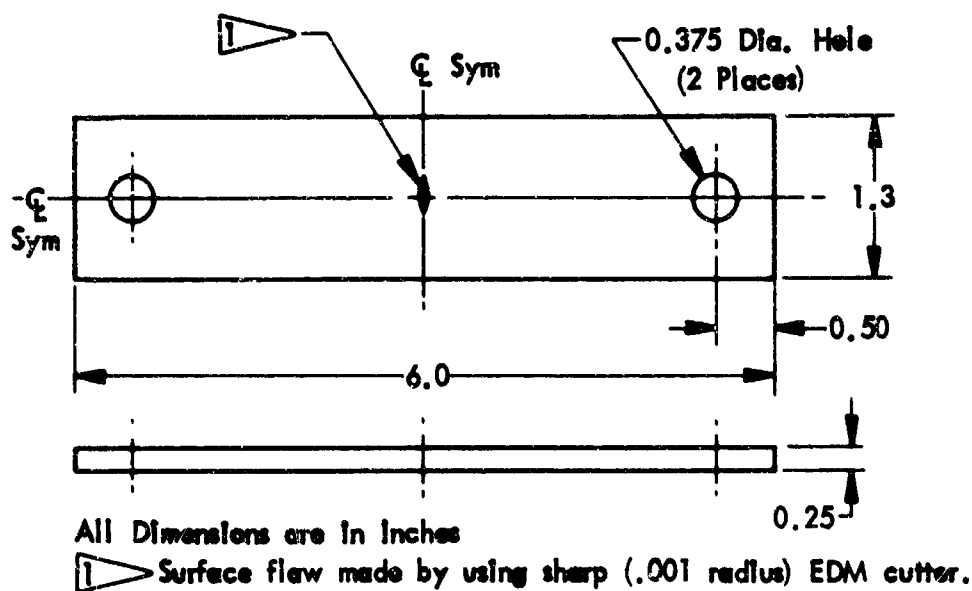
2 Weld Bead to be Removed Flush with Base Metal

(Low Stress)

Figure 20: 2021-T81 ALUMINUM WELD METAL BEND SPECIMEN

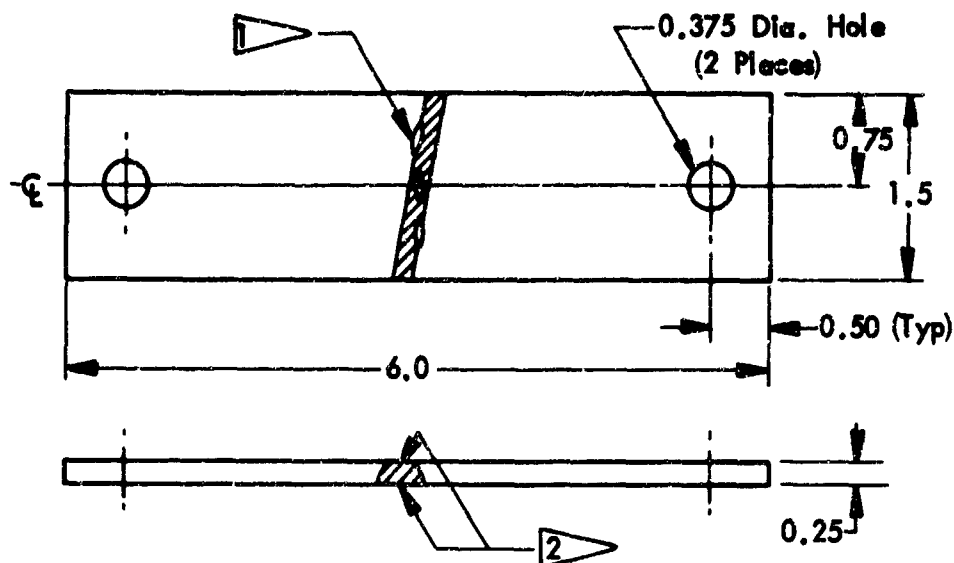


(HIGH STRESS)



(LOW STRESS)

Figure 21: 6Al-4V BASE METAL TITANIUM BEND SPECIMEN

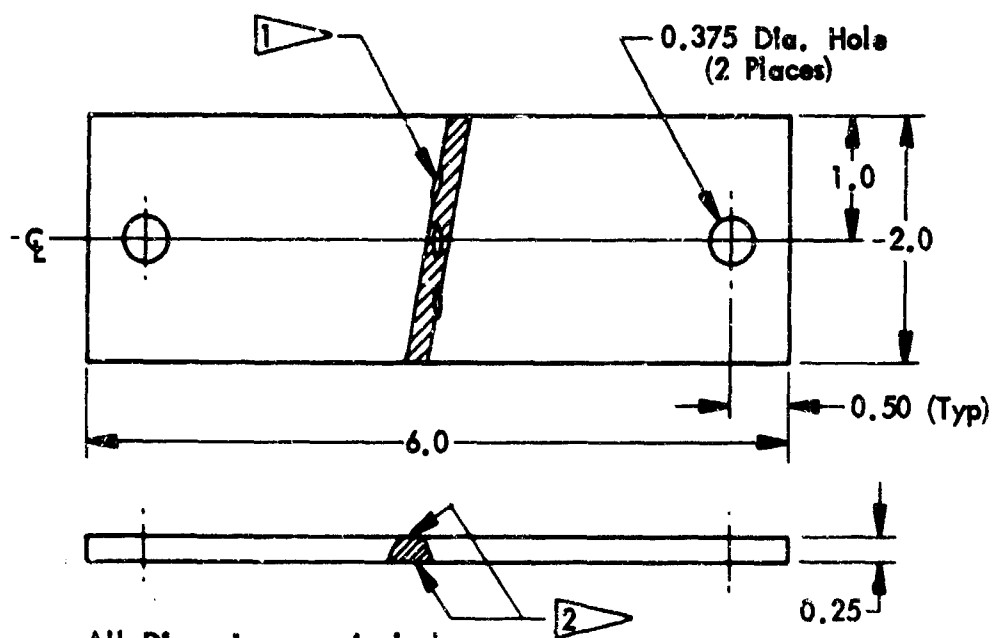


All Dimensions are In Inches

1 Surface Flaw Made by Using Sharp (.001 radius) EDM Cutter
(3 Places As Shown)

2 Weld Bead to be Removed Flush with the Base Metal

(HIGH STRESS)



All Dimensions are In Inches

1 Surface Flaw Made by Using Sharp (.001 radius) EDM Cutter
(3 Places as Shown)

2 Weld Bead to be Removed Flush with the Base Metal

(LOW STRESS)

Figure 22: 6Al-4V WELD METAL TITANIUM BEND SPECIMEN

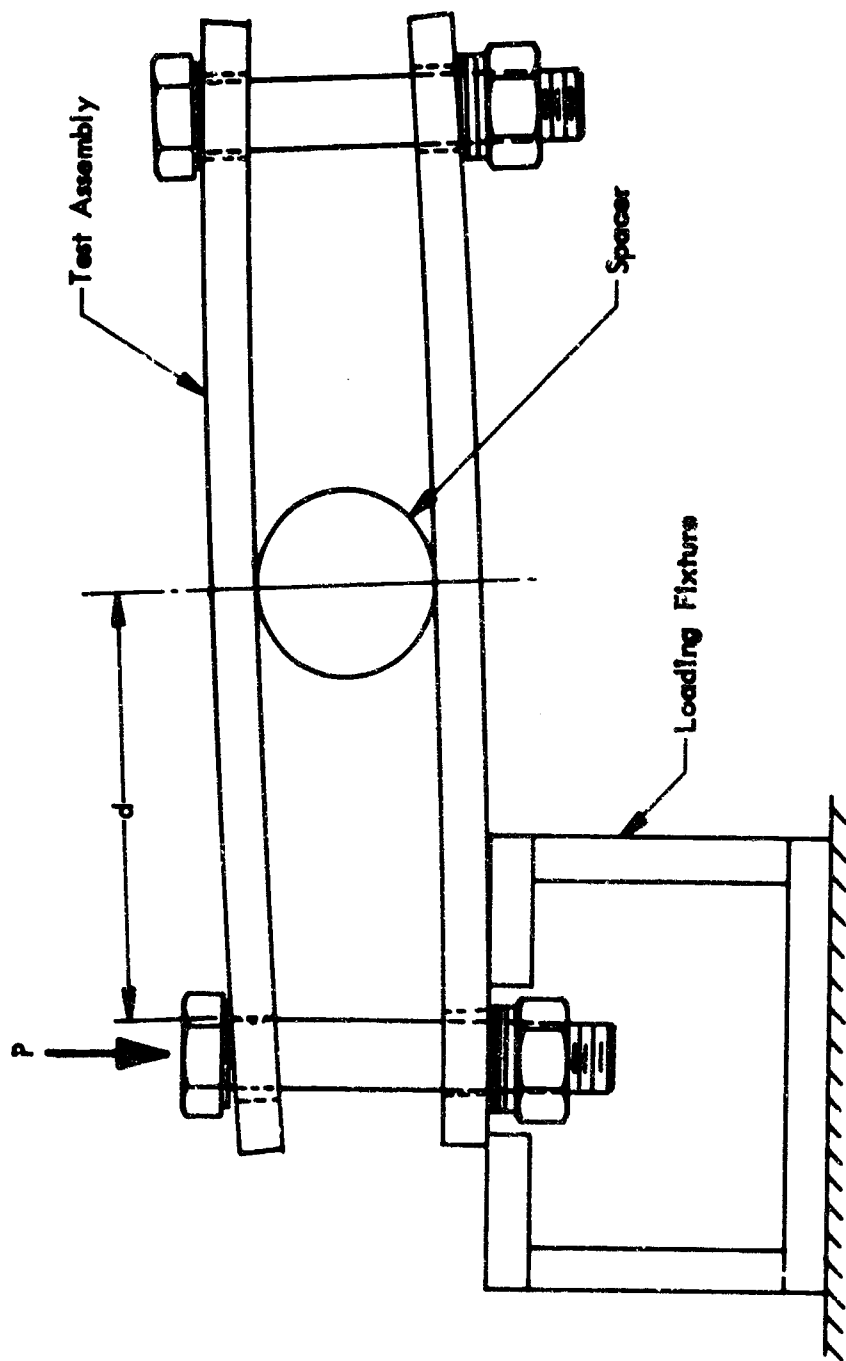


Figure 23: SFB SPECIMEN ASSEMBLY PRELOADING (Three Point Bend)

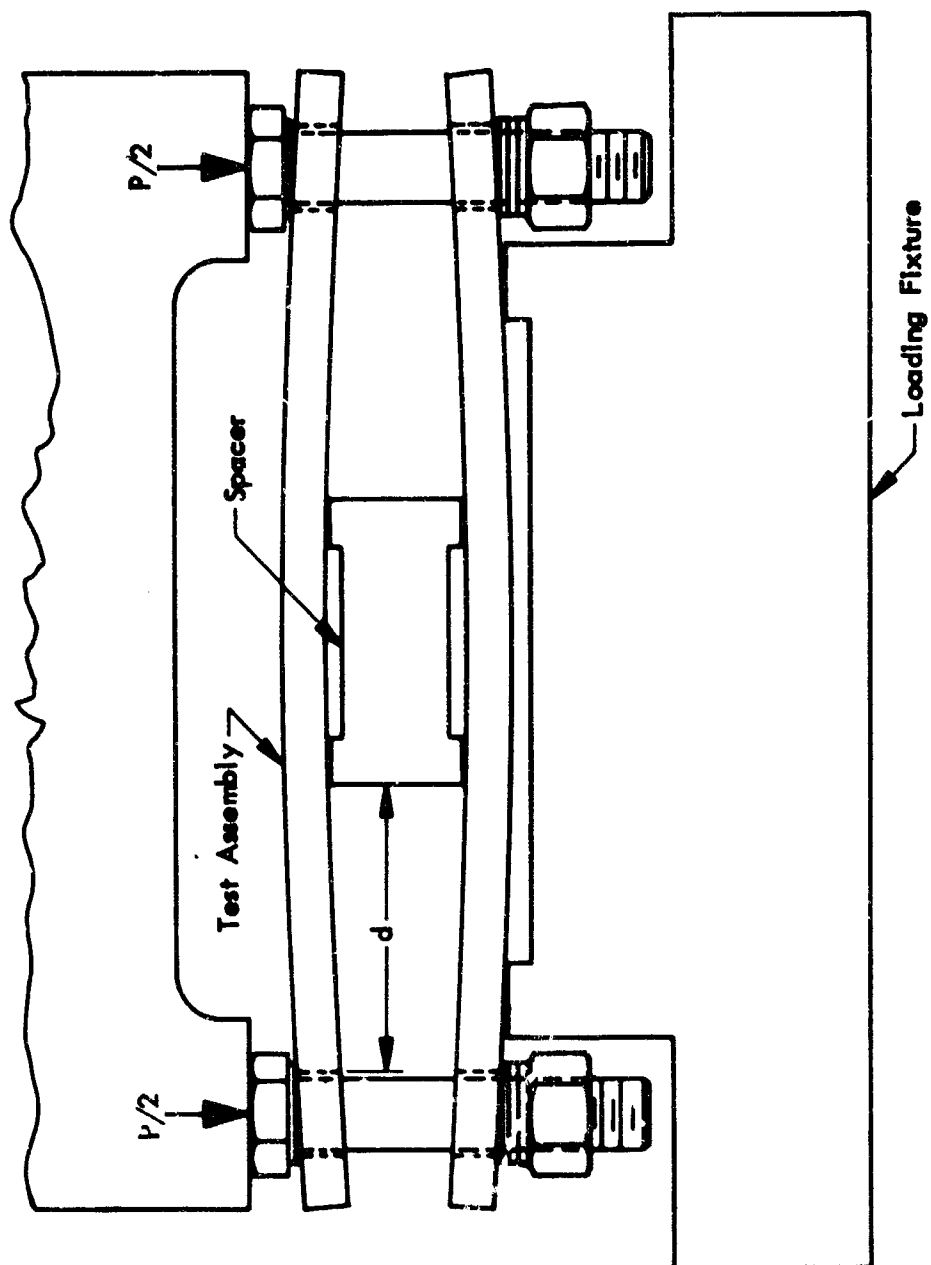


Figure 24: SFB SPECIMEN ASSEMBLY PRELOADING (Four Point Bend)

head travel curves are shown in Figures 25 and 26 for the 2021-T81 aluminum base metal and weldment, respectively.

The preloaded SFB specimen assemblies representing base metal and weldments are then exposed to the environment being evaluated. Upon conclusion of the exposure, the specimen assemblies are unloaded and examined under a wide-field microscope. The specimens are then subjected to cyclic flexing to mark outlines of the surface cracks and fractured in the three-point bend test fixture. The exposed fracture surfaces are subjected to fractographic examination and flaw size measurement. Should there be a failure or crack extension during the test run, the corresponding K_I levels may also be calculated with the aid of postfracture examination, which would indicate approximately the failure/no-failure or growth/no-growth threshold stress intensity level.

3.1.2 Double-Cantilever-Beam (DCB) Specimen

Plain and grooved DCB specimen configurations are shown in Figures 27 and 28, respectively. A typical prestressed DCB specimen tested in this program is shown in Figure 29. The specimen incorporates a constant displacement (load-holding) method by welding a bar across the specimen face to keep specimen jaws in the open (loaded) position. The specimen shown in Figure 29 further uses side grooves to suppress formation of shear lips for a more uniform growth of the crack front. Experimental effort in determining groove shape and depth proceeds along the following lines:

First, a specimen with a tentative groove depth of, say, 10% of the material thickness is subjected to cyclic loading to initiate a sharp fatigue crack, and then to propagate the crack under cyclic loading to a predetermined depth. After crack extension of some 0.1 to 0.3 inch, the specimen is pulled to failure. Examination of the fractured specimen reveals the contour of the crack front propagated under cyclic loading. The extent of the shear lip formed during the static pull to failure is also noted. Tunneling of the crack front as well as a possible formation of the shear lip would indicate excessive "plane stress" influence and would call for deeper side grooves.

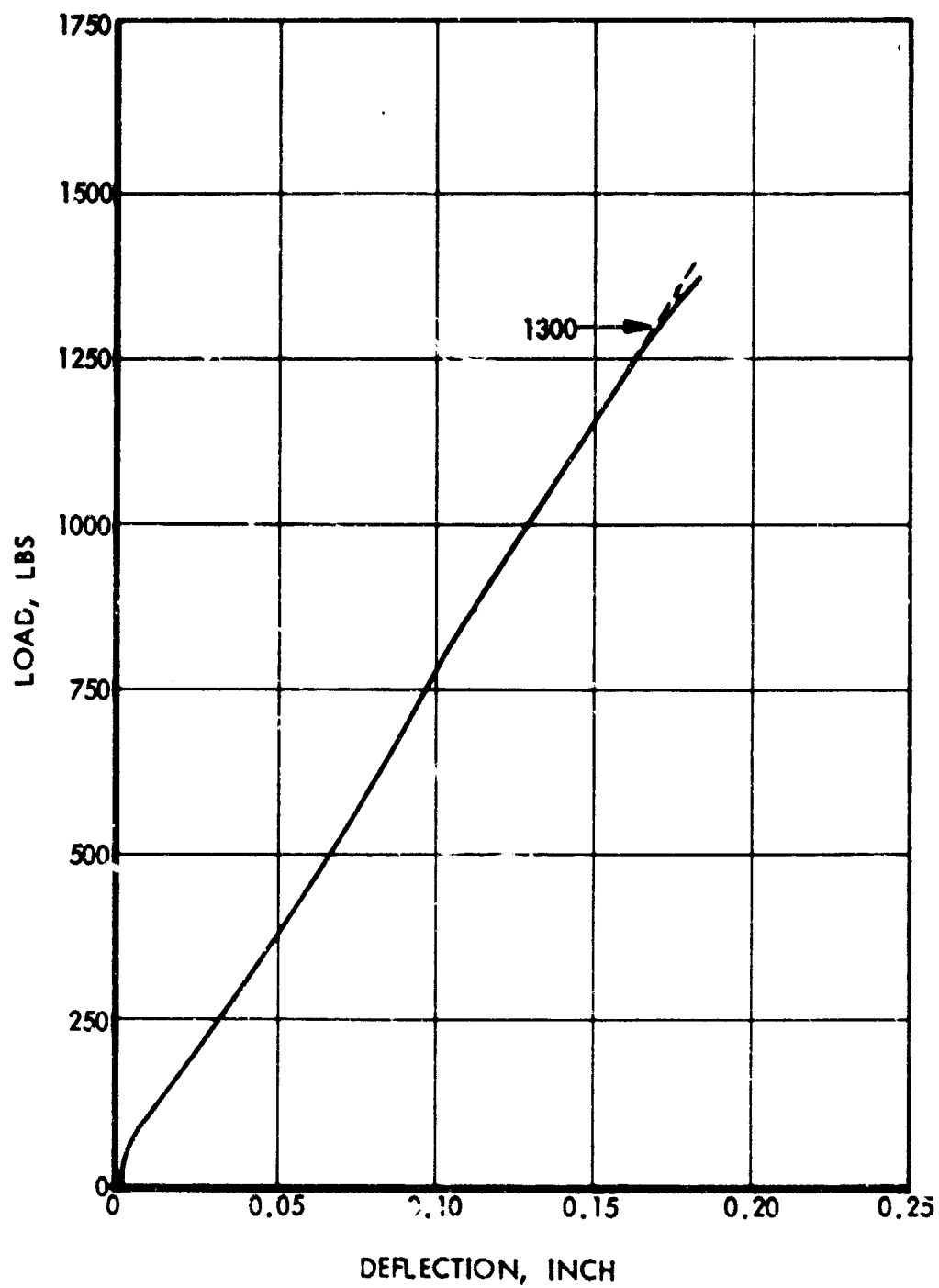


Figure 25: PREL AD CURVE FOR 2021-T81 ALUMINUM (Base Metal)

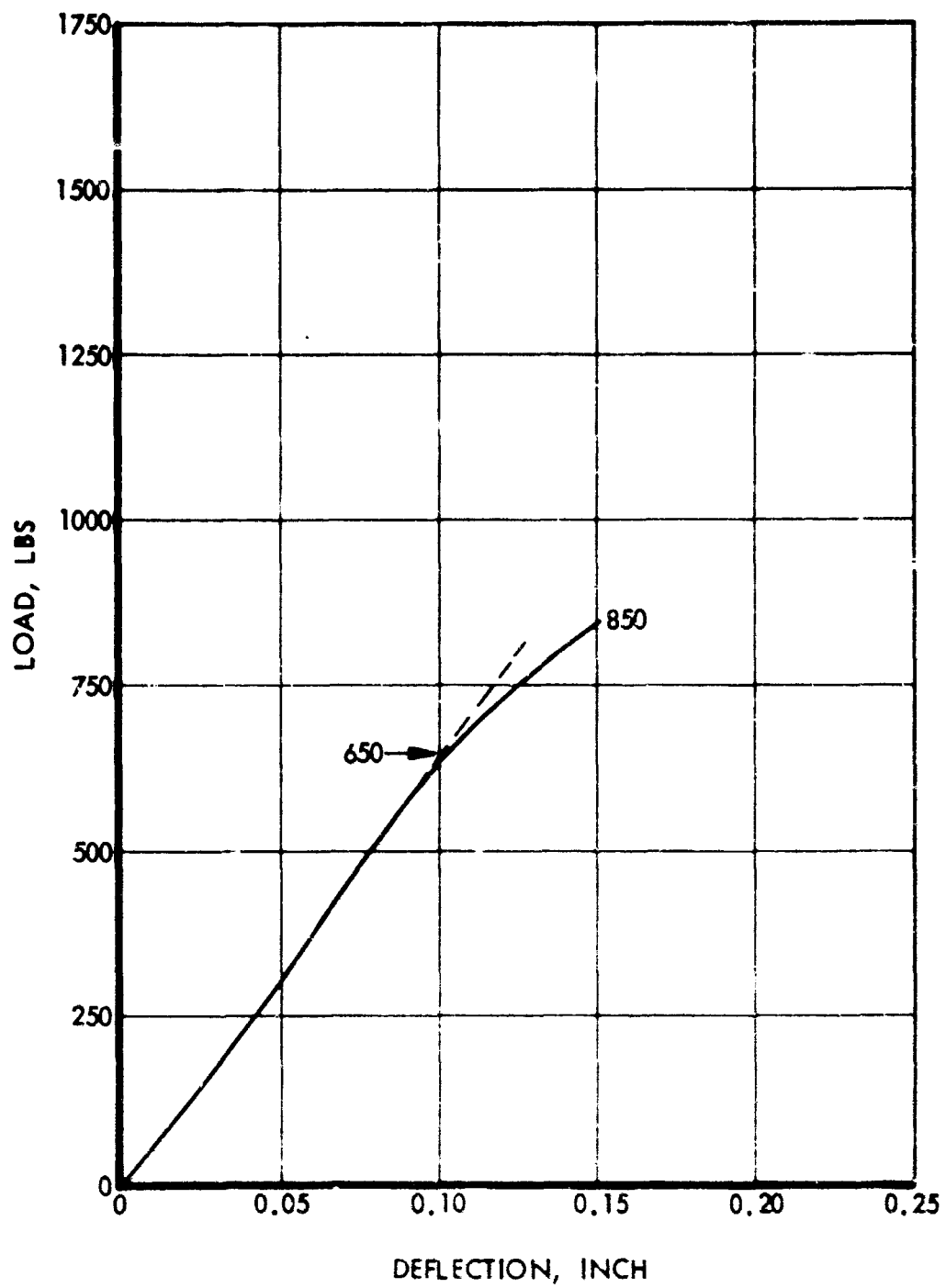


Figure 26: PRELOAD CURVE FOR 2021-T81 ALUMINUM (Weldment)

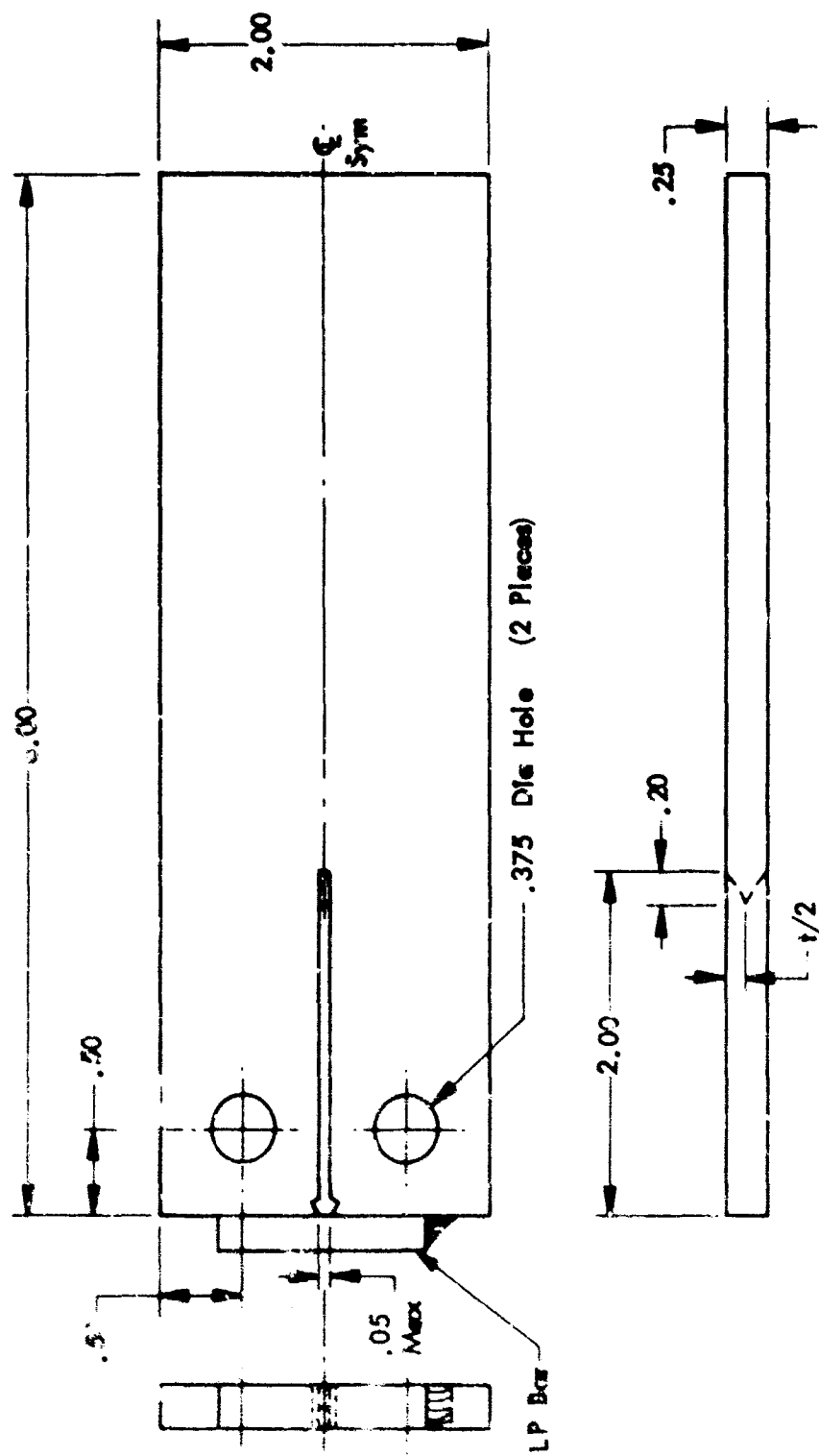


Figure 27: PLAIN DOUBLE CANTILEVER BEAM SPECIMEN

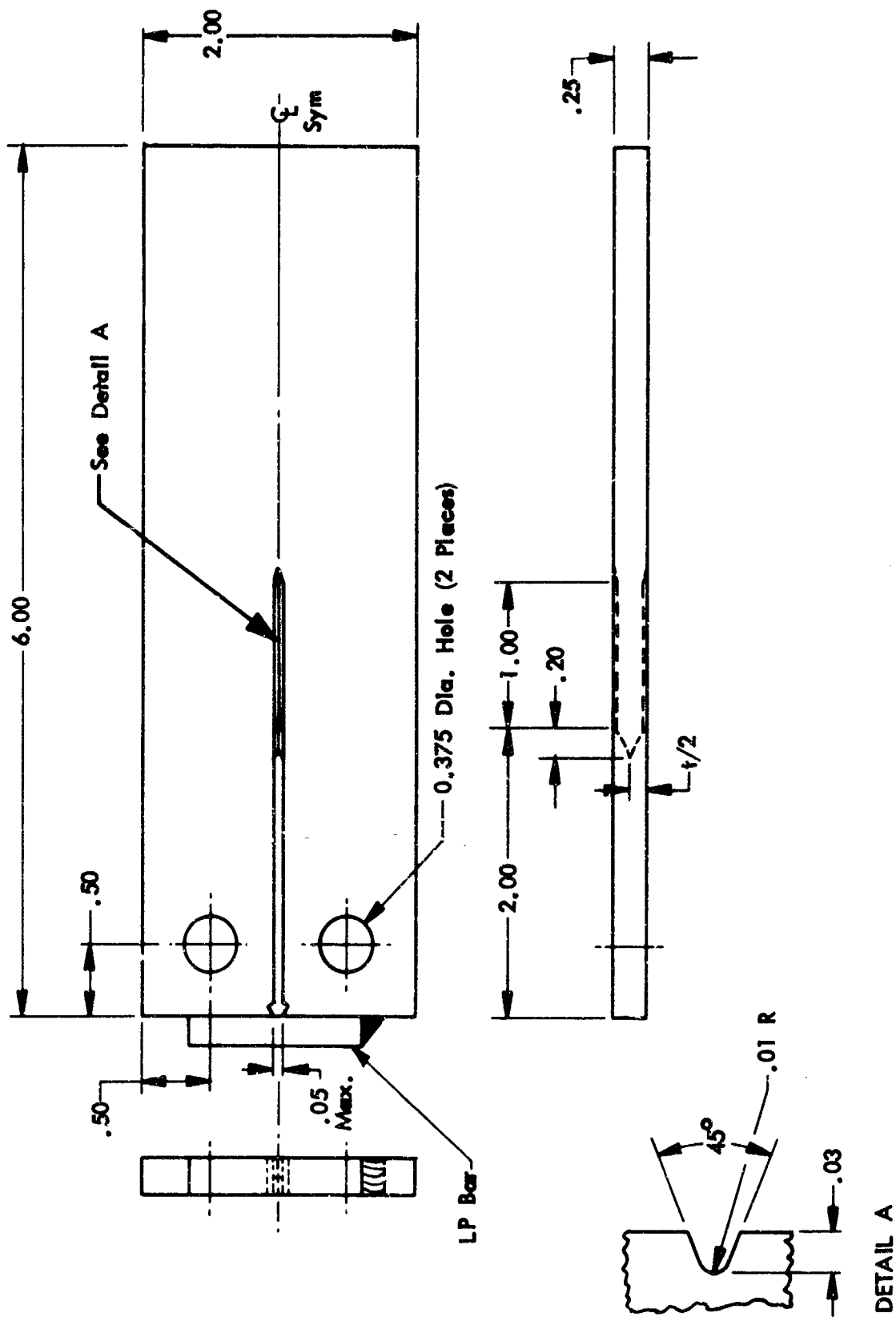


Figure 28: GROOVED DOUBLE CANTILEVER BEAM SPECIMEN

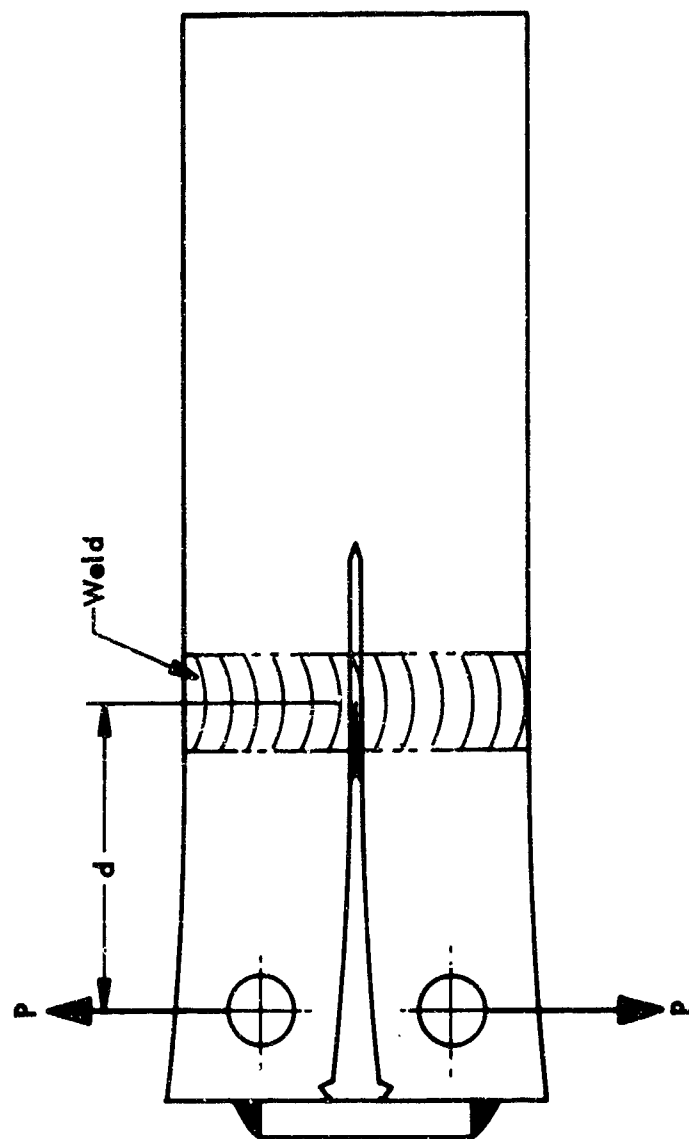


Figure 29: PRESTRESSED DCB SPECIMEN

If it should happen that the crack front in specimens with deeper grooves advanced more rapidly along the side grooves rather than at the midsection of the crack, then the groove is too deep. Some compromise between the two conditions is established so that the propagating crack front is as uniform as possible.

The required load level for DCB specimens is established by determining a compliance curve similar to the one shown in Figure 30. The load level is gradually applied in increments of 1,000 pounds. Each time, as soon as a given load level is reached, the loading is stopped for 1 minute, and a displacement mark is made on the chart to check whether the crack opening displacement continued to increase at a given load level. The process is repeated until specimen fractures or the separation of displacement points becomes noticeable. The specimens are then preloaded to a level somewhat lower than the point depicting departure from linearity or actual fracture.

3.2 Phase II -- Quantitative Crack Growth Test

Unlike Phase I testing, from which only a qualitative type of data could be derived, Phase II testing is designed to furnish test data directly applicable in engineering design. Precracked surface-flawed tensile (SFT) specimens were used for these types of tests. Configuration of a typical surface flaw is shown in Figure 31. Surface flawed specimens for 2219-T81 aluminum weldments, 6Al-4V(ELI) titanium weldments, 2021-T81 aluminum base metal and weldments, and 410(MOD) stainless steel weldments are shown in Figures 32 through 36. Configuration of the weld joints for 2219-T81 aluminum, 6Al-4V(ELI) titanium, and 2021-T81 aluminum are shown in Figures 37, 38, and 39, respectively. Environmental test systems for the N_2O_4 , F_2 , and ClF_3 propellants contained the same essential characteristics illustrated in Figures 13, 14, and 15 except that only one specimen was tested at any one time.

The generated test data is expressed in terms of threshold stress-intensity levels, which may be used for establishing defect acceptance criteria, proof and functional test requirements, and definition of minimum

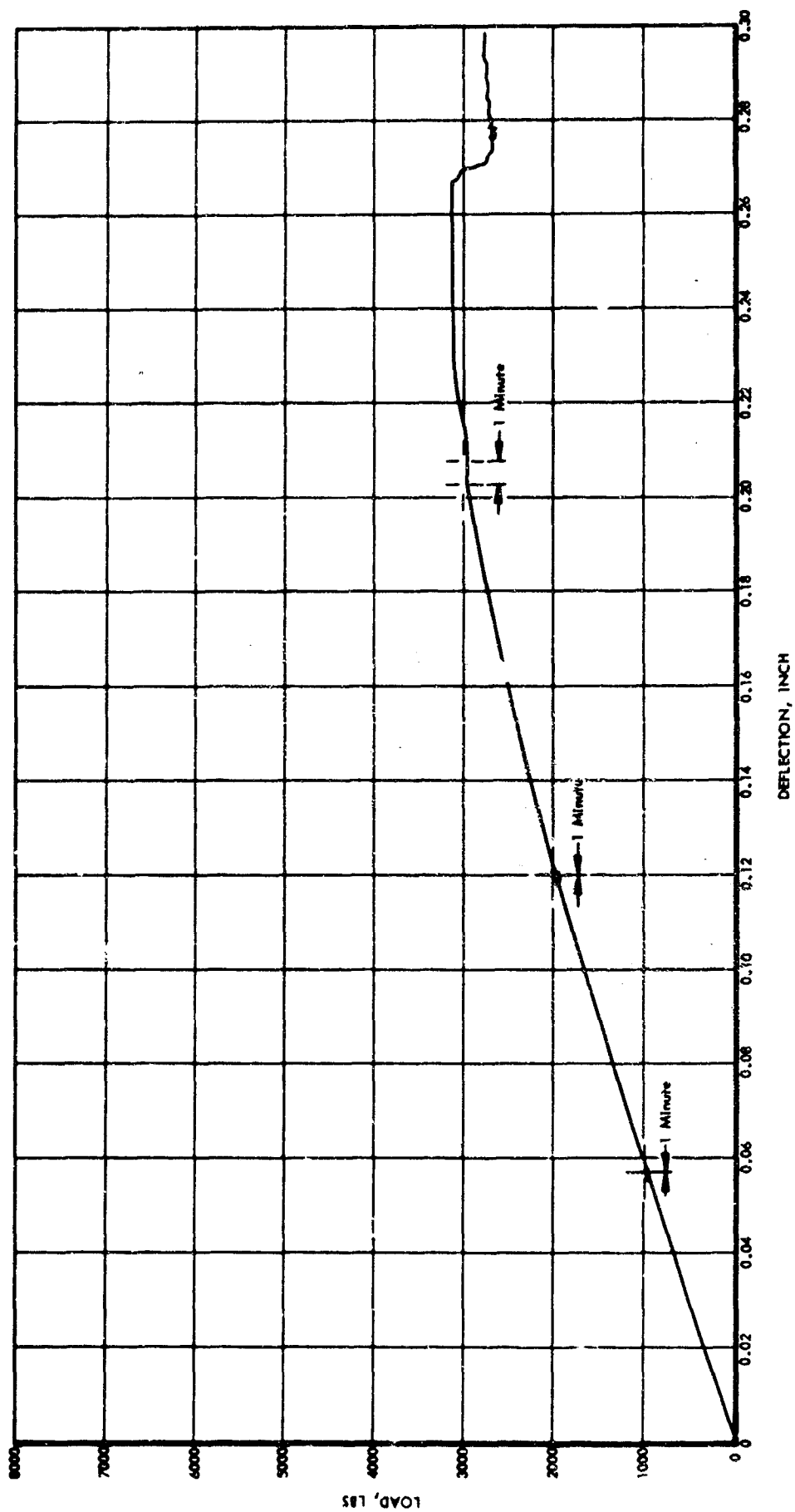
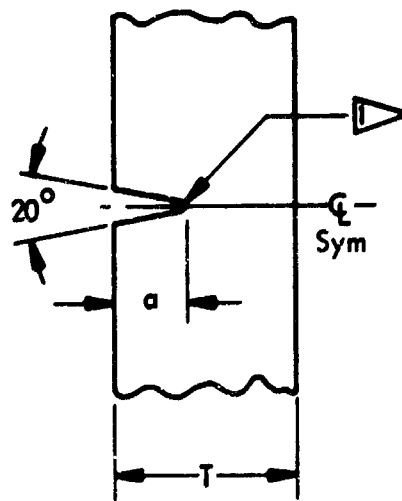
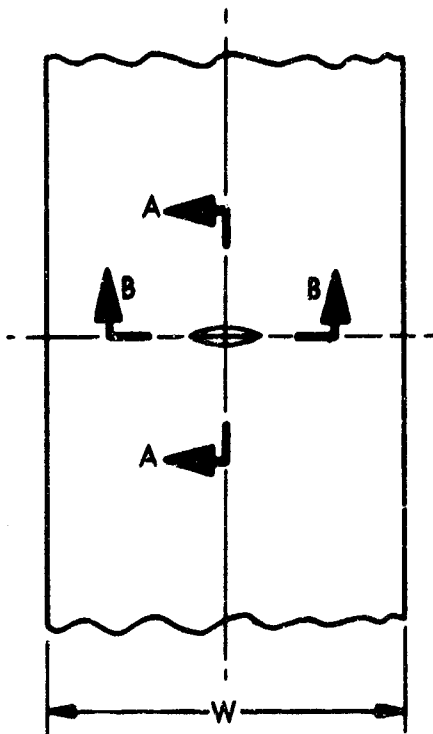
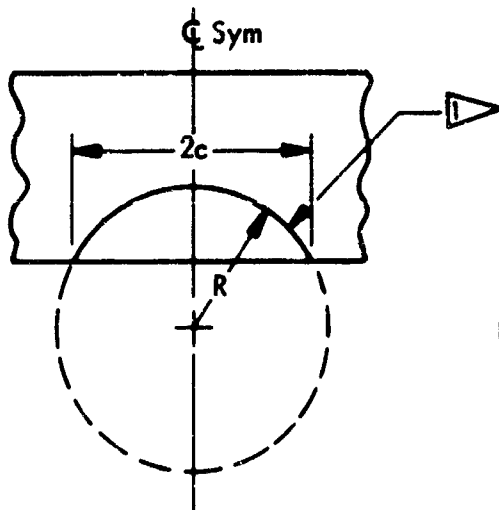


Figure 30: LOAD COMPLIANCE CURVE FOR 6Al-4V (ELI)
TITANIUM DCB SPECIMEN



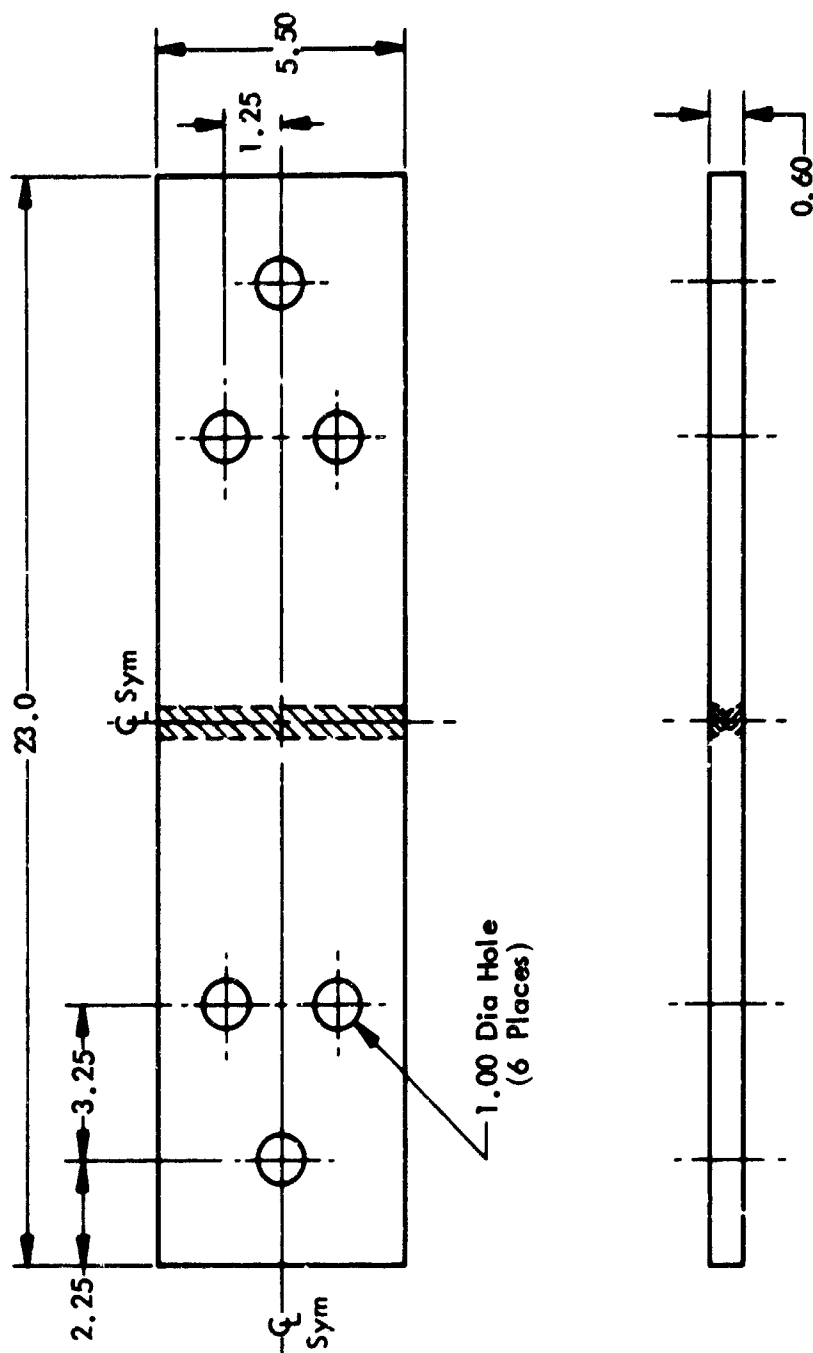
SECTION A-A
(Enlarged)



SECTION B-B
(Enlarged)

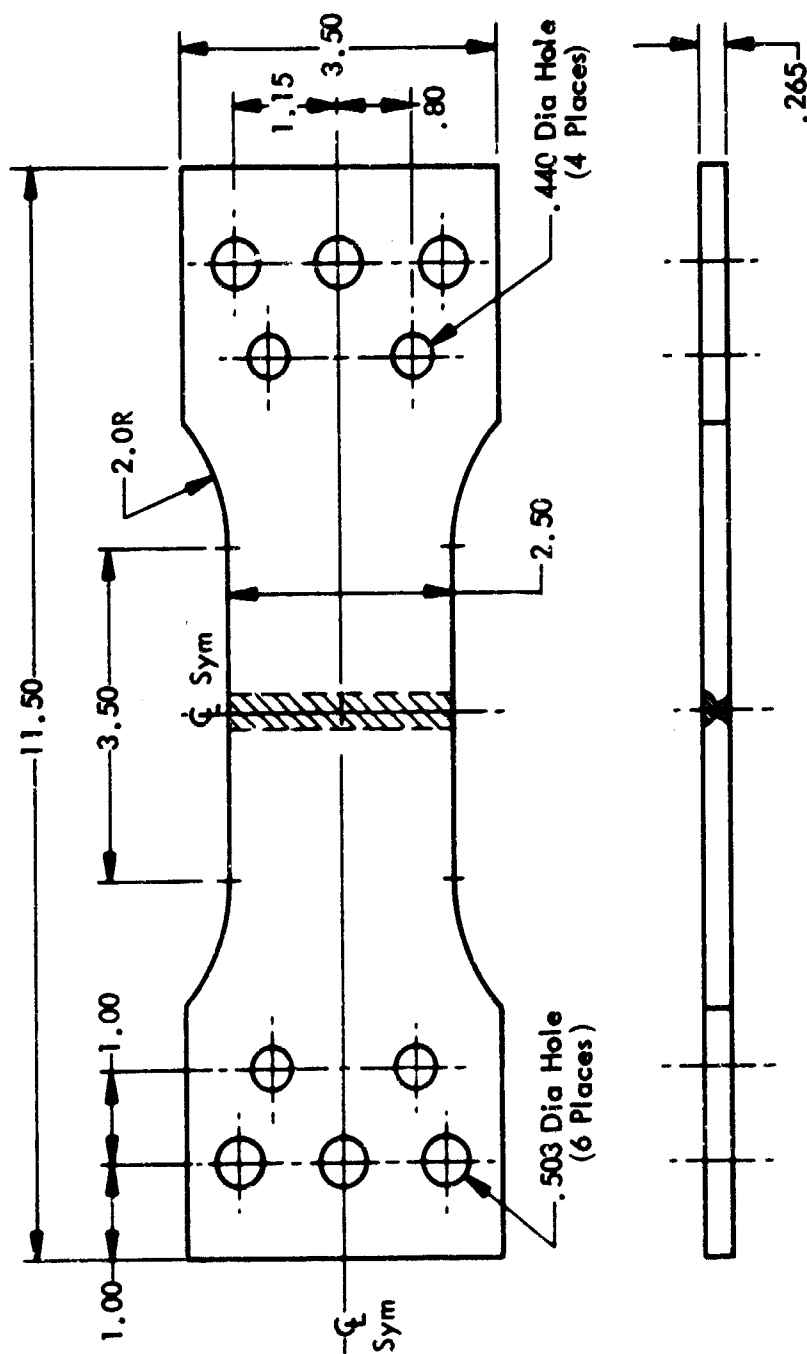
▷ Terminating Radius Along The Entire
Periphery Of The Surface Flaw Is
Not To Exceed .0015 Inch.

Figure 31: TYPICAL SURFACE FLAW



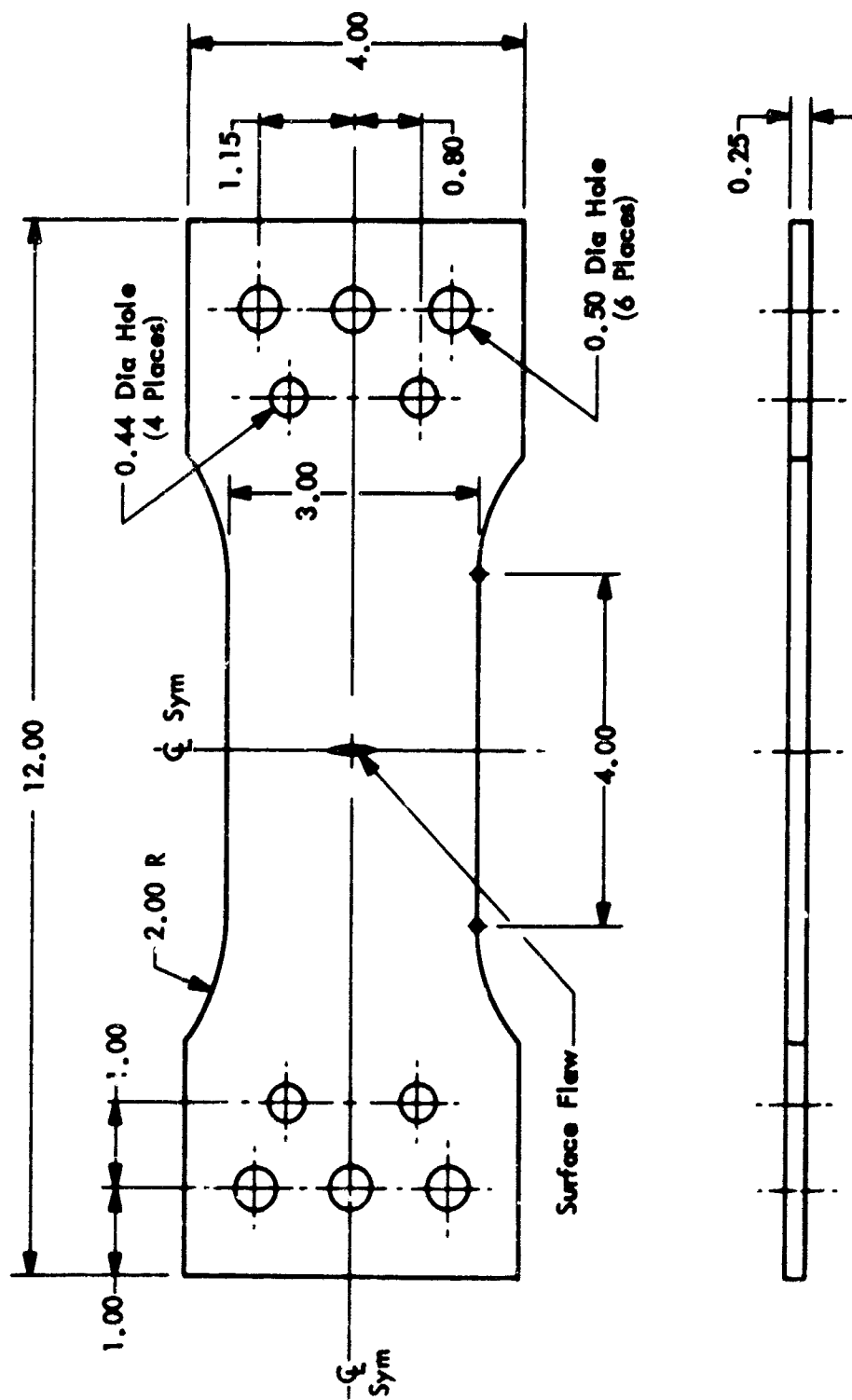
All Dimensions Are In Inches

Figure 32: 2219-T851 ALUMINUM SURFACE FLAWED SPECIMEN
(Weldment)



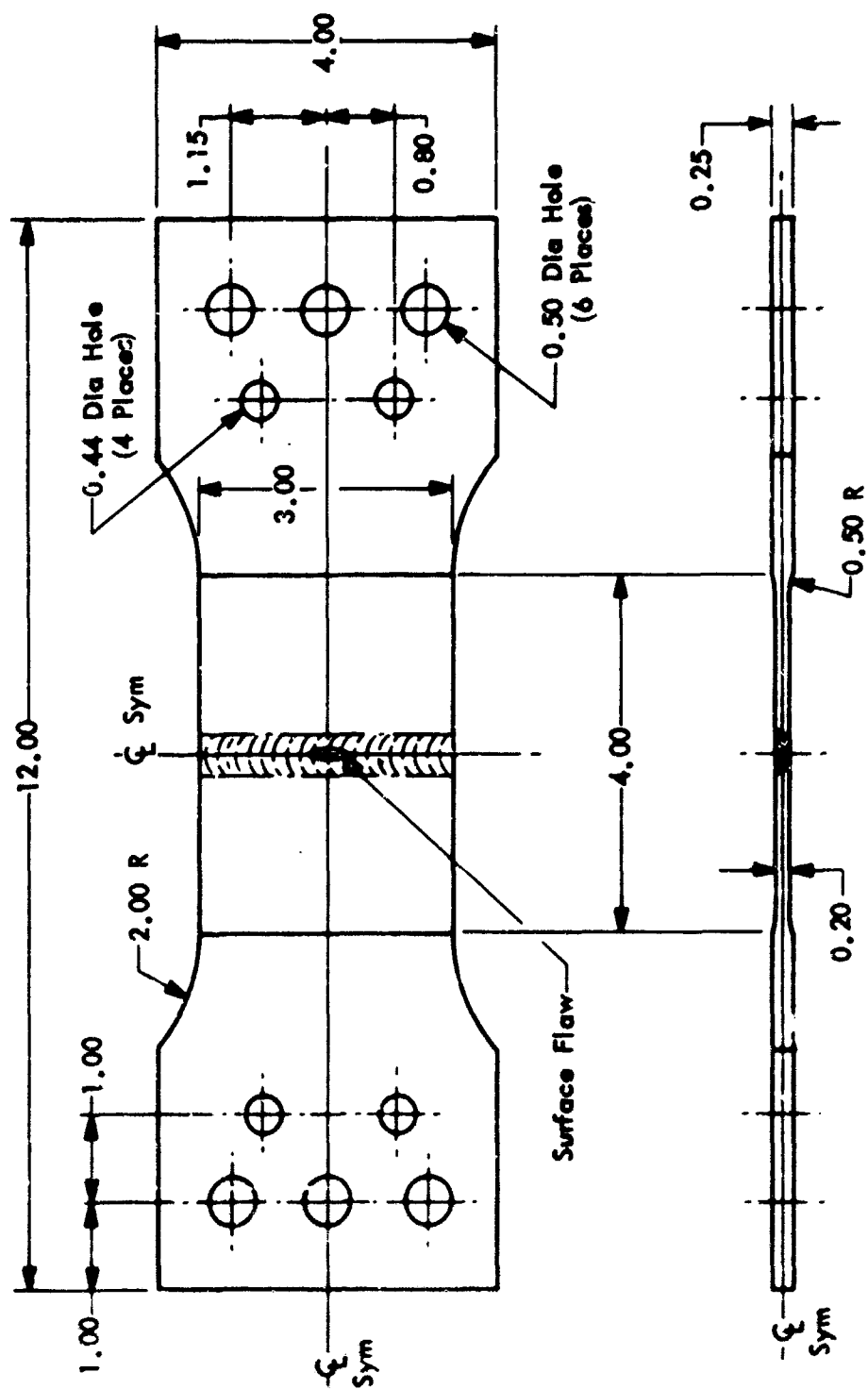
All Dimensions Are In Inches

Figure 33: 6Al-4V (ELI) TITANIUM SURFACE FLAWED SPECIMEN
(Weldment)



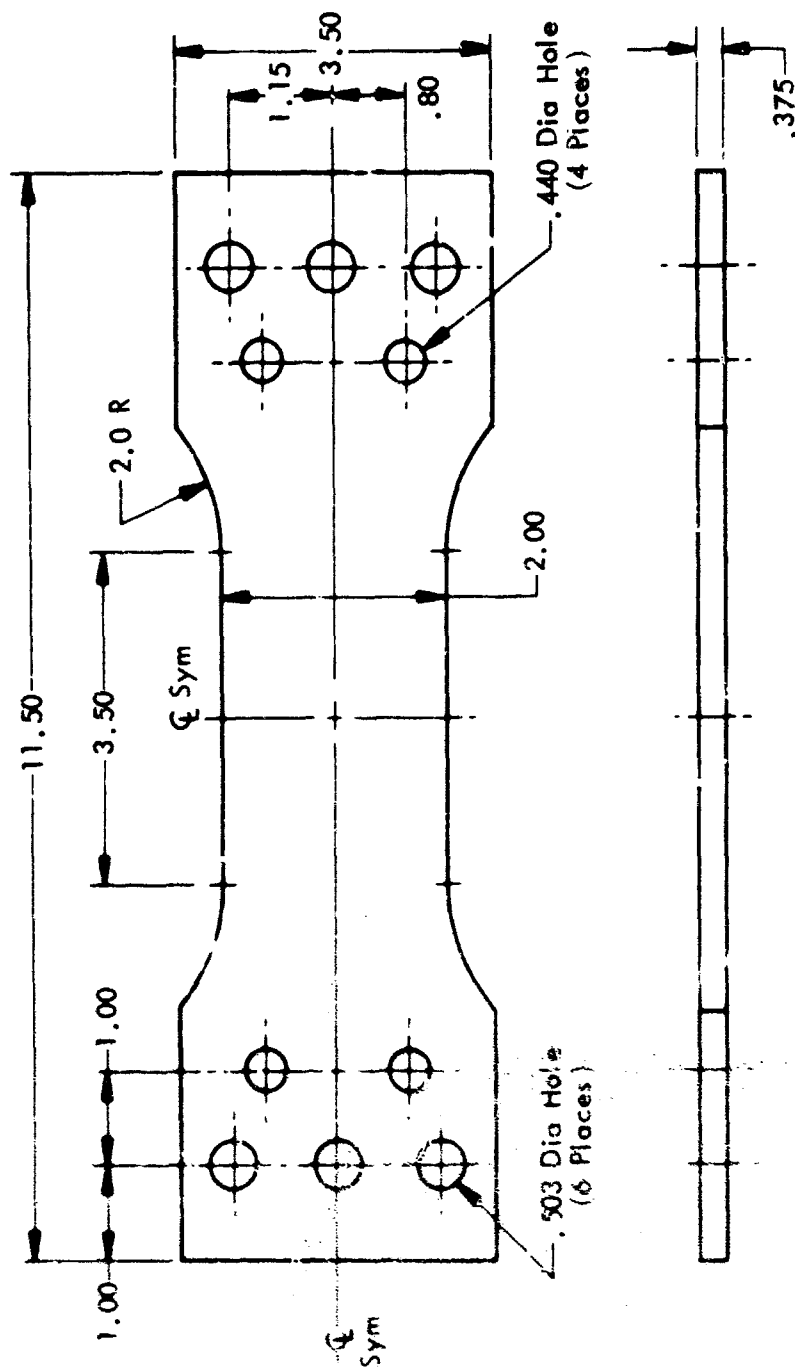
All Dimensions Are In Inches

Figure 34 : 2021 ALUMINUM SURFACE FLAWED SPECIMEN (Base Metal)



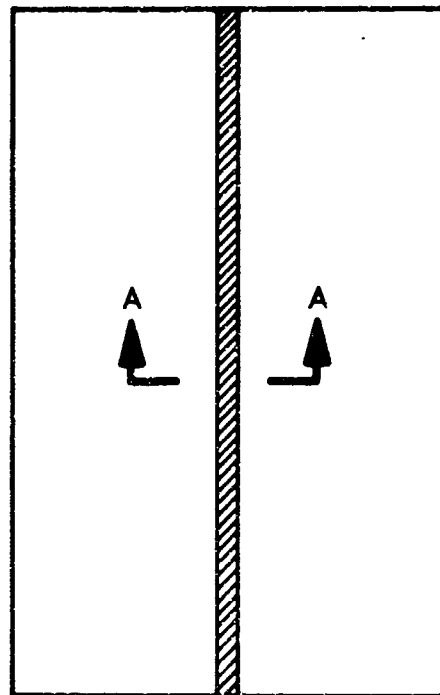
All Dimensions Are In Inches

Figure 35 : 2021 ALUMINUM SURFACE FLAWED SPECIMEN (Weld Metal)

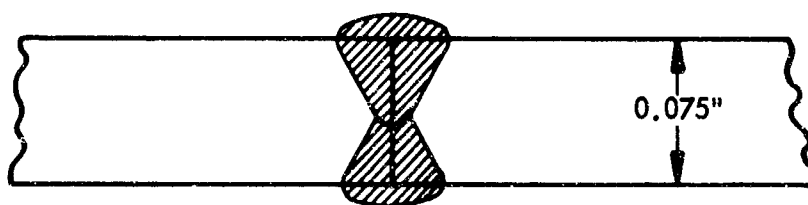


All Dimensions Are in Inches

Figure 36: 410 (Mod.) STAINLESS STEEL SURFACE FLAWED SPECIMEN
(Base Metal)

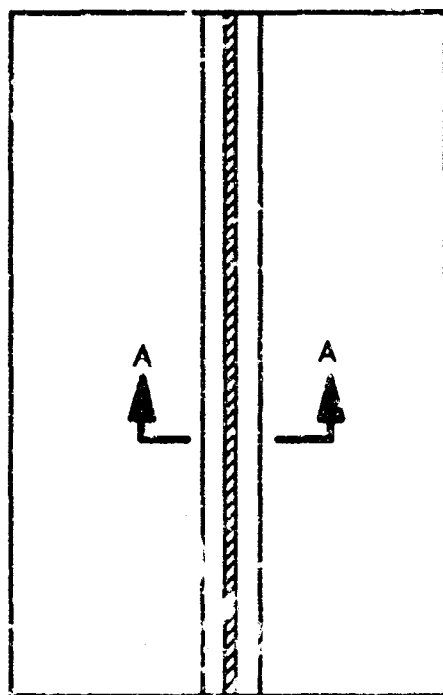


WELD PANEL

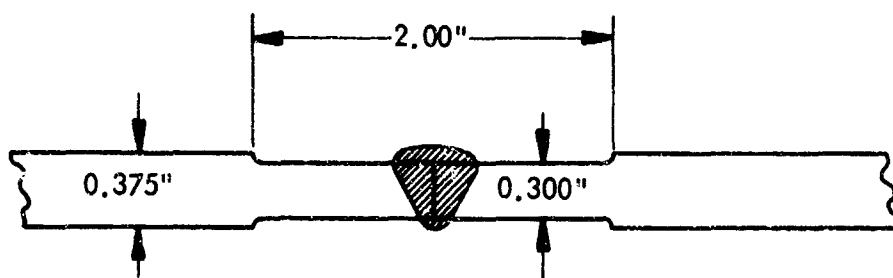


SECTION A-A

Figure 37: 2219-T851 ALUMINUM WELD TEST PANEL



WELD PANEL



SECTION A-A

Figure 38: 6Al-4V (ELI) TITANIUM WELD TEST PANEL

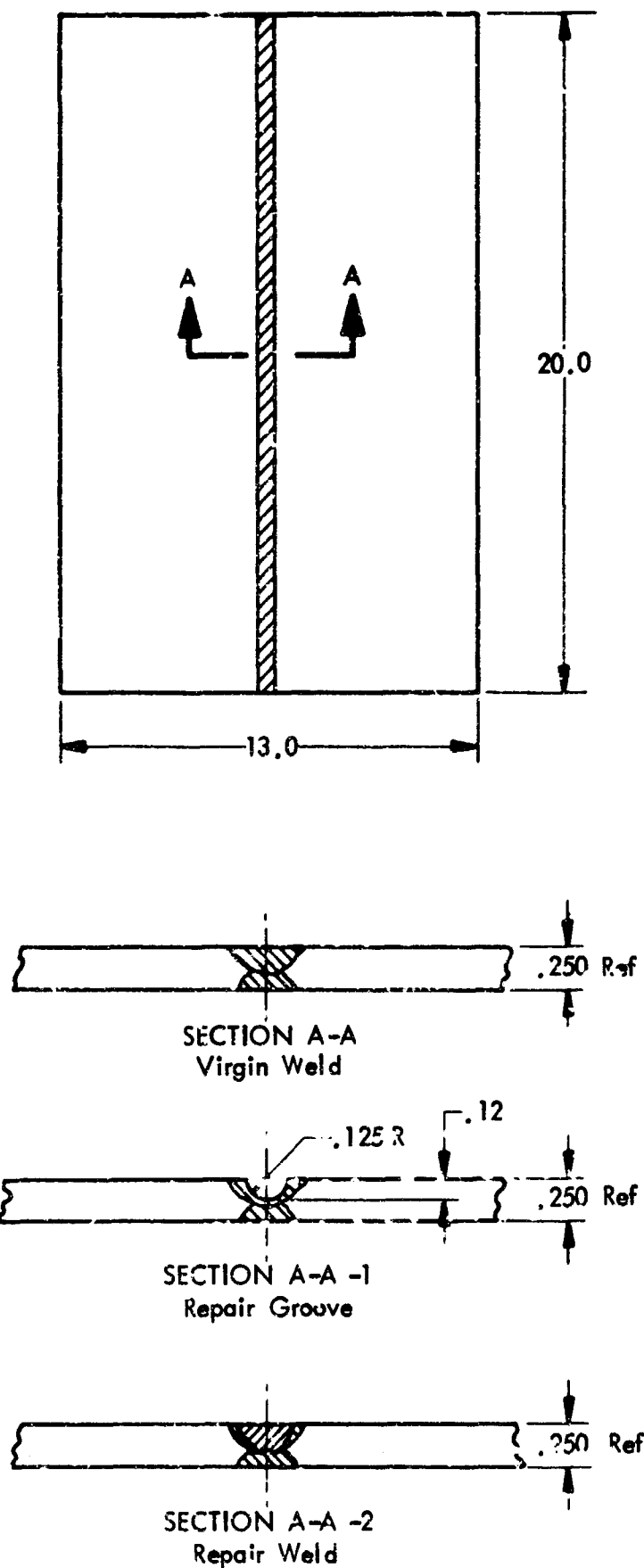


Figure 39: 2021-T81 ALUMINUM WELD TEST PANEL
(Virgin And Repair Welds)

expected service life. Preparation of SFT test specimens, testing, and specimen examination is conducted in the following manner.

3.2.1 Static K_{Ic} Test

For SFT specimens, the initial flaw is prepared using an electrical discharge machine (EDM). The specimen is then subjected to low stress cyclic loading until a fatigue crack is initiated along the entire periphery of the EDM flaw. Normally, the resultant crack front becomes semielliptical. In the presence of gross inhomogenieties or incipient delaminations in the material, orderly progression of the crack is sometimes inhibited and the crack front becomes irregular. When crack progression is normal, the final flaw depth is estimated by judging the separation of the crack opening at the bottom of the EDM flaw thus ensuring a fair degree of initial flaw uniformity from one specimen to another. The SFT specimens with prepared cracks are then pulled to failure to provide basic fracture toughness data for comparison with the data obtained in the corrosive environments.

3.2.2 Sustained Flaw Growth Test

An SFT specimen with a fatigue-extended surface flaw is mounted in the tensile machine equipped with auxiliary plumbing for transferring and pressurizing required environmental fluids. A small cup is placed over the surface crack so that the crack cavity and the adjacent area on the crack-containing surface are completely flooded with the fluid being evaluated. The cup is sealed to prevent escape of the fluid to the outside during pressurization. The clamping force was just large enough to provide required compression of the seal to prevent leakage. The fluid is introduced into the cup and pressurized to the desired level. The specimen remains unloaded.

With the crack cavity completely submerged, the specimen is then subjected to low-stress cyclic loading (50 to 100 cycles) to purge the crack cavity and to generate a fresh crack surface. The maximum cyclic load level is kept below 50% of the intended sustained load level. Cycling at a much higher load could influence the results of the sustained load testing. Once

the flaw has been purged and extended by cyclic loading, the specimen is loaded to a desired stress level and left at that stress for a predetermined period of time.

Upon conclusion of the sustained load test run, the specimen is once again subjected to low-stress fatigue to mark the outline of the crack front. The specimen is then pulled to failure and fracture surfaces examined.

3.2.3 Cyclic Flaw Growth Test

Cyclic flaw growth data is generated using SFT specimens that are prepared in an identical manner as those for static K_{IC} or sustained flaw growth testing. Programming of the load levels as well as load profiles is, to a great extent, dependent upon intended application. Normally, pressurization rates in propellant-containing pressure vessels are relatively slow. In the present program, cyclic frequency was set at about 2 to 4 cycles per minute. The loading profile was sinusoidal.

If it is necessary to obtain cyclic flaw growth data for missions involving many pressurization cycles, then programming of the specimens would call for consideration not only of the initial (K_{I1}) stress intensity levels, but also of the terminating or critical (K_{IC}) stress intensity values. The latter is important because surface flaws must remain completely confined within the material thickness and, ideally, depth should not exceed half of the material thickness. While there are approximate correction factors to account for variation in depth as well as the shape of the surface flaw, application of the test data calls for more engineering judgment than otherwise would be necessary.

3.3 Fractographic Technique

Fatigue zones on a fractured surface, while frequently visible to the naked eye in properly oriented light, are difficult to photograph under ordinary illumination. During the NAS 3-4194 program (Ref 19), attempts were made to improve fractographic resolution of cyclically tested specimens by the use of polarized white light.

The essential elements of the fractographic technique are illustrated schematically in Figure 40. The developed fractographic setup consists of a beam of white light passing through the first polaroid filter, which is positioned so that its plane of polarization is parallel to the upper edge of an optical glass reflector. Light transmitted through the first filter is plane-polarized and reflected from the glass plate vertically downward on the fracture specimens without rotating the polarization plane. Upon striking the specimen surface, some of the plane-polarized rays of light are reflected under a shallow angle with respect to the horizontal plane and are scattered outside the optical axis of a camera. Others are reflected upward, pass through the glass plate without rotation, and then are cross-polarized by the second polarizer screen. Still other rays strike the somewhat obliquely oriented flat surfaces and are reflected upward with resultant rotation of the polarizing plans. These rays pass more readily through the second polarizing plate and are recorded on film. The degree of shading or contrast attained is apparently a measure of relative density and distribution of reasonably flat and obliquely oriented surface.

One cyclically tested 2219-T87 aluminum specimen (Ref 37), sectioned and polished to show fracture profile, is pictured in Figure 41. It can be seen that profiles of the fracture faces bear distinct characteristics depending on mode of crack propagation. The low-stress initial extension region, which has numerous flat plateaus, appears to be dark in the picture. The region in which the fracture was under cyclic high-stress loading has fewer flat plateaus and is not as dark in the pictures. Finally, regions of rapidly propagating fracture are almost completely devoid of flat surfaces and appear to be quite light on the fractograph. An illustration taken from Reference 37 compares a fractograph taken with polarized light with a fractograph obtained from the same specimen using conventional illumination and is shown in Figure 42.

The same fractographic technique has been applied to the NAS 3-6290 program (Ref 19), designed to determine sustained flaw growth characteristics of the 2219-T87 aluminum and 5Al-2.5Sn(ELI) titanium in the environments of

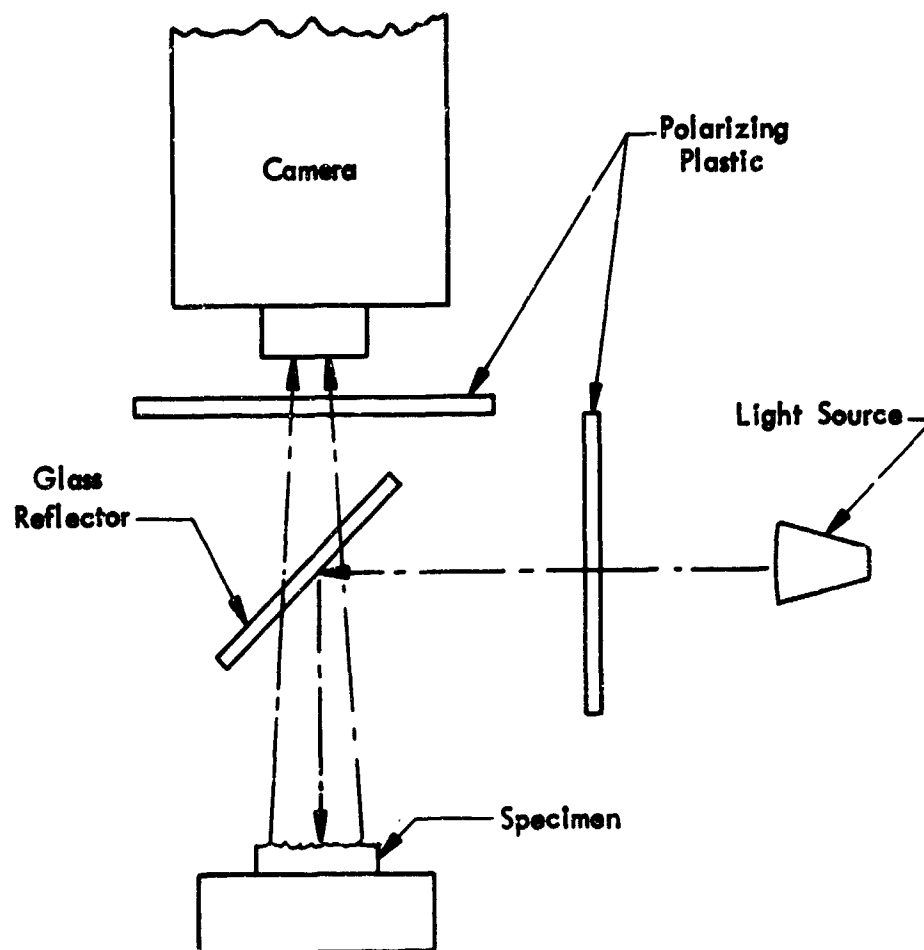


Figure 40: SCHEMATIC ILLUSTRATION OF FRACTOGRAPHIC SETUP

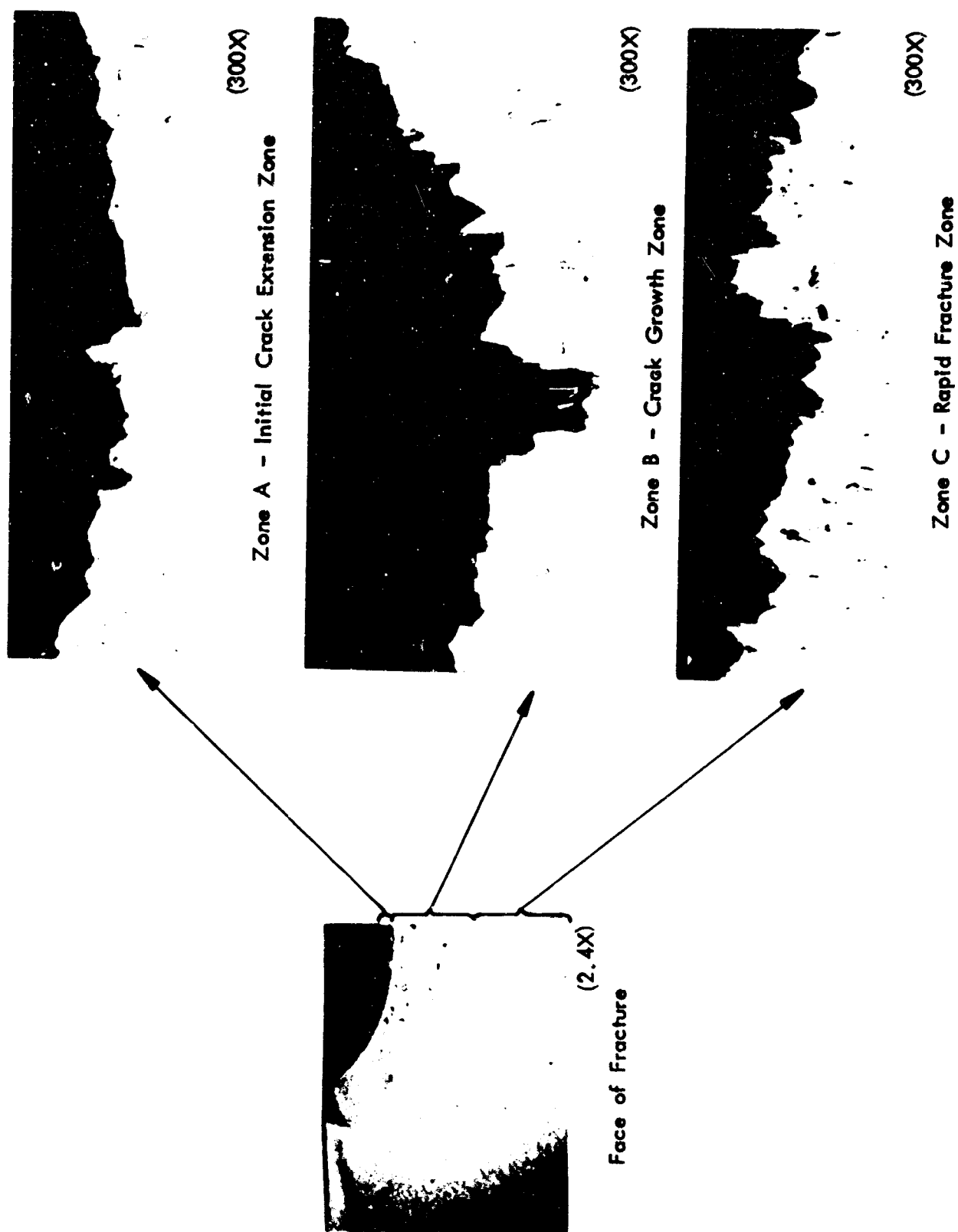
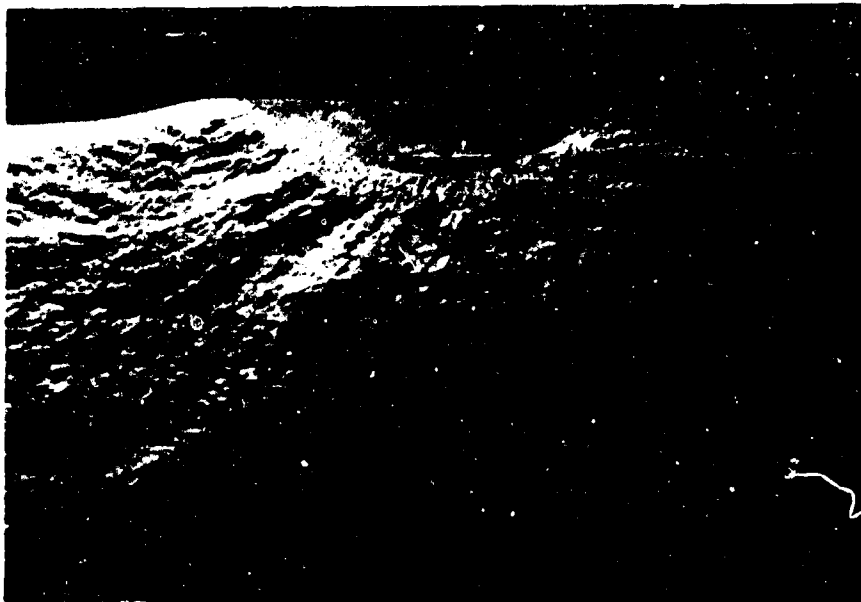


Figure 41: CROSS-SECTIONS OF PHOTOGRAPHICALLY DISCRETE ZONES
IN CYCLICALLY TESTED 2219-T87 ALUMINUM SPECIMEN



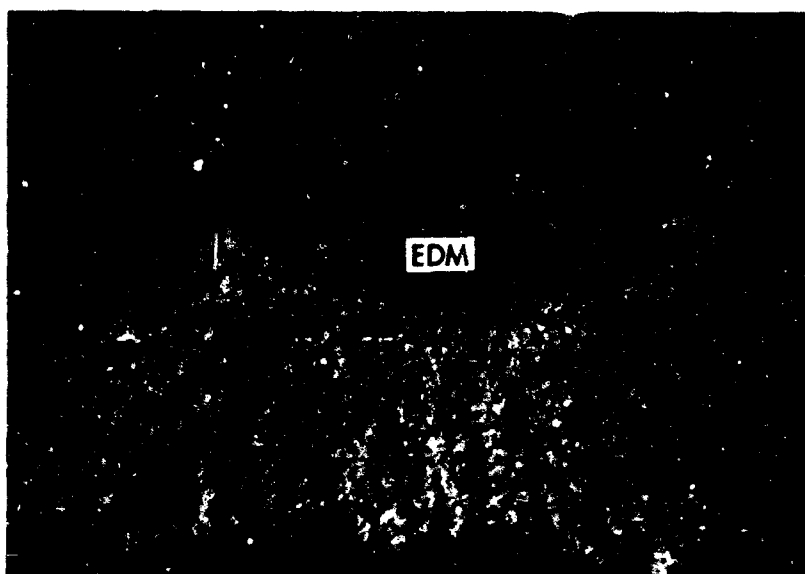
NO POLARIZATION (REFLECTED WHITE LIGHT)



LIGHT POLARIZED BY CROSSED POLARS

Figure 42: 2219 ALUMINUM FATIGUE SPECIMEN

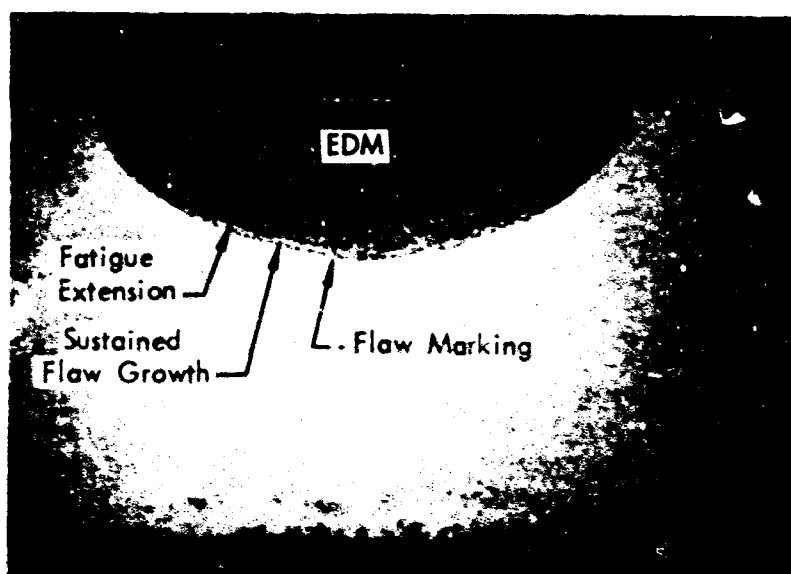
liquid nitrogen and hydrogen as well as under ambient atmospheric conditions. High degrees of reproducibility achieved by polarized light fractography is illustrated in Figure 43, showing the difference between white and polarized light illumination for sustained load test specimens. The same technique is further illustrated in Figure 44, showing fracture faces of multiple test run specimens. The advantages of the white light as a supplement to the polarized light fractograph are illustrated in Figure 45, showing a delaminated 2219-T87 aluminum tank fracture face. Application of the same fractographic techniques in the present program made both the resolution and reproduction of the crack growth data easier and more accurate.



R.T.

2.9x

SPECIMEN NO. CA-43
(White Light Illumination)



R.T.

3.6x

SPECIMEN NO. CA-43
(Polarized Light Illumination)

Figure 43 : FRACTOGRAPHS OF 2219-T87 ALUMINUM SPECIMEN
TESTED AT ROOM TEMPERATURE (Specimen No. CA-43)

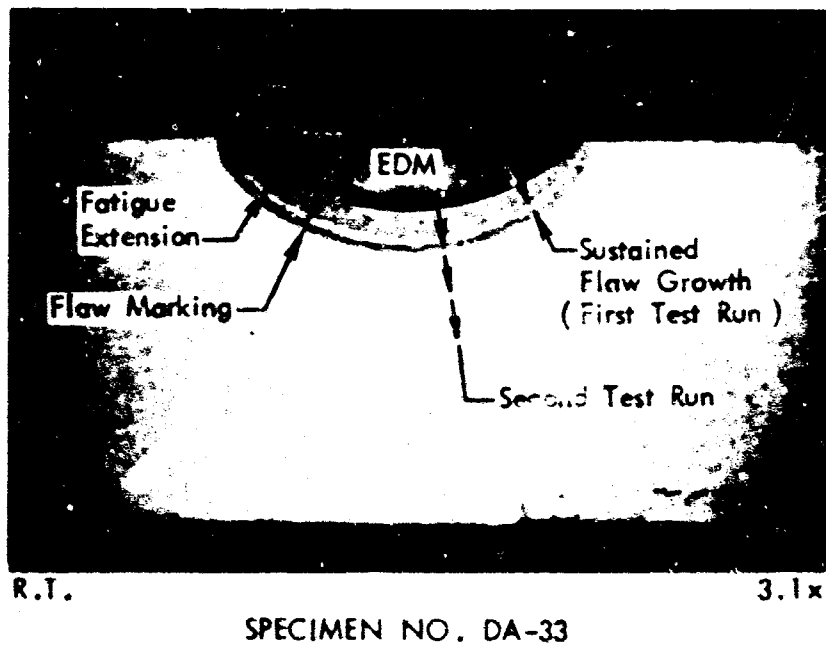
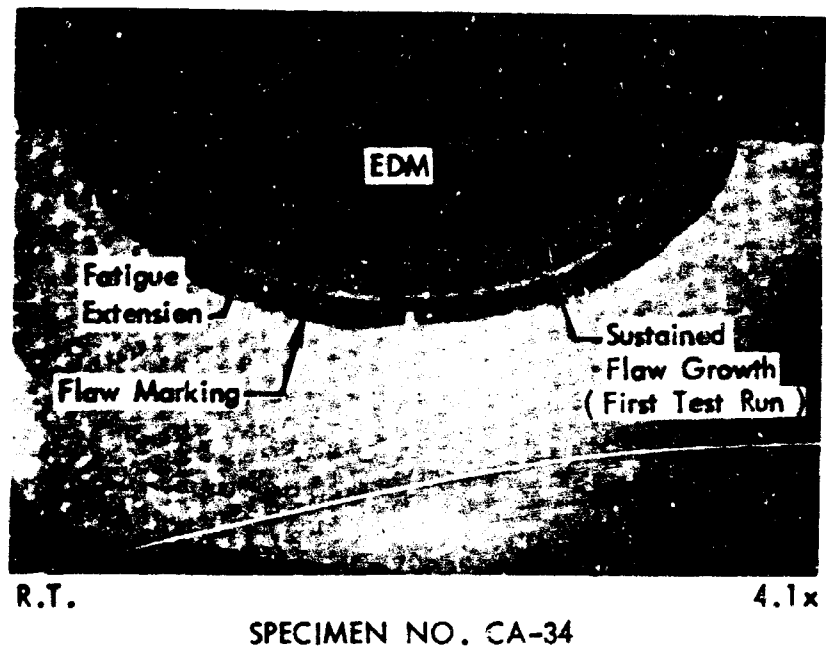
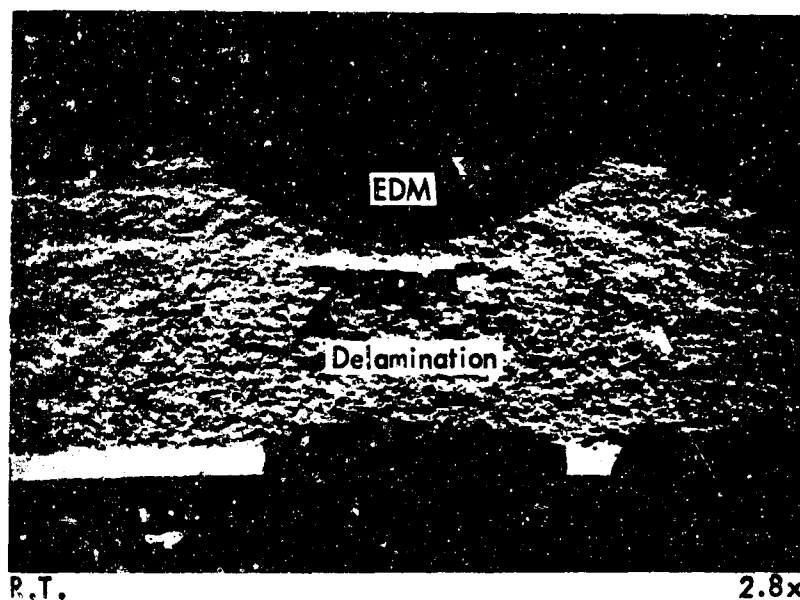
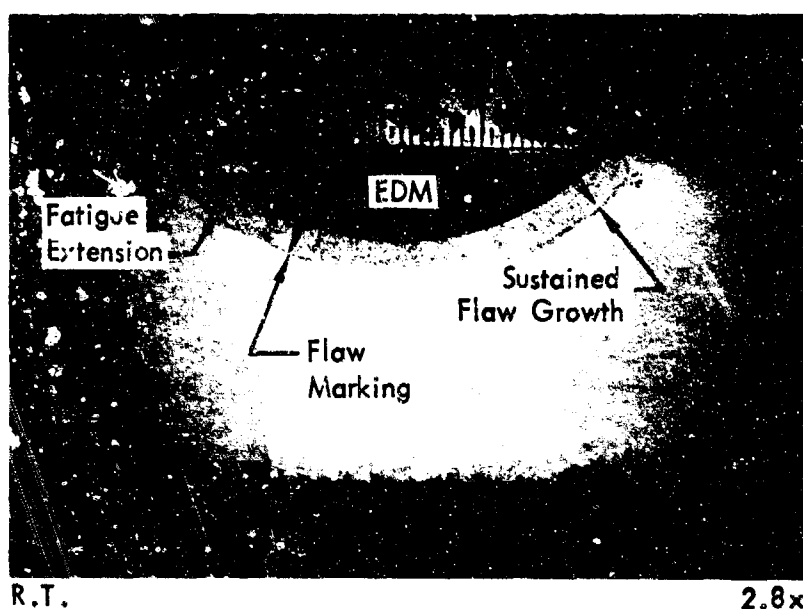


Figure 44: FRACTOGRAPHS OF 2219-T87 ALUMINUM SPECIMENS TESTED AT ROOM TEMPERATURE (Specimens CA-34 And DA-33)



TANK NO. 0001, FLAW NO. 1
(White Light Illumination)



TANK NO. 0001, FLAW NO. 1
(Polarized Light Illumination)

Figure 45: FRACTOGRAPHS OF 2219-T87 ALUMINUM TANK TESTED AT
ROOM TEMPERATURE (Tank No. 0001)

4.0 MATERIALS

Two 2219-T851 aluminum plates 0.750 by 48 by 144 inches were obtained per MIL-A-8920A (ASG). Typical mechanical properties at room temperature for this lot of material were listed by the supplier as 67.3 ksi ultimate strength, 50.5 ksi yield strength, and 10.5% elongation in the 2-inch gage length. Chemical composition of the material was reported to fall within the following percentage points: Si 0.20 max, Fe 0.30 max, Cu 6.8 to 5.8, Mn 0.40 to 0.20, Mg 0.02 max, Zn 0.10 max, Ti 0.10 to 0.002, V 0.15 to 0.05, Zr 0.25 to 0.10, others 0.15 to 0.05. The material was furnished free of charge by the Aluminum Company of America in the interest of promoting investigation of alloy behavior in aggressive environments.

Two 6Al-4V(ELI) titanium plates 0.375 by 24 by 72 inches were purchased in the annealed condition from Titanium Metals Corporation per AMS 4911A except that the interstitial content was specified not to exceed the following limits: C 0.08 max, O₂ 0.13 max, N₂ 0.05 max, H₂ 175 ppm max, and Fe 0.25 max. Chemical composition of the material was reported by the supplier to be: C 0.023, Fe 0.06, N₂ 0.009, Al 5.9, V 4.0, H₂ 0.005 to 0.004, O₂ 0.11. Typical mechanical properties of the as received material were listed as 136.0 ksi ultimate strength, 131.1 yield strength, and 16% elongation in the 2-inch gage length.

Both titanium plates were sectioned into test panels, then heat-treated at $1750 \pm 25^{\circ}\text{F}$ for one hour, water quenched to 60°F , then aged at 1050° for six hours. Due to severe warpage of the panels during solution heat treatment and water quench cycles, aging of the panels was done in a hot press.

Three 410(MOD) stainless steel plates 0.50 by 24 by 72 inches were purchased from the Republic Steel Corporation per United Technology Corporation (UTC) Specification 4MDS-20705B with several minor modifications to make 4MDS-20705B applicable to plate rather than bar and forging material for which the specification was written. The modifications consist of requesting the slab instead of the plate to be macroetched for segregations, substitution of number one surface finish in place of RMS 125 as required

for bar stock. Testing, sampling and marking to be done per WED-STD-151 as applicable to plate; the plate was to be rolled in one direction and delta ferrite was to be limited to 5 percent or less. Chemical composition of the material was reported to fall within the following percentage points: Cr 11.50 to 12.50, Ni 0.75 max, Mn 0.60 max, Si 0.50 max, Cu 0.50 max, Mo 0.20 max, C 0.12 to 0.15, Al 0.05 max, Sn 0.05 max, Pb 0.025, S 0.025, Fe - balance.

Heat treatment of the 410(MOD) plates was done in accordance with the UTC Specification 4TDS-90102B. The essential features of the heat treatment cycles were: Austenitize at $1735 \pm 15^{\circ}\text{F}$ for one hour; forced air cool below 1200°F in less than 8 minutes; cool to room temperature; double temper at $600 \pm 10^{\circ}\text{F}$ for two hours each; air cool to room temperature. Typical mechanical properties of the steel after such treatment were reported to be $F_{tu} = 192.4$ ksi, $F_{ty} = 155.1$ ksi, percent elongation in 1.0-inch gage length 15.5, reduction of area 68 percent.

The 2021-T81 aluminum weld, as well as base metal plate samples, were furnished by the Lockheed Aircraft Corporation without chemical composition or mechanical properties test data. The material, however, is being subjected to exhaustive investigation by Lockheed so that it would be possible to obtain the information if necessary.

A 2319 weld filler wire, 0.063 inch in diameter, used for welding 2219-T851 aluminum plate, has been purchased per RMS 7-75B Type II (equivalent to ASTM B-285-21T, "Tentative Specification for Aluminum Aluminum-Alloy welding Rods and Bare Electrodes"). Chemical composition of the 2319 weld filler wire was reported to be within the following limits: Mn 0.40 to 0.20, Si 0.20 max, V 0.15 to 0.05, Zr 0.25 to 0.10, Cu 6.8 to 5.8, Mg 0.02 max, Zn 0.10 max, Ti 0.20 to 0.10, Fe 0.30 max. The wire was obtained from The Boeing Company's stock.

The 6Al-4V(ELI) titanium weld filler wire heat No. 3335-D1 was purchased per AMS 4954A. Chemical composition of the wire was reported to be C 0.08,

Fe 0.20, V 3.60, Al 6.45, O₂ 0.03, N₂ 0.01, H₂ 0.002. Tensile properties of the wire were given as 136.3 ksi ultimate strength and 121.2 ksi yield strength. The weld wire was purchased from the R&D Metals Corporation.

Liquid propellants used in the program were standard grade, meeting the required military or supplier's specifications. Nitrogen tetroxide (N₂O₄) was purchased per PPD-2 NASA specification. The propellant also met the MIL-T-26539B specification. Fluorine was purchased from Allied Chemical Company. The hydrogen fluoride content was reported to be less than 0.2%. Chlorine pentafluoride (ClF₅) was purchased from the Allied Chemical Company and reportedly was produced in accordance with the best practice of the industry. No current specification was cited.

5.0 EXPERIMENTAL TEST RESULTS

5.1 Phase I -- Screening Test

Experimental test results generated using surface-flawed-bend (SFB) specimens are summarized in TABLES 1, 2, and 3 for the 2219-T851 aluminum in the environments of N_2O_4 , F_2 , and ClF_5 , respectively, in TABLE 4 for the 2021-T81 aluminum in the environment of N_2O_4 , and in TABLES 5 through 9 for the 6Al-4V(ELI) titanium in the environment of F_2 and ClF_5 . The makeup of the tables is common to all material propellant combinations and consists of the following key elements:

The first four columns list specimen identification numbers together with the symbolic notation of the specimen type (base metal or weldment, and the location of the surface flaw), specimen thickness, and width. The next two columns show initial flaw size in terms of its depth "a" and length "2c" in inches. In all cases, the "a" and "2c" dimensions are the result of EDM machining using circular disc cutter with a terminating radius less than .002 of an inch. There was no fatigue extension of the EDM flaws.

The applied stress level at the outer fiber σ_B , resulting shape parameter Q that incorporates a, 2c, and σ_B/σ_{ys} values, SFB specimen bend parameter M_B applicable for given conditions, and the calculated K_{I1} stress intensity value at the beginning of the test run are listed in the next four columns.

It should be realized that calculated values of applied stress intensity K_{I1} may not be truly representative of the actual stress intensity that would have been generated if the EDM flaws were extended by cyclic loading. The extent of the departure from the true value of applied stress intensity will be more pronounced for more brittle materials such as heat-treated titanium and may not be significant for the more ductile materials such as 2219 aluminum.

Designation of environmental media, pressure, temperature, and time under sustained loading are followed by the columns listing flaw dimensions "a" and "2c" after the test run. In cases where there was no crack extension during the sustained load run, the final flaw size is the same as the initial flaw size. There are, however, instances where the crack did grow under sustained load. To facilitate spotting of the specimens with flaw size increase, an extra column is inserted to show flaw increment in terms of depth increase Δa in inches. A corresponding increase of 2c dimension may be readily established by comparison of final and initial 2c dimensions. The resulting stress intensity value (K_{I_f}) at the end of the test run is then calculated using final flaw dimensions. Once again it should be noted that in the absence of crack extension during sustained test run, flaw dimension used in calculations are those introduced by the EDM machining.

The information pertaining to cyclic flaw marking in terms of temperature, maximum applied load level, moment arm d and number of cycles used to mark the flaw, the flaw size after marking in terms of a and 2c dimensions are listed in the next columns.

Experimental test results obtained using double-cantilever-beam (DCB) specimens are summarized in TABLE 9. The format of the table is similar to the one used for SFB specimens inasmuch as it lists specimen identification, initial crack extension by cyclic loading data, and sustained load test conditions. The table also lists post-test and post-fracture conditions and calculated stress-intensity levels. Common specimen dimensions in terms of thickness, beam depth, and Poisson ratio are also listed.

5.1.1 2219-T851 Aluminum

The 2219-T851 aluminum was tested in the environments of liquid and vapor phases of N_2O_4 , F_2 , and ClF_5 . In each case two pressure-temperature combinations were involved. For each combination there were two specimen assemblies in the vapor phase of the propellant and two specimen assemblies in the liquid phase. Of the two assemblies, one consisted of high-stress and low-stress base metal specimens. The other assembly consisted of high-stress and low-stress weld metal specimens. All base metal specimens contained

one surface flaw per specimen. All weld metal specimens contained three flaws per specimen. Configuration of the base metal and weldment high-stress and low-stress specimens is shown in Figures 17 and 18.

5.1.1.1 N_2O_4 and 2219-T851 Aluminum

Pertinent specimen dimensions, test conditions, and flaw size measurements, together with the calculated stress-intensity K values, are listed in TABLE 1. As can be seen from the column depicting flaw increment during sustained load test run, none of the surface-flawed bend specimens showed any signs of flaw growth as a result of the exposure to N_2O_4 propellant at 50 psi and 50°F as well as at 450 psi and 140°F. The test run consisted of 20 hours under sustained loading conditions. A schematic diagram of N_2O_4 pressurization system is shown in Figure 13.

5.1.1.2 F_2 and 2219-T851 Aluminum

Pertinent specimen dimensions, test conditions, and flaw size measurements together with the calculated stress-intensity K values are listed in TABLE 2. As in the environment of N_2O_4 , none of the specimens showed any signs of corrosion attack or flaw extension. Pressure temperature for high-pressure and low-pressure chambers were 450 psi and -235°F and 50 psi and -320°F. Because load levels for these specimens were the same as those used for N_2O_4 test, the applied stress intensity levels were also similar. Test runs were 21 hours under sustained load conditions in the low-pressure chamber and 24 hours in the high-pressure chamber. A schematic diagram of the F_2 pressurization system is shown in Figure 14.

5.1.1.3 ClF_5 and 2219-T851 Aluminum

Test results of this test run together with pertinent specimen dimensions and flaw sizes are listed in TABLE 3. As in the previous two environments of N_2O_4 and F_2 , exposure to ClF_5 at 450 psi and 140°F and 50 psi and 50°F did not result in crack extension. Test runs were 17:47 and 18:40 hours for the low-pressure and high-pressure chambers, respectively. A schematic diagram of the ClF_5 pressurization system is shown in Figure 15.

SPECIMEN NUMBER	TYPE	THICK- NESS t (in.)	WIDTH W (in.)	INITIAL FLAW SIZE		σ (ksi)	Q	M_B	ΔK_{I1}	ENVIRON- MENT	
				a (in.)	2c (in.)						
9BV-1	BM	.507	1.00	.052	.152	48.9	1.57	.900	14.19	N ₂ O ₄	
9BV-2	BM	.507	1.5	.054	.260	32.6	1.25	.920	10.86	N ₂ O ₄	
9BL-1	BM	.507	1.0	.054	.156	48.9	1.58	.890	14.24	N ₂ O ₄	
9BL-2	BM	.505	1.5	.050	.260	32.6	1.21	.940	10.84	N ₂ O ₄	
9WV-1	A	-	-	-	-	-	-	-	-	-	
9WV-1	B	.500	1.3	.054	.157	20.3	1.58	.895	5.96	N ₂ O ₄	
9WV-1	C	.500	1.3	.052	.152	20.3	1.57	.890	5.83	N ₂ O ₄	
9WV-2	A	.504	2.0	.048	.244	13.2	1.22	.950	4.50	N ₂ O ₄	
9WV-2	B	.507	2.0	.052	.264	13.2	1.22	.935	4.51	N ₂ O ₄	
9WV-2	C	.507	2.0	.052	.256	13.2	1.24	.930	4.46	N ₂ O ₄	
9WL-1	A	.499	1.3	.054	.154	20.3	1.60	.890	5.88	N ₂ O ₄	
9WL-1	B	.500	1.3	.052	.154	20.3	1.55	.890	5.86	N ₂ O ₄	
9WL-1	C	.497	1.3	.052	.150	20.3	1.59	.890	5.79	N ₂ O ₄	
9WL-2	A	.502	2.0	.052	.256	13.2	1.24	.930	4.46	N ₂ O ₄	
9WL-2	B	.502	2.0	.053	.252	13.2	1.26	.920	4.42	N ₂ O ₄	
9WL-2	C	.501	2.0	.052	.258	13.2	1.23	.930	4.46	N ₂ O ₄	
9BV-3	BM	.507	1.0	.054	.156	48.9	1.58	.900	14.43	N ₂ O ₄	
9BV-4	BM	.506	1.5	.055	.260	32.6	1.26	.925	10.97	N ₂ O ₄	
9BL-3	BM	.507	1.0	.052	.156	48.9	1.53	.890	14.19	N ₂ O ₄	
9BL-4	BM	.508	1.5	.055	.256	32.6	1.27	.910	10.75	N ₂ O ₄	
9WV-3	A	-	-	-	-	-	-	-	-	-	
9WV-3	B	.503	1.3	.055	.154	20.3	1.63	.880	5.80	N ₂ O ₄	
9WV-3	C	.503	1.3	.052	.152	20.3	1.57	.890	5.82	N ₂ O ₄	
9WV-4	A	.503	2.0	.052	.250	13.2	1.25	.930	4.44	N ₂ O ₄	
9WV-4	B	.503	2.0	.057	.266	13.2	1.27	.910	4.51	N ₂ O ₄	
9WV-4	C	.502	2.0	.050	.252	13.2	1.23	.940	4.44	N ₂ O ₄	
9WL-3	A	.502	1.3	.055	.152	20.3	1.64	.890	5.86	N ₂ O ₄	
9WL-3	B	.503	1.3	.060	.162	20.3	1.68	.870	5.91	N ₂ O ₄	
9WL-3	C	.502	1.3	.056	.152	20.3	1.67	.880	5.79	N ₂ O ₄	
9WL-4	A	.500	2.0	.052	.256	13.2	1.26	.925	4.39	N ₂ O ₄	
9WL-4	B	.503	2.0	.051	.252	13.2	1.23	.935	4.46	N ₂ O ₄	
9WL-4	C	.505	2.0	.052	.248	13.2	1.26	.930	4.42	N ₂ O ₄	

1 As Calculated Using Original
Dimensions of EDM Flaw

2 Whenever Applicable Flaw Growth
Increment is Added to EDM Flaw
Dimensions

A.

ID	ENVIRON- MENT	PRESSURE (psig)	TEMP. (°F)	TIME (hr)	FINAL FLAW SIZE		FLAW INCREMENT Δa (in.)	K_{If}	CYCLIC MARKING				FLAW AFTER
					a (in.)	2c (in.)			TEMP (°F)	P _{max} (lb)	D/2 (in.)	CYCLES (1000)	a (in.)
1.19	N ₂ O ₄	50	RT	20:23	.052	.152	0	14.19	RT	1,135	1.5	60	.106
0.86	N ₂ O ₄	50	RT	20:23	.054	.260	0	10.86	RT	1,870	1.5	30	.088
1.24	N ₂ O ₄	50	RT	20:23	.054	.156	0	14.24	-	-	-	-	-
0.84	N ₂ O ₄	50	RT	20:23	.050	.260	0	10.84	-	-	-	-	-
-	-	-	-	-	-	-	-	-	-	-	-	-	-
5.96	N ₂ O ₄	50	RT	20:23	.054	.157	0	5.96	RT	1,080	1.5	20	.062
5.83	N ₂ O ₄	50	RT	20:23	.052	.152	0	5.83	RT	1,080	1.5	20	.064
4.50	N ₂ O ₄	50	RT	20:23	.048	.244	0	4.50	RT	1,660	1.5	20	.052
4.51	N ₂ O ₄	50	RT	20:23	.052	.264	0	4.51	RT	1,660	1.5	20	.060
4.46	N ₂ O ₄	50	RT	20:23	.052	.256	0	4.46	RT	1,660	1.5	20	.056
5.88	N ₂ O ₄	50	RT	20:23	.054	.154	0	5.88	-	-	-	-	-
5.86	N ₂ O ₄	50	RT	20:23	.052	.154	0	5.86	-	-	-	-	-
5.79	N ₂ O ₄	50	RT	20:23	.052	.150	0	5.79	-	-	-	-	-
4.46	N ₂ O ₄	50	RT	20:23	.052	.256	0	4.46	-	-	-	-	-
4.42	N ₂ O ₄	50	RT	20:23	.053	.252	0	4.42	-	-	-	-	-
4.46	N ₂ O ₄	50	RT	20:23	.052	.258	0	4.46	-	-	-	-	-
4.43	N ₂ O ₄	450	140	20:23	.054	.156	0	14.43	-	-	-	-	-
0.97	N ₂ O ₄	450	140	20:23	.055	.260	0	10.97	-	-	-	-	-
4.19	N ₂ O ₄	450	140	20:23	.052	.156	0	14.19	-	-	-	-	-
0.75	N ₂ O ₄	450	140	20:23	.055	.256	0	10.75	-	-	-	-	-
-	-	-	-	-	-	-	-	-	-	-	-	-	-
5.80	N ₂ O ₄	450	140	20:23	.055	.154	0	5.80	-	-	-	-	-
5.82	N ₂ O ₄	450	140	20:23	.052	.152	0	5.82	-	-	-	-	-
4.44	N ₂ O ₄	450	140	20:23	.052	.250	0	4.44	-	-	-	-	-
4.51	N ₂ O ₄	450	140	20:23	.057	.266	0	4.51	-	-	-	-	-
4.44	N ₂ O ₄	450	140	20:23	.050	.252	0	4.44	-	-	-	-	-
5.86	N ₂ O ₄	450	140	20:23	.055	.152	0	5.86	-	-	-	-	-
5.91	N ₂ O ₄	450	140	20:23	.060	.162	0	5.91	-	-	-	-	-
5.79	N ₂ O ₄	450	140	20:23	.056	.152	0	5.79	-	-	-	-	-
4.39	N ₂ O ₄	450	140	20:23	.052	.256	0	4.39	-	-	-	-	-
4.46	N ₂ O ₄	450	140	20:23	.051	.252	0	4.46	-	-	-	-	-
4.42	N ₂ O ₄	450	140	20:23	.052	.248	0	4.42	-	-	-	-	-

B.


Table 1: 2219-T851 ALUMINUM IN N₂O₄
(SFB Specimen Data)

CYCLIC MARKING				FLAW SIZE AFTER MARKING		FRACTURE DATA					
TEMP(°F)	P _{max} (lb)	D/2 (in.)	CYCLES (1000)	a (in.)	2c (in.)	TEMP(°F)	a (in.)	2c (in.)	P (lb)	D/2(in.)	
RT	1,135	1.5	60	.106	.204	RT	.106	.204	4,120	2.0	
RT	1,870	1.5	30	.088	.284	RT	.088	.284	6,090	2.0	
-	-	-	-	-	-	RT	.054	.156	4,415	2.0	
-	-	-	-	-	-	RT	.050	.260	6,400	2.0	
-	-	-	-	-	-	-	-	-	-	-	
RT	1,080	1.5	20	.062	.164	RT	.054	.157	3,020	2.0	
RT	1,080	1.5	20	.064	.174	RT	.052	.152	3,020	2.0	
RT	1,660	1.5	20	.052	.248	RT	.048	.244	5,010	2.0	
RT	1,660	1.5	20	.060	.272	RT	.052	.264	5,010	2.0	
RT	1,660	1.5	20	.056	.260	RT	.052	.256	5,010	2.0	
-	-	-	-	-	-	RT	.054	.154	3,285	2.0	
-	-	-	-	-	-	RT	.052	.154	3,285	2.0	
-	-	-	-	-	-	RT	.052	.150	3,285	2.0	
-	-	-	-	-	-	RT	.052	.256	5,460	2.0	
-	-	-	-	-	-	RT	.053	.252	5,460	2.0	
-	-	-	-	-	-	RT	.052	.258	5,460	2.0	
-	-	-	-	-	-						
-	-	-	-	-	-	RT	.054	.156	4,495	2.0	
-	-	-	-	-	-	RT	.055	.260	6,560	2.0	
-	-	-	-	-	-	RT	.052	.156	4,455	2.0	
-	-	-	-	-	-	RT	.055	.256	6,500	2.0	
-	-	-	-	-	-	-	-	-	-	-	
-	-	-	-	-	-	RT	.055	.154	3,570	2.0	
-	-	-	-	-	-	RT	.052	.152	3,570	2.0	
-	-	-	-	-	-	RT	.052	.250	5,400	2.0	
-	-	-	-	-	-	RT	.057	.260	5,400	2.0	
-	-	-	-	-	-	RT	.050	.252	5,400	2.0	
-	-	-	-	-	-	RT	.055	.152	3,560	2.0	
-	-	-	-	-	-	RT	.060	.162	3,560	2.0	
-	-	-	-	-	-	RT	.056	.152	3,560	2.0	
-	-	-	-	-	-	RT	.052	.256	5,400	2.0	
-	-	-	-	-	-	RT	.051	.252	5,400	2.0	
-	-	-	-	-	-	RT	.052	.248	5,400	2.0	

SPECIMEN NUMBER	TYPE	THICK- NESS t (in.)	WIDTH W (in.)	INITIAL FLAW SIZE		σ (ksi)	Q	M_B	K_{Ti}	ENVIRON- MENT	PRESSURE (psi)
				a (in.)	2c (in.)						
9BV-9	BM	.506	1.00	.053	.154	48.9	1.576	.905	14.38	F ₂	50
9EV-10	BM	.504	1.50	.053	.256	32.6	1.250	.930	10.88	F ₂	50
9BL-9	BM	.506	1.00	.053	.158	48.9	1.544	.903	14.51	F ₂	50
9BL-10	BM	.505	1.50	.054	.262	32.6	1.244	.926	10.93	F ₂	50
9WV-9	A	.502	1.30	.049	.156	20.3	1.466	.920	6.06	F ₂	50
9WV-9	B	.502	1.30	.050	.156	20.3	1.491	.913	6.05	F ₂	50
9WV-9	C	.501	1.30	.050	.152	20.3	1.520	.916	5.98	F ₂	50
9WV-10	A	.503	2.00	.051	.248	13.2	1.250	.939	4.44	F ₂	50
9WV-10	B	.503	2.00	.052	.254	13.2	1.250	.935	4.46	F ₂	50
9WV-10	C	.502	2.00	.052	.254	13.2	1.250	.932	4.45	F ₂	50
9WL-9	A	.500	1.30	.053	.146	20.3	1.620	.903	5.82	F ₂	50
9WL-9	B	.501	1.30	.048	.154	20.3	1.460	.912	5.95	F ₂	50
9WL-9	C	.502	1.30	.052	.152	20.3	1.570	.905	5.92	F ₂	50
9WL-10	A	.503	2.00	.050	.252	13.2	1.230	.944	4.46	F ₂	50
9WL-10	B	.505	2.00	.051	.254	13.2	1.240	.940	4.46	F ₂	50
9WL-10	C	.507	2.00	.053	.258	13.2	1.250	.930	4.44	F ₂	50
9BV-11	BM	.505	1.00	.052	.155	48.9	1.544	.910	14.47	F ₂	450
9BV-12	BM	.505	1.50	.050	.258	32.6	1.212	.950	10.96	F ₂	450
9BL-11	BM	.507	1.00	.054	.157	48.9	1.542	.905	14.68	F ₂	450
9BL-12	BM	.506	1.50	.054	.262	32.6	1.244	.926	10.93	F ₂	450
9WV-11	A	.505	1.30	.052	.152	20.3	1.570	.910	5.96	F ₂	450
9WV-11	B	.505	1.30	.053	.154	20.3	1.542	.908	6.06	F ₂	450
9WV-11	C	.505	1.30	.055	.155	20.3	1.620	.898	5.95	F ₂	450
9WV-12	A	.501	2.00	.051	.249	13.2	1.250	.931	4.40	F ₂	450
9WV-12	B	.502	2.00	.052	.256	13.2	1.240	.930	4.45	F ₂	450
9WV-12	C	.502	2.00	.051	.248	13.2	1.250	.930	4.39	F ₂	450
9WL-11	A	.501	1.30	.052	.146	20.3	1.624	.908	5.85	F ₂	450
9WL-11	B	.502	1.30	.052	.157	20.3	1.528	.910	6.03	F ₂	450
9WL-11	C	.503	1.30	.056	.154	20.3	1.640	.890	5.91	F ₂	450
9WL-12	A	.501	2.00	.052	.256	13.2	1.240	.930	4.45	F ₂	450
9WL-12	B	.506	2.00	.051	.256	13.2	1.234	.943	4.50	F ₂	450
9WL-12	C	.510	2.00	.052	.262	13.2	1.230	.943	4.54	F ₂	450

1 As Calculated Using Original
Dimensions of EDM Flaw


2 Whenever Applicable Flaw Growth
Increment is Added to EDM Flaw
Dimensions


ENVIRON- MENT	PRESSURE (psig)	TEMP. (°F)	TIME (hr)	FINAL FLAW SIZE		FLAW INCREMENT Δa (in.)	K_{If} 	CYCLIC MARKING				FLAW SIZE AFTER MARKING	
				a (in.)	c (in.)			TEMP (°F)	P _{max} (lb)	D/2 (in.)	CYCLES (1000)	a (in.)	c (in.)
F ₂	50	-320	21:00	.053	.154	0	14.38	-	-	-	-	-	-
F ₂	50	-320	21:00	.053	.256	0	10.88	-	-	-	-	-	-
F ₂	50	-320	21:00	.053	.158	0	14.51	-	-	-	-	-	-
F ₂	50	-320	21:00	.054	.262	0	10.93	-	-	-	-	-	-
F ₂	50	-320	21:00	.049	.156	0	6.06	-	-	-	-	-	-
F ₂	50	-320	21:00	.050	.156	0	6.05	-	-	-	-	-	-
F ₂	50	-320	21:00	.050	.152	0	5.98	-	-	-	-	-	-
F ₂	50	-320	21:00	.051	.248	0	4.44	-	-	-	-	-	-
F ₂	50	-320	21:00	.052	.254	0	4.46	-	-	-	-	-	-
F ₂	50	-320	21:00	.052	.254	0	4.45	-	-	-	-	-	-
F ₂	50	-320	21:00	.053	.146	0	5.82	-	-	-	-	-	-
F ₂	50	-320	21:00	.048	.154	0	5.95	-	-	-	-	-	-
F ₂	50	-320	21:00	.052	.152	0	5.92	-	-	-	-	-	-
F ₂	50	-320	21:00	.050	.252	0	4.46	-	-	-	-	-	-
F ₂	50	-320	21:00	.051	.254	0	4.46	-	-	-	-	-	-
F ₂	50	-320	21:00	.053	.258	0	4.44	-	-	-	-	-	-
F ₂	450	-235	24:07	.052	.155	0	14.47	-	-	-	-	-	-
F ₂	450	-235	24:07	.050	.258	0	10.96	-	-	-	-	-	-
F ₂	450	-235	24:07	.054	.157	0	14.68	-	-	-	-	-	-
F ₂	450	-235	24:07	.054	.262	0	10.93	-	-	-	-	-	-
F ₂	450	-235	24:07	.052	.152	0	5.96	-	-	-	-	-	-
F ₂	450	-235	24:07	.053	.154	0	6.06	-	-	-	-	-	-
F ₂	450	-235	24:07	.055	.155	0	5.95	-	-	-	-	-	-
F ₂	450	-235	24:07	.051	.249	0	4.40	-	-	-	-	-	-
F ₂	450	-235	24:07	.052	.256	0	4.45	-	-	-	-	-	-
F ₂	450	-235	24:07	.051	.248	0	4.39	-	-	-	-	-	-
F ₂	450	-235	24:07	.052	.146	0	5.85	-	-	-	-	-	-
F ₂	450	-235	24:07	.052	.157	0	6.03	-	-	-	-	-	-
F ₂	450	-235	24:07	.056	.154	0	5.91	-	-	-	-	-	-
F ₂	450	-235	24:07	.052	.256	0	4.45	-	-	-	-	-	-
F ₂	450	-235	24:07	.051	.256	0	4.50	-	-	-	-	-	-
F ₂	450	-235	24:07	.052	.262	0	4.54	-	-	-	-	-	-


B.

Table 2: 2219-T851 ALUMINUM IN F₂
(SFB Specimen Data)

CYCLIC MARKING				FLAW SIZE AFTER MARKING		FRACTURE DATA					
TEMP (°F)	P _{max} (lb)	D/2 (in.)	CYCLES (1000)	a (in.)	2c (in.)	TEMP (°F)	a (in.)	2c (in.)	P (lb)	D/2 (in.)	
-	-	-	-	-	-	RT	.053	.154	4,450	2.0	
-	-	-	-	-	-	RT	.053	.256	6,480	2.0	
-	-	-	-	-	-	RT	.053	.158	4,380	2.0	
-	-	-	-	-	-	RT	.054	.262	6,520	2.0	
-	-	-	-	-	-	RT	.049	.156	3,615	2.0	
-	-	-	-	-	-	RT	.050	.156	3,615	2.0	
-	-	-	-	-	-	RT	.050	.152	3,615	2.0	
-	-	-	-	-	-	RT	.051	.248	5,300	2.0	
-	-	-	-	-	-	RT	.052	.254	5,300	2.0	
-	-	-	-	-	-	RT	.052	.254	5,300	2.0	
-	-	-	-	-	-	RT	.053	.146	3,650	2.0	
-	-	-	-	-	-	RT	.048	.154	3,650	2.0	
-	-	-	-	-	-	RT	.052	.152	3,650	2.0	
-	-	-	-	-	-	RT	.050	.252	5,240	2.0	
-	-	-	-	-	-	RT	.051	.254	5,240	2.0	
-	-	-	-	-	-	RT	.053	.258	5,240	2.0	
-	-	-	-	-	-						
-	-	-	-	-	-	RT	.052	.155	4,490	2.0	
-	-	-	-	-	-	RT	.050	.258	6,540	2.0	
-	-	-	-	-	-	RT	.054	.157	4,450	2.0	
-	-	-	-	-	-	RT	.054	.262	6,560	2.0	
-	-	-	-	-	-	RT	.052	.152	3,350	2.0	
-	-	-	-	-	-	RT	.053	.154	3,350	2.0	
-	-	-	-	-	-	RT	.055	.155	3,350	2.0	
-	-	-	-	-	-	RT	.051	.249	5,140	2.0	
-	-	-	-	-	-	RT	.052	.256	5,140	2.0	
-	-	-	-	-	-	RT	.051	.248	5,140	2.0	
-	-	-	-	-	-	RT	.052	.146	3,470	2.0	
-	-	-	-	-	-	RT	.052	.157	3,470	2.0	
-	-	-	-	-	-	RT	.056	.154	3,470	2.0	
-	-	-	-	-	-	RT	.052	.256	5,000	2.0	
-	-	-	-	-	-	RT	.051	.256	5,000	2.0	
-	-	-	-	-	-	RT	.052	.262	5,000	2.0	

SPECIMEN NUMBER	TYPE	THICK- NESS t (in.)	WIDTH W (in.)	INITIAL FLAW SIZE		σ (ksi)	Q	M _B	 K _{II}	ENVIRON- MENT	PR
				a (in.)	2c (in.)						
9BV-5	BM	.507	1.00	.053	.157	48.9	1.552	.906	14.29	C1F ₅	
9BV-5	BM	.506	1.50	.055	.262	32.6	1.254	.923	10.98	C1F ₅	
9BL-5	BM	.507	1.00	.056	.158	48.9	1.615	.895	14.46	C1F ₅	
9BL-6	BM	.500	1.50	.056	.262	32.6	1.266	.920	10.99	C1F ₅	
9WV-5	A	.504	1.30	.054	.160	20.3	1.550	.900	6.04	C1F ₅	
9WV-5	B	.503	1.30	.052	.158	20.3	1.520	.910	6.06	C1F ₅	
9WV-5	C	.504	1.30	.053	.158	20.3	1.540	.907	6.05	C1F ₅	
9WV-6	A	.501	2.00	.052	.252	13.2	1.250	.930	4.44	C1F ₅	
9WV-6	B	.502	2.00	.053	.256	13.2	1.250	.926	4.46	C1F ₅	
9WV-6	C	.502	2.00	.052	.252	13.2	1.250	.930	4.44	C1F ₅	
9WL-5	A	.502	1.30	.055	.156	20.3	1.610	.892	5.93	C1F ₅	
9WL-5	B	.503	1.30	.054	.157	20.3	1.576	.900	5.99	C1F ₅	
9WL-5	C	.503	1.30	.054	.153	20.3	1.610	.897	5.90	C1F ₅	
9WL-6	A	.505	2.00	.052	.250	13.2	1.252	.930	4.44	C1F ₅	
9WL-6	B	.503	2.00	.052	.254	13.2	1.250	.931	4.44	C1F ₅	
9WL-6	C	.500	2.00	.052	.253	13.2	1.250	.930	4.44	C1F ₅	
9BV-7	BM	.506	1.00	.056	.156	48.9	1.634	.890	14.28	C1F ₅	
9BV-8	BM	.504	1.50	.056	.264	32.6	1.250	.918	11.03	C1F ₅	
9BL-7	BM	.508	1.00	.055	.158	48.9	1.592	.908	14.63	C1F ₅	
9BL-8	BM	.506	1.50	.052	.260	32.6	1.230	.932	10.88	C1F ₅	
9WV-7	A	.498	1.30	.050	.152	20.3	1.520	.920	6.00	C1F ₅	
9WV-7	B	.498	1.30	.052	.160	20.3	1.505	.910	6.09	C1F ₅	
9WV-7	C	.498	1.30	.052	.152	20.3	1.570	.909	5.95	C1F ₅	
9WV-8	A	.502	2.00	.052	.252	13.2	1.250	.920	4.39	C1F ₅	
9WV-8	B	.502	2.00	.050	.255	13.2	1.220	.944	4.47	C1F ₅	
9WV-8	C	.503	2.00	.051	.256	13.2	1.230	.940	4.47	C1F ₅	
9WL-7	A	.501	1.30	.052	.150	20.3	1.588	.909	5.92	C1F ₅	
9WL-7	B	.500	1.30	.052	.155	20.3	1.543	.910	6.01	C1F ₅	
9WL-7	C	.501	2.00	.052	.148	20.3	1.600	.908	5.89	C1F ₅	
9WL-8	A	.501	2.00	.052	.250	13.2	1.250	.920	4.39	C1F ₅	
9WL-8	B	.502	2.00	.053	.252	13.2	1.260	.918	4.40	C1F ₅	
9WL-8	C	.503	2.00	.053	.251	13.2	1.260	.918	4.40	C1F ₅	

 As Calculated Using Original
Dimensions of EDM Flaw

 Whenever Applicable Flaw Growth
Increment is Added to EDM Flaw
Dimensions

A.

I	ENVIRON- MENT	PRESSURE (psig)	TEMP. (°)	TIME (hr)	FINAL FLAW SIZE		FLAW INCREMENT Δa (in.)	K_{If}	CYCLIC MARKING				FLAW AFTER
					a (in.)	2c (in.)			TEMP (°F)	P_{max} (lb)	D/2 (in.)	CYCLES (1000)	a (in.)
29	C1F ₅	50	RT	17:47	.053	.157	0	14.29	-	-	-	-	-
98	C1F ₅	50	RT	17:47	.055	.262	0	10.98	-	-	-	-	-
46	C1F ₅	50	RT	17:47	.056	.158	0	14.46	-	-	-	-	-
99	C1F ₅	50	RT	17:47	.056	.262	0	10.98	-	-	-	-	-
04	C1F ₅	50	RT	17:47	.054	.160	0	6.04	-	-	-	-	-
06	C1F ₅	50	RT	17:47	.052	.158	0	6.06	-	-	-	-	-
05	C1F ₅	50	RT	17:47	.053	.158	0	6.05	-	-	-	-	-
44	C1F ₅	50	RT	17:47	.052	.252	0	4.44	-	-	-	-	-
46	C1F ₅	50	RT	17:47	.053	.256	0	4.46	-	-	-	-	-
44	C1F ₅	50	RT	17:47	.052	.252	0	4.44	-	-	-	-	-
93	C1F ₅	50	RT	17:47	.055	.152	0	5.93	-	-	-	-	-
99	C1F ₅	50	RT	17:47	.054	.157	0	5.99	-	-	-	-	-
90	C1F ₅	50	RT	17:47	.054	.153	0	5.90	-	-	-	-	-
44	C1F ₅	50	RT	17:47	.052	.250	0	4.44	-	-	-	-	-
44	C1F ₅	50	RT	17:47	.052	.254	0	4.44	-	-	-	-	-
44	C1F ₅	50	RT	17:47	.052	.253	0	4.44	-	-	-	-	-
28	C1F ₅	450	140	18:40	.056	.156	0	14.28	-	-	-	-	-
03	C1F ₅	450	140	18:40	.056	.264	0	11.03	-	-	-	-	-
63	C1F ₅	450	140	18:40	.055	.158	0	14.63	-	-	-	-	-
88	C1F ₅	450	140	18:40	.052	.260	0	10.88	-	-	-	-	-
00	C1F ₅	450	140	18:40	.050	.152	0	6.00	-	-	-	-	-
09	C1F ₅	450	140	18:40	.052	.160	0	6.09	-	-	-	-	-
95	C1F ₅	450	140	18:40	.052	.152	0	5.95	-	-	-	-	-
39	C1F ₅	450	140	18:40	.052	.252	0	4.39	-	-	-	-	-
47	C1F ₅	450	140	18:40	.050	.255	0	4.47	-	-	-	-	-
47	C1F ₅	450	140	18:40	.051	.256	0	4.47	-	-	-	-	-
92	C1F ₅	450	140	18:40	.052	.150	0	5.92	-	-	-	-	-
01	C1F ₅	450	140	18:40	.052	.155	0	6.01	-	-	-	-	-
89	C1F ₅	450	140	18:40	.052	.148	0	5.89	-	-	-	-	-
39	C1F ₅	450	140	18:40	.052	.250	0	4.39	-	-	-	-	-
40	C1F ₅	450	140	18:40	.053	.252	0	4.40	-	-	-	-	-
40	C1F ₅	450	140	18:40	.053	.251	0	4.40	-	-	-	-	-

B.

Table 3: 2019-T851 ALUMINUM IN ClF_5
(SFB Specimen Data)

CYCLIC MARKING				FLAW SIZE AFTER MARKING		FRACTURE DATA					
TEMP (°F)	P _{max} (lb)	D/2 (in.)	CYCLES (1000)	a (in.)	2c (in.)	TEMP (°F)	a (in.)	2c (in.)	P (lb)	D/2 (in.)	
-	-	-	-	-	-	RT	.053	.157	4,390	2.0	
-	-	-	-	-	-	RT	.055	.262	6,460	2.0	
-	-	-	-	-	-	RT	.056	.158	4,410	2.0	
-	-	-	-	-	-	RT	.056	.262	6,260	2.0	
-	-	-	-	-	-	RT	.054	.160	3,390	2.0	
-	-	-	-	-	-	RT	.052	.158	3,390	2.0	
-	-	-	-	-	-	RT	.053	.158	3,390	2.0	
-	-	-	-	-	-	RT	.052	.252	4,900	2.0	
-	-	-	-	-	-	RT	.053	.256	4,900	2.0	
-	-	-	-	-	-	RT	.052	.252	4,900	2.0	
-	-	-	-	-	-	RT	.055	.152	3,340	2.0	
-	-	-	-	-	-	RT	.054	.157	3,340	2.0	
-	-	-	-	-	-	RT	.054	.153	3,340	2.0	
-	-	-	-	-	-	RT	.052	.250	5,400	2.0	
-	-	-	-	-	-	RT	.052	.254	5,400	2.0	
-	-	-	-	-	-	RT	.052	.253	5,400	2.0	
-	-	-	-	-	-						
-	-	-	-	-	-	RT	.056	.156	4,415	2.0	
-	-	-	-	-	-	RT	.056	.264	6,380	2.0	
-	-	-	-	-	-	RT	.055	.158	4,535	2.0	
-	-	-	-	-	-	RT	.052	.260	6,500	2.0	
-	-	-	-	-	-	RT	.050	.152	3,630	2.0	
-	-	-	-	-	-	RT	.052	.160	3,630	2.0	
-	-	-	-	-	-	RT	.052	.152	3,630	2.0	
-	-	-	-	-	-	RT	.052	.252	5,300	2.0	
-	-	-	-	-	-	RT	.050	.255	5,300	2.0	
-	-	-	-	-	-	RT	.051	.256	5,300	2.0	
-	-	-	-	-	-	RT	.052	.150	3,730	2.0	
-	-	-	-	-	-	RT	.052	.155	3,730	2.0	
-	-	-	-	-	-	RT	.052	.148	3,730	2.0	
-	-	-	-	-	-	RT	.052	.250	5,000	2.0	
-	-	-	-	-	-	RT	.053	.252	5,000	2.0	
-	-	-	-	-	-	RT	.053	.251	5,000	2.0	

5.1.2 2021-T81 Aluminum and N_2O_4

The 2021-T81 aluminum was tested in N_2O_4 only. The test specimens, however, consisted of a.c. as well as d.c. weldments prepared by the Lockheed Missiles and Space Company in their assessments of potential use of the alloy in space hardware. Configuration of test specimens used is shown in Figures 19 and 20 for base metal and for a.c. and d.c. weldments, respectively. The test setup for the SFB specimens used four- rather than three-point bending because of the surface irregularities along the weld deposit. There were two surface flaws in each weld specimen but only one flaw in each base metal specimen. Pertinent specimen dimensions and flaw sizes, together with calculated stress intensity values and test conditions, are listed in TABLE 4. The test lasted 20:25 hours. Temperature and pressure in the test chamber were 100 psi and 140°F.

5.1.3 6Al-4V(ELI) Titanium

The 6Al-4V(ELI) titanium was tested in environments of liquid and vapor phases of F_2 and ClF_5 . With F_2 and 6Al-4V(ELI) titanium, there were two pressure-temperature combinations in one test run, with ClF_5 and 6Al-4V(ELI) titanium, a total of five pressure-temperature combinations and a total of three test runs. Furthermore, during the last test run of the titanium with ClF_5 , a set of DCB specimens was added. Configuration of the SFB titanium base metal specimen is shown in Figure 21 for high-stress and low-stress levels. Each base metal specimen contained one surface flaw. Configurations of high-stress and low-stress SFB weldment specimens are shown in Figure 22. Weld location in DCB specimen is illustrated in Figure 29. At the time of DCB specimen fabrication there was not enough material left to place weld longitudinally within the specimen. The F_2 and ClF_5 pressurization systems used for aluminum were also used for titanium specimens after proper cleaning and passivation procedure to eliminate possible interaction between corrosion products of the two materials.

K _{Ti}	ENVIRON- MENT	PRESSURE (psig)	TEMP. (°F)	TIME (hr)	FINAL FLAW SIZE		FLAW INCREMENT Δa(in.)	K _{If}	CYCLIC MARKING				FL AFTER
					a (in.)	c (in.)			TEMP (°F)	P _{max} (lb)	D/2 (in.)	CYCLES (1000)	a (in.)
13.7	N ₂ O ₄	100	140	20:25	.065	.190	0	13.7	RT	340	2.0	20	.06
10.8	N ₂ O ₄	100	140	20:25	.066	.188	0	10.8	-	-	-	-	-
7.8	N ₂ O ₄	100	140	20:25	.073	.200	0	7.8	RT	340	2.0	20	.07
-	N ₂ O ₄	100	140	20:25	-	-	-	-	RT	340	2.0	20	-
6.0	N ₂ O ₄	100	140	20:25	.065	.185	0	6.0	-	-	-	-	-
-	N ₂ O ₄	100	140	20:25	-	-	-	-	-	-	-	-	-
8.0	N ₂ O ₄	100	140	20:25	.074	.235	0	8.0	RT	340	2.0	30	.07
-	N ₂ O ₄	100	140	20:25	-	-	-	-	RT	340	2.0	30	-
6.4	N ₂ O ₄	100	140	20:25	.065	.187	0	6.4	-	-	-	-	-
-	N ₂ O ₄	100	140	20:25	-	-	-	-	-	-	-	-	-
13.7	N ₂ O ₄	100	140	20:25	.064	.189	0	13.7	RT	340	2.0	30	.06
10.8	N ₂ O ₄	100	140	20:25	.065	.187	0	10.8	-	-	-	-	-
8.0	N ₂ O ₄	100	140	20:25	.076	.202	0	8.0	RT	340	2.0	30	.08
-	N ₂ O ₄	100	140	20:25	-	-	-	-	RT	340	2.0	30	-
5.9	N ₂ O ₄	100	140	20:25	.067	.188	0	5.9	-	-	-	-	-
-	N ₂ O ₄	100	140	20:25	-	-	-	-	-	-	-	-	-
7.7	N ₂ O ₄	100	140	20:25	.068	.210	0	7.7	RT	340	2.0	20	.08
-	N ₂ O ₄	100	140	20:25	-	-	-	-	RT	-	2.0	-	-
6.4	N ₂ O ₄	100	140	20:25	.066	.188	0	6.4	-	-	-	-	-
-	N ₂ O ₄	100	140	20:25	-	-	-	-	-	-	-	-	-

B.

Table 4: 2021-T81 ALUMINUM IN N_2O_4
(SFB Specimen Data)

[illegible]

5.1.3.1 F₂ and 6Al-4V(ELI) Titanium


TABLE 5 lists pertinent specimen dimensions, flaw sizes, and calculated stress-intensity values, together with test conditions for this test run. Gaseous fluorine was liquified in the test chamber, which was submerged in liquid nitrogen at atmospheric pressure. Once the sufficient quantity of fluorine had been admitted to each test chamber, the system was pressurized to 450 psig in the high-pressure chamber and 50 psig in the low-pressure chamber. The high-pressure chamber was then warmed up to -230°F and held at that temperature for the duration of the test run. The low-pressure chamber was left at -320°F. Upon conclusion of the test run, the specimens were removed from the chambers and examined.


The 6Al-4V(ELI) titanium specimens exposed to fluorine vapors at 450 psig and -230°F temperature showed marked staining along the specimen surfaces. However, titanium specimens submerged in liquid fluorine remained relatively clean. High-stress specimens were subjected to low-stress flexing to mark EDM flaws, then fractured to expose fracture faces for fractographic examination. Laboratory examination of stained specimens failed to reveal any corrosion penetration into the material. Low-stress specimens were fractured without cyclic marking and examined. No flaw growth was detected.


5.1.3.2 ClF₅ and 6Al-4V(ELI) Titanium (First Test Run)

Pertinent specimen dimensions, flaw sizes, and test conditions, together with calculated stress-intensity values, are listed in TABLE 6.


The chlorine pentafluoride test run with 6Al-4V(ELI) titanium was to be conducted like the 2219-T851 aluminum test run. The pressure and temperature conditions were to be 450 psi and 140°F in the high-pressure chamber and 50 psi and 50°F in the lower chamber. One hour before completion of the scheduled 16-hour test run, the high-pressure chamber suddenly exploded, wrecking the test setup and scattering debris over a wide area. The rise of temperature and pressure as recorded by the test instruments was instantaneous.

SPECIMEN NUMBER	TYPE	THICK- NESS t (in.)	WIDTH W (in.)	INITIAL FLAW SIZE		σ (ksi)	Q	M_B	K_{Ii} 	ENVIRON- MENT	RES (psi)	
				a (in.)	2c (in.)							
TBV-9	BM	.255	1.0	.034	.144	143.00	1.21	.882	37.5	F ₂	50	5
TBV-10	BM	.255	1.5	.035	.146	98.50	1.34	.880	24.8	F ₂	50	8
TBL-9	BM	.255	1.0	.038	.149	143.00	1.26	.864	38.6	F ₂	50	6
TBL-10	BM	.246	1.5	.038	.150	98.50	1.38	.860	24.9	F ₂	50	9
TWV-9	A	.236	1.3	.034	.143	124.00	1.23	.870	31.8	F ₂	50	8
TWV-9	B	.236	1.3	.035	.143	124.00	1.25	.860	31.6	F ₂	50	6
TWV-9	C	.236	1.3	.036	.143	124.00	1.27	.860	31.8	F ₂	50	6
TWV-10	A	.236	2.0	.037	.143	80.60	1.42	.850	19.6	F ₂	50	6
TWV-10	B	.236	2.0	.040	.152	80.60	1.43	.848	20.3	F ₂	50	3
TWV-10	C	.236	2.0	.037	.143	80.66	1.42	.852	19.7	F ₂	50	7
TWL-9	A	.233	1.3	.035	.145	128.90	1.24	.864	33.1	F ₂	50	1
TWL-9	B	.233	1.3	.035	.145	128.90	1.24	.864	33.1	F ₂	50	1
TWL-9	C	.233	1.3	.034	.146	128.90	1.22	.870	33.2	F ₂	50	2
TWL-10	A	.237	2.0	.035	.134	79.60	1.42	.870	19.3	F ₂	50	3
TWL-10	B	.237	2.0	.034	.136	79.60	1.39	.870	19.2	F ₂	50	2
TWL-10	C	.237	2.0	.035	.134	79.60	1.42	.870	19.3	F ₂	50	3
TBV-11	BM	.254	1.0	.037	.144	143.00	1.27	.872	37.7	F ₂	450	7
TBV-12	BM	.255	1.5	.037	.150	98.50	1.37	.875	25.1	F ₂	450	1
TBL-11	BM	.255	1.0	.035	.149	143.00	1.21	.884	38.0	F ₂	450	0
TBL-12	BM	.257	1.5	.036	.136	96.20	1.42	.870	23.6	F ₂	450	6
TWV-11	A	.235	1.3	.035	.147	125.60	1.24	.870	32.5	F ₂	450	5
TWV-11	B	.235	1.3	.036	.149	125.60	1.25	.858	32.4	F ₂	450	4
TWV-11	C	.235	1.3	.036	.148	125.60	1.25	.858	32.4	F ₂	450	4
TWV-12	A	.234	2.0	.037	.146	82.60	1.39	.850	20.3	F ₂	450	3
TWV-12	B	.234	2.0	.036	.148	82.60	1.36	.856	20.4	F ₂	450	4
TWV-12	C	.234	2.0	.034	.149	82.60	1.31	.873	20.6	F ₂	450	6
TWL-11	A	.233	1.3	.034	.140	128.90	1.24	.873	33.0	F ₂	450	0
TWL-11	B	.233	1.3	.034	.140	128.90	1.24	.873	33.0	F ₂	450	0
TWL-11	C	.233	1.3	.034	.140	128.90	1.24	.873	33.0	F ₂	450	0
TWL-12	A	.234	2.0	.037	.150	82.60	1.37	.852	20.5	F ₂	450	5
TWL-12	B	.234	2.0	.038	.149	82.60	1.40	.844	20.3	F ₂	450	3
TWL-12	C	.234	2.0	.038	.149	82.60	1.40	.844	20.3	F ₂	450	3

1  As Calculated Using Original
Dimensions of EDM Flaw

2  Whenever Applicable Flow Growth
Increment Is Added to EDM Flaw
Dimensions


A.

ENVIRONMENT	PRESSURE (psig)	TEMP (°F)	TIME (hrs.)	FINAL FLAW SIZE		FLAW INCREMENT a (in.)	K _{If} 	CYCLIC MARKING				FLAW AFTER a (in.)	C
				a (in.)	2c (in.)			TEMP (°F)	P _{max} (1b)	D (in.)	CYCLES (1000)		
F ₂	50	-320	24:50	.034	.144	0	37.5	RT	1,235	3.0	71	.126	
F ₂	50	-320	24:50	.035	.146	0	24.8	-	-	-	-	-	
F ₂	50	-320	24:50	.038	.149	0	38.6	RT	1,235	3.0	50	.068	
F ₂	50	-320	24:50	.038	.150	0	24.9	-	-	-	-	-	
F ₂	50	-320	24:50	.034	.143	0	31.8	RT	1,316	3.0	34	.136	
F ₂	50	-320	24:50	.035	.143	0	31.6	RT	1,316	3.0	34	.110	
F ₂	50	-320	24:50	.036	.143	0	31.8	RT	1,316	3.0	34	.107	
F ₂	50	-320	24:50	.037	.143	0	19.6	-	-	-	-	-	
F ₂	50	-320	24:50	.040	.152	0	20.3	-	-	-	-	-	
F ₂	50	-320	24:50	.037	.143	0	19.7	-	-	-	-	-	
F ₂	50	-320	24:50	.035	.145	0	33.1	RT	1,316	3.0	15	.151	
F ₂	50	-320	24:50	.035	.145	0	33.1	RT	1,316	3.0	15	.149	
F ₂	50	-320	24:50	.034	.146	0	33.2	RT	1,316	3.0	15	.096	
F ₂	50	-320	24:50	.035	.134	0	19.3	-	-	-	-	-	
F ₂	50	-320	24:50	.034	.136	0	19.2	-	-	-	-	-	
F ₂	50	-320	24:50	.035	.134	0	19.3	-	-	-	-	-	
F ₂	450	-230	24:50	.037	.144	0	37.7	RT	1,235	3.0	45	.121	
F ₂	450	-230	24:50	.037	.150	0	25.1	-	-	-	-	-	
F ₂	450	-230	24:50	.035	.149	0	38.0	RT	1,124	3.0	40	.056	
F ₂	450	-230	24:50	.036	.136	0	23.6	-	-	-	-	-	
F ₂	450	-230	24:50	.035	.147	0	32.5	-	-	-	-	-	
F ₂	450	-230	24:50	.036	.149	0	32.4	-	-	-	-	-	
F ₂	450	-230	24:50	.036	.148	0	32.4	-	-	-	-	-	
F ₂	450	-230	24:50	.037	.146	0	20.3	-	-	-	-	-	
F ₂	450	-230	24:50	.036	.148	0	20.4	-	-	-	-	-	
F ₂	450	-230	24:50	.034	.149	0	20.6	-	-	-	-	-	
F ₂	450	-230	24:50	.034	.140	0	33.0	RT	1,316	3.0	24	.137	
F ₂	450	-230	24:50	.034	.140	0	33.0	RT	1,316	3.0	24	.134	
F ₂	450	-230	24:50	.034	.140	0	33.0	RT	1,316	3.0	24	.160	
F ₂	450	-230	24:50	.037	.150	0	20.5	-	-	-	-	-	
F ₂	450	-230	24:50	.038	.149	0	20.3	-	-	-	-	-	
F ₂	450	-230	24:50	.038	.149	0	20.3	-	-	-	-	-	

B.

Table 5: 6Al-4V(ELI) TITANIUM IN F₂
(SFB Specimen Data)

CYCLIC MARKING				FLAW SIZE AFTER MARKING		FRACTURE DATA					
°F)	P _{max} (lb)	D (in.)	CYCLES (1000)	a (in.)	2c (in.)	TEMP (°F)	a (in.)	2c (in.)	P (lb)	D (in.)	
	1,235	3.0	71	.126	.405	RT	.126	.405	2,800	3.0	
	-	-	-	-	-	RT	-	-	6,070	3.0	
	1,235	3.0	50	.068	.168	RT	.068	.168	3,220	3.0	
	-	-	-	-	-	RT	-	-	5,680	3.0	
	1,316	3.0	34	.136	-	RT	.136	-	2,080	3.0	
	1,316	3.0	34	.110	.320	RT	.110	.320	2,080	3.0	
	1,316	3.0	34	.107	.340	RT	.107	.340	2,080	3.0	
	-	-	-	-	-	RT	.037	.143	5,930	3.0	
	-	-	-	-	-	RT	.040	.152	5,930	3.0	
	-	-	-	-	-	RT	.037	.143	5,930	3.0	
	1,316	3.0	15	.151	-	RT	.151	-	1,790	3.0	
	1,316	3.0	15	.149	-	RT	.149	-	1,790	3.0	
	1,316	3.0	15	.096	.310	RT	.096	-	1,790	3.0	
	-	-	-	-	-	RT	.035	.134	6,020	3.0	
	-	-	-	-	-	RT	.034	.136	6,020	3.0	
	-	-	-	-	-	RT	.035	.134	6,020	3.0	
	1,235	3.0	45	.121	.400	RT	.121	.400	2,540	3.0	
	-	-	-	-	-	RT	.037	.150	5,770	3.0	
	1,124	3.0	40	.056	.160	RT	.056	.160	3,290	3.0	
	-	-	-	-	-	RT	.036	.136	5,660	3.0	
	-	-	-	-	-	-	-	-	-	-	
	-	-	-	-	-	-	-	-	-	-	
	-	-	-	-	-	-	-	-	-	-	
	-	-	-	-	-	-	-	-	-	-	
	-	-	-	-	-	-	-	-	-	-	
	-	-	-	-	-	-	-	-	-	-	
	1,316	3.0	24	.137	-	RT	.137	-	1,200	3.0	
	1,316	3.0	24	.134	.380	RT	.134	.380	1,200	3.0	
	1,316	3.0	24	.160	-	RT	.160	-	1,200	3.0	
	-	-	-	-	-	RT	-	-	5,935	3.0	
	-	-	-	-	-	RT	-	-	5,935	3.0	
	-	-	-	-	-	RT	-	-	5,935	3.0	

SPECIMEN NUMBER	TYPE	THICK- NESS t (in.)	WIDTH W (in.)	INITIAL FLAW SIZE		σ (ksi)	Q	M_B	K_{I1} 	ENVIRON- MENT	PRESSURE (psig)	ENVIRONMENTAL MATERIAL
				a (in.)	2c (in.)							
TBV-1	BM	.255	1.0	.034	.149	143.00	1.19	.88	38.2	C1F ₅	50	C
TBV-2	BM	.253	1.5	.039	.150	146.50	1.28	.85	38.7	C1F ₅	50	C
TBL-1	BM	.255	1.0	.039	.150	97.80	1.40	.84	24.9	C1F ₅	50	C
TBL-2	BM	.255	1.5	.033	.140	98.50	1.32	.90	24.8	C1F ₅	50	C
TWV-1	A	.235	1.3	.035	.133	134.00	1.30	.85	33.2	C1F ₅	50	C
TWV-1	B	.235	1.3	.034	.142	134.00	1.22	.87	34.6	C1F ₅	50	C
TWV-1	C	.235	1.3	.033	.141	134.00	1.20	.85	33.6	C1F ₅	50	C
TWV-2	A	.236	2.0	.034	.144	130.50	1.21	.86	33.2	C1F ₅	50	C
TWV-2	B	.236	2.0	.035	.148	130.50	1.21	.85	33.4	C1F ₅	50	C
TWV-2	C	.236	2.0	.040	.153	130.50	1.29	.83	33.8	C1F ₅	50	C
TWL-1	A	.237	1.3	.035	.140	83.00	1.38	.85	19.85	C1F ₅	50	C
TWL-1	B	.237	1.3	.033	.150	83.00	1.29	.87	20.45	C1F ₅	50	C
TWL-1	C	.237	1.3	.035	.142	83.00	1.37	.85	20.00	C1F ₅	50	C
TWL-2	A	.230	2.0	.036	.139	88.00	1.40	.82	20.40	C1F ₅	50	C
TWL-2	B	.230	2.0	.039	.152	88.00	1.39	.80	20.85	C1F ₅	50	C
TWL-2	C	.230	2.0	-	-	88.00	-	-	-	C1F ₅	50	C
TBV-3	BM	.253	1.0							C1F ₅	450	C
TBV-4	BM	.255	1.5							C1F ₅	450	C
TBL-3	BM	.255	1.0							C1F ₅	450	C
TBL-4	BM	.255	1.5							C1F ₅	450	C
TWV-3	A	.236	1.3							C1F ₅	450	C
TWV-3	B	.236	1.3							C1F ₅	450	C
TWV-3	C	.236	1.3							C1F ₅	450	C
TWV-4	A	.235	2.0							C1F ₅	450	C
TWV-4	B	.235	2.0							C1F ₅	450	C
TWV-4	C	.235	2.0							C1F ₅	450	C
TWL-3	A	.238	1.3							C1F ₅	450	C
TWL-3	B	.238	1.3							C1F ₅	450	C
TWL-3	C	.238	1.3							C1F ₅	450	C
TWL-4	A	.235	2.0							C1F ₅	450	C
TWL-4	B	.235	2.0							C1F ₅	450	C
TWL-4	C	.235	2.0							C1F ₅	450	C

VERY SIMILAR
TO THE VALUES ABOVE

1 As Calculated Using Original
Dimensions of EDM Flaw

2 Whenever Applicable Flaw Growth
Increment Is Added to EDM Flaw
Dimensions

A.

1

[illegible]

THESE SPECIMENS WERE
IN THIRD C1 F 5

It was presumed that during the 15-hour test time, the material slowly reacted with the ClF_5 , causing the cracks to grow, and eventually led to fracture of one of the prestressed specimen assemblies. Upon fracture, it is speculated that the broken specimen assembly impacted upon adjacent specimens or the pressure chamber wall and started the spontaneous reaction. The conditions in the high-pressure chamber just prior to the accident were 450 psi pressure and 146°F temperature. A general view of the test apparatus just after the explosion is shown in Figure 46. A close-up view of the test chamber and the only two remaining specimen assemblies from the high-pressure chamber are shown in Figures 47 and 48.

5.1.3.3 ClF_5 and 6Al-4V(ELI) Titanium (Second Test Run)

The second test run involving ClF_5 and 6Al-4V(ELI) titanium was conducted to determine the conditions that led to explosion during the first test run. The requirements for pressure-temperature combinations were set at 450 psi and 146°F for the high-pressure chamber and 200 psi and 100°F in the low-pressure chamber. The duration of the test run was to be limited to approximately 6 hours. Each chamber was instrumented for sonic pickup of noises that could indicate specimen fracture. The temperatures selected were to duplicate conditions existing in the high-pressure chamber on one hand and to provide intermediate temperature ranges between 50 and 146°F in case the high-pressure chamber exploded again. The pressure in the low-pressure chamber was raised to its maximum allowable of 200 psi, which was thought to provide a closer simulation of the high-pressure chamber. Pertinent specimen dimensions and test data are summarized in TABLE 7.

The second test run was completed as scheduled, but malfunction of the heating unit limited the test temperature of the high-pressure chamber to 138°F , or 8°F below the target temperature. There were no sonic pickups. The test run was terminated after 8 hours. cursory examination of the specimens failed to reveal any signs of corrosion attack. The specimens were then to be flexed and fractured for fractographic examination. Failure to reach target temperature in the high-pressure chamber and absence of superficial




Figure 46: GENERAL VIEW OF THE TEST APPARATUS AFTER EXPLOSION



Figure 47: CLOSE-UP VIEW OF HIGH PRESSURE TEST CHAMBER




Figure 48: CLOSE-UP VIEW OF THE ONLY TWO REMAINING SPECIMEN ASSEMBLIES

SPECIMEN NUMBER	TYPE	THICK- NESS t (in.)	WIDTH W (in.)	INITIAL FLAW SIZE		(ksi)	Q	M _B	K _{II} 	ENVIRON- MENT	PRESS. (psi)
				a (in.)	2c (in.)						
TBV-5	BM	.255	1.0	.032	.142	143.00	1.18	.90	37.5	ClF ₅	250
TBV-6	BM	.256	1.5	.032	.142	98.50	1.27	.90	25.0	ClF ₅	250
TBL-5	BM	.255	1.0	.032	.142	143.00	1.18	.90	37.5	ClF ₅	250
TBL-6	BM	.256	1.5	.033	.144	98.50	1.31	.89	24.7	ClF ₅	250
TWV-5	A	.235	1.3	.0345	.142	125.60	1.23	.87	32.2	ClF ₅	250
TWV-5	B	.235	1.3	.034	.143	125.60	1.23	.87	32.2	ClF ₅	250
TWV-5	C	.235	1.3	.032	.141	125.60	1.20	.88	32	ClF ₅	250
TWV-6	A	-	1.5	-	-	98.50	-	-	-	ClF ₅	250
TWV-6	B	-	1.5	-	-	98.50	-	-	-	ClF ₅	250
TWV-6	C	-	1.5	-	-	98.50	-	-	-	ClF ₅	250
TWL-5	A	.230	1.3	.034	.140	134.00	1.23	.87	34.2	ClF ₅	250
TWL-5	B	.230	1.3	.035	.141	134.00	1.25	.86	34.0	ClF ₅	250
TWL-5	C	.230	1.3	.034	.142	134.00	1.22	.87	34.0	ClF ₅	250
TWL-6	A	-	1.5	-	-	98.50	-	-	-	ClF ₅	250
TWL-6	B	-	1.5	-	-	98.50	-	-	-	ClF ₅	250
TWL-6	C	-	1.5	-	-	98.50	-	-	-	ClF ₅	250
TBV-7	BM	.258	1.0	.034	.141	143.00	1.22	.89	37.6	ClF ₅	450
TBV-8	BM	.255	1.5	.034	.143	98.50	1.34	.89	24.8	ClF ₅	450
TBL-7	BM	.250	1.0	.033	.142	143.00	1.19	.90	37.8	ClF ₅	450
TBL-8	BM	.258	1.5	.035	.143	98.50	1.35	.88	24.8	ClF ₅	450
TWV-7	A	.236	1.3	.032	.130	124.00	1.25	.88	31.0	ClF ₅	450
TWV-7	B	.236	1.3	.032	.142	124.00	1.19	.89	32.1	ClF ₅	450
TWV-7	C	.236	1.3	.032	.140	124.00	1.20	.88	31.7	ClF ₅	450
TWV-8	A	-	1.5	-	-	98.50	-	-	-	ClF ₅	450
TWV-8	B	-	1.5	-	-	98.50	-	-	-	ClF ₅	450
TWV-8	C	-	1.5	-	-	98.50	-	-	-	ClF ₅	450
TWL-7	A	.230	1.3	-	-	134.00	-	-	-	ClF ₅	450
TWL-7	B	.230	1.3	.036	.140	134.00	1.27	.85	33.9	ClF ₅	450
TWL-7	C	.230	1.3	.034	.146	134.00	1.20	.86	34.3	ClF ₅	450
TWL-8	A	-	1.5	-	-	98.50	-	-	-	ClF ₅	450
TWL-8	B	-	1.5	-	-	98.50	-	-	-	ClF ₅	450
TWL-8	C	-	1.5	-	-	98.50	-	-	-	ClF ₅	450

1 As Calculated Using Original
Dimensions of EDM Flaw

2 Whenever Applicable Flaw Growth
Increment Is Added to EDM Flaw
Dimensions

ENVIRON- MENT	PRESSURE (psig)	TEMP. (°F)	TIME (hr)	FINAL FLAW SIZE		FLAW INCREMENT Δa (in.)	K_{If} 	CYCLIC MARKING				FLAW AFTER a (in.)	IP(°F)
				a (in.)	2c (in.)			TEMP(°F)	P_{max} (lb)	(in.)	CYCLES (1,000)		
ClF ₅	250	110	8:00	.032	.142	0	37.5	RT	1,235	1.5	141	.135	RT
ClF ₅	250	110	8:00	.032	.142	0	25.0	-	-	-	-	-	-
ClF ₅	250	110	8:00	.032	.142	0	37.5	RT	1,124	1.5	154	.034	RT
ClF ₅	250	110	8:00	.033	.144	0	24.7	-	-	-	-	-	-
ClF ₅	250	110	8:00	.034	.142	0	32.2	RT	1,316	1.5	35	.050	RT
ClF ₅	250	110	8:00	.034	.143	0	32.2	RT	1,316	1.5	35	.048	RT
ClF ₅	250	110	8:00	.032	.141	0	32.1	RT	1,316	1.5	35	.145	RT
ClF ₅	250	110	8:00	-	-	-	-	-	-	-	-	-	-
ClF ₅	250	110	8:00	-	-	-	-	-	-	-	-	-	-
ClF ₅	250	110	8:00	-	-	-	-	-	-	-	-	-	-
ClF ₅	250	110	8:00	.034	.140	0	34.2	RT	1,316	1.5	25	.170	RT
ClF ₅	250	110	8:00	.035	.141	0	34.0	RT	1,316	1.5	25	.069	RT
ClF ₅	250	110	8:00	.034	.142	0	34.0	RT	1,316	1.5	25	.034	RT
ClF ₅	250	110	8:00	-	-	-	-	-	-	-	-	-	-
ClF ₅	250	110	8:00	-	-	-	-	-	-	-	-	-	-
ClF ₅	250	110	8:00	-	-	-	-	-	-	-	-	-	-
ClF ₅	450	138	8:00	.034	.141	0	37.6	RT	1,235	1.5	60	.037	RT
ClF ₅	450	138	8:00	.034	.143	0	24.8	-	-	-	-	-	-
ClF ₅	450	138	8:00	.034	.144	0	37.8	RT	1,235	1.5	196	.162	RT
ClF ₅	450	138	8:00	.035	.143	0	24.8	-	-	-	-	-	-
ClF ₅	450	138	8:00	.041	.130	.009	29.7	RT	1,316	1.5	18	.060	RT
ClF ₅	450	138	8:00	.066	.142	.034	16.8	RT	1,316	1.5	18	.066	RT
ClF ₅	450	138	8:00	.036	.140	.004	31.7	RT	1,316	1.5	18	.043	RT
ClF ₅	450	138	8:00	-	-	-	-	-	-	-	-	-	-
ClF ₅	450	138	8:00	-	-	-	-	-	-	-	-	-	-
ClF ₅	450	138	8:00	-	-	-	-	-	-	-	-	-	-
ClF ₅	450	138	8:00	-	-	-	-	RT	1,316	1.5	20	-	RT
ClF ₅	450	138	8:00	.040	.140	.004	30.1	RT	1,316	1.5	20	.044	RT
ClF ₅	450	138	8:00	.034	.146	0	34.3	RT	1,316	1.5	20	.072	RT
ClF ₅	450	138	8:00	-	-	-	-	-	-	-	-	-	-
ClF ₅	450	138	8:00	-	-	-	-	-	-	-	-	-	-
ClF ₅	450	138	8:00	-	-	-	-	-	-	-	-	-	-

B.

Table 7: 6Al-4V(ELI) TITANIUM IN CIF₅
(SFB Specimen Data, Second Run)

CYCLIC MARKING				FLAW SIZE AFTER MARKING		FRACTURE DATA					
(°F)	P _{max} (lb)	(in.)	CYCLES (1,000)	a (in.)	2c (in.)	TEMP. (°F)	a (in.)	2c (in.)	P (lb)	(in.)	
	1,235	1.5	141	.135	.300	RT	.135	.300	2,465	1.5	
	-	-	-	-	-	RT	.032	.142	5,430	1.5	
	1,124	1.5	154	.034	.142	RT	.034	.142	3,910	1.5	
	-	-	-	-	-	RT	.033	.144	5,750	1.5	
	1,316	1.5	35	.050	.150	RT	.050	.150	2,500	1.5	
	1,316	1.5	35	.048	.158	RT	.048	.158	2,500	1.5	
	1,316	1.5	35	.145	-	RT	.145	-	2,500	1.5	
	-	-	-	-	-	-	-	-	-	-	
	-	-	-	-	-	-	-	-	-	-	
	-	-	-	-	-	-	-	-	-	-	
	1,316	1.5	25	.170	-	RT	.170	-	2,240	1.5	
	1,316	1.5	25	.069	-	RT	.069	-	2,240	1.5	
	1,316	1.5	25	.034	-	RT	.034	-	2,240	1.5	
	-	-	-	-	-	-	-	-	-	-	
	-	-	-	-	-	-	-	-	-	-	
	-	-	-	-	-	-	-	-	-	-	
	1,235	1.5	60	.037	.143	RT	.037	.143	3,450	1.5	
	-	-	-	-	-	RT	.034	.143	5,720	1.5	
	1,235	1.5	196	.162	.780	RT	.162	.780	1,200	1.5	
	-	-	-	-	-	RT	.035	.143	5,790	1.5	
	1,316	1.5	18	.060	.140	RT	.060	.140	3,550	1.5	
	1,316	1.5	18	.066	.142	RT	.066	.142	3,550	1.5	
	1,316	1.5	18	.043	.146	RT	.043	.146	3,550	1.5	
	-	-	-	-	-	-	-	-	-	-	
	-	-	-	-	-	-	-	-	-	-	
	-	-	-	-	-	-	-	-	-	-	
	1,316	1.5	20	-	-	RT	-	-	3,445	1.5	
	1,316	1.5	20	.044	.140	RT	.044	.140	3,445	1.5	
	1,316	1.5	20	.072	.172	RT	.072	.172	3,445	1.5	
	-	-	-	-	-	-	-	-	-	-	
	-	-	-	-	-	-	-	-	-	-	
	-	-	-	-	-	-	-	-	-	-	

signs of corrosive attack on specimens exposed to ClF_5 during the second test run prompted scheduling of another run of 6Al-4V(ELI) titanium in the environment of ClF_5 .

The third run was to be done in one chamber only at 450 psi but at a temperature of 160° to 170°F. Furthermore, it was decided that in addition to the SFB specimen, a DCB specimen would be used to improve initiation and detection of crack extension during the test run.

5.1.3.4 ClF_5 and 6Al-4V(ELI) Titanium (Third Test Run)

The third and final test run involving ClF_5 and 6Al-4V(ELI) titanium was completed using DCB as well as SFB specimens. The DCB weld specimens per Figure 29 were machined from a remnant of the weld test panel previously used for fabrication of the SFB specimens. One of the specimens was used to establish a compliance curve for this type of specimen; the compliance curve is shown in Figure 30. Another specimen was pulled to failure. The remaining two specimens were then used for the sustained load test rerun with ClF_5 .

The compliance curve was generated and the preload level for the DCB specimens was determined with DCB specimen XAT-2. (Pertinent dimensions of this as well as the remaining three DCB specimens are given in TABLE 8.) The compliance curve was determined by incrementally increasing the load. Upon reaching the 1,000-pound level, the loading was stopped for one minute to verify whether the displacement, as measured with the compliance strain gage, remained stationary. The load was then increased to 2,000 pounds and the loading stopped for another minute. The displacement was once again noted. The load was then increased to 3,000 pounds and stopped. This time, holding the specimen under 3,000 pounds load resulted in an increase of displacement, suggesting gradual crack extension. Increase of load level above 3,000 pounds caused rapid crack extension and fracture.

The preload level for the DCB specimens to be exposed to ClF_5 was set at 2,900 pounds so that a relatively high value of applied stress intensity was generated to ensure some crack movement during the test run, even if the material did not exhibit pronounced susceptibility to the corrosive environment

[illegible]

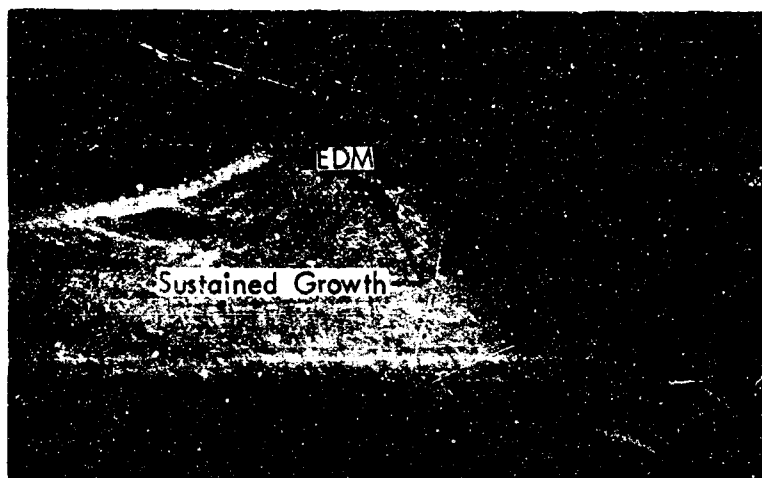
Table 8: 6Al-4V(ELI) TITANIUM IN ClF_5
(SFB Specimen Data, Third Run)

[illegible]

being evaluated. The indication of the threshold value would not be jeopardized by the high preload level because stress intensity level in DCB specimens decreases as the crack length increases. The preload level for the SFB specimens was the same as in previous test runs. There were no new SFB specimens available for this run, so it was decided to use the SFB specimens previously used for the ClF_5 rerun of 8 hours at 100°F and 200 psi in the environment of ClF_5 in the low-pressure chamber. Pertinent dimensions and flaw sizes of the SFB specimen, together with calculated K values, are shown in TABLE 9.

The actual rerun thus involved 6Al-4V(ELI) titanium SFB as well as DCB specimens. The temperature requirement was set at 160° to 170°F , pressure at 450 psi. Both conditions were met with no trouble; however, one hour after test conditions were reached, one valve in the ClF_5 pressurization system sprang a leak. The remaining 30 minutes of the exposure time were actually above the boiling point of the ClF_5 because pressure could not be maintained. To a considerable dismay of test personnel, the test rerun was stopped at the end of two hours. Actually, premature termination of the test run may very well have averted another explosion of the test site, because all high-stress SFB specimens in 6Al-4V(ELI) titanium weldments and base metal exposed to the liquid phase of ClF_5 and both DCB specimens (one in liquid and one in vapor) showed considerable crack growth. Fracture of any one of the SFB specimens could have led to conditions which, it is suspected, were the cause of the explosion in the original test run.

The extent of crack extension in SFB specimens exposed to the liquid phase of ClF_5 is shown in Figure 49. Similar specimens (Figure 50) exposed to the vapor phase of ClF_5 showed no signs of crack extension. It may be noted that in the specimen subjected to the liquid phase, the crack extension increased in depth without significant increase in length at the surface. The increase of crack depth brought about a reduction of K values due to increase of the flaw shape parameter Q as the $a/2c$ ratio was increasing. Further reduction of K was caused by the lowering of tensile bend stresses at the tip of the crack as it grew deeper.

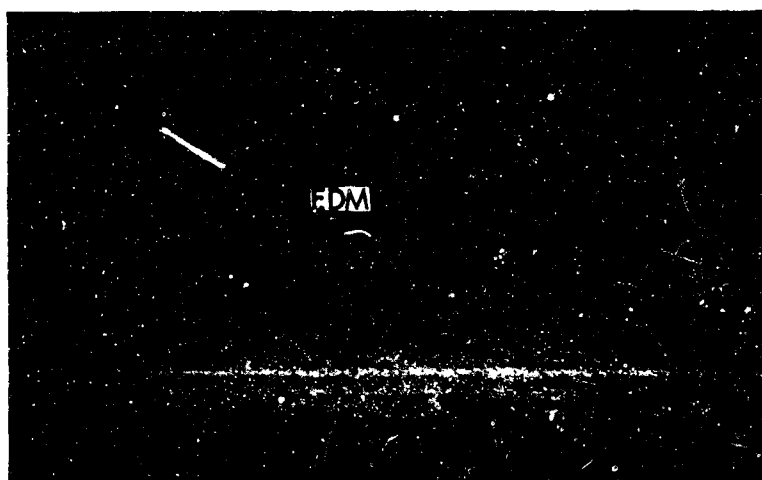


SPECIMEN TBL-1
BASE METAL

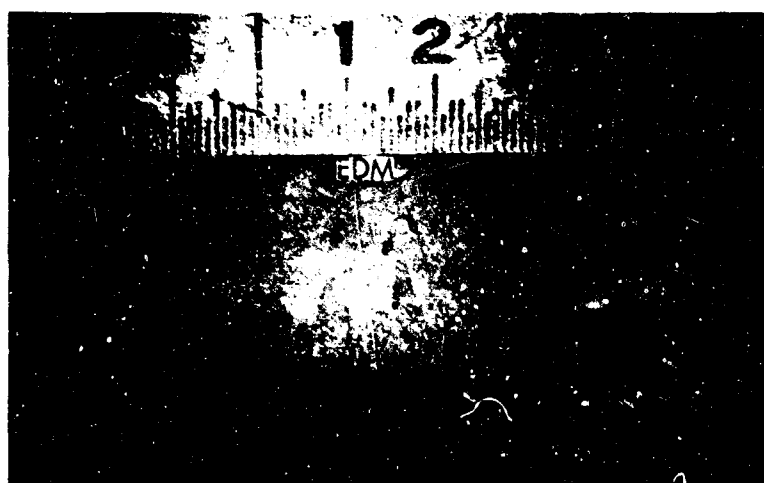


SPECIMEN TWL-1
WELDMENT

Figure 49: SUSTAINED FLAW GROWTH IN 6Al-4V (ELI)
TITANIUM IN LIQUID ClF_5



SPECIMEN TBV-1



SPECIMEN TWV-1

Figure 50: ABSENCE OF SUSTAINED FLAW GROWTH IN 6Al-4V (ELI) TITANIUM IN VAPOR ClF_5

[illegible]

Table

[illegible]

B.

Table 9: 6Al-4V(ELI) TITANIUM IN ClF_5
(DCB Specimen Data, Third Run)

[illegible]

By the time the third run of ClF_5 6Al-4V(ELI) titanium was completed, the test specimens used in the second test run at 450 psi and 138°F temperature were cycled and fractured. Both high-stress weldment specimens (one exposed to vapor, the other to the liquid phase of ClF_5) showed signs of crack extension in depth. Fractographs of both specimens are shown in Figure 51.

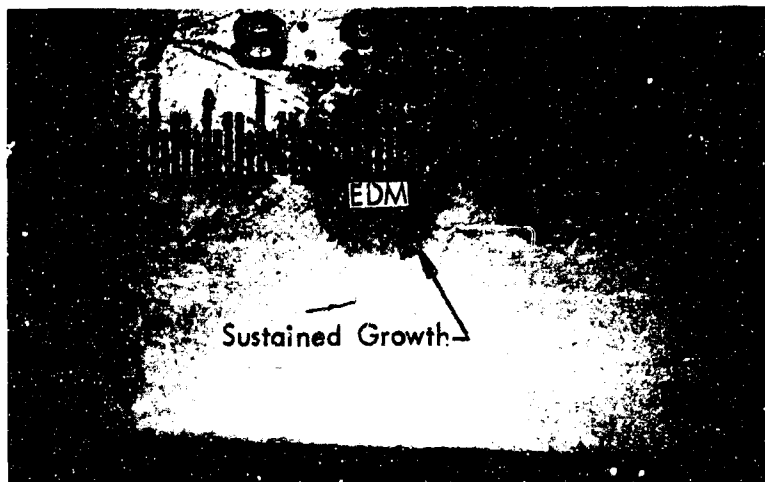
5.2 Phase II -- Fracture Toughness Test

Experimental data generated during this portion of the program consists of mechanical properties test data, static fracture toughness and flaw growth data generated under cyclic and sustained loading conditions.

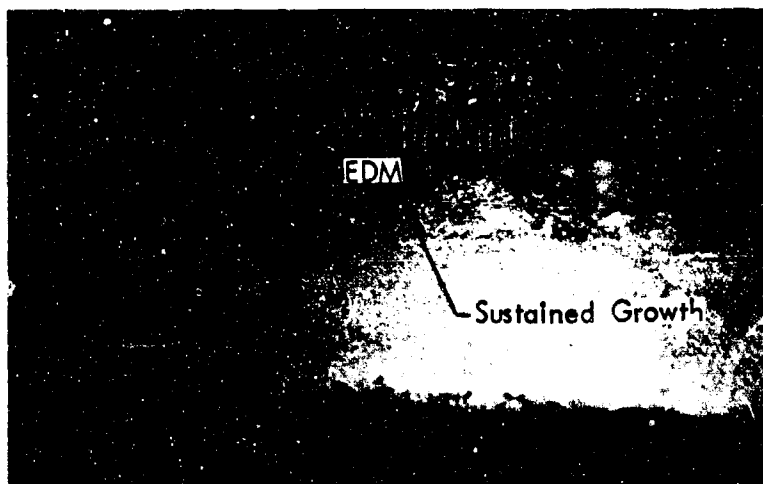
Typical makeup of the sustained flaw growth tables includes nine major headings beginning with the column for specimen number and concluding with the column on test condition at fracture. The second column from the left shows specimen size in terms of specimen thickness in inches and its width in the test gage section. The information on cyclic extension of the EDM flaw and flaw size before the test run is given under the third and fourth headings.

Sustained test data is listed in the fifth column. Under this heading, together with the indication of test temperature, maximum stress across the specimen test gage area and time under sustained load, while in the environmental media being evaluated. There are three sets of applied stress intensity values calculated using initial flaw size in the fourth column and applied max stress shown in the fifth column. The three sets of stress intensity values are calculated using Irwin's Equation 2, Kobayashi's Equation 3, and Smith's Equation 6. Symbolically, the values are denoted by K_{I1} and represent the initial stress intensity applied to the specimens at the beginning of the sustained test run.

Under flaw-size-after-the-test-run heading, there are once again three stress intensity values calculated for each specimen at the end of the sustained test run. Stress intensities are designated by K_{If} symbols where K is the stress intensity calculated using Equations 2, 3, and 6, and subscript If depicts plane strain condition at the end of the sustained test run. Stress



SPECIMEN TWV-7



SPECIMEN TWL-7

Figure 51: INITIATION OF THE SUSTAINED FLAW GROWTH IN
6Al-4V (ELI) TITANIUM IN ClF_5

level used in calculations is the same as applied during sustained load test run but the flaw sizes include any incremental flaw growth that may have occurred during sustained test run. Direction of the maximum flaw growth (in degrees) is the included angle between semiminor axis of the ellipse and the direction of maximum flaw growth at some point on flaw periphery. Flaw increment along the direction of maximum flaw growth is measured at a point corresponding to maximum flaw increment but perpendicular to the flaw curvature at that point.

The next two columns contain data on cyclic flaw marking in terms of temperature, maximum stress, and number of cycles and flaw size after cyclic marking. Flaw depth and flaw length are measured directly from fractographs or via wide field microscope. The flaw size (a/Q) is calculated on the basis of direct measurements of flaw depth and Q value read from Figure 1 for a corresponding $a/2c$ and fracture stress value. Fracture stress together with the test temperature and the calculated stress intensity values are listed in the remaining columns.

5.2.1 2219-T851 Aluminum As-Welded Weldments

Mechanical properties of the 2219-T851 aluminum as-welded weldments are listed in TABLE 10. Three tensile specimens were pulled to failure at each of the following test temperatures: room temperature, $+140^{\circ}\text{F}$, -230°F , and -320°F . The -320°F test data was obtained while specimens were completely submerged in liquid nitrogen. The -230°F test data was obtained by cooling specimens with cold nitrogen gas out of the liquid nitrogen bottle. The $+140^{\circ}\text{F}$ tests were conducted by heating test specimens with electrically heated air. Ultimate strength (σ_{ult}) and yield strength (σ_{ys}) data is plotted in Figure 52 as a function of test temperature. The solid lines drawn in Figure 52 for σ_{ult} and σ_{ys} values correspond to the average data points for each test temperature. Tensile specimens were machined in a manner that weldments were oriented transversely with respect to the longitudinal axis of the specimens.

Table 10: MECHANICAL PROPERTIES OF 2219-T851 ALUMINUM
AS-WELDED WELDMENTS

SPECIMEN NUMBER	THICKNESS (IN)	AREA (IN ²)	TEST ATMOSPHERE	WELD DIRECTION L = LONGITUDINAL T = TRANSVERSE	TEST TEMPERATURE (°F)	ULTIMATE STRENGTH (KSI)	YIELD STRENGTH (KSI)	ELONGATION % PER INDICATED LENGTH			REDUCTION IN AREA (%)
								0.5 INCH	1.0 INCH	2.0 INCHES	
AW200	.2536	.1265	AIR	TW	75	41.5	26.2	14	7	3	20
AW18A	.2506	.1252				42.4	28.2	16	7	3	17
AW19A	.2501	.1239				41.8	26.6	14	7	3	17
						<u>41.9</u>	<u>27.0</u>				
AW18B	.2492	.1246	AIR	TW	140	42.6	30.0	10	7	4	16
AW19B	.2504	.1250				41.7	27.5	16	8	4	20
AW20B	.2500	.1239				41.5	26.7	14	8	4	21
						<u>41.9</u>	<u>28.0</u>				
AW18C	.2508	.1248	N ₂	TW	-230	47.5	33.1	16	10	5	27
AW19C	.2560	.1272				46.1	29.5	20	10	5	27
AW20C	.2502	.1245				45.8	28.9	24	12	6	31
						<u>46.5</u>	<u>30.5</u>				
AW18D	.2503	.1244	LN ₂	TW	-320	58.2	35.2	16	8	4	18
AW19D	.2512	.1249				58.4	31.2	16	8	4	19
AW20A	.2532	.1261				57.3	31.3	16	10	5	18
						<u>58.0</u>	<u>32.6</u>				

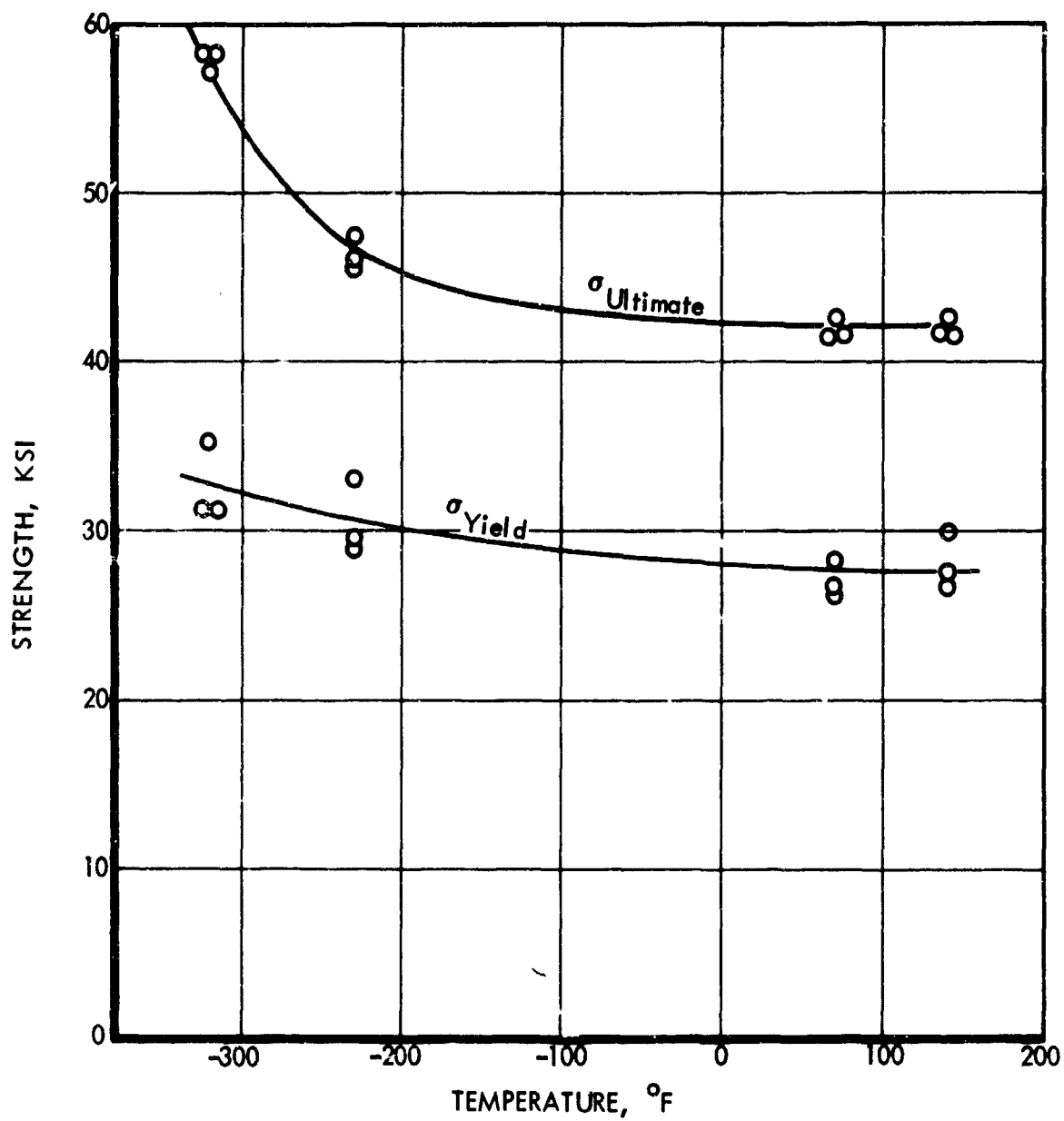


Figure 52: MECHANICAL PROPERTIES OF 2219-T851 ALUMINUM AS-WELDED WELDMENTS

Static fracture toughness data for the 2219-T851 aluminum weldments at different test temperatures is listed in TABLE 11. Specimens AW-1, -2, and -3 were pulled to failure at room temperature. Of the three specimens tested at room temperature, specimens AW-2 and -3 fractured at a stress level above the uniaxial yield strength. Specimen AW-22 and AW-24 were pulled to failure at +140°F. Both specimens fractured at stress level in excess of uniaxial yield strength. Specimen AW-23 was pulled to failure at -320°F and also exceeded its uniaxial yield strength. Static fracture toughness data, as calculated using Irwin's equation, is plotted in Figure 53 as a function of test temperature.

Fracture toughness data generated at room temperature has been augmented by the end-point data obtained upon conclusion of the sustained load testing. The plot of such data points together with static test data points at room temperature is shown in Figure 54 as a function of depth-to-thickness ratio. On the basis of the obtained data it was decided to use 28.0, 29.0, and 33.0 ksi $\sqrt{\text{in}}$ stress intensity values for 140°F, room temperature, and -320°F, respectively, as representative values of the material fracture toughness.

5.2.1.1 N_2O_4 and 2219-T851 Aluminum

The sustained flaw growth data for 2219-T851 aluminum in the environment of liquid nitrogen tetroxide (N_2O_4) at 155°F and under 100 psig pressure is summarized in TABLE 12. Of the five specimens tested (specimens AW-4 through -8), one specimen broke upon loading (AW-8), the other four were subjected to sustained test runs from 6.0 to 11.5 hours duration. The applied stress levels varied from 60 percent of the uniaxial yield strength to 99 percent. Test specimen AW-4 with the lowest stress level of 17.0 ksi which corresponds to K_{I1} value of 15.9 ksi $\sqrt{\text{in}}$, showed no signs of flaw growth. The remaining specimens (AW-5, -6, and -7) had flaw growth as seen in Figure 55 showing fractographs of the tested specimens.

The sustained flaw growth data is plotted in Figure 56 in terms of applied stress intensity K_{I1} in ksi $\sqrt{\text{in}}$ versus time under load in hours. The numbers next to data points indicate total flaw growth increment in the

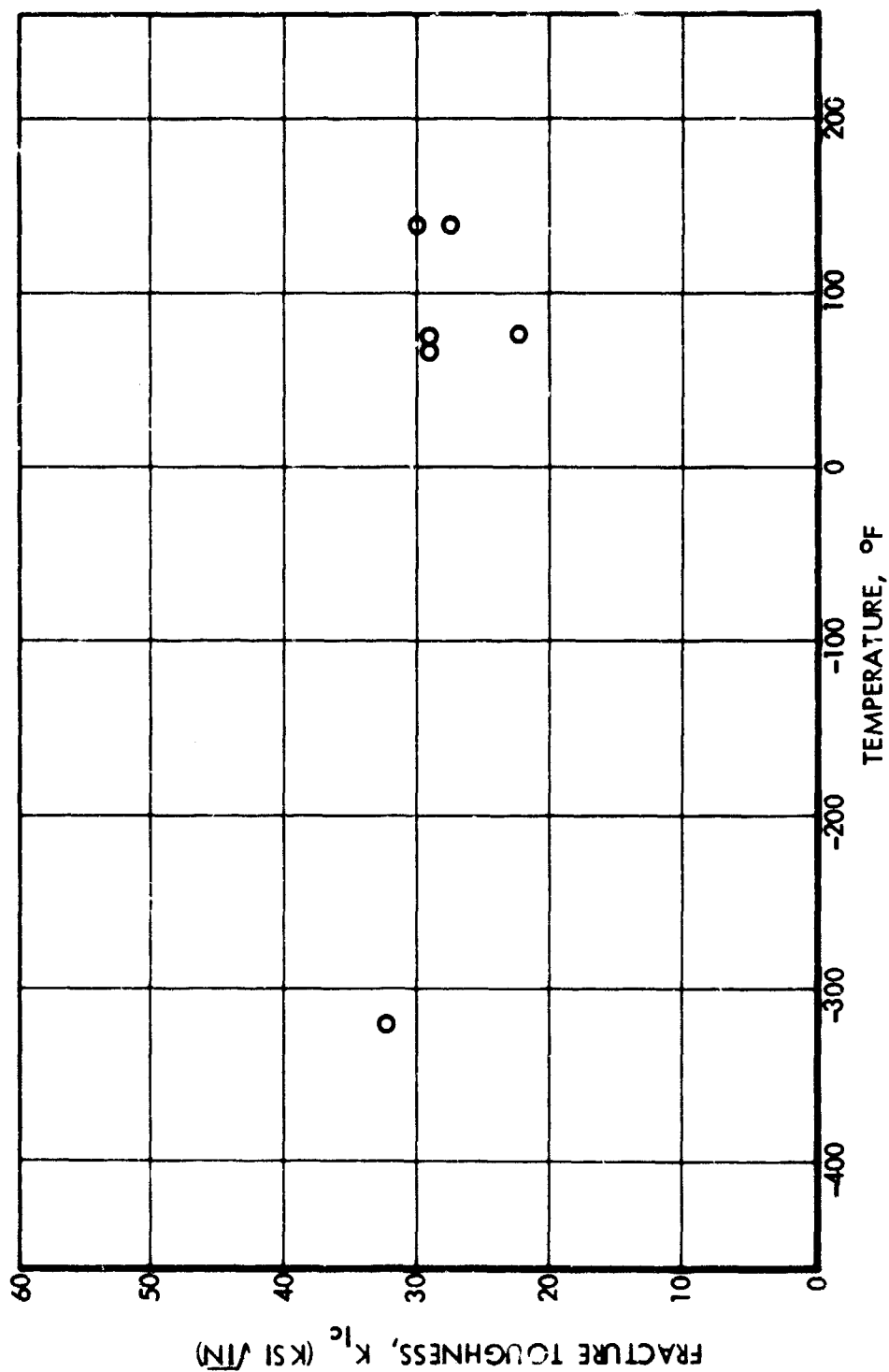


Figure 53: STATIC FRACTURE TOUGHNESS DATA FOR 2219-T851 ALUMINUM
AS-WELDED WELDMENT

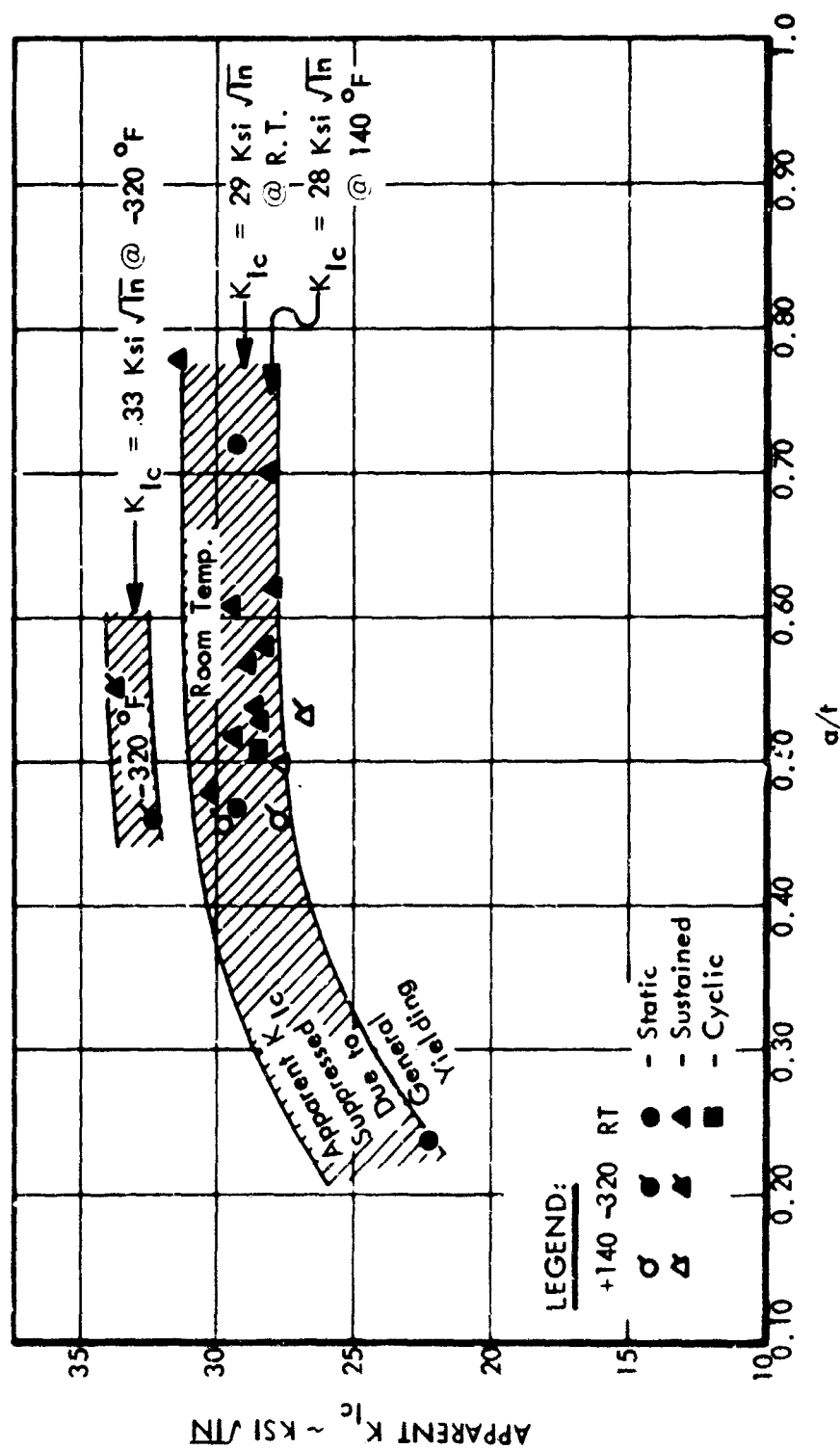
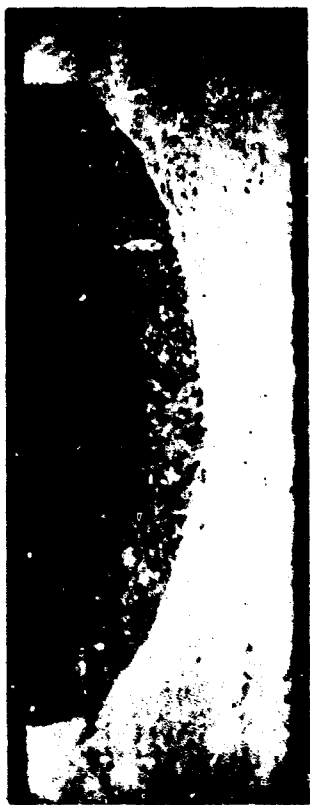
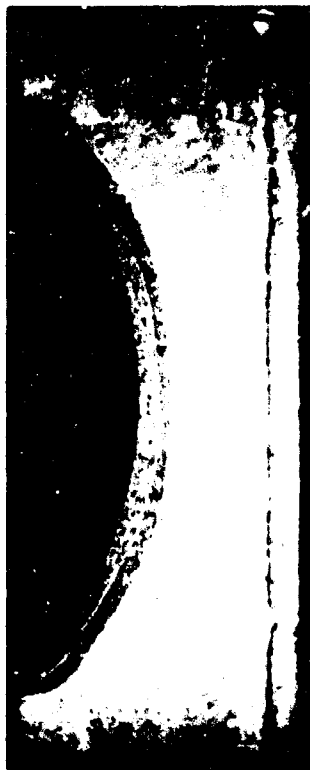


Figure 54: STATIC FRACTURE TOUGHNESS FOR 2219-T851 ALUMINUM AS-WELDED WELDMENTS



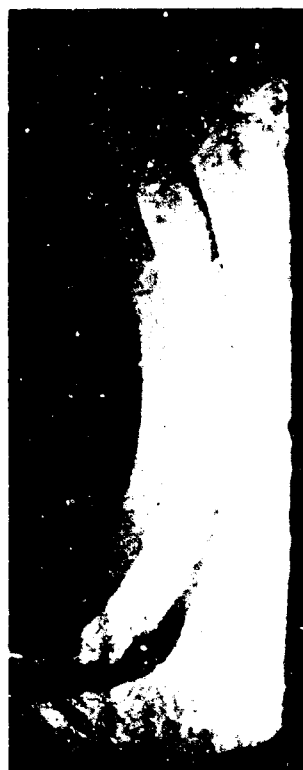
Specimen AW-4



Specimen AW-6



Specimen AW-5



Specimen AW-7



Specimen AW-8

Figure 55 : FRACTOGRAPHS OF 2219-T851 ALUMINUM AS-WELDED WELDMENT
SPECIMENS (Sustained Test In N_2O_4)

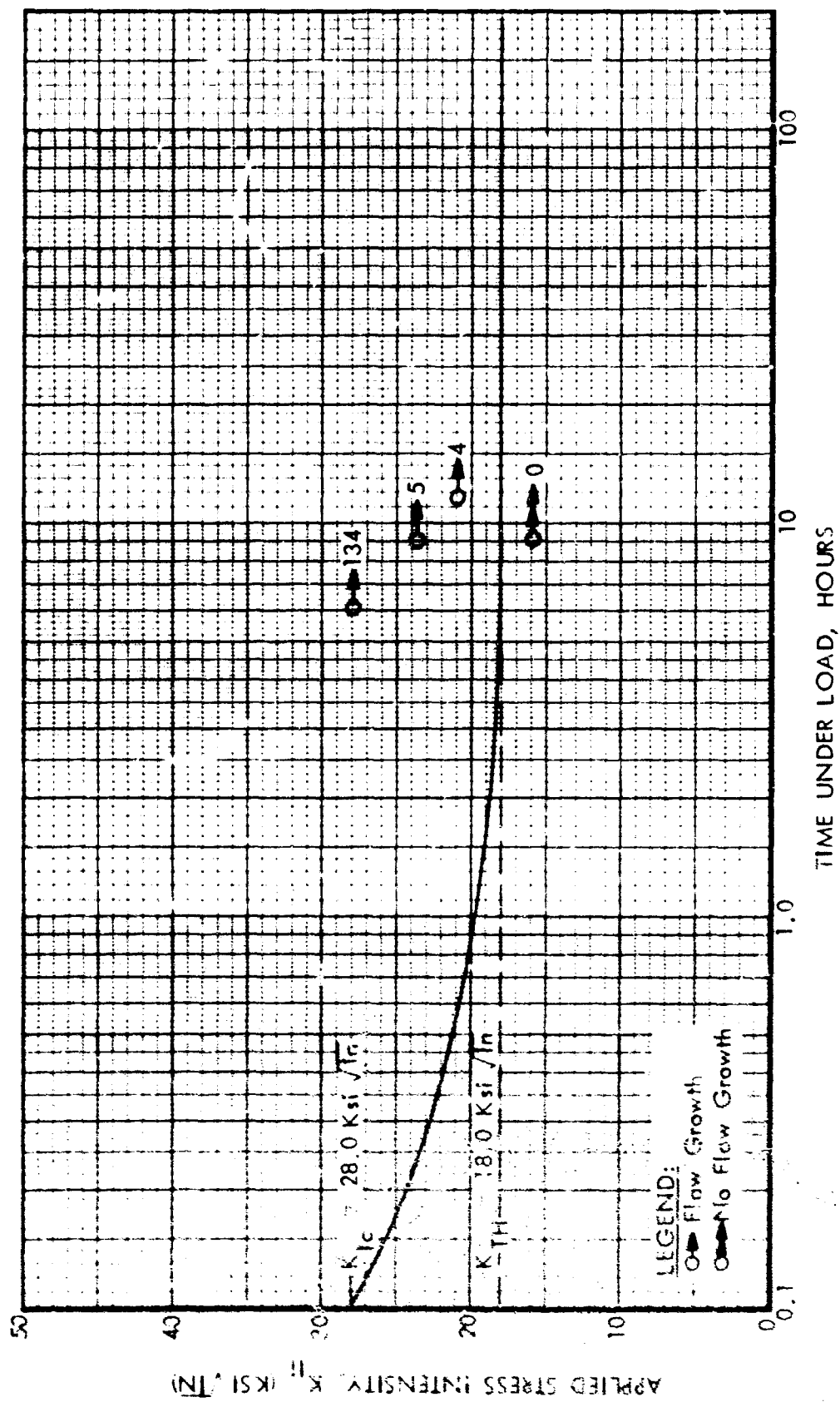


Figure 56 : SUSTAINED FLAW GROWTH DATA FOR 2219-T851 ALUMINUM
AS-WELDED WELDMENTS (N_2O_4 @ 155 °F And 100 Pslg)

[illegible]

TABLE 11: STATIC FRACTURE TOUGHNESS DATA
2219-T851 ALUMINUM AS-WELDED
WELDMENTS

[illegible]

[illegible]

ECIMEN FAILED ON LOADING

B.

Table 12: SUSTAINED FLAW GROWTH DATA 2219-T851
ALUMINUM WELDMENT IN THE ENVIRONMENT
OF N₂O₄ AT 155°F AND 100 PSIG PRESSURE

[illegible]

direction of maximum flaw extension in thousandths of an inch. The solid line was visually fitted to separate data points with flaw growth from those having no flaw growth. On the ordinate the lines intersect a point corresponding to $28.0 \text{ ksi } \sqrt{\text{in.}}$ which was designated earlier as the fracture toughness value for the material at $+140^\circ\text{F}$. The threshold value then becomes equal to $18.0 \text{ ksi } \sqrt{\text{in.}}$

Cyclic flaw growth data for 2219-T851 aluminum as-welded weldment in the environment of N_2O_4 at 155°F and 100 psig pressure is summarized in TABLE 13. There were two specimens tested. Specimen AW-9 was cycled at a gross stress level of 21.8 ksi maximum and 0.4 ksi minimum. Specimen AW-10 was cycled at 25.3 ksi maximum stress level and the same minimum stress of 0.4 ksi. Surface flaws in both specimens increased in size (grew) under cyclic loading. The growth, as seen from Figure 57, was more pronounced in the direction of 65 to 75 degrees from the minor axis of the surface flaw. Cyclic data is plotted in Figure 58 in terms of applied stress intensity (K_{I1}) versus flaw growth rate $\Delta(a/Q)/\Delta N$ in micro-inches per cycle. Superimposed on the plot are threshold stress intensity level (K_{TH}) of $18.0 \text{ ksi } \sqrt{\text{in.}}$ as well as fracture toughness value for the material (K_{IC}) of $28.0 \text{ ksi } \sqrt{\text{in.}}$

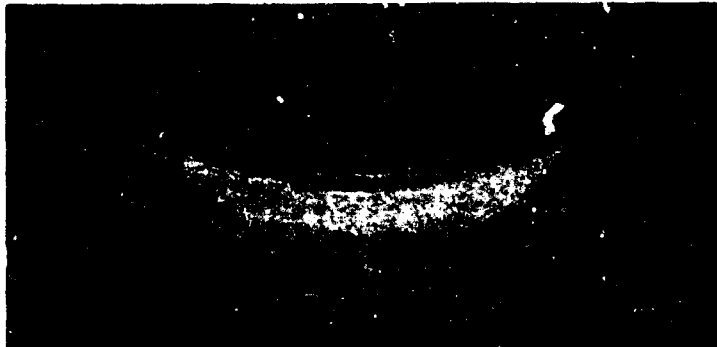
5.2.1.2 F_2 and 2219-T851 Aluminum

The sustained flaw growth data for 2219-T851 aluminum in the environment of liquid fluorine (F_2) at -320°F and under 450 psig pressure is summarized in TABLE 14. Of the five specimens tested (specimens AW-11 through -15) specimen AW-13 was subjected to two consecutive test runs of 5.0 and 1.7 hours, respectively. The first run of 5.0 hours was done at 18.0 ksi stress level. The second test run was done at 25.0 ksi. The remaining specimens were subjected to one test run each at stress level ranging between 18.4 and 27.6 ksi. The resultant applied stress intensity levels ranged between 16.7 and $25.5 \text{ ksi } \sqrt{\text{in.}}$. Figure 59 shows fractographs of test specimens listed in TABLE 14.

The data is plotted in Figure 60 in terms of applied stress intensity in $\text{ksi } \sqrt{\text{in.}}$ versus time under load in hours. The numbers next to data points indicate the amount of flaw growth in thousandths of an inch. A solid line is drawn visually to separate data points with flaw growth from those showing



Specimen AW-9



Specimen AW-10

Figure 57: FRACTOGRAPHS OF 2219-T851 ALUMINUM AS-WELDED
WELDMENT SPECIMENS (Cyclic Test In N_2O_4)

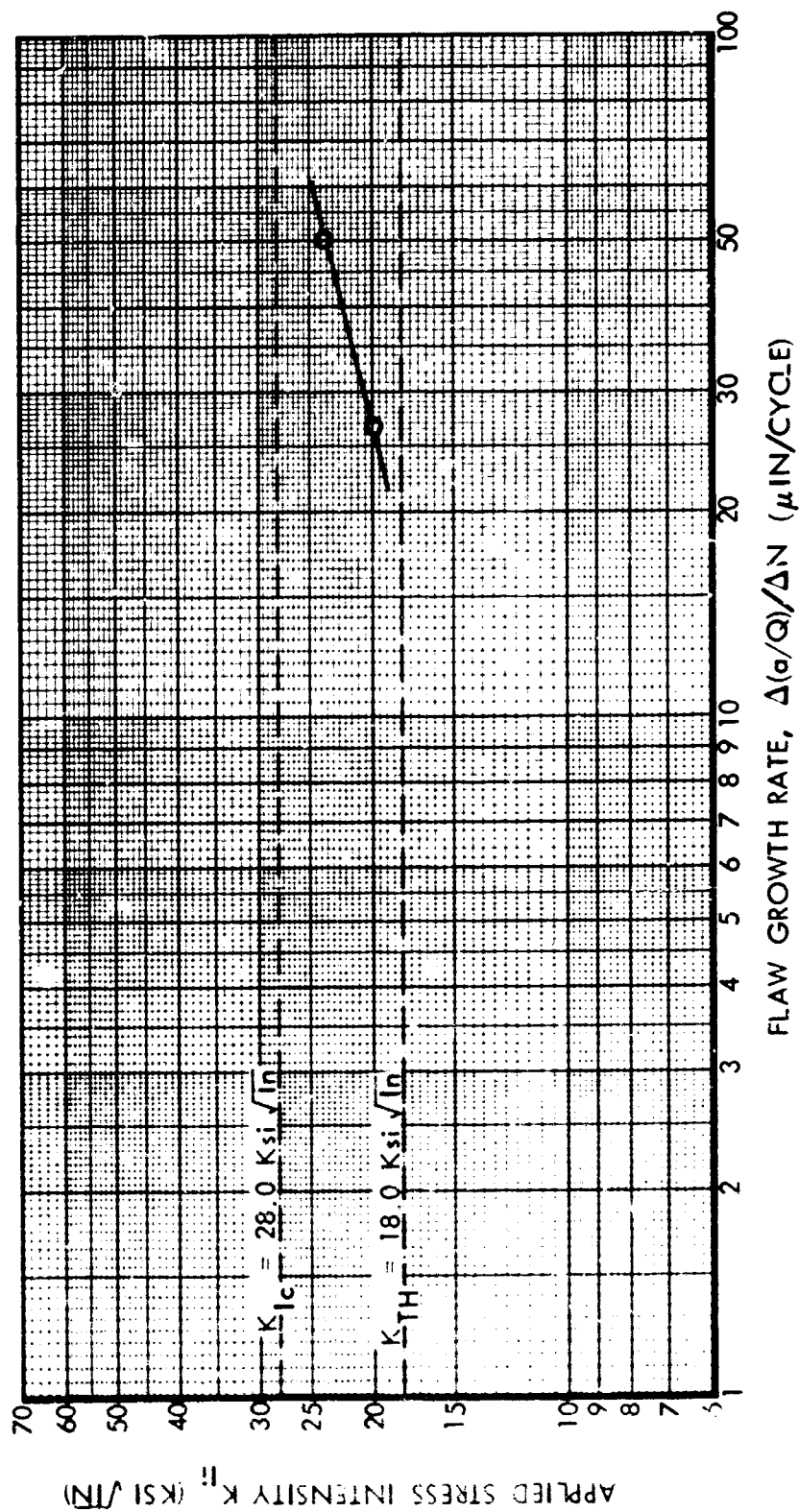


Figure 58: CYCLIC FLAW GROWTH DATA FOR 2219-T851 ALUMINUM AS-WELDED WELDMENTS (N_2O_4 @ 155 °F And 100 Psig)



Specimen AW-11



Specimen AW-13



Specimen AW-12



Specimen AW-14



Specimen AW-15

Figure 59 : FRACTOGRAPHS OF 2219-T851 ALUMINUM AS-WELDED WELDMENT
SPECIMENS (Sustained Test In F₂ @ -320 °F And 450 Psig)

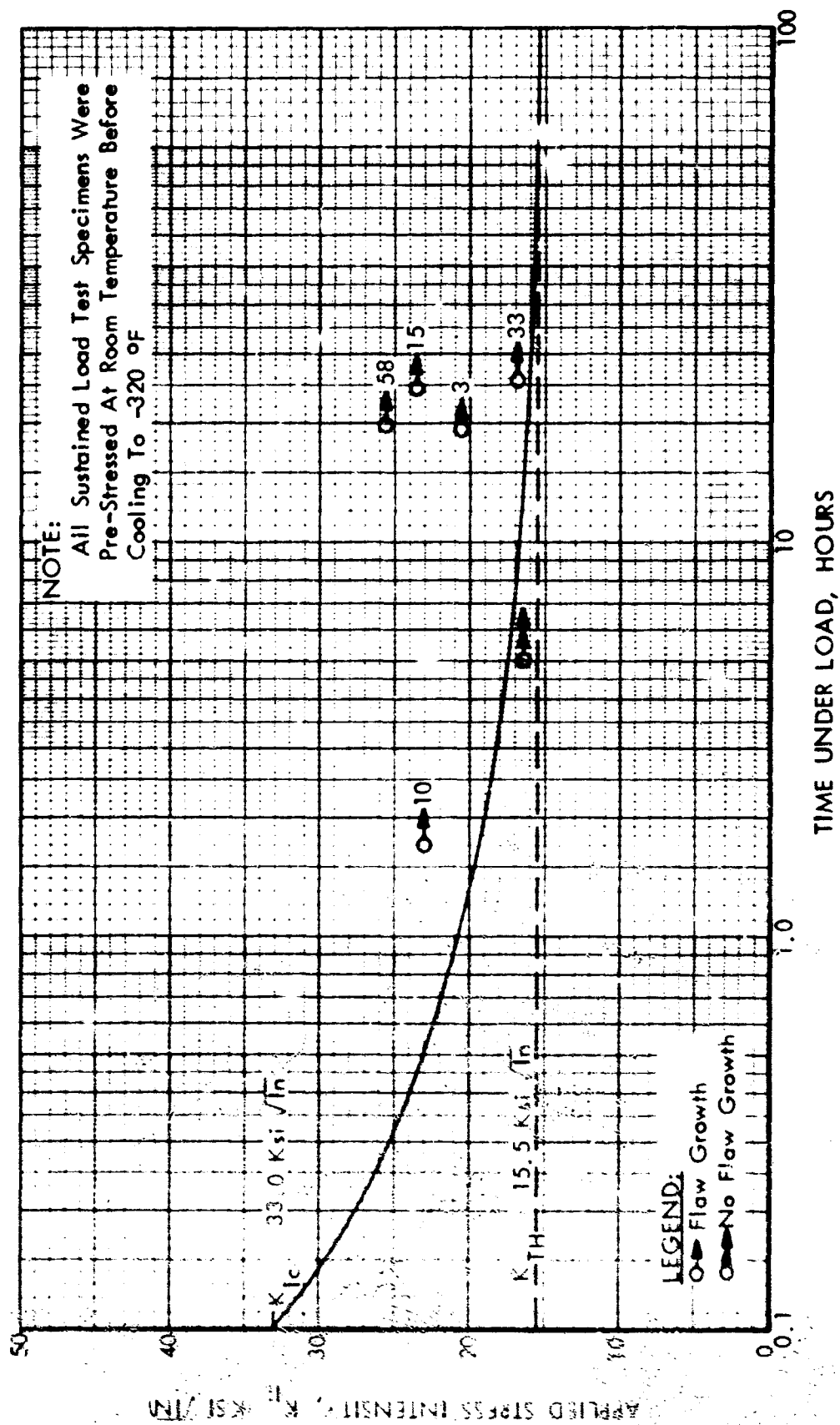


Figure 60 : SUSTAINED FLAW GROWTH DATA FOR 2219-T851 ALUMINUM AS-WELDED WELDMENTS (F_2 @ -320 °F And 450 Psig)

[illegible]

Table 1

[illegible]

B.

Table 13: CYCLIC FLAW GROWTH DATA 2219-T851
ALUMINUM WELDMENT IN THE ENVIRON-
MENT OF N_2O_4 AT 155°F AND 100 PSIG PRESSURE

[illegible]

[illegible]

SUS
AL
MEY

B

Table 14: SUSTAINED FLAW GROWTH DATA 2219-T851
ALUMINUM WELDMENT IN THE ENVIRON-
MENT OF F₂, AT -320°F AND 450 PSIG PRESSURE

[illegible]

no flaw growth and also to intersect the ordinate at a point corresponding to 33.0 ksi $\sqrt{\text{in.}}$ — apparent fracture toughness of the material. The sustained load threshold stress intensity level (K_{TH}) is set at 15.5 ksi $\sqrt{\text{in.}}$

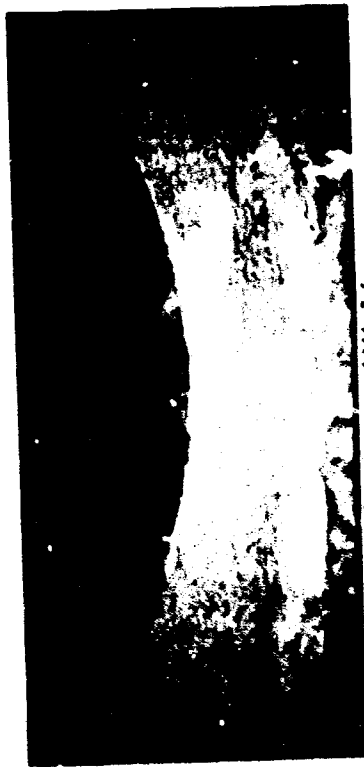
Because of the problems associated with containing pressurized liquid fluorine, no attempts were made to generate cyclic flaw growth data in that environment. Under cyclic load the seal inevitably would spring a leak in a very short time, which in turn could easily have resulted in loss of specimens and destruction of the test apparatus. In place of cyclic testing, extra specimens were tested under sustained loading in N_2O_4 and F_2 .

5.2.1.3 ClF_5 and 2219-T851 Aluminum

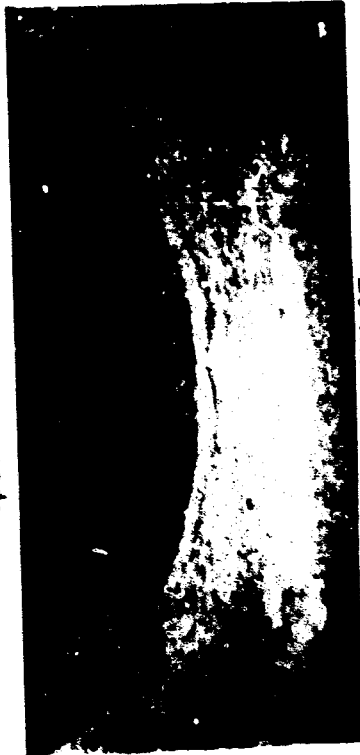
The sustained flaw growth data for 2219-T851 aluminum in the environment of liquid chlorine pentafluoride (ClF_5) at 145°F and under 450 psig pressure is summarized in TABLE 15. There was a total of four specimens tested (specimens AW-16 through -19). Specimens were subjected to sustained test run from 12.7 to 44.4 hours duration, then cyclically marked and pulled to failure at room temperature. Fractographs of specimens AW-16 through -19 are shown in Figure 61 together with cyclically tested specimens AW-20 and AW-21.

Sustained flaw growth data for 2219-T851 as-welded aluminum in the environment of ClF_5 is plotted in Figure 62 in terms of applied stress intensity (K_{I_2}) versus time under load in hours. The numbers next to data points with arrows indicate total flaw growth increment in thousandths of an inch. The sustained threshold stress intensity is set at 18.0 ksi $\sqrt{\text{in.}}$

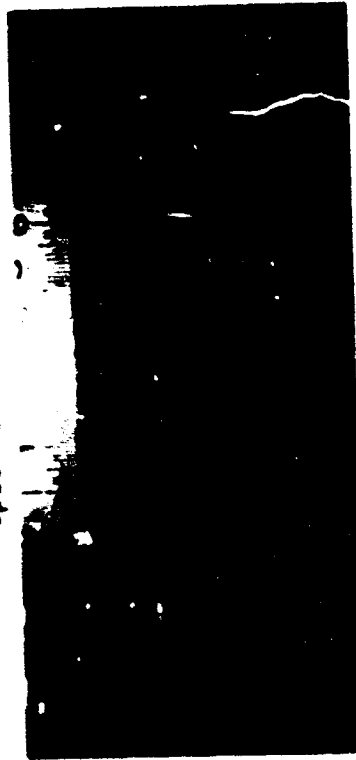
Cyclic flaw growth data is summarized in TABLE 16 and is plotted in Figure 63. The applied stress intensities were above the threshold stress intensity level of 18.0 ksi $\sqrt{\text{in.}}$. Tests were conducted from 2 to 3 cycles per minute under sinusoidal loading profile. Calculated rates were established by dividing total flaw growth increment (a/Q) by the number of cycles.



Specimen AW-16



Specimen AW-17



Specimen AW-18



Specimen AW-19



Specimen AW-20



Specimen AW-21

Figure 61 : FRACTOGRAPHES OF 2219-T851 ALUMINUM AS-WELDED WELDMENT
SPECIMENS (Sustained Test In CIF5 @ 155 °F And 450 Pslg)

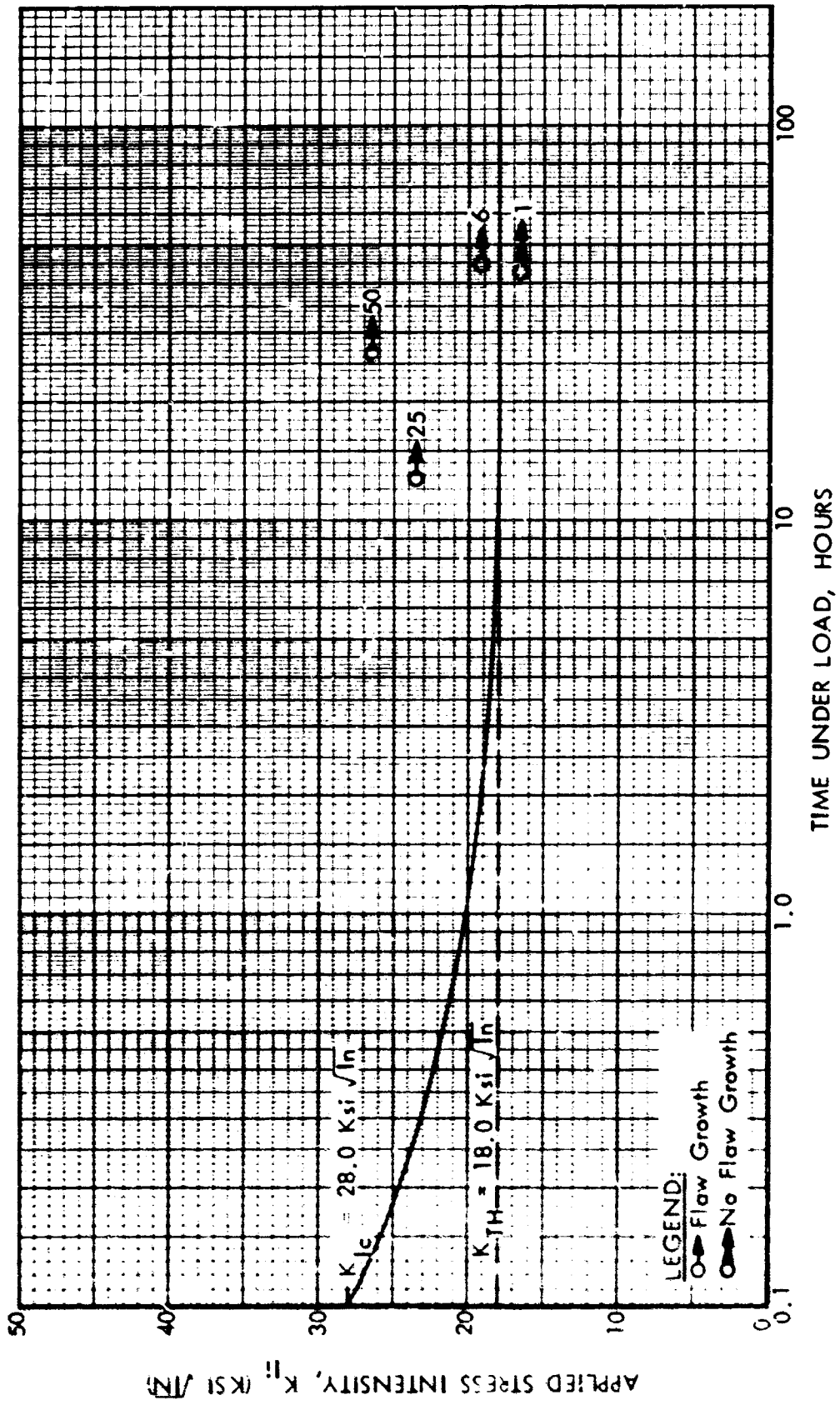


Figure 62 : SUSTAINED FLAW GROWTH DATA FOR 2219-T851 ALUMINUM
AS-WELDED WELDMENTS (CIF₅ @ 145 °F And 450 Psig)

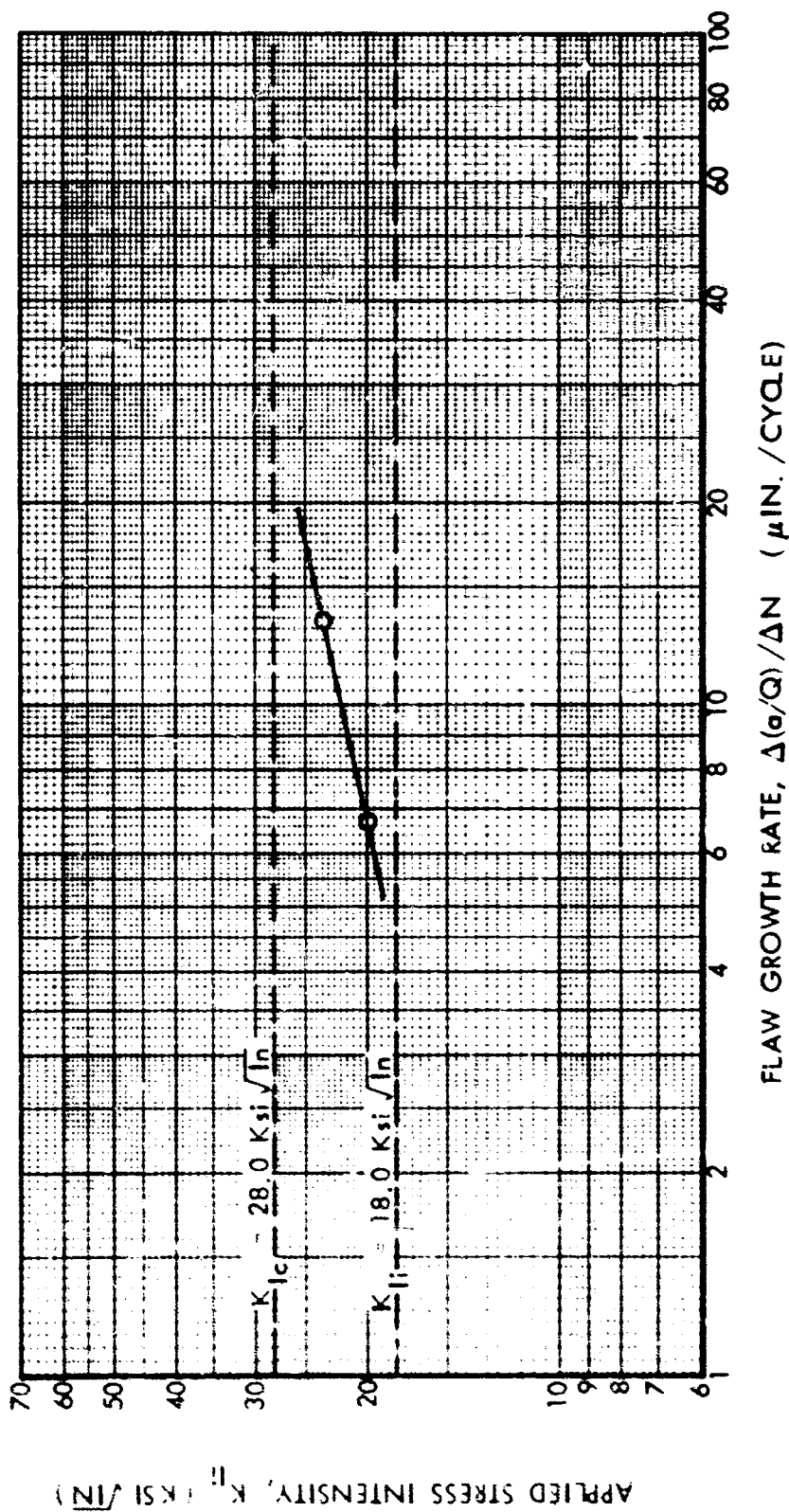


Figure 63: CYCLIC FLAW GROWTH DATA FOR 2219-T87 ALUMINUM AS-WELDED WELDMENTS (CIF₅ @ 145 °F And 450 Psig)

[illegible]

SUS
ALL
MEI

B

Smith's K 18

Smith's K 18

[illegible]

A.

Table 16: CYC
ALL
MEN

[illegible]

B.

5.2.2 2021-T81 Aluminum

Testing of the 2021-T81 aluminum base metal as well as heat treated weldments was done in the N_2O_4 environment. Yield strength of the heat treated weldments was reported by the supplier of weld panels to be 31.0 ksi for repaired weldments and 40.3 ksi for heat treated weldments. Yield strength of the 2021-T81 base metal was reported to be 65.0 ksi. These values were used in calculating stress intensities for static as well as sustained load test specimens.

5.2.2.1 N_2O_4 and 2021-T81 Aluminum (Base Metal)

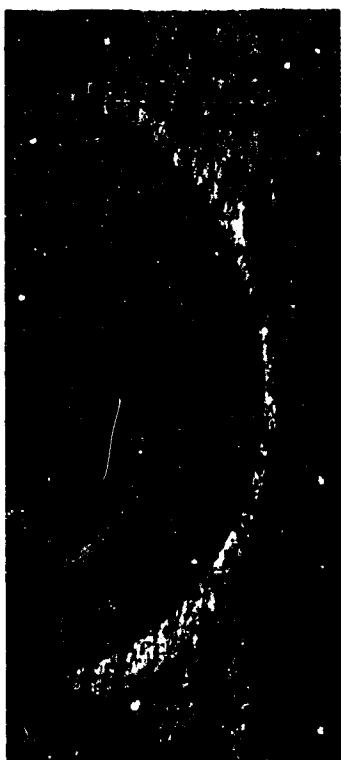
Static as well as sustained load test data is summarized in TABLE 17. Specimens SA-1, -5, -6, and -7 were pulled to failure at room temperature in ambient air. Specimen SA-6 was pulled to failure at room temperature after additional extension of the initial flaw at $-320^{\circ}F$. This was done in an effort to prevent delamination during static tests. Specimen SA-11 was pulled to failure in the environment of pressurized N_2O_4 at $135^{\circ}F$ test temperature. Fractographs of the static test specimens are shown in Figures 64 and 65.

Static fracture toughness data points together with the end points of the sustained load test specimens are plotted in Figure 66 in terms of apparent K_{Ic} versus flaw-depth-to-specimen thickness ratio a/t . From the plot of the data it is concluded that fracture toughness of the 2021-T81 aluminum base metal may be taken to be $32.5 \text{ ksi } \sqrt{\text{in.}}$.

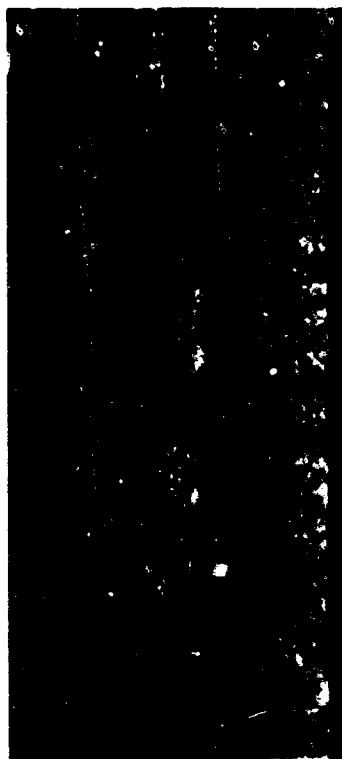
Fractographs of the sustained load test specimens are shown in Figures 67 and 68. The sustained flaw growth for 2021-T81 aluminum in the environment of N_2O_4 at $145^{\circ}F$ and 100 psig pressure is plotted in Figure 69. The plot is made in terms of applied stress intensity values (K_{I1}) versus time under sustained load in hours. The threshold stress intensity is established by visually drawing a curve that would place test data points with flaw growth above the line. All specimens tested did show some flaw growth. Test specimens SA-3, -4, and -10 had only three to four thousandths of an inch flaw growth. Placing of the curve below these two points was motivated by the fact that



Specimen SA-1



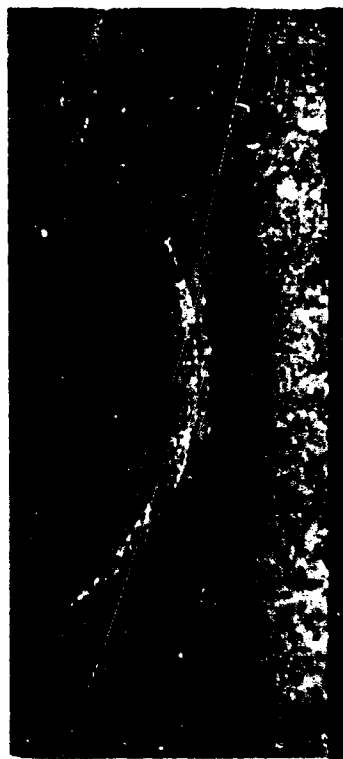
Specimen SA-7



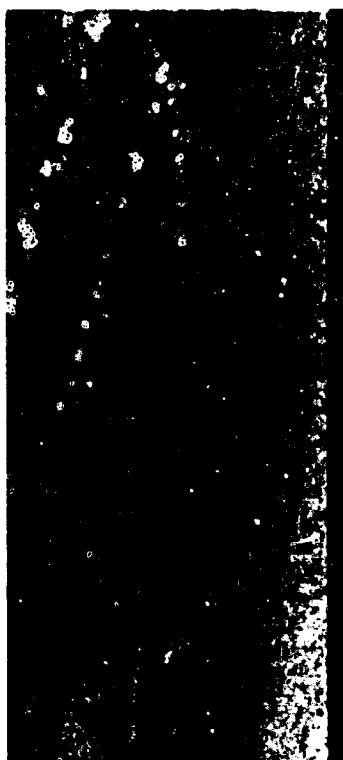
Specimen SA-5



Specimen SA-11



Specimen SA-6

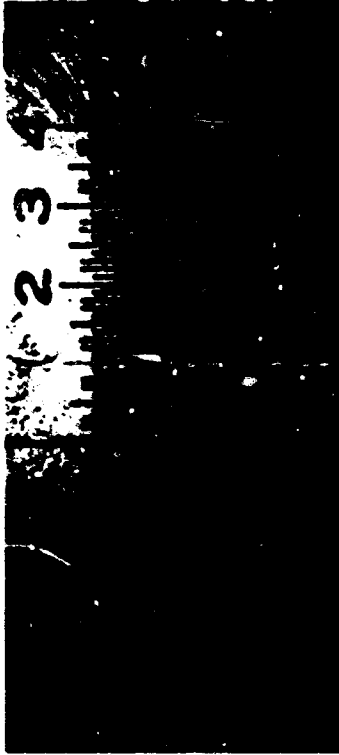


Specimen SA-12

Figure 64 : FRACTOGRAPHS OF 2021-T81 ALUMINUM BASE METAL
(Static Test, White Light Illumination)



Specimen SA-1



Specimen SA-5



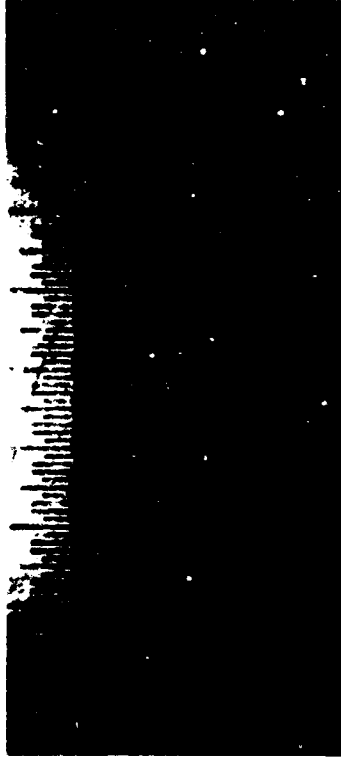
Specimen SA-6



Specimen SA-7



Specimen SA-11



Specimen SA-12

Figure 65 : FRACTOGRAPHES OF 2021-T81 ALUMINUM BASE METAL
(Static Test, Polarized Light Illumination)

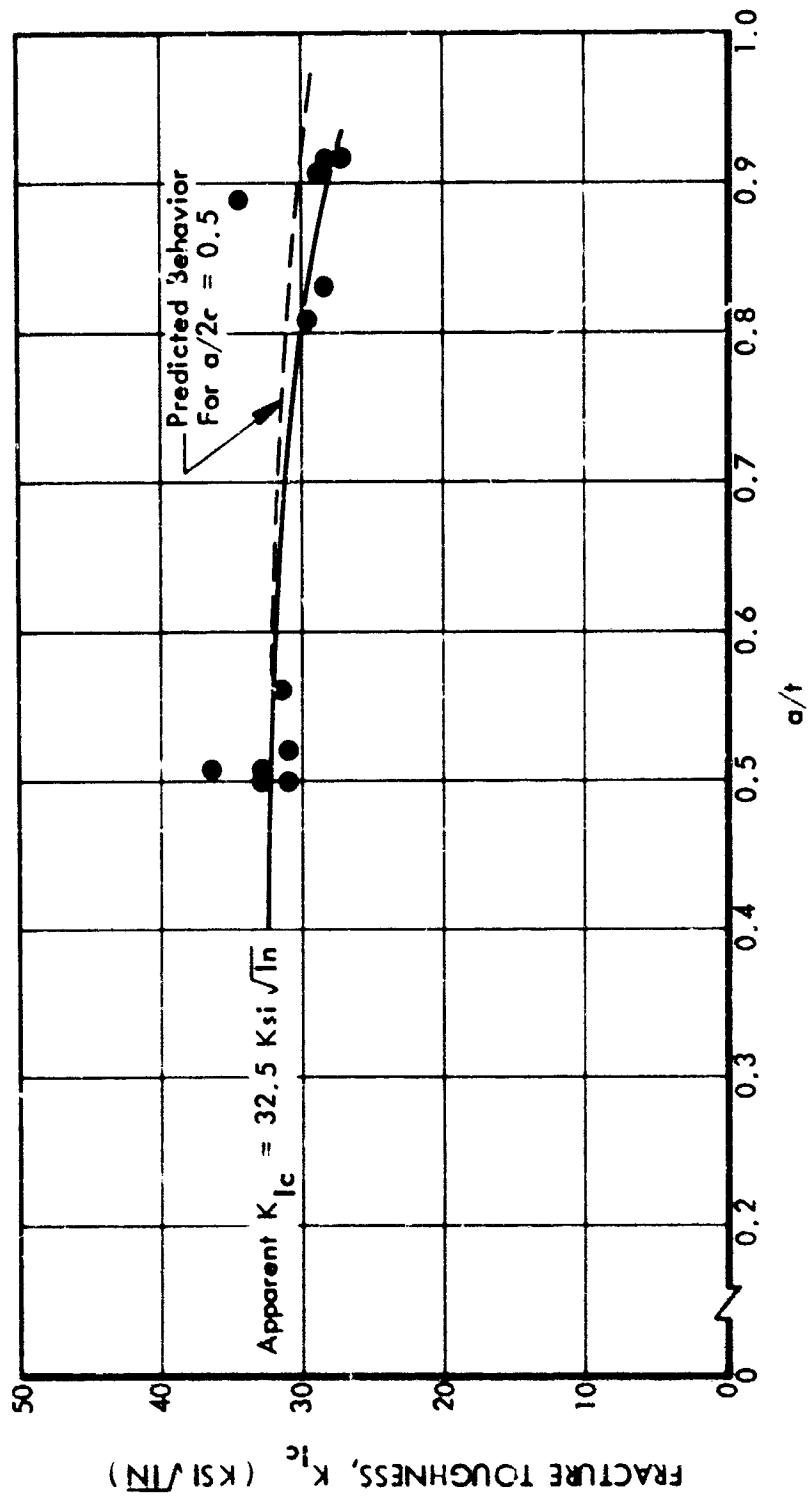


Figure 66: STATIC FRACTURE TOUGHNESS DATA FOR 2021-T81 ALUMINUM
BASE METAL



Specimen SA-2



Specimen SA-3



Specimen SA-4



Specimen SA-8



Specimen SA-9

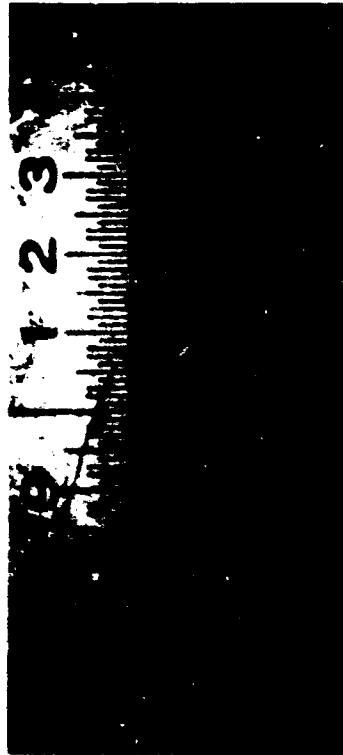


Specimen SA-10

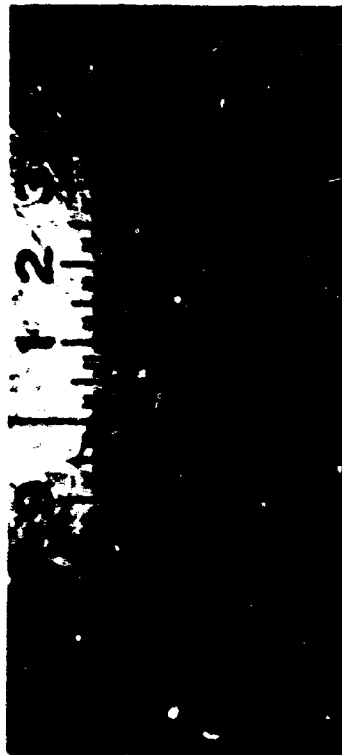
Figure 67 : FRACTOGRAPHS OF 2021-T81 ALUMINUM BASE METAL
(Sustained Test, White Light Illumination)



Specimen SA-2



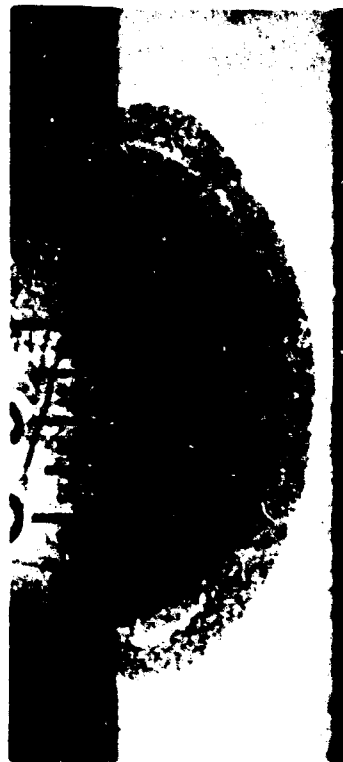
Specimen SA-3



Specimen SA-4



Specimen SA-8



Specimen SA-9



Specimen SA-10

Figure 68 : FRACTOGRAPHS OF 2021-T81 ALUMINUM BASE METAL
(Sustained Test, Polarized Light Illumination)

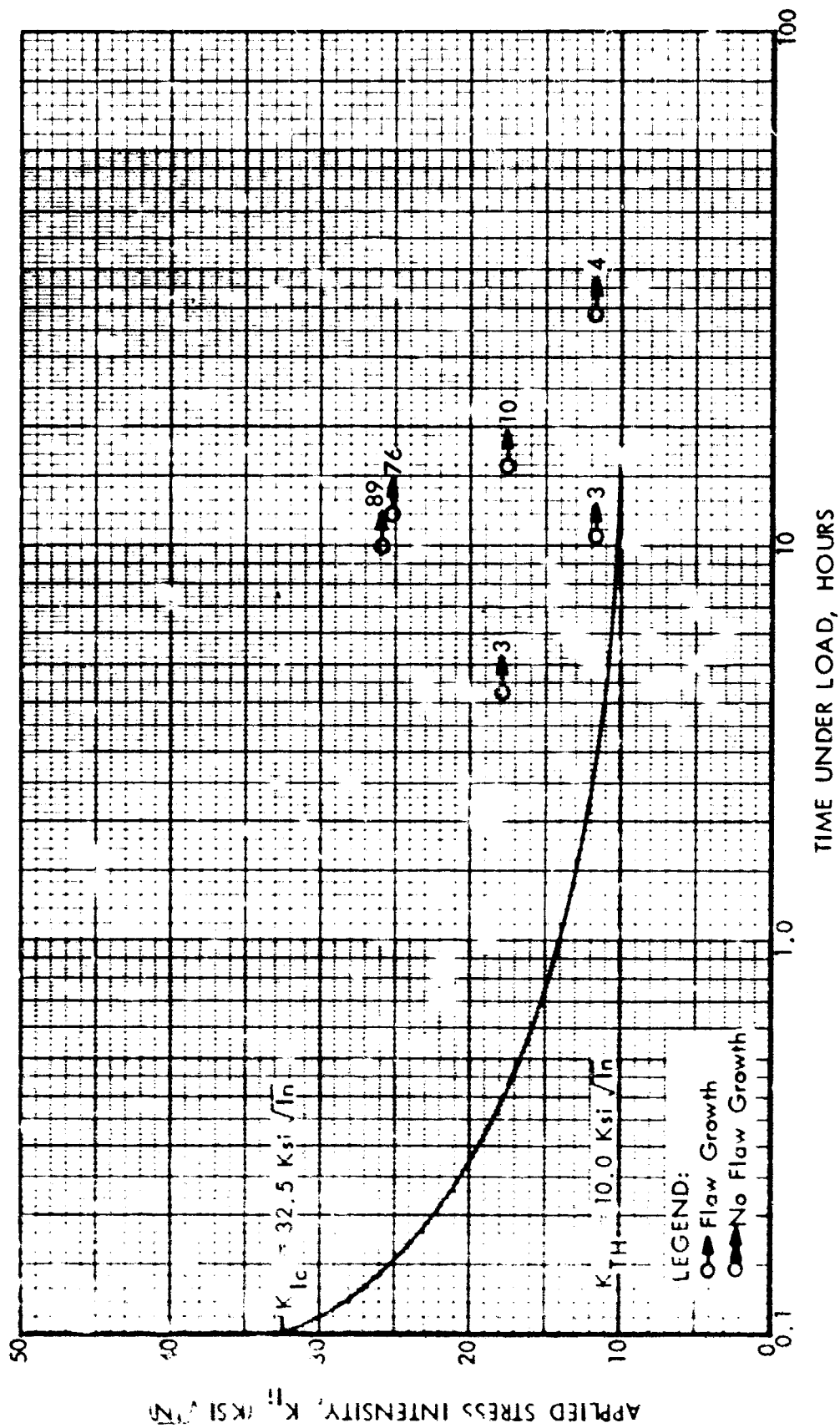


Figure 69 : SUSTAINED FLAW GROWTH DATA FOR 2021-T81 ALUMINUM
BASE METAL (N_2O_4 @ 145 °F And 100 Psig)

SPECIMEN NUMBER	SPECIMEN SIZE		CYCLIC EXTENSION OF EDM FLAW			FLAW SIZE BEFORE THE TEST RUN			SUSTAINED TEST RUN					
	Thickness (Inches)	Width (Inches)	Temperature (°F)	Max Stress (Ksi)	Number of Cycles (1,000)	Flaw Depth a (Inches)	Flaw Length 2c (Inches)	Flaw Size a/Q (Inches)	Test Temperature (°F)	Max Stress σ_{max} (Ksi)	Time @ σ_{max} (Hours)	Irwln's K_{II} (Ksi \sqrt{In})	Kobayashi's K_{II} (Ksi \sqrt{In})	Smith's K_{II} @ α (Ksi \sqrt{In})
SA-1	.236	2.996	RT	15.0	12.0	-	-	-	-	-	-	-	-	-
			RT	20.0	3.0	.118	.420	.083	-	-	-	-	-	-
SA-2	.238	2.997	RT	20.0	8.0	.118	.420	.081	143	46.6	10.0	25.9	29.7	24.3
SA-3	.238	2.997	RT	20.0	8.0	.117	.420	.078	142	32.9	4.2	17.9	20.5	19.4
SA-4	.238	2.998	RT	20.0	10.0	.116	.410	.075	141	21.9	10.5	11.7	13.4	10.9
SA-5	.238	2.997	RT	20.0	8.0	.118	.410	.100	-	-	-	-	-	-
SA-6	.237	2.998	RT	20.0	4.0	-	-	-	-	-	-	-	-	-
			-320	20.0	8.0	.123	.424	.085	-	-	-	-	-	-
SA-7	.238	2.997	RT	15.0	11.5	.192	.519	.109	-	-	-	-	-	-
SA-8	.237	2.997	RT	15.0	16.0	.196	.518	.106	139	39.7	12.0	25.2	37.5	-
SA-9	.237	2.999	RT	15.0	14.0	.198	.520	.105	144	27.9	16.0	17.6	26.2	-
SA-10	.237	2.999	RT	15.0	14.0	.199	.515	.103	142	18.7	38.5	11.7	17.5	-
SA-11	.236	2.999	RT	15.0	11.2	.195	.512	.106	-	-	1	-	-	-
SA-12	.236	2.999	RT	15.0	12.0	.216	.524	.109	155	42.5	2	-	-	-
SA-13	.236	2.999	RT	15.0	11.0	-	-	-	155	34.0	10.5	-	-	-



STATIC TEST IN THE ENVIRONMENT OF N_2O_4



FAILED ON LOADING



SPECIMEN TO BE DELIVERED TO CAPT. PHIL MERRILL

* EXTRAPOLATED

A.

FERRIL

B.

**Table 17: SUSTAINED FLAW GROWTH DATA
2021-T81 ALUMINUM BASE METAL
IN THE ENVIRONMENT OF N₂O₄
AT 155°F AND 100 PSIG PRESSURE**

[illegible]

the specimen with longer hold time (SA-10) did have somewhat larger flaw extension as compared to specimen SA-4. Both specimens were subjected to identical stress intensity values of $11.7 \text{ ksi } \sqrt{\text{in.}}$. The threshold stress intensity for 2021-T81 aluminum and N_2O_4 at 145°F and 100 psig is taken to be at $10.0 \text{ ksi } \sqrt{\text{in.}}$ level.

5.2.2.2 N_2O_4 and 2021-T81 Aluminum Weldment

Static as well as sustained load flaw growth data for 2021-T81 aluminum weldments in the environment of N_2O_4 at 155°F and 100 psig pressure is summarized in TABLE 18. There were three different panels used for fabrication of these specimens. Panels A and B represent repaired, then heat-treated weldments of 2021 aluminum. Panel AW represents welded, then heat-treated 2021 aluminum weldments. Code number of each specimen reflects its origin (panels A, B, and AW) as well as approximate location within the panel.

Of the 14 specimens tested, three specimens (A1-3, A1-4, and A2-3) broke upon loading in the environment of heated and pressurized N_2O_4 . Specimens A2-4, B1-3, A2-1, B1-1, and A1-2 were subjected to sustained load test run, then cyclically marked and either pulled to failure or fractured during cyclic marking. Specimens B1-4, A2-2, B1-2, AW1-1, and AW1-3 were pulled to failure at room temperature to obtain static fracture toughness for the material. Specimen AW1-4 was subjected to sustained test run of 11.6 hours, then sent to Alcoa for further analysis.

Static fracture toughness data for 2021-T81 aluminum weldments as well as end points from the sustained load test specimens are plotted in Figure 70. The data is plotted in terms of fracture toughness K_{Ic} versus flaw-depth-to-specimen-thickness (a/t) ratio. The plot contains data points obtained by pulling specimen to failure at room temperature in ambient air as well as specimens that fracture upon application of load in the environment of heated N_2O_4 . All end points of the sustained test specimens are also included.

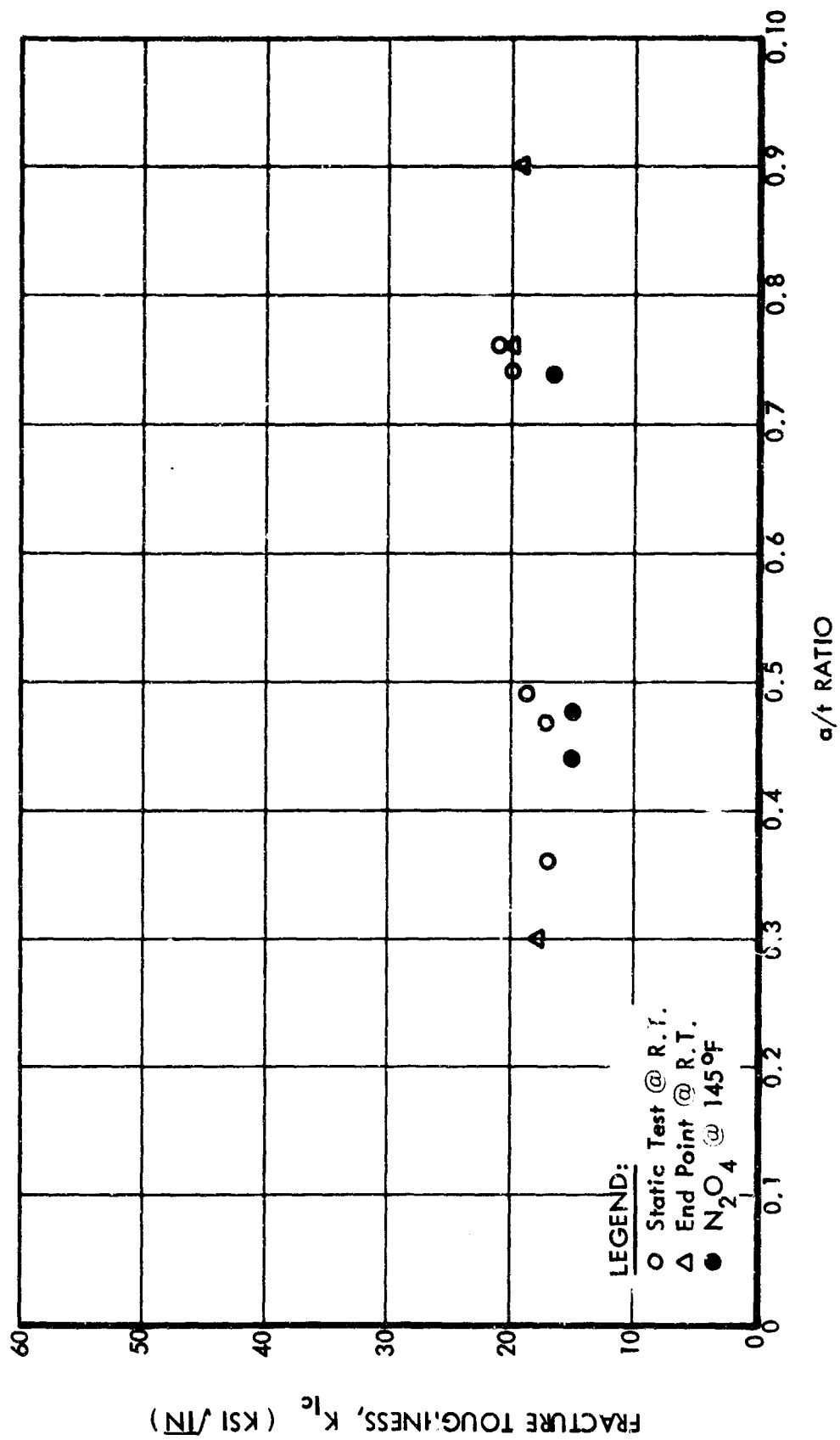
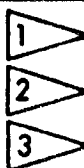


Figure 70: STATIC FRACTURE TOUGHNESS FOR 2021-T81 ALUMINUM WELDMENT

SPECIMEN NUMBER	SPECIMEN SIZE		CYCLIC EXTENSION OF EDM FLAW			FLAW SIZE BEFORE THE TEST RUN			SUSTAINED TEST RUN						Flaw Depth (Inches)
	Thickness (Inches)	Width (Inches)	Temperature (°F)	Max Stress (Ksi)	Number of Cycles (1,000)	Flaw Depth a (Inches)	Flaw Length 2c (Inches)	Flaw Size a/Q (Inches)	Test Temperature (°F)	Max Stress σ_{max} (Ksi)	Time @ σ_{max} (Hours)	Irwin's K_{II} (Ksi \sqrt{In})	Kobayashi's K_{II} (Ksi \sqrt{In})	Smith's K_{II} @ α (Ksi \sqrt{In})	
A2-4	.233	2.999	RT	14.0	38.0	.110	.460	.081	155	17.9	9.0	9.9	11.2	11.2	.11
B1-3	.232	2.998	RT	14.0	33.0	.105	.461	.082	155	23.7	28.3	13.3	14.8	15.1	.18
A1-3	.231	2.998	RT	14.0	35.0	.110	.451	.085	151	26.3	2	-	-	-	-
A1-4	.229	2.997	RT	14.0	20.0	.100	.460	.083	153	26.8	2	-	-	-	-
A2-3	.227	2.998	RT	14.0	10.0	.168	.745	.132	154	23.3	2	-	-	-	-
A2-1	.222	2.998	RT	14.2	30.0	.112	.467	.082	155	17.8	13.1	-	-	-	-
-	-	-	-	-	-	-	-	-	RT	1.1	1.6	-	-	-	-
-	-	-	-	-	-	-	-	-	155	17.8	7.2	-	-	-	-
-	-	-	-	-	-	-	-	-	RT	0.9	2.8	-	-	-	-
-	-	-	-	-	-	-	-	-	154	17.8	10.1	9.9	11.5	11.5	.11
B1-1	.231	2.998	RT	14.0	12.0	.175	.737	.128	154	16.7	16.3	11.7	16.4	-	.17
A1-2	.231	2.997	RT	16.0	45.0	.064	.220	.045	153	26.1	12.5	10.8	11.2	10.8	.06
B1-4	.230	2.999	RT	14.0	32.0	.109	.455	.088	-	-	-	-	-	-	-
A2-2	.226	2.998	RT	14.0	12.0	.168	.730	.136	-	-	-	-	-	-	-
B1-2	.233	3.000	RT	14.0	20.0	.177	.735	.141	-	-	-	-	-	-	-
AW1-1	.223	3.002	RT	26.5	40.0	.081	.230	.050	-	-	-	-	-	-	-
AW1-3	.226	3.000	RT	14.0	35.0	.110	.460	.085	-	-	-	-	-	-	-
AW1-4	.224	2.998	RT	14.0	35.0	3	3	-	158	26.6	11.6	-	-	-	-



FLAW GREW THROUGH THE THICKNESS

BROKE UPON LOADING

SAME SIZE AS AW1-3
SPECIMEN SENT TO CAPT. MERRIL
FOR ANALYSIS

A.

**Table 18: SUSTAINED FLAW GROWTH DATA
2021-T81 ALUMINUM WELDMENT
IN THE ENVIRONMENT OF N₂O₄
AT 155°F AND 100 PSIG PRESSURE**

[illegible]

All fractured 2021-T81 weld metal specimens were sectioned and etched in the manner to provide some insight on the microstructural composition of the weldments as well as location and propagation path of the surface flaws. Figures 71 through 77 show such fractographs together with cross sectional view of each specimen. Considering location of the propagating crack path with respect to weld fusion zone, it may be deduced that of the 13 specimens tested, only the A1-3, A1-4, B1-4, and AW1-1 could be considered as reflecting properties of weld fusion zone. Calculated fracture toughness values for these specimens are 15.0, 15.0, 17.2, and 17.0 ksi $\sqrt{\text{in.}}$ respectively. Specimens A1-3, and A1-4 were tested at 145°F. The average value of these two specimens is 15.0 ksi $\sqrt{\text{in.}}$ and is taken to represent fracture toughness of 2021-T81 weldment fusion zone at 145°F. Specimens B1-4 and AW1-1 were tested in ambient air. Their average K_{Ic} value is 17.1 ksi $\sqrt{\text{in.}}$ and is taken to represent fracture toughness of 2021-T81 aluminum fusion zone area at room temperature.

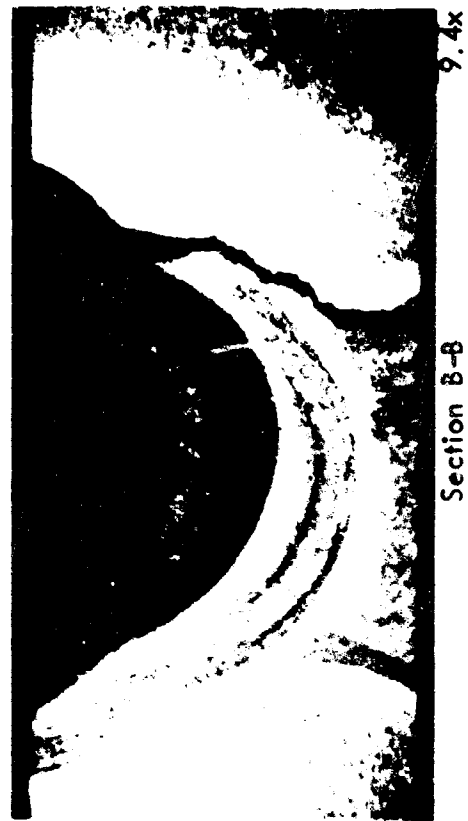
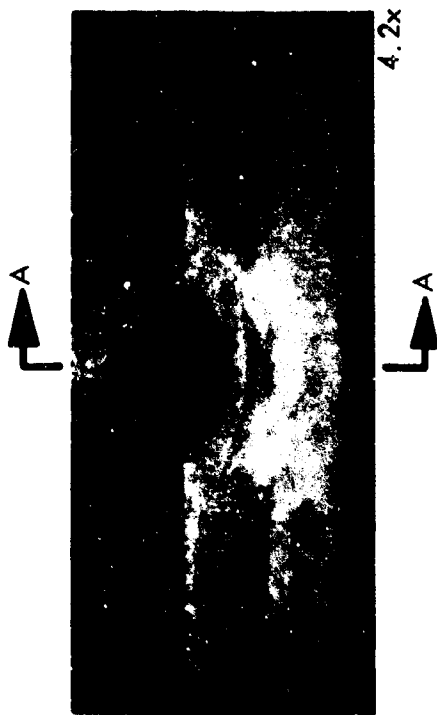
Sustained flaw growth data for 2021-T81 aluminum weldments is plotted in Figure 78 in terms of applied stress intensity K_{I1} versus time under load in hours. The threshold stress intensity level is set at 9.0 ksi $\sqrt{\text{in.}}$ by drawing a curve to separate data points reflecting flaw growth from those that show no flaw growth. On the ordinate the curve passes through a point for K_{I1} equal to 15.0 ksi $\sqrt{\text{in.}}$ which is the assumed fracture toughness for the material.

5.2.3 6A1-4V(ELI) Titanium

Two material-propellant combinations were evaluated for 6A1-4V(ELI) titanium. In both cases, the evaluation was conducted using as-welded weldments. The two propellants evaluated were liquid fluorine (F_2) at -320°F and liquid chlorine pentafluoride (ClF_5) at 145°F. Mechanical properties of as-welded 6A1-4V(ELI) titanium weldments are plotted in Figure 79 as a function of test temperature. The mechanical properties test data was generated as part of the NASA contract (NAS 3-7993) with The Boeing Company. Tensile



SPECIMEN A1-2



SPECIMEN A1-3

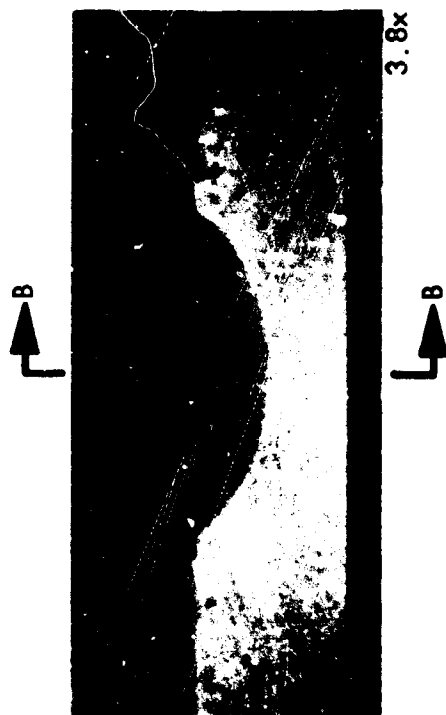
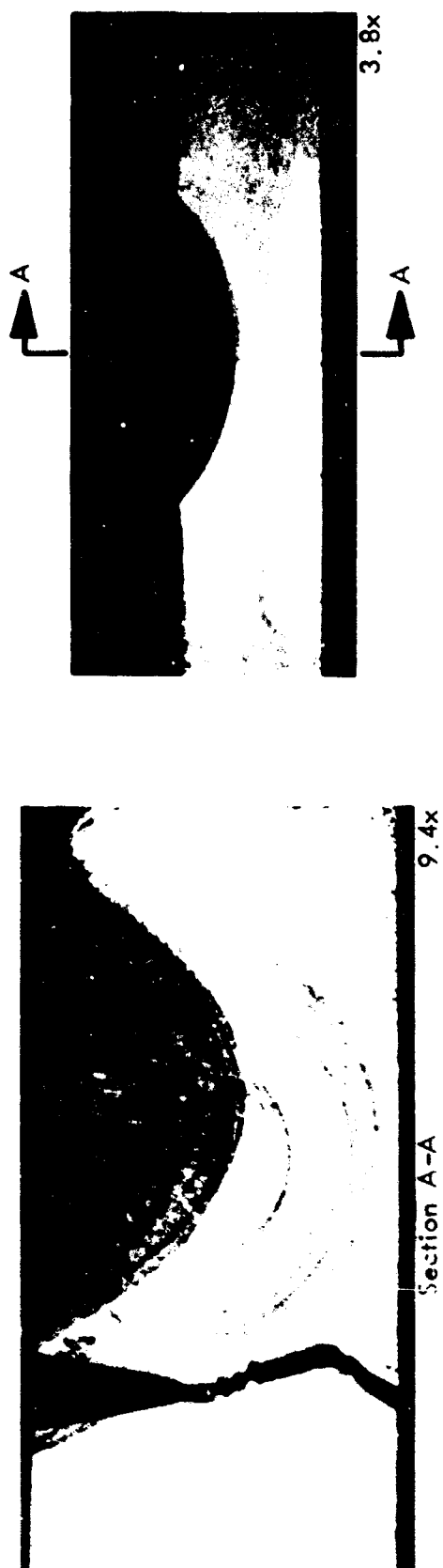
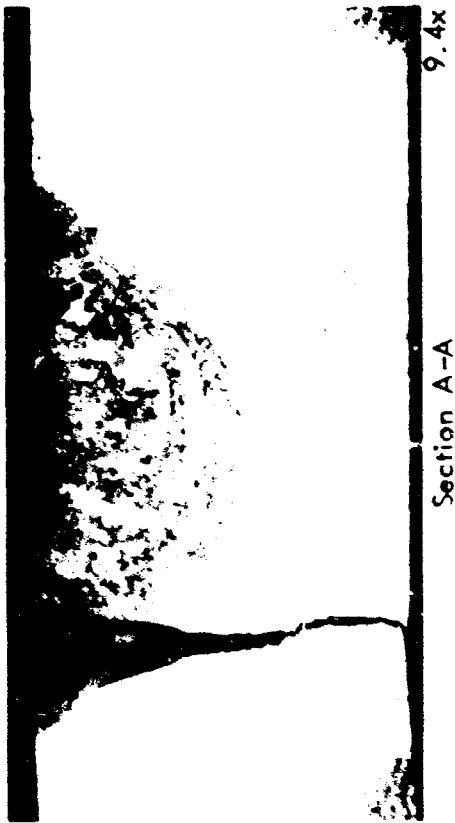


Figure 71 : CRACK PATH AND FRACTURE APPEARANCE IN 2021-T81 ALUMINUM
WELDMENT (Specimens A1-2 And A1-3)

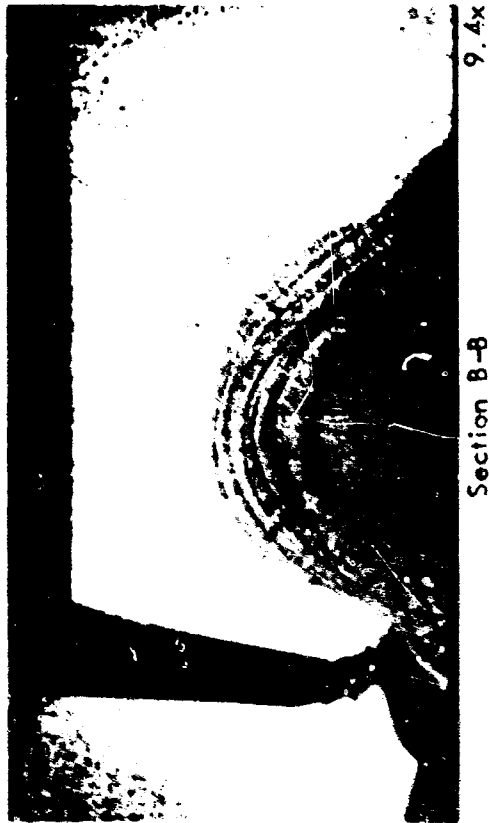
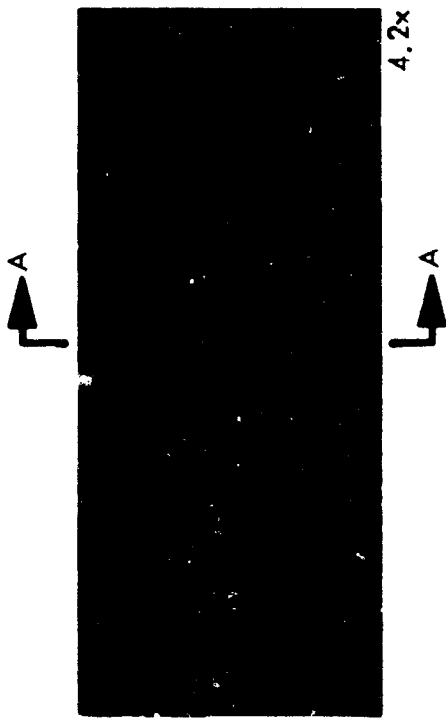


SPECIMEN AI-4

Figure 72 : CRACK PATH AND FRACTURE APPEARANCE IN 2021-T81 ALUMINUM
WELDMENT (Specimen AI-4)



SPECIMEN A2-1



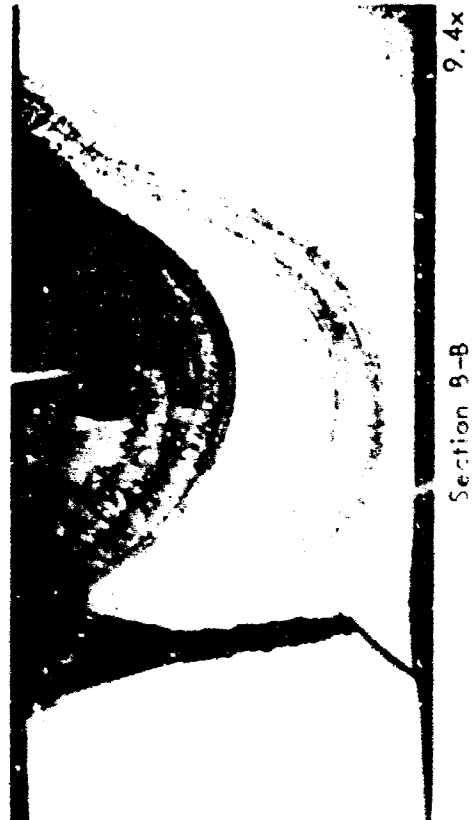
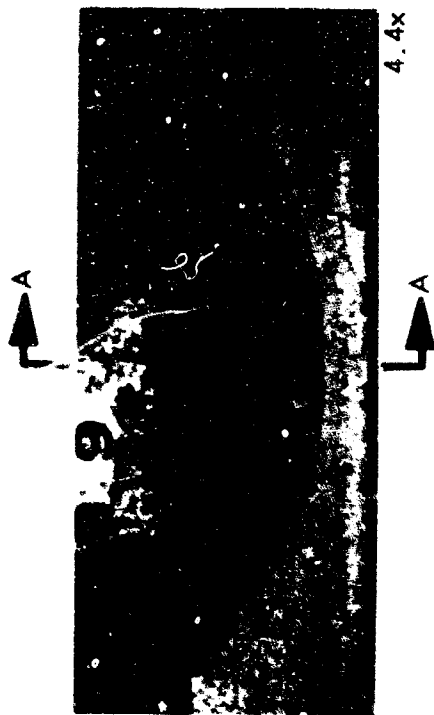
SPECIMEN A2-2



Figure 73 : CRACK PATH AND FRACTURE APPEARANCE IN 2021-T81 ALUMINUM WELDMENT (Specimens A2-1 And A2-2)



SPECIMEN A2-3



SPECIMEN A2-4

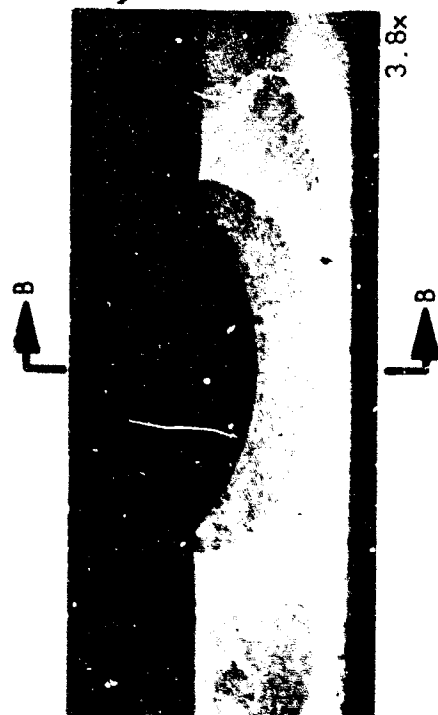


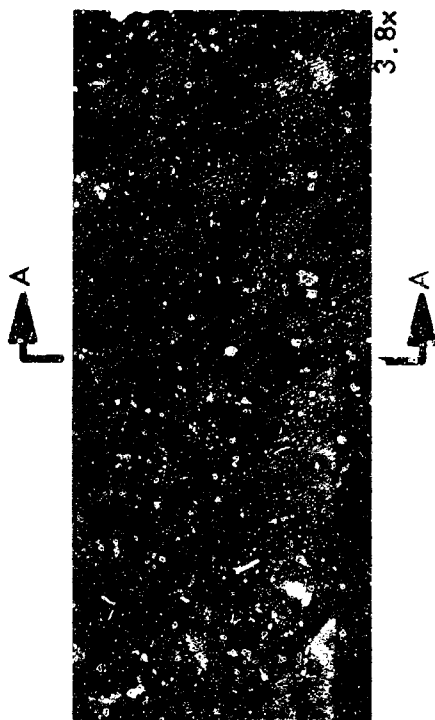
Figure 74: CRACK PATH AND FRACTURE APPEARANCE IN 2021 T81 ALUMINUM WELDMENT (Specimens A2-3 And A2-4)



Section A-A

9.4x

SPECIMEN B1-1



Section B-B

9.4x

SPECIMEN B1-2

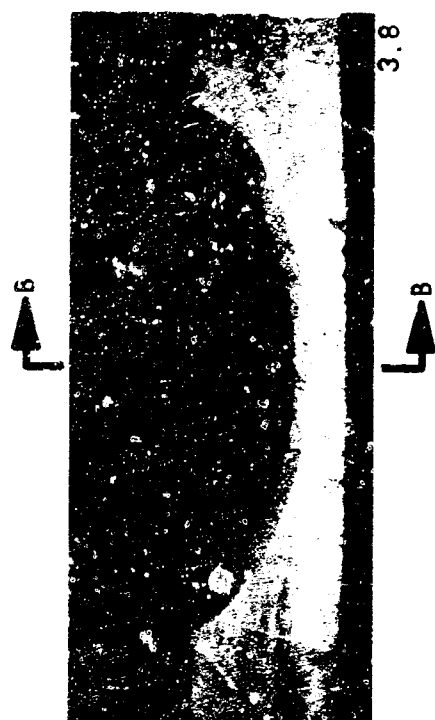
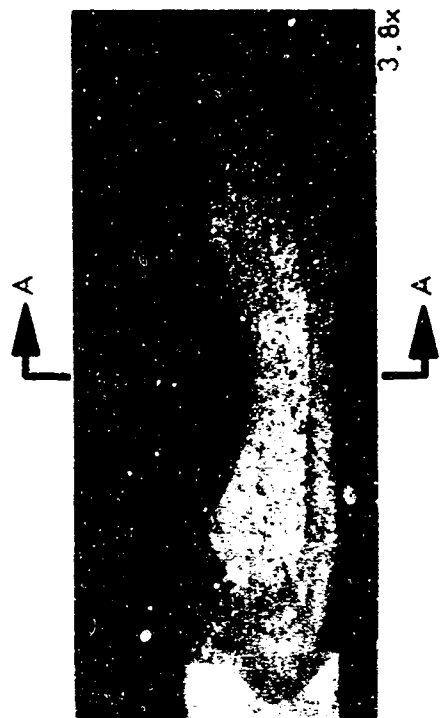
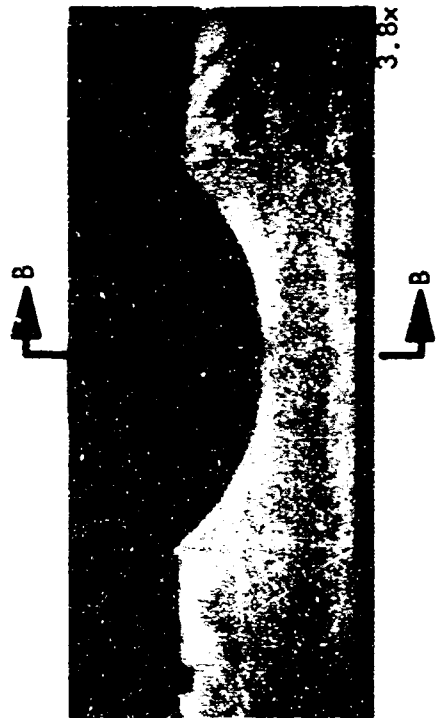
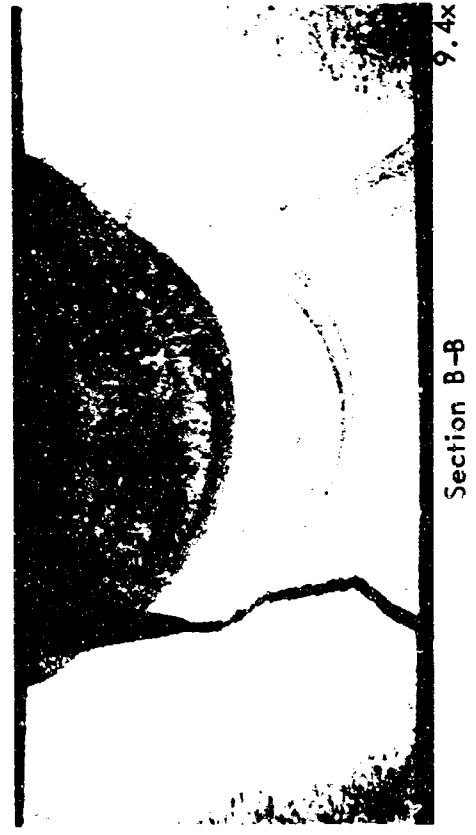


Figure 75: CRACK PATH AND FRACTURE APPEARANCE IN 2021-T81 ALUMINUM
WELDMENT (Specimens B1-1 And B1-2)



SPECIMEN B1-3



SPECIMEN B1-4

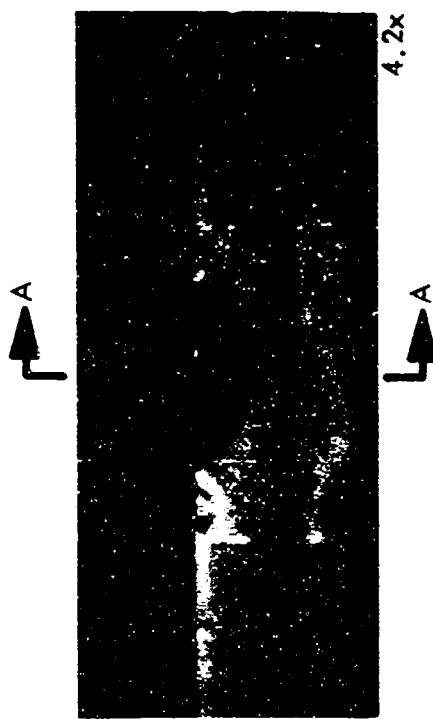
Figure 76: CRACK PATH AND FRACTURE APPEARANCE IN 2021-T81 ALUMINUM WELDMENT (Specimens B1-3 And B1-4)



Section A-A

9.4x

SPECIMEN AW1-1



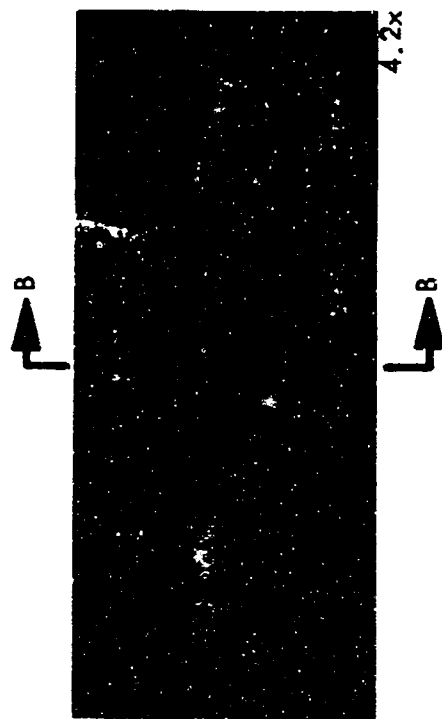
4.2x



Section B-B

9.4x

SPECIMEN AW1-3



4.2x

Figure 77 : CRACK PATH AND FRACTURE APPEARANCE IN 2021-T81 ALUMINUM WELDMENT (Specimens AW1-1 And AW1-3)

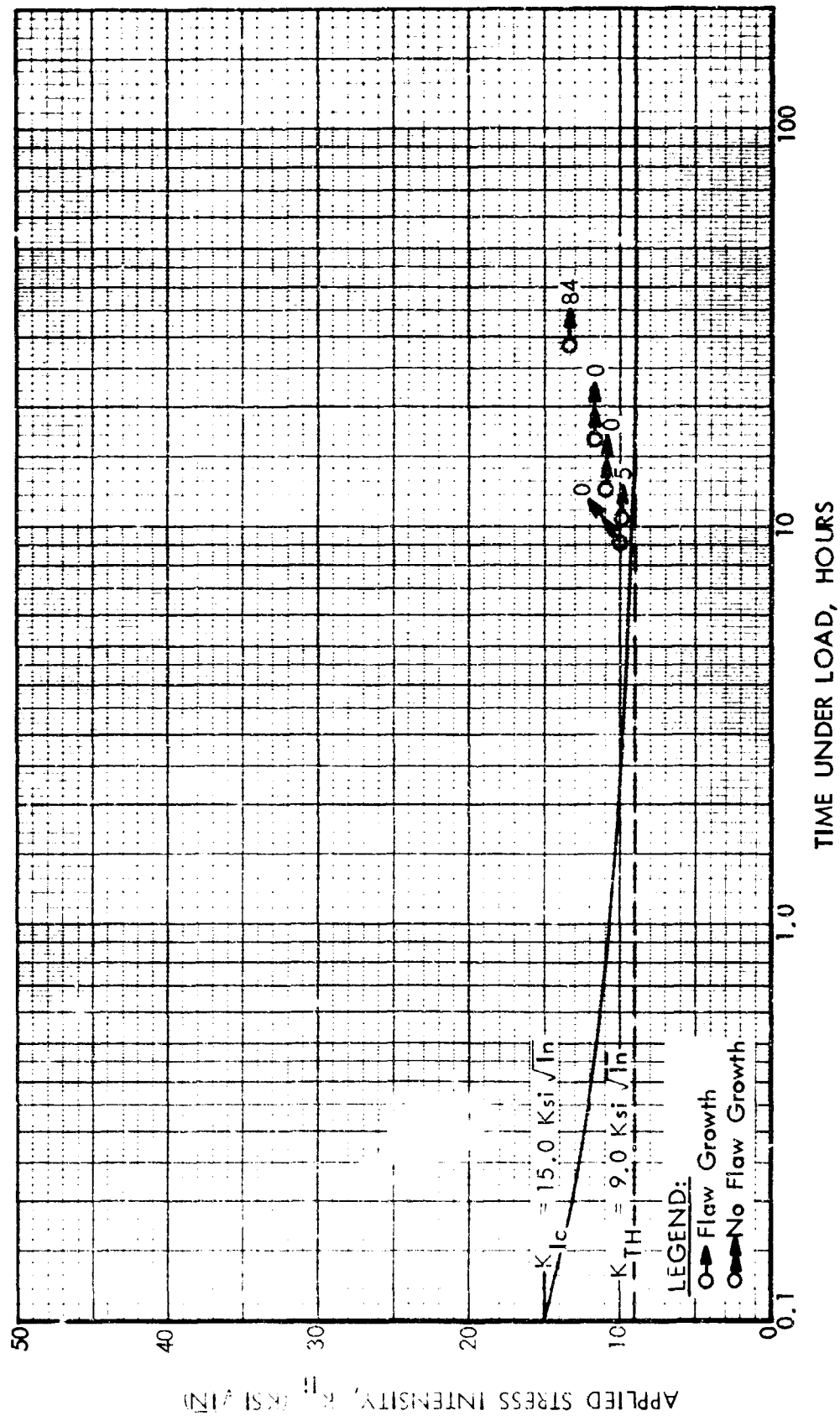


Figure 78: SUSTAINED FLAW GROWTH DATA FOR 2021-T81 ALUMINUM WELDMENTS
(N₂O₄ @ 145 °F And 100 Psig)

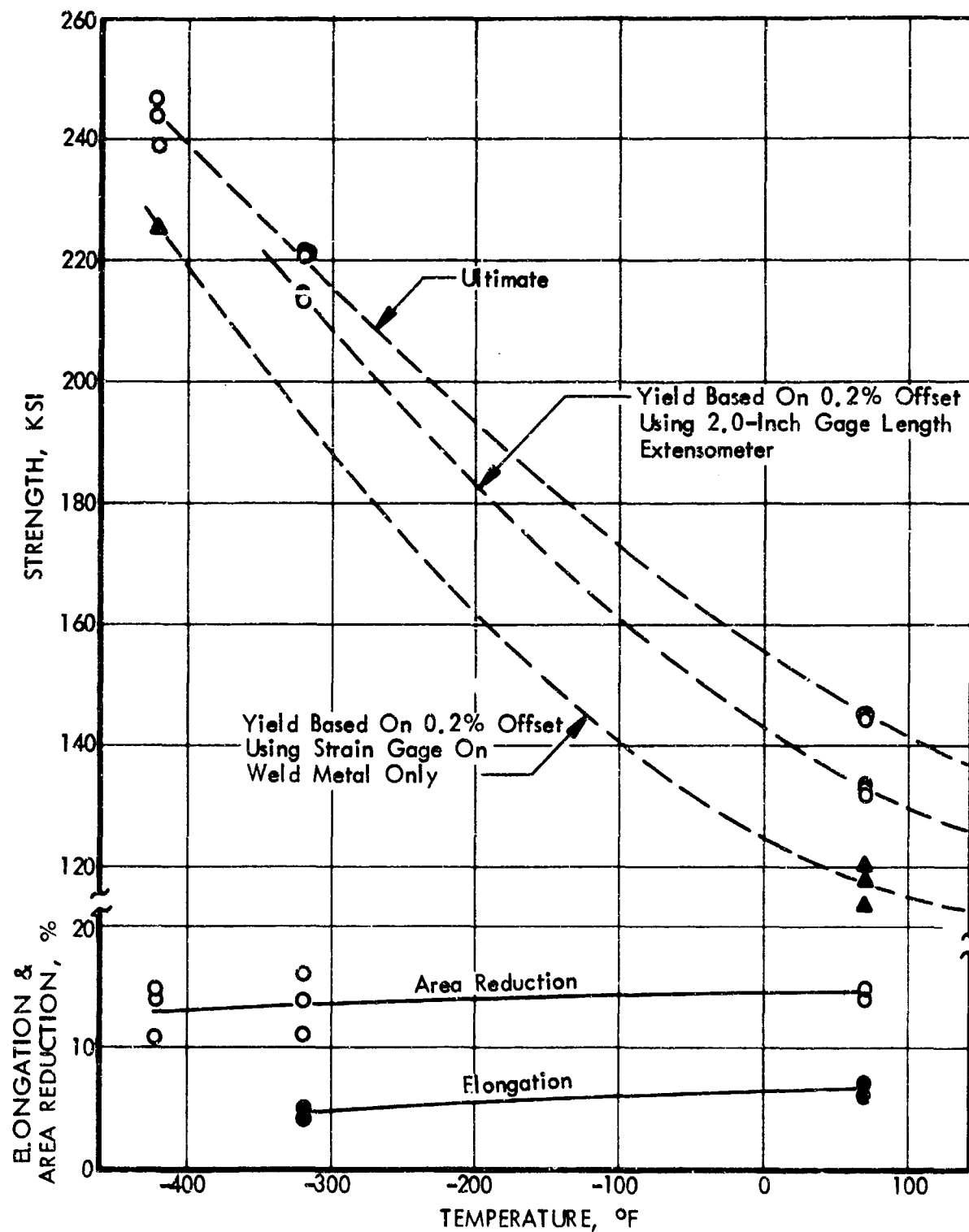


Figure 79 : MECHANICAL PROPERTIES FOR 6Al-4V (ELI) TITANIUM AS-WELDED WELDMENTS

test data for 140-150°F test temperatures, while not specifically obtained in the referenced test program, has been estimated by considering effect of temperature increase from 75 to 140°F as shown in ASM Metals Handbook, Vol 1 for 6Al-4V titanium alloy.


The yield strength (as measured using 2.0 inch extensionmeter) is 133.0 ksi for the material at room temperature while at the same temperature the indicated yield strength drops down to 117.0 ksi if 3/8 of an inch long strain gage is used. For the purpose of calculating applied stress intensity levels and fracture toughness values yield strengths of 127.0, 133.0, 190.0, and 215.0 ksi were used for test temperatures of 140, RT, -230, and -320°F, respectively. Mechanical properties data is summarized in TABLE 19.

Static fracture toughness data for 6Al-4V(ELI) titanium at different test temperatures is summarized in TABLE 20. There were three specimens tested for each test temperature. The flaws in all fracture toughness specimens were located in the center of the weld bead. Fractographs of static test specimens tested at room temperature and at -320°F are shown in Figure 80. Those tested at +140°F and -230°F are shown in Figure 81. A plot of static fracture toughness data as a function of test temperature is shown in Figure 82. The plot consists of fracture toughness (K_{IC}) on the ordinate and test temperature in degrees Fahrenheit on the abscissa. Static fracture toughness data for 6Al-4V(ELI) titanium weldments at room temperature is plotted for static as well as sustained load test specimens in Figure 83 as a function of flaw-depth-to-thickness ratio. The data is very consistent between static and end point specimens. Static fracture toughness for the 6Al-4V(ELI) titanium as-welded weldment is set to be 62.5 ksi $\sqrt{\text{in.}}$ at room temperature, 64.0 ksi $\sqrt{\text{in.}}$ at +140°F, 55.0 ksi $\sqrt{\text{in.}}$ at -230°F, and 44.0 ksi $\sqrt{\text{in.}}$ at -320°F.

5.2.3.1 F_2 and 6Al-4V(ELI) Titanium

The sustained flaw growth data for 6Al-4V(ELI) titanium as-welded weldments in the environment of liquid fluorine at -320°F test temperature and 450 psig

Table 19: MECHANICAL PROPERTIES OF 6Al-4V (ELI)
TITANIUM AS-WELDED WELDMENT

SPECIMEN IDENTIFICATION	TEST TEMPERATURE (°F)	GRAIN ORIENTATION	SPECIMEN SIZE		ULTIMATE STRENGTH (KSI)	YIELD STRENGTH (KSI)	ELONGATION (%)	REDUCTION OF AREA (%)
			THICKNESS (IN)	WIDTH (IN)				
	RT	T	0.317	0.40	144.1	131.8	7	-
	RT	T	0.316	0.40	144.6	134.0	7	-
	RT	T	0.313	0.40	144.0	132.9	7	-
	-320	T	0.315	0.40	221.7	215.8	5	16
	-320	T	0.319	0.40	220.7	213.7	4	11
	-320	T	0.319	0.40	220.6	214.3	4	14
	-423	T	0.320	0.40	243.8	-	-	14
	-423	T	0.320	0.40	246.5	-	-	15
	-423	T	0.316	0.40	238.2	-	-	11

 SPECIMEN TEST DATA WAS ABSTRACTED FROM D2-114465

T TENSILE PROPERTIES MEASURED ACROSS WELDMENT



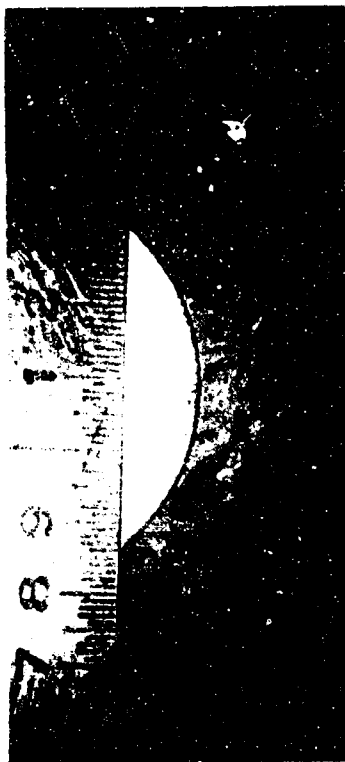
Specimen TW-1



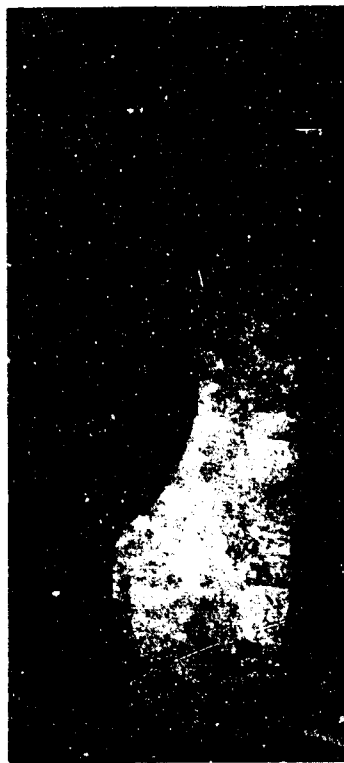
Specimen TW-2



Specimen TW-3



Specimen TW-4



Specimen TW-5

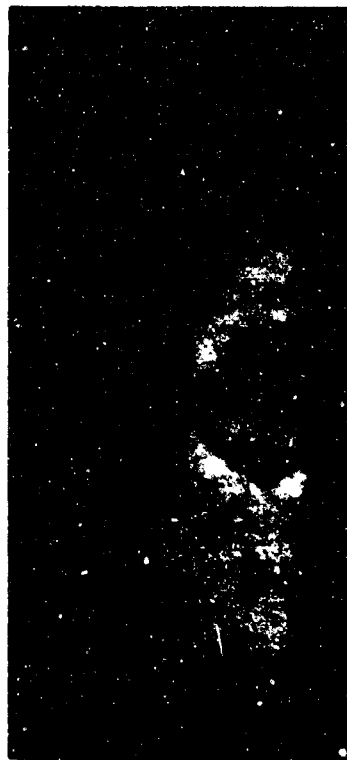


Specimen TW-6

Figure 80 : FRACTOGRAPHS OF 6Al-4V (ELI) TITANIUM AS-WELDED WELDMENTS
(Static Test @ Room Temperature And -320 °F)



Specimen TW-7



Specimen TW-10



Specimen TW-8



Specimen TW-11



Specimen TW-9



Specimen TW-12

Figure 81: FRACTOGRAPHS OF 6Al-4V (ELI) TITANIUM AS-WELDED WELDMENT
(Static Test @ 140 °F And -230 °F)

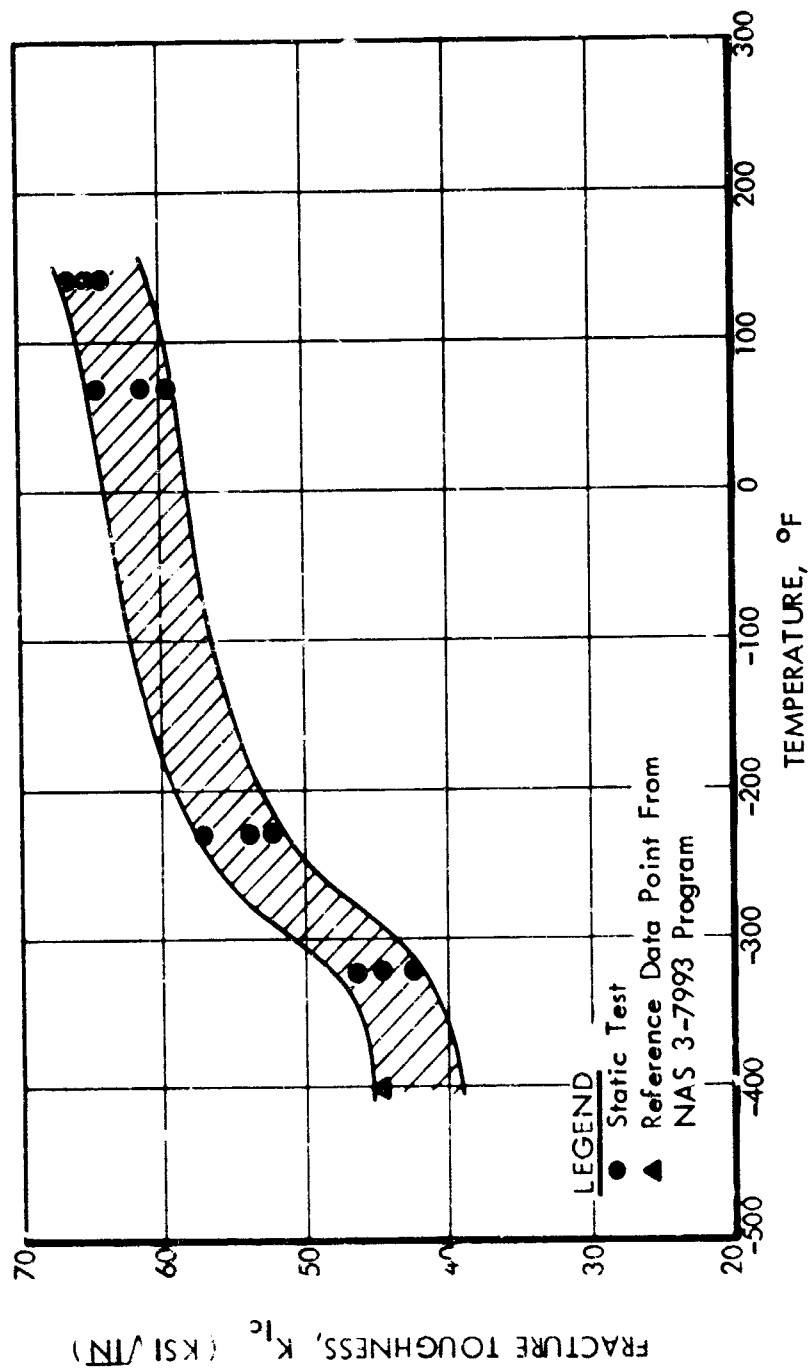


Figure 82: STATIC FRACTURE TOUGHNESS DATA FOR 6Al-4V (ELI) TITANIUM AS-WELDED WELDMENTS

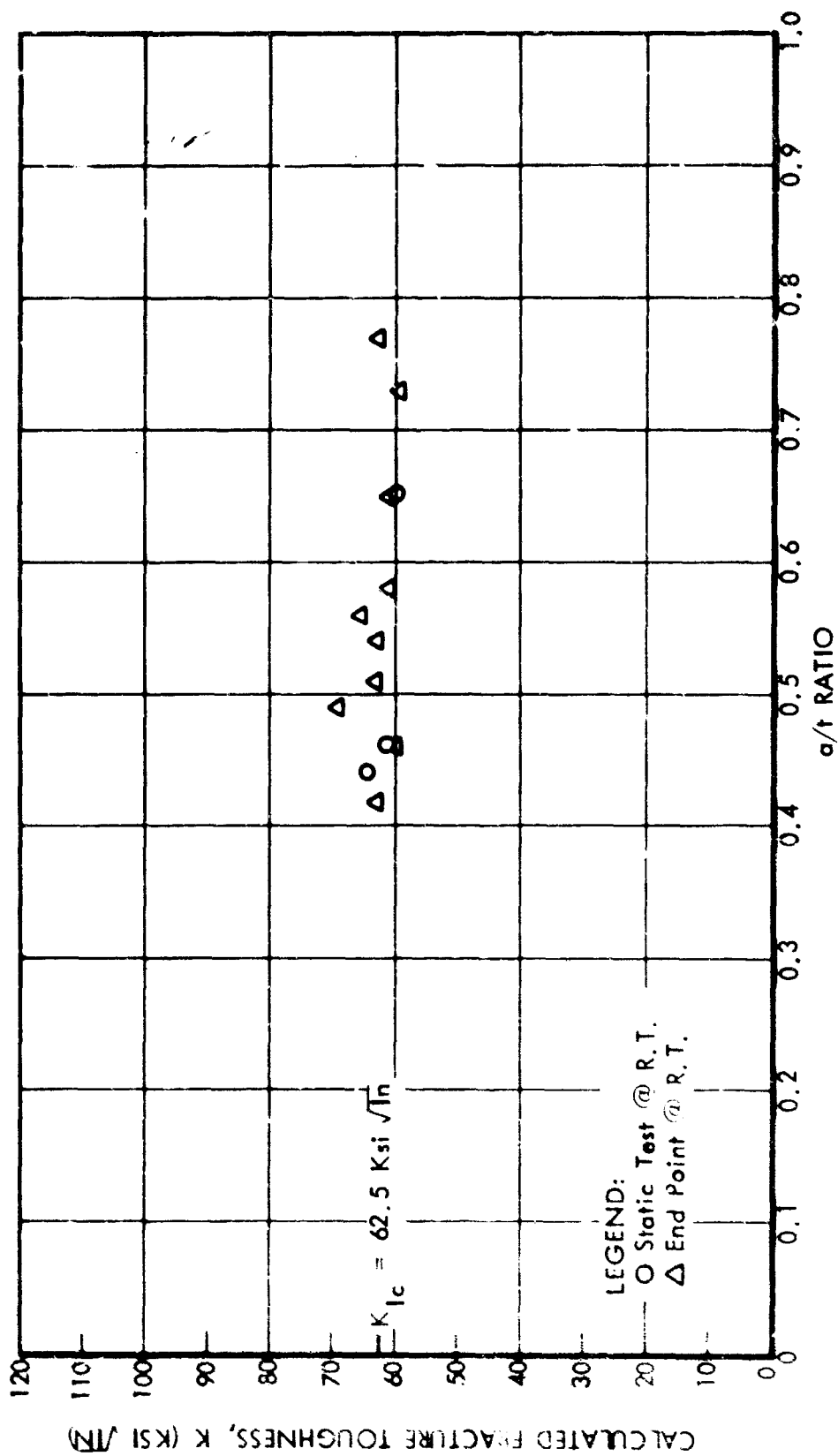


Figure 83: EFFECT OF FLAW DEPTH UPON CALCULATED FRACTURE TOUGHNESS
 (6Al-4V (ELI) Titanium As-Welded Weldment)

[illegible]

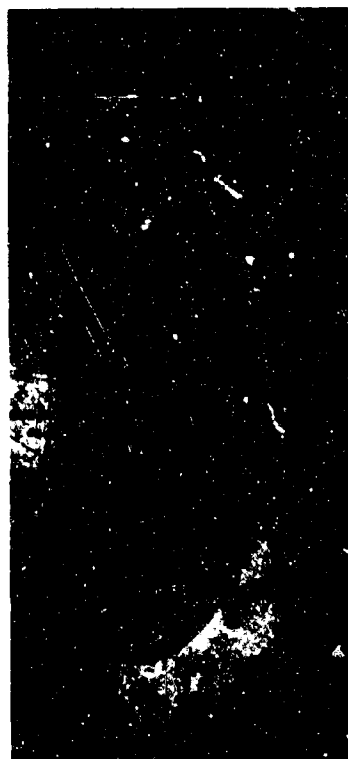
Table 20: STATIC FRACTURE TOUGHNESS DATA
FOR 6Al-4V(ELI) TITANIUM AS-WELDED
WELDMENTS

CYCLIC FLAW MARKING			FLAW SIZE AFTER CYCLIC MARKING			TEST CONDITION AT FRACTURE							
(°F)	Max Stress (Ksi)	Number of Cycles (1,000)	Flaw Depth a (Inches)	Flaw Length 2c (Inches)	Flaw Size a/Q (Inches)	Temperature (°F)	Flaw Depth a (Inches)	Flaw Length 2c (Inches)	Flaw Size a/Q (Inches)	Fracture Stress (Ksi)	Irwin's K_{Ic} (Ksi $\sqrt{\text{In}}$)	Kobayashi's K_{Ic} (Ksi $\sqrt{\text{In}}$)	Smith's K_{Ic} (Ksi $\sqrt{\text{In}}$)
-	-	-	-	-	-	RT	.169	.492	.101	96.1	59.5	76.7	64.3
-	-	-	-	-	-	RT	.119	.448	.086	106.8	61.2	68.7	66.4
-	-	-	-	-	-	RT	.117	.445	.086	112.9	64.7	71.8	69.8
-	-	-	-	-	-	-320	.117	.448	.079	80.9	44.5	49.1	47.9
-	-	-	-	-	-	-320	.122	.445	.081	76.4	42.3	47.3	45.3
-	-	-	-	-	-	-320	.112	.447	.078	85.1	46.4	51.6	50.8
-	-	-	-	-	-	140	.118	.442	.089	114.6	66.8	73.9	71.5
-	-	-	-	-	-	140	.118	.452	.090	110.1	64.2	71.4	69.5
-	-	-	-	-	-	140	.118	.442	.089	111.7	64.8	72.8	70.3
-	-	-	-	-	-	-230	.118	.445	.081	94.3	52.2	57.9	56.1
-	-	-	-	-	-	-230	.121	.451	.082	96.3	53.9	60.0	58.0
-	-	-	-	-	-	-230	.117	.447	.081	103.4	57.4	63.3	61.7

pressure is summarized in TABLE 21. Of the five specimens tested (TWLS-1 through -5) each specimen was exposed to sustained load test run for nearly 20 hours. All specimens showed various degrees of flaw growth and after cyclic marking were pulled to failure to give additional static fracture toughness data at room temperature. Additional information was acquired with specimen TWLS-4 by cyclic marking it at -320°F rather than at room temperature as was done with other specimens. The purpose of such cyclic marking at -320°F was to see if the small indication of flaw growth (in the order of about 0.001 of an inch) in specimen TWLS-1 was indeed brought about by physical separation of material at the crack tip and was not merely a reflection of a differently textured region caused by cyclic marking at room temperature. In the case of 2219-T87 aluminum, such indications of flaw growth disappeared by resorting to cyclic marking at -320°F (Reference 19).

Figure 84 shows fractographs of sustained test specimens exposed to F_2 . Cyclic marking at -320°F in specimen TWLS-4 still exhibited the same degree of differently textured area, suggested that small amounts of flaw growth indeed took place in both the TWLS-1 and TWLS-4 test specimens or that prior preloading at room temperature before cooling specimen assembly to -320°F had formed yield zone size considerably larger than corresponding zone that would have been formed if one specimen was loaded at -320°F . Propagation of the crack through such yield zone could have produced differently textured area without prior separation of material at the crack tip and also could have been responsible for apparently higher initial K_{I1} values that were reached during sustained load testing.

Sustained flaw growth data summarized in TABLE 21 is plotted in Figure 85 in terms of applied stress intensity (K_{I1}) versus time under load (hours). The sustained threshold stress intensity level is established by drawing a curve below data points showing some flaw growth including specimens TWLS-1 and -4 with .001 of an inch flaw growth indication in each. On the ordinate the line intersects K_{Ic} value of 44.0 ksi $\sqrt{\text{in.}}$ as established in Figure 82 for static fracture toughness data for the material at -320°F . Under these conditions the threshold stress intensity (K_{TH}) becomes 28.0 ksi $\sqrt{\text{in.}}$



Specimen TWLS-1



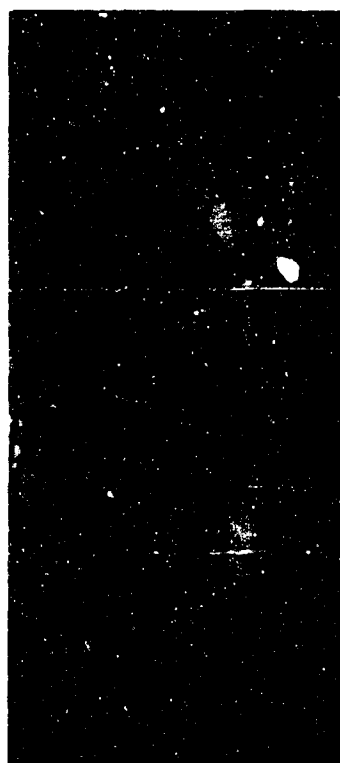
Specimen TWLS-3



Specimen TWLS-2



Specimen TWLS-4



Specimen TWLS-5

Figure 84 : FRACTOGRAPHS OF 6Al-4V (ELI) TITANIUM AS-WELDED WELDMENT
(Sustained Test In F₂ @ -320 °F And 450 Psig)

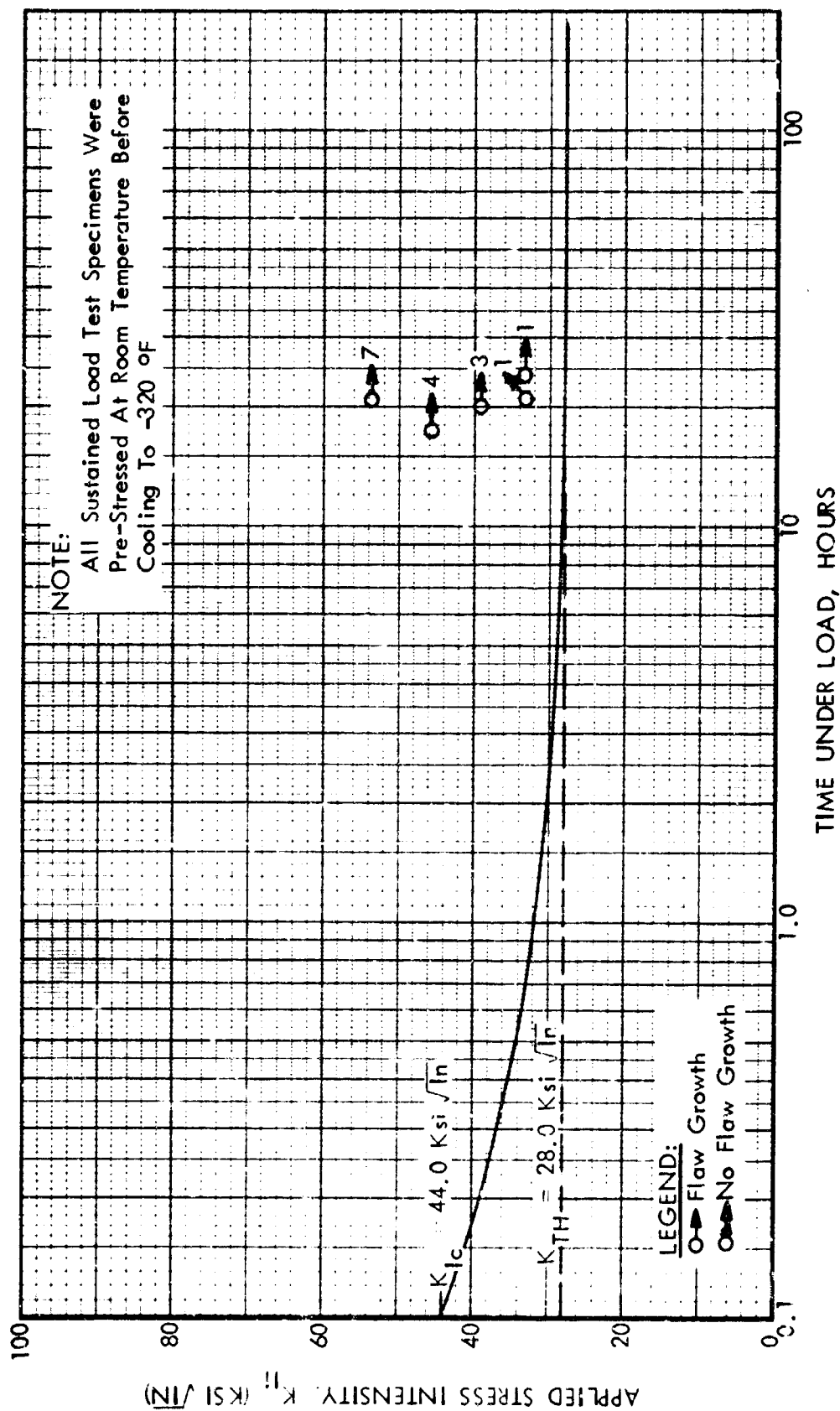


Figure 85: SUSTAINED FLAW GROWTH DATA FOR 6Al-4V (ELI) TITANIUM
 AS-WELDED WELDMENT (F_2 @ -320 °F And 450 Psig)

[illegible]

A.

Table 21: SUSTAINED FLAW GROWTH DATA FOR
6Al-4V(ELI) TITANIUM AS-WELDED
WELDMENT (F₂ AT -320°F AND 450 PSIG)

[illegible]

Flaw growth indications of the entire group of five test specimens were very consistent. All specimens were held under sustained load for approximately the same time. Specimens TWLS-1 and -4 had .001 of an inch flaw growth (or at least an indication of differently textured region which suggests flaw growth under sustained loading). Specimen TWLS-5 at the stress intensity of 38.8 ksi $\sqrt{\text{in.}}$ and approximately the same exposure time, had 0.003 flaw extension. Specimens TWLS-2 and -3 at progressively higher stress intensity levels had 0.004 and 0.007 of an inch flaw extensions, respectively. Gradual increase of flaw growth as a function of applied stress intensity tends to suggest that threshold stress intensity indeed would be in the close proximity to the selected value of 28.0 ksi $\sqrt{\text{in.}}$

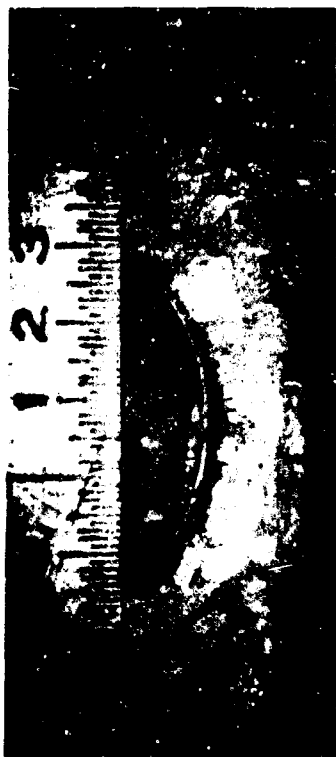
Referring back to Figure 85, it may be noted that fracture toughness value of 44.0 ksi $\sqrt{\text{in.}}$ as plotted on the ordinate, is actually lower than some of stress intensity levels that specimens TWLS-2 and -3 were subjected to during sustained load testing. Apparent explanation of this behavior may be drawn from the fact that loading sequence of test specimens subjected to liquid fluorine at -320°F consisted of first loading test specimen at room temperature to a target load, then tightening pressure cup over the surface flaw, filling cup with gaseous fluorine and cooling the entire assembly down to -320°F . Fresh supply of gaseous fluorine was provided during fluorine liquidation in the pressure cup. The resulting test data appears to have been affected to the extent that at -320°F specimens were able to withstand loads higher than during direct static testing at -320°F without prior prestressing at room temperature.

5.2.3.2 ClF_3 and 6Al-4V(ELI) Titanium

The sustained flaw growth data for 6Al-4V(ELI) titanium as-welded weldments in the environment of chlorine pentafluoride heated to 140°F and pressurized to 450 psig pressure is summarized in TABLE 22. Hold time under sustained load in view of the explosion and appreciable crack extension encountered during Phase I testing, was deliberately held short to make sure that rapid flaw growth would not precipitate spontaneous reaction. Specimen TWLS-8 was tested first, followed by TWLS-9, then -6 and -7. Each of these specimens was subjected to progressively lower stress intensity levels for a longer period of time. Fractographs of fractured specimens are shown in Figure 86. Included in the figure is also specimen TWLC-1 which was tested under cyclic loading conditions summarized in TABLE 23.



Specimen TWLS-6



Specimen TWLS-8



Specimen TWLS-7



Specimen TWLS-9



Specimen TWLC-1

Figure 86 : FRACTOGRAPHES OF 6Al-4V (ELI) TITANIUM AS-WELDED WELDMENT
(Sustained And Cyclic Test In ClF₅ @ 140 °F And 450 Pslg)

[illegible]

B

Table 22: SUSTAINED FLAW GROWTH DATA FOR 6Al-4V(ELI) TITANIUM AS-WELDED WELDMENT (ClF₅ AT 140°F AND 450 PSIG)

[illegible]

[illegible]

B.

Smith's K₁₂ @ n[illegible]

The sustained flaw growth data summarized in Table 22 is plotted in Figure 87. The plot is made in the usual manner of plotting applied stress intensity on the ordinate versus time under load on the abscissa. Solid curve separates data points with flaw growth from those showing no flaw growth. The ordinate is intersected by the solid line at a point of 64.0 ksi $\sqrt{\text{in.}}$ that corresponds to static fracture toughness of the material at +140°F as shown in Figure 82. For the short time exposure the threshold stress intensity level for the 6Al-4V(ELI) titanium in the environment of ClF_5 at 140°F and 450 psig pressure becomes 8.0 ksi $\sqrt{\text{in.}}$

Fractographic appearance of the sustained load test specimens shown in Figure 86 offers some interesting suggestions of apparent interaction between 6Al-4V(ELI) titanium and ClF_5 at 140°F. Unlike all other cases of sustained flaw growth observed during the course of this program, 6Al-4V(ELI) titanium specimens seem to react with ClF_5 in the manner that results not only in the flaw growth at exceptionally low stress intensity levels but also in selective directionality along preferred path of the flaw periphery causing rugged and irregular crack front.

Specimen TWLS-8 in Figure 86 was exposed to ClF_5 under higher stress intensity than any other specimen in this group. The flaw growth is large along the entire crack front periphery. Specimen TWLS-9, while still at a stress intensity above the threshold level, showed preferential flaw growth in the direction along $\alpha = 38$ degrees, as well as nucleation of cracks along several other points along the flaw periphery. Specimen TWLS-6 had only two nucleated crack spots: one along minor axis of the ellipse, i.e., $\alpha = 0$; the other along about 35-40 degrees away from it. Specimen TWLS-7 had no detectable signs of flaw growth and is considered to be below the threshold stress intensity level of 8.0 ksi $\sqrt{\text{in.}}$

Cyclic flaw growth data for 6Al-4V(ELI) titanium in the environment of ClF_5 at 140°F and 450 psig pressure is summarized in TABLE 23. Of the two specimens tested (TWLC-1 and -2) only one yielded some partial crack growth data. Specimen TWLC-2 after cyclic testing in the environment of ClF_5 was accidentally destroyed during cyclic marking. Specimen TWLC-1, while successfully completing the intended test sequence, yielded results that are not readily suitable for assessment of cyclic flaw growth characteristics of 6Al-4V(ELI) titanium in the environment of chlorine pentafluoride.

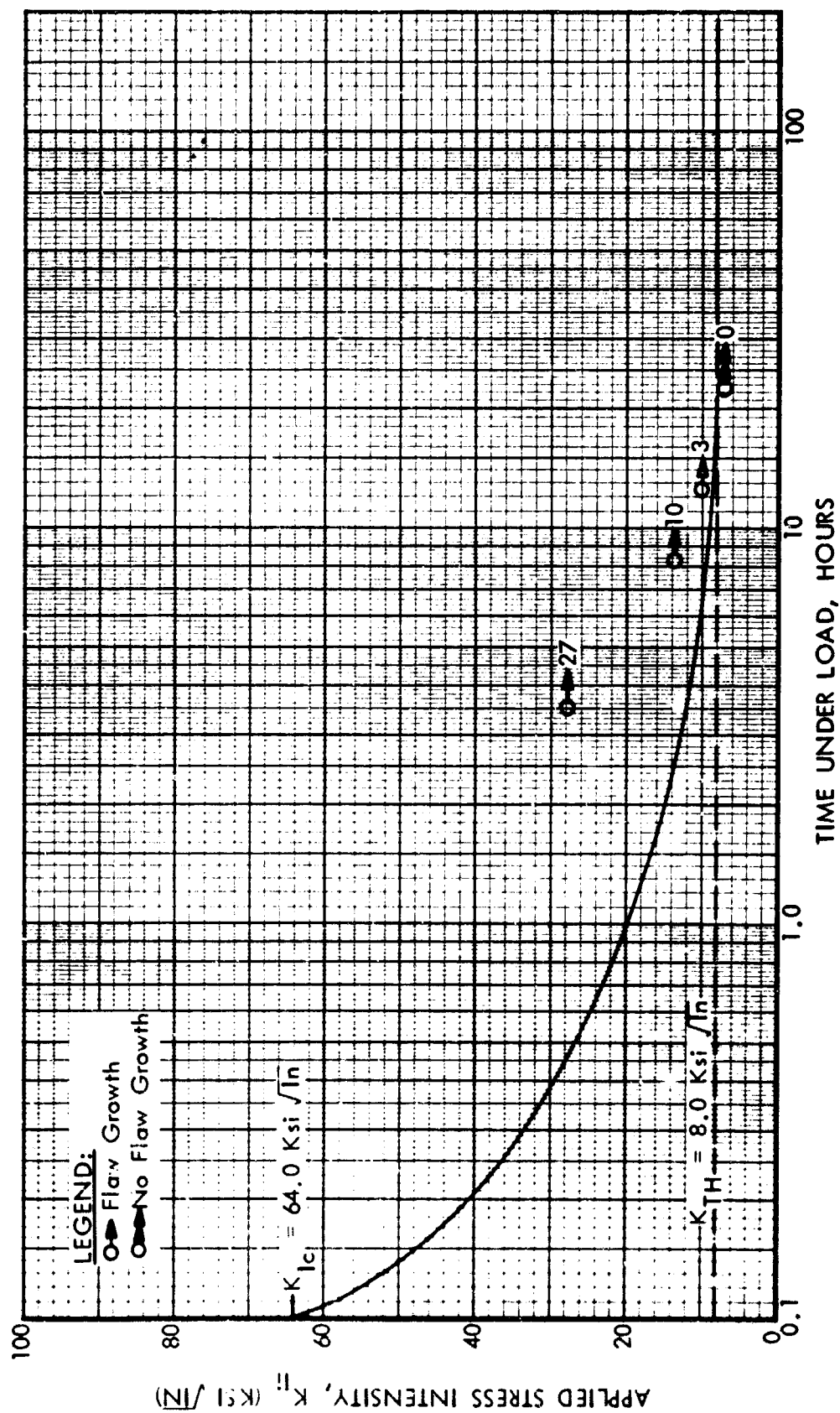


Figure 87 : SUSTAINED FLAW GROWTH DATA FOR 6Al-4V (ELI) TITANIUM AS-WELDED WELDMENT (CIF₅ @ 140 °F And 450 Psig)

5.2.4 410(MOD) Stainless Steel

Testing of the 410(MOD) stainless steel base metal was done in the environment of N_2O_4 at 120°F and 450 psig. Mechanical properties for the heat treated 410(MOD) stainless steel plate are listed in TABLE 24. Together with the two specimens pulled in long-transverse grain direction (specimens T-1 and -2), there was one specimen (TL-1) pulled in the longitudinal (along the plate rolling direction) grain orientation. Microstructure of the plate was exceptionally fine and was very uniform. Closeness of the data point values between TL-1, -2, and TT-1 specimens also tends to suggest high degree of uniformity within the material. Average yield and ultimate strengths of the material at room temperature are 155.1 and 192.4 ksi, respectively.

In response to the request by the Air Force Program Manager, and as an added factor in checking conformance of the material properties to the specification, three V-Charpy test specimens were tested at room temperature. Each of the three specimens tested was oriented in a different grain direction. Specimen TS-1 was machined in a manner that V-notch was oriented parallel to the plate rolling direction with the actual fracture running into the plate thickness. V-notch in specimen TE-1 was oriented parallel to the plate thickness in a manner that actual fracture ran along longitudinal grain direction and edgewise with respect to the plate. Specimen LE-1 was similar to TE-1 except that its fracture would run along the long-transverse grain direction but still edgewise with respect to the plate. The resultant Charpy impact values for specimens TS-1, LE-1, and TE-1, were 81.0, 70.0, and 61 ft-lbs, respectively.

Static fracture toughness data for the material was determined by testing two static fracture toughness specimens and is summarized in TABLE 25. Fractographs of the two static specimens tested are shown in Figure 88. Static fracture toughness data, together with end point values for the sustained test specimens summarized in TABLE 26, are plotted in Figure 89 in terms of fracture stress (σ) in ksi versus flaw size (a/Q) in inches. Superimposed on the plot are range of yield and ultimate strength levels for the material as listed in TABLE 24. As seen from Figure 89, both static test data points exceeded yield strength by a wide margin and consequently could not yield valid fracture toughness values.

Table 24: MECHANICAL PROPERTIES OF 410 (Mod)
STAINLESS STEEL BASE METAL

SPECIMEN IDENTIFICATION	TEST TEMPERATURE (°F)	GRAIN ORIENTATION	SPECIMEN SIZE		ULTIMATE STRENGTH (KSI)	YIELD STRENGTH (KSI)	ELONGATION (%)	REDUCTION OF AREA (%)
			DIAMETER (IN)	GAGE LENGTH (IN)				
T-1	RT	T	0.247	1.0	192.7	156.4	15	68
T-2	RT	T	0.247	1.0	192.0	153.8	16	68
L-1	RT	L	0.249	1.0	193.6	158.1	16	63



Specimen S-1



Specimen S-2

Figure 88 : FRACTOGRAPHS OF 410 (Mod.) STAINLESS STEEL BASE METAL SPECIMENS (Static Test In Air At Room Temperature)

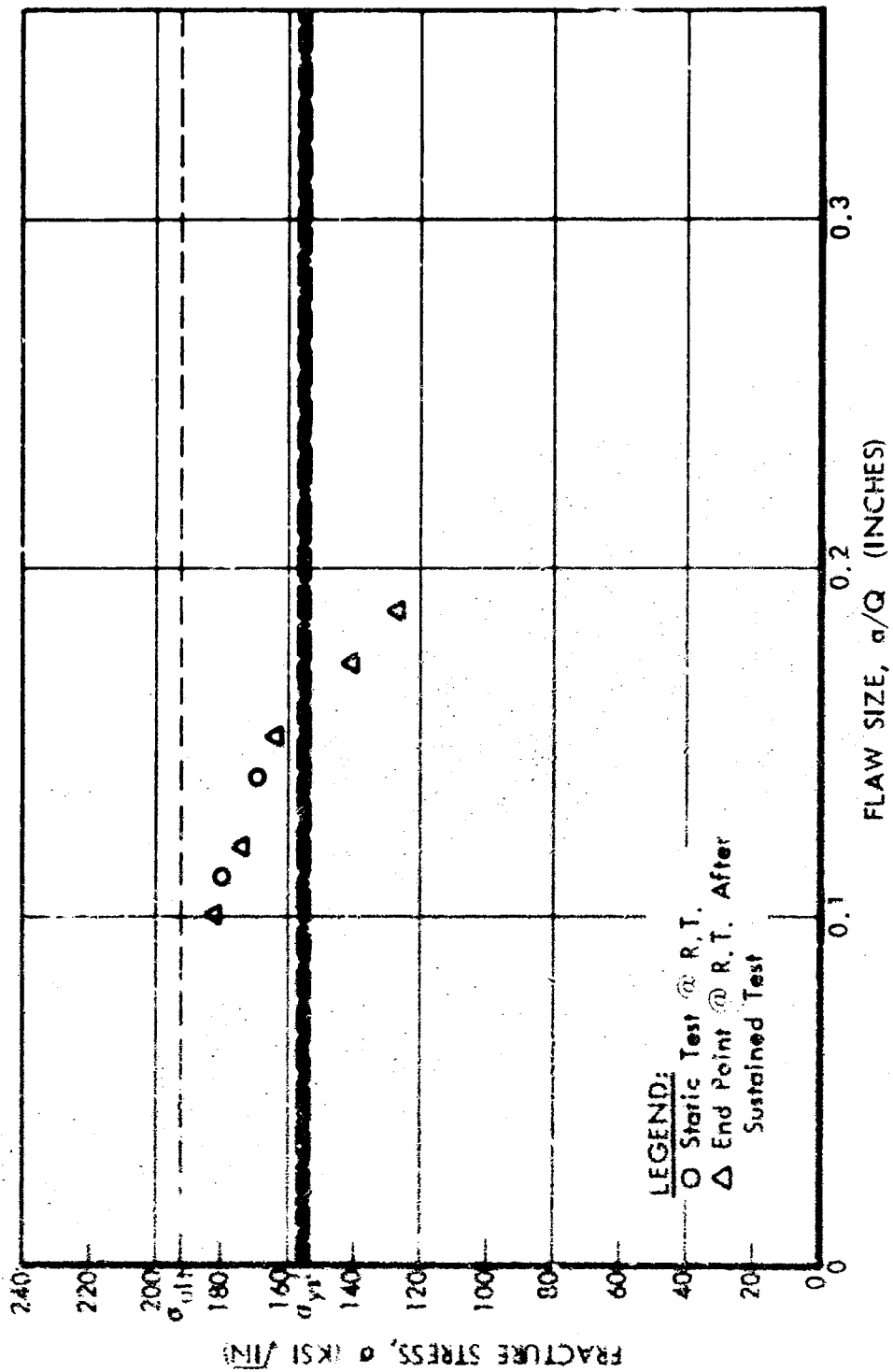


Figure 89 : STATIC FRACTURE TOUGHNESS DATA FOR 410 (Mod.)
STAINLESS STEEL BASE METAL

**Table 25: STATIC FRACTURE TOUGHNESS DATA
410 (MOD) STAINLESS STEEL BASE METAL**

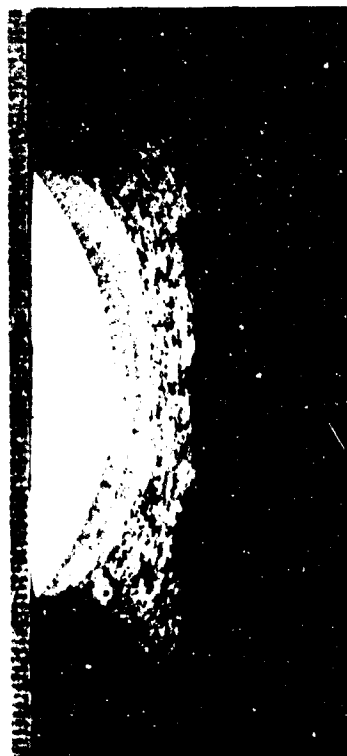
[illegible]

Likewise, three end point values from the sustained test specimens exceeded uniaxial yield strength of the material. Of the remaining three end point specimens whose gross stresses fall below uniaxial yield strength are likewise invalid because each of these specimens, while being subjected to gross stress levels below uniaxial yield strength in reality were experiencing net area stresses in excess of the yield strength. Because of that, none of the specimens tested did yield actual fracture toughness and it may be only assumed that fracture toughness of the material is larger than 124 ksi $\sqrt{\text{in.}}$.

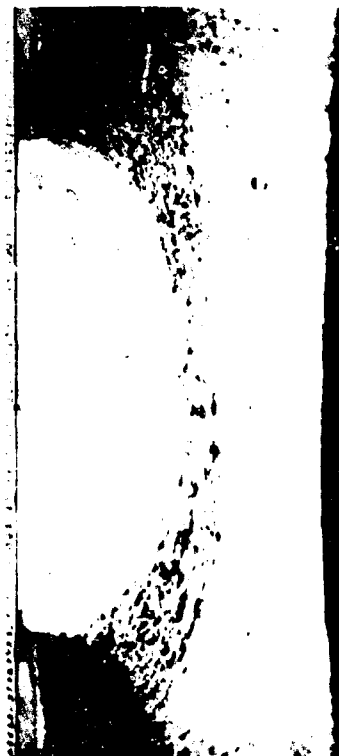
5.2.4.1 N_2O_4 and 410(MOD) Stainless Steel

The sustained flaw growth data for 410(MOD) stainless steel in the environment of N_2O_4 at 120°F and 450 psig pressure is summarized in TABLE 26. Fractographs of the sustained flaw growth test specimens are shown in Figure 90. Of the six specimens tested (specimens S-3 through S-8) specimen S-3 and -4 had relatively shallow flaws. The remaining specimens had considerably deeper flaws in order to generate high stress intensity without exceeding uniaxial yield strength of the material. Specimens S-6, -7, and -8 met that criteria even with respect to the net area stress level. All of the sustained test data points are plotted in Figure 91.

The plot of the sustained data in Figure 91 is made in terms of applied stress intensity (K_{II}) on the ordinate versus time under load on the abscissa in hours. Included on the plot as well as in TABLE 26 is specimen S-7 which was actually subjected to cyclic loading in the manner that total hold time at maximum stress did add up to 5 hours for direct comparison with Specimen S-8. The cyclic loading profile was trapezoidal with hold time at maximum load 5 minutes each cycle. Loading and unloading sequences were completed in 15 seconds each. There was also a 15 second hold time at zero load. Purpose of this cyclic test was to see if the cyclic loading would precipitate a "run-away" cyclic flaw growth rate. Such was not the case. The extent of flaw growth in cyclically loaded specimen was considerably larger (0.004 versus 0.001 of an inch). The threshold stress intensity for the 410(MOD) stainless steel was set at 72.0 ksi $\sqrt{\text{in.}}$ level.



Specimen S-3



Specimen S-4



Specimen S-5



Specimen S-6



Specimen S-7



Specimen S-8

Figure 90 · FRACTOGRAPHS OF 410 (Mod.) STAINLESS STEEL BASE METAL
SPECIMENS (Sustained Test In N_2O_4)

Table

[illegible]

B

Table 26: SUSTAINED FLAW GROWTH DATA
410 (MOD) STAINLESS STEEL BASE
METAL IN THE ENVIRONMENT OF
N₂O₄ AT 120°F AND 450 PSIG PRESSURE

[illegible]

6.0 DISCUSSION

6.1 Application to Pressure Vessel Design

Application of experimental data to engineering problems confronting designers of propellant containing pressure vessels may be facilitated by considering various interlocking factors, first independently, then in conjunction with one another. Present program consisted of two distinct phases. The first phase was designed to give a qualitative indication of critical parameter-affecting behavior of a given material. The second was intended to provide data that would assist the designers in selecting the material for service in a given environment and to enable them to make a reasonable forecast of its behavior under service conditions.

The Phase I screening test, while potentially very promising in providing an inexpensive method for checking various critical variables, may not be sensitive enough to distinguish less pronounced influences affecting behavior of the material. Failure to pass a screening test, as in the case of 6Al-4V(ELI) titanium and ClF_5 , is an obvious indication that the selected material is not compatible with a given propellant. The converse is not always true, however. If the material passes a screening test, one should be careful to provide additional testing like the one proposed for Phase II testing to make sure that the selected combination is indeed suitable for structural application.

Further refinements of the Phase I testing will lead to improved specimen design and flaw preparation that would provide greater sensitivity and a more refined categorizing of different material-propellant combinations. In the present program, with the one notable exception of ClF_5 in combination with titanium, the materials failed to react with the propellants calling for a more sophisticated Phase II testing.

Inasmuch as the Phase I test approach was never intended to be more than a qualitative screening method, the generated data would not be directly usable in design. The Phase II testing, on the other hand, was meant to provide design data and, within certain limits for material-propellant

combinations, offers plausible opportunities to use it as a means for establishing service and proof stress test levels, prediction of cyclic and sustained load carrying capability, and determination of the nondestructive inspection criteria.

The concept of critical stress intensity (K_{IC}) or fracture toughness, it may be pointed out, is as essential in design as yield or ultimate strength of the material. For a given set of conditions the load carrying capability of the material is intimately dependent upon size, shape and orientation of crack-like defects inadvertently present in the component. The higher the toughness, the larger is the defect that can be tolerated for a given stress level. From equations 2, 3, and 6, it is apparent that for a given crack-like defect oriented perpendicularly to the principal tensile stress, the fracture stress is directly proportional to the fracture toughness K_{IC} . The higher the toughness -- the higher will be the fracture stress.

In the absence of sizable flaws, fracture stress will be equal to the ultimate strength of the material. For most engineering materials of practical interest presence of small flaws is likely to lead to fracture at stress levels below the ultimate strength but still above material's yield strength. Not uncommon are the situations when relatively small flaws would cause fracture at stress levels considerably lower than the uniaxial yield strength. This may occur either due to very low fracture toughness of the material or when a relatively small flaw grows in size under sustained load until critical combination of load-crack size is reached.

Gradual flaw growth will occur whenever applied stress intensity (K_{II}) exceeds the threshold stress intensity level (K_{TH}) for a given material-propellant combination. The relationship between fracture toughness (K_{IC}), threshold stress intensity level (K_{TH}) and the applied stress intensity level (K_{II}) is illustrated in the following three examples.

EXAMPLE 1: Effective proof test - safe life - critical burst

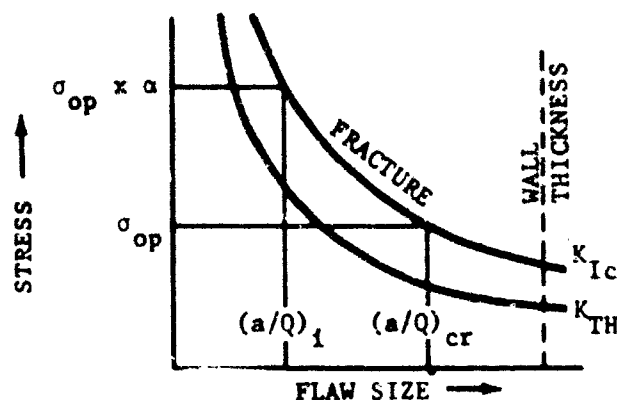


FIGURE a

Fracture toughness (K_{Ic}) threshold stress intensity level (K_{TH}), operating stress level (σ_{op}) and proof test factor (σ) are schematically plotted in Figure a. A pressure vessel that successfully passed proof test at $\sigma_{op} \times \alpha$ stress level may be presumed not to have defects larger than $(a/Q)_1$. Any pre-existing defect larger than $(a/Q)_1$ would have caused burst because the intersection of $\sigma_{op} \times \alpha$ horizontal line with the vertical projection of a flaw larger than $(a/Q)_1$ would fall to the right of the K_{Ic} curve or into the fracture region.

At the operating stress level a pre-existing flaw as large as $(a/Q)_1$ would remain stationary because the resultant stress intensity (K_{I1}) is actually smaller than the threshold stress intensity (K_{TH}) as seen from the fact that intersection of σ_{op} and $(a/Q)_1$ lines falls to the left of the intersection between K_{TH} curve and the σ_{op} line. It may be further noted that should the vessel be subjected to cyclic loading at σ_{op} the initial flaw $(a/Q)_1$ would grow in size until eventually it would reach $(a/Q)_{cr}$ size and cause burst at operating stress level. In the absence of cyclic loading the flaw would remain stationary at sustained stress level σ_{op} .

EXAMPLE 2: Effective proof test - safe life - leak instead of burst

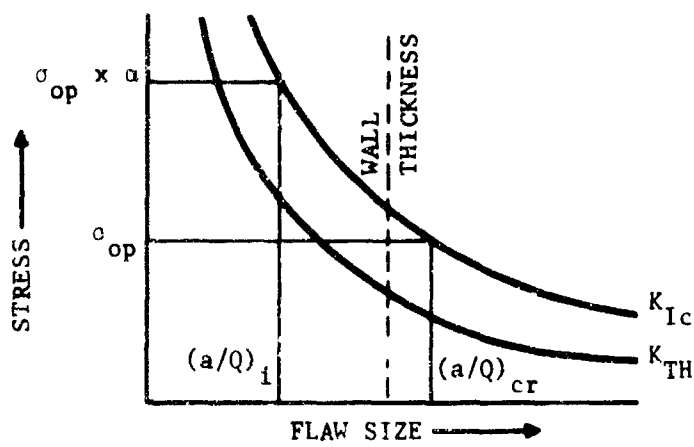


FIGURE b

This example characterizes a relatively thin-walled pressure vessel schematically illustrated in Figure b. Fracture toughness (K_{IC}), threshold stress intensity level (K_{TH}), operating stress, σ_{op} , and proof test level, $\sigma_{op} \times \alpha$ where α is once again the proof test factor, are plotted in Figure b, in the same manner as in Figure a. Marked difference stems from the fact that, unlike in Example 1, critical flaw size $(a/Q)_{cr}$ falls to the right of (is larger than) the tank wall thickness. This seemingly subtle difference has a very significant effect upon mode of fracture.

A pressure vessel characterized in Figure b would be safe to operate at σ_{op} sustained pressure because, as in the previous case, the maximum possible initial flaw size $(a/Q)_i$ that could remain in the vessel after proof test is still smaller than the one that would be required to generate K_{II} above K_{TH} level. Thus the pressure vessel would be safe to operate at σ_{op} sustained load. Should the vessel undergo unscheduled cyclic loading of stress level equal to σ_{op} the flaw would grow in size. However, because pressure vessel wall thickness is smaller than the critical flaw size $(a/Q)_{cr}$, the pressure vessel will leak and depressurize rather than burst as would be the case with the tank illustrated in Example 1.

EXAMPLE 3: No effective proof test - safe life - leak instead of burst

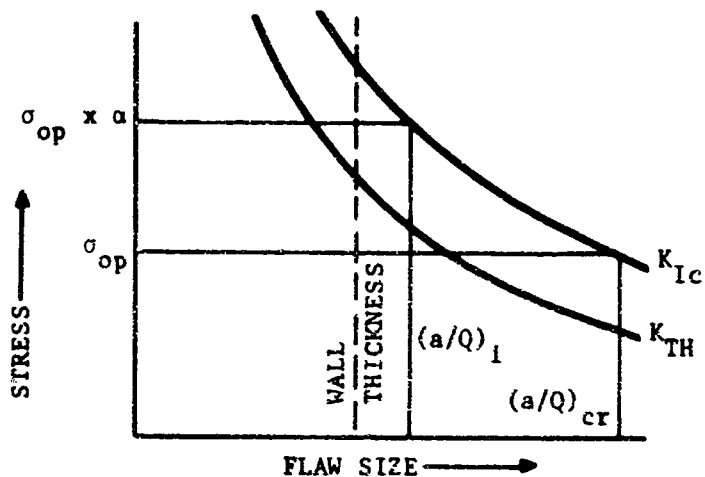


FIGURE c

This example characterizes a pressure vessel made from a material possessing high fracture toughness (K_{Ic}) and high threshold stress intensity (K_{TH}). The pressure vessel wall thickness is such that at the proof test level of $\sigma_{op} \times \alpha$ no burst is possible because intersection of the K_{Ic} curve and the $\sigma_{op} \times \alpha$ line falls to the right of (is larger than) the tank wall thickness. The most that a successful proof test under these conditions would reveal is that the tank did not leak, i.e., there were no initial flaw sizes larger than the wall thickness.

At the operating stress level, such a tank will be safe to operate under sustained pressure because even for a flaw that is almost as deep as the tank wall thickness, the generated stress intensity (K_{Ic}) is still below the threshold stress intensity (K_{TH}) level. Cyclic loading at stress levels as high as proof test stress level would cause a leak rather than a burst, thus providing substantial extra margin in safe operating conditions.

6.2 Limitations Inherent in Specific Cases

The preceding discussion of some typical cases encountered in pressure vessel design and operation by necessity are short and greatly simplified to illustrate basic principles supporting the so-called proof test logic. More specific information as applied to actual service vessel in the NASA

spacecraft may be found in References 41, 42, and 43. It would be appropriate to discuss some of the most significant qualifying limitations inherent in the approach based upon linear elastic fracture mechanics.

6.2.1 Baseline Fracture Toughness, K_{Ic}

In all three figures characterizing several types of pressure vessels, in Section 6.1, fracture toughness of each material was represented by a single curve. Such curve was drawn using Equation 2 as the only one at the present time permitting discussion of very deep flaws. Aside from the approximate nature of Equation 2, particularly its flaw depth correction factor, M_K , there is also the unavoidable data scatter that is encountered in any set of experimental results. Fracture stresses for a given set of specimens with identical flaw sizes generally fall within 5 to 7 percent, but can vary by as much as 10 to 15 percent or even greater. Some of the variations may be brought about by differences in specimen preparation, inaccuracies in flaw size measurements, and metallurgical variability of the material. In actual cases, therefore, the fracture toughness (K_{Ic}) baseline data should be characterized by drawing upper and lower bounds so that every valid data point falls within that range. For fracture stresses well within the elastic limit of the material and in general conformance with the requirements for valid fracture toughness measurements, both the upper and the lower K_{Ic} bounds may be drawn using the appropriate stress intensity equation.

For the situations where failure stresses approach or even exceed uniaxial yield strength of the material, rigorous characterization of the fracture toughness becomes impossible. Fracture data points when plotted on fracture stress versus critical flaw size on cartesian coordinates cannot be bounded by the loci following equations for fracture toughness measurements. In such cases, experimental data points usually follow a very regular path and still may be used to characterize flaw growth behavior as long as a strict similitude between test specimen and actual pressure vessel is maintained.

6.2.2 Threshold Stress Intensity, K_{TH}

Experimental techniques for determination of the threshold stress intensity levels were described in Section 3.2.2. By definition it is a stress intensity level below which flaw growth will not occur. It is presumed that occurrence of the flaw growth, while insignificantly small at the time of short run test, is likely to continue and eventually would lead to fracture or a leak depending on whether one is dealing with vessels typified by Example 1 and 2 or 3. Generally, the sustained threshold stress intensity levels will be considerably lower than actual fracture toughness of the material. Thus, calculated values would be more valid or are in greater conformance with the requirements of linear elastic fracture mechanics.

Considerable difficulties in establishing threshold stress intensity level may be avoided by insisting that only the lower bound of the experimental data be used to characterize threshold stress intensity level. This also provides an extra safety margin because the threshold stress intensity parameter reflects chemical as well as metallurgical interaction between a given propellant and a selected material. This extra margin together with the natural tendency of being on the conservative side in interpreting short test time data for prolonged service requirements should be carefully assessed lest it inflicts undue level of safety factors that eventually annihilate structural efficiency of a component.

6.2.3 Proof Test Factor, α

Selection of the adequate proof test factor in conjunction with required operating pressure level is an indispensable, and most crucial part in ensuring safe, reliable and efficient service capability. Effectiveness of the proof test hinges upon the ability to eliminate destructively pressure vessels containing defects larger than $(a/Q)_i$. Once this is done, the operating stress level is set at a level that for an established $(a/Q)_i$ value would not generate stress intensity greater than the threshold stress intensity level K_{TH} . As the break-even point proof test factor α can be set to be numerically equal to the K_{IC}/K_{TH} ratio, provided that both the K_{TH} as well

as K_{Ic} values are indeed valid, i.e., determined in strict compliance with the requirements of linear elastic fracture mechanics.

A great deal of care should be exercised whenever the K_{Ic}/K_{TH} ratio is deficient in one or both values. Quite often, for a given thickness of the material of interest, the full fracture toughness potential cannot be utilized, i.e., valid measurements cannot be obtained. This may not necessarily imply that the K_{TH} value is likewise deficient, or departs to the same degree from the requirements for valid measurements. Thus, characterization of proof test requirements using K_{Ic}/K_{TH} ratio should be judiciously applied, particularly in the areas where sustained as well as cyclic flaw growth rates are used to predict useful service life.

6.2.4 Data Scatter and Proof Test Logic

Whenever destructive elimination of pressure vessels containing flaws larger than $(a/Q)_i$ is possible (see Figures a and b in the preceding section), assurance of safe operating life through proof test logic may be confidently predicted. The concept is not only simple in principle but quite realistic in its application. Selection of adequate proof test factor is subject to considerable interpretation of confidence levels for the K_{Ic} as well as K_{TH} values. Nevertheless, once the proof factor is selected and a given vessel successfully passes proof test, every region in the vessel containing a defect would have been proofed to that factor regardless of the expected variations of properties from one region within the material to another.

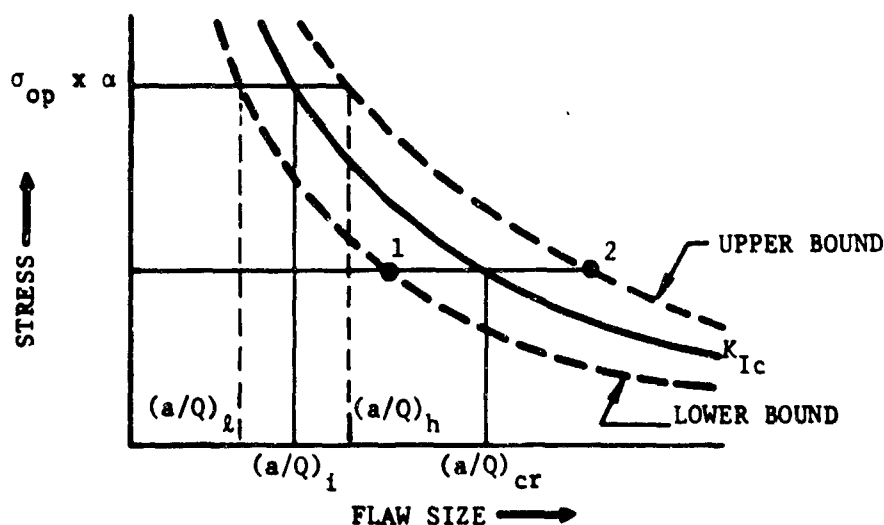


FIGURE d

To illustrate this, consider now once again the example of a pressure vessel fabricated from a material whose toughness can be characterized as shown schematically in Figure d. Using the baseline reference K_{Ic} value (solid line), successful completion of proof test provides an assurance that at operating stress level σ_{op} flaw growth potential in the region that can be characterized with the basic K_{Ic} line is the difference between $(a/Q)_{cr}$ and the $(a/Q)_1$.

Suppose now there is a region in the pressure vessel wall that is actually tougher than the toughness of the bulk of the material and is characterized by upper bound K_{Ic} curve. Successful completion of the proof test in this case cannot assure absence of flaws larger than $(a/Q)_1$. As a matter of fact, flaws as large as $(a/Q)_h$ may be present. Does that decrease the flaw growth potential? The answer to that is "no" because, as seen from the intersection of the σ_{op} line and the upper bound K_{Ic} curve, the flaw growth potential now is equal to the difference between $(a/Q)_2$ and the $(a/Q)_h$. Following the same reasoning, lower bound of the fracture toughness may be likewise considered. Successful proof test will now assure absence of defects smaller than $(a/Q)_1$. The flaw growth potential will be the difference between $(a/Q)_2$ and $(a/Q)_1$.

Thus, it may be concluded that even in the presence of differently behaving regions within a given pressure vessel, the proof test factor provides a flaw growth potential which can be derived by considering average K_{Ic} value for the material and its actual K_{TH} stress intensity level. Whether or not the selected proof test factor α will be sufficient to ascertain that applied K_{I1} is below threshold stress intensity level K_{TH} will depend on the margin that will be provided between K_{I1} and K_{TH} values and the degree with which regions of higher toughness (upper bound K_{Ic}) are also regions of correspondingly higher K_{TH} value.

It should be also noted that proof test logic is based on the assumption that upon conclusion of the proof test as the pressure is dropped, no further growth (certainly not to a significant degree) takes place. The pre-existing

flaw of the size somewhat smaller than $(a/Q)i$ may grow during the rising-load portion of the proof test cycle; however, unless depressurization rate is exceedingly low, the flaw growth occurring during the proof test cycle does not invalidate the approach and can still be looked at as a realistic method for ascertaining structural integrity of pressurized components.

7.0 CONCLUSIONS

1. Experimental techniques employed in this program are suitable for generation of reproducible crack growth data even though not all Phase I test specimens were sensitive enough for effective screening of engineering materials.
2. Generated Phase II data is usable in the design of propellant-containing pressure vessels.
3. Of the materials tested, 6Al-4V(ELI) titanium was found to be incompatible with chlorine pentafluoride (ClF_5); 2021-T81 aluminum is likely to create functional problems if used as N_2O_4 storage pressure vessel material; 2219-T851 aluminum and 410(MOD) stainless steel showed no pronounced susceptibility to N_2O_4 environment.
4. Several examples on application of this type of data to engineering design may serve as an inducement for further evaluation of specific cases in order to establish proof test criteria, NDT acceptance standards and provide adequate assurance of safe operating conditions.

REFERENCES

1. G. R. Irwin, "Crack Extension Force for a Part-Through Crack in a Plate", Appl. Mech., Vol. 29; Trans. ASME, Vol. 84, Series E, December 1962.
2. A. S. Kobayashi, "On the Magnification Factors of Deep Surface Flaws", Structural Development Research Memorandum No. 16, The Boeing Company, December 1965.
3. F. W. Smith, "Stresses Near a Semi-Circular Edge Crack", Ph. D. Dissertation, University of Washington, 1966.
4. F. W. Smith, "Stress Intensity Factor for a Semi-Elliptical Flaw", Structural Development Research Memorandum No. 17, The Boeing Company, August 1966.
5. B. Gross, J. E. Srawley, and W. F. Brown, "Stress Intensity Factors for a Single Edge Notch Tension Specimen by Boundary Collocation of a Stress Function", NASA TN D-2395, 1964.
6. S. Mostovoy, P. B. Crosley, and E. J. Ripling, "Use of Crack-Line-Loaded Specimens for Measuring Plane-Strain Fracture Toughness", Journal of Materials, Vol. 2, No. 3, September 1967.
7. S. O. Davis, N. G. Tupper, and R. M. Niemi, "Plane Strain Fracture Toughness Properties of Three Aluminum Alloys as a Function of Specimen Geometry", AFML-TR-65-150, July 1965.
8. C. N. Freed and J. M. Krafft, "Effect of Side Grooving on Measurements of Plane Strain Fracture Toughness", Journal of Materials, Vol. 1, No. 4, December 1966.
9. B. Gross, "Stress Intensity Factors for Single Edge Notch Specimens in Bending or Combined Bending and Tension by Boundary Collocation of a Stress Function", NASA TN D-2603, 1965.
10. C. D. Beachem and B. F. Brown, "A Comparison of Three Specimens for Evaluating the Susceptibility of High Strength Steel to Stress-Corrosion Cracking", Internal Report, U.S. Naval Research Laboratory.
11. H. R. Smith, D. E. Piper, and F. K. Downey, "A Study of Stress Corrosion Cracking by Wedge Force Loading", Boeing Document D6-19768, June 1967 (to be published in the Journal of Engineering, Fracture Mechanics, 1968).
12. B. F. Brown, "A New Stress-Corrosion Cracking Test for High-Strength Alloys", ASTM Materials Research and Standards 66, 129 (1966).

REFERENCES - (Continued)

13. D. E. Piper, S. H. Smith, and R. V. Carter, "Corrosion Fatigue and Stress Corrosion Cracking in Aqueous Environments", ASM National Metal Congress, October 31, 1966.
14. G. G. Hancock and H. H. Johnson, "Subcritical Crack Growth in AM 350 Steel", Materials Research and Standards 6, 431 (1966).
15. H. H. Johnson and A. M. Willner, "Moisture and Stable Crack Growth in a High Strength Steel", Applied Materials Research 4, 34 (1965).
16. E. A. Steigerwald and W. D. Benjamin, "Stress Corrosion Cracking Mechanisms in Martensitic High Strength Steels", Third Quarterly Progress Report, Contract AF 33(615)-3651, Air Force Materials Laboratory, 1967.
17. M. H. Peterson, B. F. Brown, R. L. Newbegin, and R. E. Groover, "Stress Corrosion Cracking of High Strength Steels and Titanium Alloys in Chloride Solution at Ambient Temperature", Corrosion 23, 142, 1967.
18. G. R. Irwin, "Moisture Assisted Slow Crack Extension in Glass Plates" Naval Research Laboratory Memorandum Report 1678, 1966.
19. C. F. Tiffany, P. M. Lorenz, and R. C. Shah, "Extended Loading of Cryogenic Tanks", NASA CR-72252, July 1966. (NAS 3-4194 Program)
20. P. C. Paris, M. P. Gomez, and W. E. Anderson, "A Rational Analytic Theory of Fatigue", Trend in Engr. (Univ. of Washington), Vol. 13, No. 1, 1961.
21. P. C. Paris, "The Growth of Cracks Due to Variations in Loads", Ph. D. Thesis, Lehigh University, 1962.
22. P. C. Paris and F. Erdogan, "A Critical Analysis of Crack Propagation Laws", Trans. ASME, Series D (J. Basic Engr.), Vol. 85, No. 4, 1963.
23. D. R. Donaldson and W. E. Anderson, "Crack Propagation Behavior of Some Airframe Materials", in Proceedings of the Crack Propagation Symposium, Cranfield, College of Aeronautics, 1962.
24. J. Schijve and F. A. Jacobs, "Fatigue Crack Propagation in Unnotched and Notched Aluminum Alloy Specimens, NLR-TR M.2128 (Amsterdam), 1964.
25. D. Broek and J. Schijve, "The Effect of Sheet Thickness on the Fatigue-Crack Propagation in 2024-T3 Alclad Sheet Material", NLR-TR M.2129 (Amsterdam), 1963.
26. A. J. McEvily and W. Illg, "The Rate of Fatigue Crack Propagation in Two Aluminum Alloys", NASA-TN 4384, 1958.
27. N. E. Frost and D. S. Dugdale, "The Propagation of Fatigue Cracks in Sheet Specimens", J. Mech. Phys. Sol., Vol. 6, No. 2, 1958.
28. H. W. Liu, "Crack Propagation in Thin Metal Sheets Under Repeated Loading", Trans. ASME, Series D (J. Basic Engr.), Vol. 83, No. 1, 1961.

REFERENCES - (Continued)

29. H. W. Liu, "Fatigue Crack Propagation and Applied Stress Range--An Energy Approach", Trans. ASME, Series D (J. Basic Engr.), Vol. 85, No. 1, 1963.
30. A. K. Head, "The Growth of Fatigue Cracks", Phil. Mag., Vol. 44, Series 7, 1953.
31. A. K. Head, "The Propagation of Fatigue Cracks", J. Appl. Mech., Vol. 23, September 1956.
32. F. A. McClintock, "On the Plasticity of the Growth of Fatigue Cracks", Fracture of Solids (editors Drucker and Gilman), Wiley, 1963.
33. J. R. Rice, "Fatigue Crack Growth Model: Some General Comments and Preliminary Study of the Rigid Plastic Strip Model", Lehigh University Inst. Res. Report, December 1962.
34. J. Weertman, "Rate of Growth of Fatigue Cracks as Calculated from the Theory of Infinitesimal Dislocations Distributed on a Plane", to appear in Proc. of Intl. Conf. Fract., Sendai, Japan, 1965.
35. J. M. Krafft, "A Comparison of Cyclic Fatigue Crack Propagation with Single Cycle Crack Toughness and Plastic Flow", Report to ASTM Fracture Toughness of High-Strength Materials Special Committee, September 1964.
36. R. G. Forman, V. E. Kearney, and R. M. Engle, "Numerical Analysis of Crack Propagation in Cyclic-Loaded Structures", ASME Paper No. 66-WA/Met-4, 1967.
37. C. F. Tiffany, P. M. Lorenz, and L. R. Hall, "Investigation of Plane Strain Flaw Growth in Thick-Walled Tanks", NASA CR-54837, February 1966.
38. L. R. Hall, "Plane-Strain Cyclic Flaw Growth in 2014-T62 Aluminum and 6Al-4V(ELI) Titanium", NASA Technical Report CR-72477, January 1969.
39. R. Roberts and F. Erdogan, "The Effect of Mean Stress on Fatigue Crack Propagation in Plates under Extension and Bending", ASME paper No. 67-WA1, Met-2, 1967.
40. J. N. Masters, "Cyclic and Sustained Load Flaw Growth Characteristics of 6Al-4V(ELI) Titanium", NASA CR-92231, July 1968.
41. C. F. Tiffany, J. N. Masters, and R. C. Shah, "Fracture Mechanics Assessment of Apollo Launch Vehicle and Spacecraft Pressure Vessels", Volume I. Boeing Document D2-114248-1, January 1969.
42. S. V. Glorioso, et al., "Lunar Module Pressure Vessel Operating Criteria Specification", SE-V-0024, October 25, 1968, NASA MSC Houston, Texas.
43. D. M. Ecord, et al., "Apollo Command and Service Module Pressure Vessel Operating Criteria Specification", SE-V-0028, October 1968, NASA MSC Houston, Texas.

14. KEY WORDS	LINK A		LINK B		LINK C	
	ROLE	WT	ROLE	WT	ROLE	WT
Fracture Mechanics						
Flaw Growth						
Sustained Load						
Aluminum						
Stainless Steel						
Titanium						
Nitrogen Tetroxide						
Flourine						
Chlorine Pento Flouride						

INSTRUCTIONS

1. **ORIGINATING ACTIVITY:** Enter the name and address of the contractor, subcontractor, grantee, Department of Defense activity or other organization (corporate author) issuing the report.
2. **REPORT SECURITY CLASSIFICATION:** Enter the overall security classification of the report. Indicate whether "Restricted Data" is included. Marking is to be in accordance with appropriate security regulations.
3. **GROUP:** Automatic downgrading is specified in DoD Directive 5200.10 and Armed Forces Industrial Manual. Enter the group number. Also, when applicable, show that optional markings have been used for Group 3 and Group 4 as authorized.
3. **REPORT TITLE:** Enter the complete report title in all capital letters. Titles in all cases should be unclassified. If a meaningful title cannot be selected without classification, show title classification in all capitals in parenthesis immediately following the title.
4. **DESCRIPTIVE NOTES:** If appropriate, enter the type of report, e.g., interim, progress, summary, annual, or final. Give the inclusive dates when a specific reporting period is covered.
5. **AUTHOR(S):** Enter the name(s) of author(s) as shown on or in the report. Enter last name, first name, middle initial. If military, show rank and branch of service. The name of the principal author is an absolute minimum requirement.
6. **REPORT DATE:** Enter the date of the report as day, month, year; or month, year. If more than one date appears on the report, use date of publication.
- 7a. **TOTAL NUMBER OF PAGES:** The total page count should follow normal pagination procedures, i.e., enter the number of pages containing information.
- 7b. **NUMBER OF REFERENCES:** Enter the total number of references cited in the report.
- 8a. **CONTRACT OR GRANT NUMBER:** If appropriate, enter the applicable number of the contract or grant under which the report was written.
- 8b, 8c, & 8d. **PROJECT NUMBER:** Enter the appropriate military department identification, such as project number, subproject number, system numbers, task number, etc.
- 9a. **ORIGINATOR'S REPORT NUMBER(S):** Enter the official report number by which the document will be identified and controlled by the originating activity. This number must be unique to this report.
- 9b. **OTHER REPORT NUMBER(S):** If the report has been assigned any other report numbers (either by the originator or by the sponsor), also enter this number(s).
10. **AVAILABILITY/LIMITATION NOTICES:** Enter any limitations on further dissemination of the report, other than those

imposed by security classification, using standard statements such as:

- (1) "Qualified requesters may obtain copies of this report from DDC."
- (2) "Foreign announcement and dissemination of this report by DDC is not authorized."
- (3) "U. S. Government agencies may obtain copies of this report directly from DDC. Other qualified DDC users shall request through _____."
- (4) "U. S. military agencies may obtain copies of this report directly from DDC. Other qualified users shall request through _____."
- (5) "All distribution of this report is controlled. Qualified DDC users shall request through _____."

If the report has been furnished to the Office of Technical Services, Department of Commerce, for sale to the public, indicate this fact and enter the price, if known.

11. **SUPPLEMENTARY NOTES:** Use for additional explanatory notes.

12. **SPONSORING MILITARY ACTIVITY:** Enter the name of the departmental project office or laboratory sponsoring (paying for) the research and development. Include address.

13. **ABSTRACT:** Enter an abstract giving a brief and factual summary of the document indicative of the report, even though it may also appear elsewhere in the body of the technical report. If additional space is required, a continuation sheet shall be attached.

It is highly desirable that the abstract of classified reports be unclassified. Each paragraph of the abstract shall end with an indication of the military security classification of the information in the paragraph, represented as (TS), (S), (C), or (U).

There is no limitation on the length of the abstract. However, the suggested length is from 150 to 225 words.

14. **KEY WORDS:** Key words are technically meaningful terms or short phrases that characterize a report and may be used as index entries for cataloging the report. Key words must be selected so that no security classification is required. Identifiers, such as equipment model designation, trade name, military project code name, geographic location, may be used as key words but will be followed by an indication of technical context. The assignment of links, rules, and weights is optional.